## Aus der

Abteilung für Transfusionsmedizin, Zelltherapeutika und Hämostaseologie Klinikum der Ludwig-Maximilians-Universität München



# **Enhancement of Antibody-Dependent Cellular Phagocytosis** of Lymphoma Cells by the Blockade of HLA Class I Receptors

Dissertation

zum Erwerb des Doktorgrades der Medizin an der Medizinischen Fakultät der Ludwig-Maximilians-Universität München

vorgelegt von
Tobias Sebastian Zeller

aus

Augsburg

Jahr

2025

# Mit Genehmigung der Medizinischen Fakultät der Ludwig-Maximilians-Universität zu München

Erstes Gutachten: Prof. Dr. rer. nat. Christian Kellner

Zweites Gutachten: Priv. Doz. Dr. Andreas Moosmann

Drittes Gutachten: Prof. Dr. Anne Krug

ggf. weitere Gutachten: Prof. Dr. Stefan Endres

Dekan: Prof. Dr. med. Thomas Gudermann

Tag der mündlichen Prüfung: 16.10.2025

This work was supported by the Deutsche José Carreras Leukämie-Stiftung and Deutsche Gesellschaft für Hämatologie und Medizinische Onkologie with the José Carreras-DGHO scholarship for doctoral research (05 PSD/2021).	

#### Essential parts of this thesis have previously been published in the following articles:

#### Original research articles

Schewe, D. M., Vogiatzi, F., Munnich, I. A., <u>Zeller, T.</u>, Windisch, R., Wichmann, C., Muller, K., Bhat, H., Felix, E., Mougiakakos, D., Bruns, H., Lenk, L., Valerius, T., Humpe, A., Peipp, M. & Kellner, C. 2024. Enhanced potency of immunotherapy against B-cell precursor acute lymphoblastic leukemia by combination of an Fc-engineered CD19 antibody and CD47 blockade. *Hemasphere*, 8, e48.

Zeller, T., Lutz, S., Munnich, I. A., Windisch, R., Hilger, P., Herold, T., Tahiri, N., Banck, J. C., Weigert, O., Moosmann, A., von Bergwelt-Baildon, M., Flamann, C., Bruns, H., Wichmann, C., Baumann, N., Valerius, T., Schewe, D. M., Peipp, M., Rosner, T., Humpe, A. & Kellner, C. 2022. Dual checkpoint blockade of CD47 and LILRB1 enhances CD20 antibody-dependent phagocytosis of lymphoma cells by macrophages. *Front Immunol*, 13, 929339.

#### **Review articles**

**Zeller, T.**, Munnich, I. A., Windisch, R., Hilger, P., Schewe, D. M., Humpe, A. & Kellner, C. 2023. Perspectives of targeting LILRB1 in innate and adaptive immune checkpoint therapy of cancer. *Front Immunol*, 14, 1240275.

Peipp, M., Klausz, K., Boje, A. S., **Zeller, T.**, Zielonka, S. & Kellner C. 2022. Immunotherapeutic targeting of activating natural killer cell receptors and their ligands in cancer. *Clin Exp Immunol*, 209, 22-32.

#### **Abstracts**

Kiepe, N., Zimmermann, P., Pauls, I., **Zeller, T.**, Kreissig, S., Wichmann, C., Peipp, M., Humpe, A., Lenk, L. & Kellner, C. 2025. Targeting FMS-Like Tyrosine Kinase 3 (FLT3) in B-Cell Acute Lymphoblastic Leukemia with an Fc-Engineered Antibody. *Ann Hematol, accepted for publication* 

Zeller, T., Munnich, I. A., Hilger P., Pauls, I., Windisch R., Kreissig, S., Zimmermann, P., Kiepe, N., Wichmann, C., Moosmann A., Humpe, A., Schewe, D. M., Peipp, M. & Kellner, C. 2024. Die Kombination von Daratumumab mit dualer Immun-Checkpoint-Blockade von CD47 und LILRB1 steigert die Phagozytose von T-ALL-Zellen durch Makrophagen. *Oncol Res Treat*, 47 (Supplement 2), 318.

**Zeller, T.**, Munnich, I. A., Hilger, P., Pauls, I., Windisch, R., Kreissig, S., Wichmann, C., Peipp, M., Humpe, A., Schewe, D. M. & Kellner, C. 2023. Co-Blockade of CD47 and LILRB1 Enhances Daratumumab-Mediated Phagocytosis of T Lineage Acute Lymphoblastic Leukemia Cells by Macrophages. *Ann Hematol*, 102 (Supplement 1), 14.

**Zeller, T.**, Lutz, S., Munnich, I. A., Windisch, R., Hilger, P., Herold, T., Tahiri, N., Banck, J. C., Weigert, O., Moosmann, A., von Bergwelt-Baildon, M., Flamann, C., Bruns, H., Wichmann, C., Baumann, N., Valerius, T., Schewe, D. M., Peipp, M., Rosner, T., Humpe, A. & Kellner, C. 2022. Immun-Checkpoint Co-Blockade von CD47 und HLA-Klasse I-Rezeptoren zur Steigerung der CD20-Antikörper-vermittelten Phagozytose von Lymphomzellen. *Oncol Res Treat*, 45 (Supplement 2), 162.

Hilger, P., **Zeller, T.**, Vogiatzi, F., Muller, K., Munnich, I. A., Windisch, R., Wichmann, C., Nimmerjahn, F., Valerius, T., Peipp, M., Humpe, A., Schewe, D. M. & Kellner, C. 2022. Steigerung der CD38 Antikörper-vermittelten Phagozytose von T-ALL Zellen durch Fc Engineering und CD47 Blockade. *Oncol Res Treat*, 45 (Supplement 2), 92.

**Zeller, T.**, Lutz, S., Munnich, I. A., Windisch, R., Hilger, P., Herold, T., Tahiri, N., Banck, J. C., Weigert, O., Moosmann, A., von Bergwelt-Baildon, M., Flamann, C., Bruns, H., Wichmann, C., Baumann, N., Valerius, T., Schewe, D. M., Peipp, M., Rosner, T., Humpe, A. & Kellner, C. 2022. Dual immune checkpoint blockade of LILRB1 and CD47 enhances antibody-dependent cellular phagocytosis of lymphoma cells by CD20 antibodies. *Eur J Immunol*, 52 (Supplement 1), 136.

## **Table of Contents**

Tal	ble o	of Conte	nts	I
Zu	samı	menfass	sung	<b>V</b>
Ab	stra	ct		VI
Lis	t of	Figures		VII
Lis	t of	Tables		IX
Lis	t of	Abbrevi	ations	X
1.			tion	
	1.1	Antibo	dy-Based Immunotherapy of Cancer	1
		1.1.1	CD20 Antibody Therapy of B-Cell Non-Hodgkin Lymphoma	2
		1.1.2	Structure and Formats of Therapeutic Antibodies	
		1.1.2		
		1.1.2 1.1.2		
		1.1.2		
		1.1.3	•	
		1.1.3		
		1.1.4		
		1.1.4	1.1 NK Cells	14
		1.1.4	_	
		1.1.4	,	
		1.1.4	, , ,	
	1.2	_	gies to Improve Macrophage ADCP of Cancer Cells	
		1.2.1	Antibody Fc Engineering	
		1.2.2	Phagocytosis Checkpoints	20
	1.3		cyte Immunoglobulin-Like Receptors as Targets nune Checkpoint Blockade	21
			Genetics, Structure and Signaling of LILRB1 and LILRB2	
		1.3.2	Broad Recognition of HLA Class I by LILRB1 and LILRB2	
		1.3.3	LILRB1 and LILRB2 in the Regulation of Macrophages	
		1.3.4	LILRB1 and LILRB2 in Cancer	
	1.4	Aims a	ınd Objectives	29
2.	ı	Materials	s and Methods	31
	2.1	Materia	als	31
		2.1.1	Chemicals	
		2.1.2	Kits	_
		2.1.3	Buffers, Solutions and Media	
		2.1.4	Cell Lines	
		2.1.5	Cultivation of Cell Lines	35

## Table of Contents

	2.1.6	Bacteria	35
	2.1.7	Vectors	35
	2.1.8	Primers	36
	2.1.9	Antibodies	36
	2 1 10		
		•	
	_		
2.2			
		- · · · · · · · · · · · · · · · · · · ·	
		·	
	2.2.1		
	2.2.1	·	
	2.2.2		
	2.2.2		
	2.2.2	2.2 Transfection of Mammalian Cells	48
		2.2.2.2.1 Calcium Phosphate Transfection	48
		2.2.2.2.2 Lipofectamine Transfection	49
	2.2.2	2.3 Flow Cytometry	49
		2.2.2.3.1 Cell Surface Antigen Expression	49
		2.2.2.3.2 Binding of Recombinant Antibodies	
		•	
		•	
		1 3	
		• •	
	2.2.2	2.7 Statistical and Graphical Analysis	53
F	Results		54
3.1			<b>54</b>
	-		54
	3.1.2	•	EE
	0.4.0		
		·	
	3.1.4	LILRB1 and LILRB2 Expression on M0 Macrophages	57
	F	2.1.7 2.1.8 2.1.9 2.1.10 2.1.11 2.1.12 2.1.13 2.1.14  2.2 Method 2.2.1 2.2. 2.2. 2.2. 2.2. 2.2. 2.2. 2.	2.1.7 Vectors

3.2	Genera	tion of Fc-silent anti-LILRB1 and anti-LILRB2 Antibodies	58
	3.2.1	Cloning of Expression Vectors	58
	3.2.2	Expression and Purification of LILRB1-lgGσ and LILRB2-lgGσ	58
	3.2.3	Biochemical Characterization of LILRB1-IgGσ	
		and LILRB2-IgGσ	59
3.3	Binding	g Properties of LILRB1-IgG $\sigma$ and LILRB2-IgG $\sigma$	61
	3.3.1	Binding of LILRB1-IgGσ and LILRB2-IgGσ to Macrophages	61
	3.3.2	Antigen-Specific Binding of LILRB1-IgG $\sigma$ and LILRB2-IgG $\sigma$	61
3.4	Recept	or Blocking by LILRB1-lgGσ and LILRB2-lgGσ	62
3.5		is of the Impact of LILRB1 or LILRB2 Blockade CP in Lymphoma Cell Line Models	64
	3.5.1	ADCP of Lymphoma Cell Lines upon HLA Receptor Blockade	64
	3.5.2	Depletion of Lymphoma Cells upon HLA Receptor Blockade	67
	3.5.3	Impact of LILRB1-IgGσ on IgA Antibody-Mediated ADCP	67
	3.5.4	Serial Phagocytosis of Lymphoma Cell Lines upon HLA Receptor Blockade	68
	3.5.5	Kinetics of ADCP upon HLA Receptor Blockade	69
	3.5.6	Dose-Dependent Enhancement of ADCP by LILRB1-IgGσ	70
	3.5.7	Impact of Enhanced FcγR Activation on ADCP under LILRB1 and CD47 Dual Immune Checkpoint Blockade	71
3.6		tion of LILRB1 or LILRB2 Blockade in Differentially ed Macrophages	72
3.6			
3.6	Polariz	ed Macrophages  Expression of M1 and M2c Marker Antigens by	73
3.6	Polariz 3.6.1	ed Macrophages  Expression of M1 and M2c Marker Antigens by Polarized Macrophages  Expression of Immune Checkpoint Molecules on	73 74
3.6	<b>Polariz</b> 3.6.1 3.6.2	Expression of M1 and M2c Marker Antigens by Polarized Macrophages  Expression of Immune Checkpoint Molecules on Polarized Macrophages  Influence of Macrophage Activation by LPS and IFN-γ on the Expression of LILRB1, LILRB2 and SIRPα  Phagocytosis of Lymphoma Cells by Polarized Macrophages	73 74 74
3.6	3.6.1 3.6.2 3.6.3	Expression of M1 and M2c Marker Antigens by Polarized Macrophages  Expression of Immune Checkpoint Molecules on Polarized Macrophages  Influence of Macrophage Activation by LPS and IFN-γ on the Expression of LILRB1, LILRB2 and SIRPα  Phagocytosis of Lymphoma Cells by Polarized Macrophages  Serial Phagocytosis of Lymphoma Cells by Polarized Macrophages	73 74 74 75
3.6	3.6.1 3.6.2 3.6.3 3.6.4	Expression of M1 and M2c Marker Antigens by Polarized Macrophages  Expression of Immune Checkpoint Molecules on Polarized Macrophages  Influence of Macrophage Activation by LPS and IFN-γ on the Expression of LILRB1, LILRB2 and SIRPα  Phagocytosis of Lymphoma Cells by Polarized Macrophages  Serial Phagocytosis of Lymphoma Cells by Polarized Macrophages  Influence of Macrophage Activation by LPS and IFN-γ on the Phagocytosis of Lymphoma Cells	73 74 74 75
3.6	3.6.1 3.6.2 3.6.3 3.6.4 3.6.5	Expression of M1 and M2c Marker Antigens by Polarized Macrophages  Expression of Immune Checkpoint Molecules on Polarized Macrophages  Influence of Macrophage Activation by LPS and IFN-γ on the Expression of LILRB1, LILRB2 and SIRPα  Phagocytosis of Lymphoma Cells by Polarized Macrophages  Serial Phagocytosis of Lymphoma Cells by Polarized Macrophages  Influence of Macrophage Activation by LPS and IFN-γ	73 74 75 76
3.6	3.6.1 3.6.2 3.6.3 3.6.4 3.6.5 3.6.6 3.6.7 Efficac	Expression of M1 and M2c Marker Antigens by Polarized Macrophages  Expression of Immune Checkpoint Molecules on Polarized Macrophages  Influence of Macrophage Activation by LPS and IFN-γ on the Expression of LILRB1, LILRB2 and SIRPα  Phagocytosis of Lymphoma Cells by Polarized Macrophages  Serial Phagocytosis of Lymphoma Cells by Polarized Macrophages  Influence of Macrophage Activation by LPS and IFN-γ on the Phagocytosis of Lymphoma Cells  Kinetics of ADCP of Lymphoma Cells by Differentially	73 74 75 76 77
	3.6.1 3.6.2 3.6.3 3.6.4 3.6.5 3.6.6 3.6.7 Efficac	Expression of M1 and M2c Marker Antigens by Polarized Macrophages  Expression of Immune Checkpoint Molecules on Polarized Macrophages  Influence of Macrophage Activation by LPS and IFN-γ on the Expression of LILRB1, LILRB2 and SIRPα  Phagocytosis of Lymphoma Cells by Polarized Macrophages  Serial Phagocytosis of Lymphoma Cells by Polarized Macrophages  Influence of Macrophage Activation by LPS and IFN-γ on the Phagocytosis of Lymphoma Cells  Kinetics of ADCP of Lymphoma Cells by Differentially Polarized Macrophages  y of LILRB1-IgGσ and LILRB2-IgGσ in Enhancing	73 74 75 76 77 78
	3.6.1 3.6.2 3.6.3 3.6.4 3.6.5 3.6.6 3.6.7 Efficacy	Expression of M1 and M2c Marker Antigens by Polarized Macrophages  Expression of Immune Checkpoint Molecules on Polarized Macrophages  Influence of Macrophage Activation by LPS and IFN-γ on the Expression of LILRB1, LILRB2 and SIRPα.  Phagocytosis of Lymphoma Cells by Polarized Macrophages  Serial Phagocytosis of Lymphoma Cells by Polarized Macrophages  Influence of Macrophage Activation by LPS and IFN-γ on the Phagocytosis of Lymphoma Cells  Kinetics of ADCP of Lymphoma Cells by Differentially Polarized Macrophages  y of LILRB1-IgGσ and LILRB2-IgGσ in Enhancing of Patient-Derived Lymphoma Cells  Expression of CD20, CD47 and HLA Class I	73 74 75 76 77 78 80

## Table of Contents

		3.7.4	ADCP of Patient-Derived Mantle Cell Lymphoma Cells	84
4.	[	Discussi	on	85
	4.1	Further	Critical Factors Affecting ADCP	86
	4.2	•	ement of CD47 Co-Blockade and the Presence of ctivation for the Efficacy of Anti-LILRB1 Antibodies	87
	4.3	Inability	y of LILRB2-lgG $\sigma$ to Promote Phagocytosis	89
	4.4		ncer Effects of LILRB Blockade in Different e Effector Cells	91
	4.5		nges in the Development of LILRB1-Directed dies and Potential Pitfalls in their Application	93
	4.6	•	ctives of Immune Checkpoint Co-Blockade cer Immunotherapy	95
5.	E	Bibliogra	phy	98
6.	A	Acknowle	edgements	120
7.	A	Affidavit		120
8.	į	Jbereins	timmungserklärung	122
9.	L	_ist of Pւ	ublications	123

## Zusammenfassung

Die antikörperabhängige zelluläre Phagozytose (ADCP) von Tumorzellen durch Makrophagen ist eine wichtige Effektorfunktion therapeutischer Antikörper. ADCP wird jedoch durch "Don't Eat Me!"-Signale wie CD47 gehemmt. Klinische Studien in Lymphompatienten ergaben vielversprechende Ergebnisse für eine Kombination des CD20-Antikörpers Rituximab (RTX) mit dem CD47-blockierenden Antikörper Magrolimab. Kürzlich wurde in Modellen solider Tumoren auch eine hemmende Rolle für Klasse I humane Leukozytenantigene (HLA) aufgedeckt, die Makrophagen mit den Rezeptoren leukocyte immunoglobulin-like receptor subfamily B member 1 (LILRB1) und LILRB2 erkennen. Ob ADCP von Lymphomzellen durch LILRB1- oder LILRB2-Blockade gesteigert werden kann ist noch nicht bekannt und wurde in dieser Arbeit untersucht. So ergab die Analyse verschiedener Lymphom-Zelllinien eine positive Korrelation zwischen dem Expressionsverhältnis von CD20 zu HLA Klasse I und der durch RTX und einem CD47-Antikörper induzierten ADCP. Dies zeigte, dass die HLA Klasse I-Expression ADCP unter CD47-Blockade hemmte. Zur Blockade der HLA Klasse I-Rezeptoren wurden Antikörper gegen LILRB1 oder LILRB2 (LILRB1-IgGσ bzw. LILRB2-IgGσ) in einem Fc-stummen Format hergestellt, um Interaktionen mit Fcy-Rezeptoren (FcyR) zu vermeiden. Beide wurden in humanen Zellen exprimiert und affinitätschromatographisch gereinigt. Die spezifische Bindung wurde durchflusszytometrisch nachgewiesen. ADCP wurde durch Fluoreszenzmikroskopie oder Live-Cell Imaging bestimmt. Hierzu wurden Monozyten aus dem Blut gesunder Spender isoliert und ex vivo zu Makrophagen mit M0, M1- oder M2-Polarisation differenziert. Als Ergebnis steigerte LILRB1-IgGσ die ADCP verschiedener Lymphom-Zelllinien durch M0-, M1- und M2-Makrophagen, wenn der Antikörper mit RTX und einer Fc-stummen Version von Magrolimab (CD47-lgGσ) kombiniert wurde. LILRB1-IgGo steigerte sogar die ADCP von DG-75 Burkitt-Lymphom-Zellen, die in Präsenz von nur RTX und CD47-IgGσ kaum phagozytiert wurden. Dagegen war LILRB2-IgGσ aus unbekannten Gründen unwirksam, obwohl er die Rezeptor-Bindung von HLA blockierte. LILRB1-IgGo förderte die ADCP multipler Lymphom-Zellen durch individuelle Makrophagen, erforderte jedoch die Anwesenheit eines CD20-Antikörpers zur FcyR-Aktivierung und eine Ko-Blockade von CD47, um wirksam zu werden. Bedeutenderweise steigerte LILRB1-IgGo die ADCP frisch isolierter Tumorzellen von Patienten mit chronischer lymphatischer Leukämie oder Mantelzell-Lymphom. Folglich limitiert HLA Klasse I die durch Kombinationen aus CD20- und CD47-Antikörpern induzierte ADCP. Diese Limitation kann durch Blockade von LILRB1, nicht aber von LILRB2, überwunden werden. Duale CD47 und LILRB1-Checkpoint-Blockade stellt somit eine vielversprechende Strategie zur weiteren Verbesserung der CD20-Antikörpertherapie von Lymphomen dar.

## **Abstract**

Antibody-dependent cellular phagocytosis (ADCP) of cancer cells by macrophages is a major mechanism of action of therapeutic antibodies. However, ADCP is hampered by the expression of 'Don't Eat Me!' signals such as CD47 on tumor cells. In clinical studies in lymphoma patients, encouraging outcomes were obtained by combining the CD20 antibody rituximab (RTX) with the CD47 blocking antibody magrolimab. Recently, in solid tumor models also class I human leukocyte antigens (HLA), which ligate the macrophage receptors leukocyte immunoglobulin-like receptor subfamily B member 1 (LILRB1) and LILRB2, were found to protect cells from phagocytosis. Whether ADCP of lymphoma cells can be augmented by antibody blockade of LILRB1 or LILRB2 is currently not known and was analyzed in this thesis. Along this line, investigations in a set of lymphoma cell lines showed a positive correlation between the CD20-to-HLA class I expression ratio and the extent of ADCP induced by co-treatment with RTX and a CD47 antibody. This indicates that the expression of HLA class I hampered ADCP under CD47 blockade. To specifically block HLA class I receptors, anti-LILRB1 and anti-LILRB2 antibodies were generated as Fc-silent versions (LILRB1-lgGσ and LILRB2-lgGσ, respectively) with abrogated Fcy receptor (FcyR) binding. Both were produced by expression in human cells and purification via affinity chromatography. Antigen-specificity was demonstrated using flow cytometry. ADCP was analyzed by fluorescence microscopy or live cell imaging. To this, monocytes were enriched from peripheral blood and differentiated to macrophages with M0, M1 or M2 polarization status ex vivo. As a result, LILRB1-IgGo significantly improved ADCP of different lymphoma cell lines by M0, M1 or M2 macrophages when the antibody was combined with RTX and an Fc-silent magrolimab variant (CD47-IgGσ). LILRB1-IgGσ was even effective with DG-75 Burkitt lymphoma cells, which were barely phagocytozed upon treatment with RTX and CD47-IgGσ only. LILRB1-IgGσ facilitated the uptake of multiple target cells by individual macrophages, but constantly required the simultaneous blockade of CD47 and the combination with a CD20 antibody for FcyR activation to unfold its effect. Remarkably, LILRB1-IgGσ notably increased the phagocytosis of freshly isolated cancer cells from patients with chronic lymphocytic leukemia or mantle cell lymphoma. LILRB2-lgGσ, on the other hand, was ineffective for yet unknown reasons, even though the antibody effectively impeded receptor ligation by HLA class I. Consequently, the expression of HLA class I by lymphoma cells limits the potential of the combination of CD20 and CD47 antibodies to initiate phagocytosis. This hinderance can be overcome by masking LILRB1, but not LILRB2. Thus, dual LILRB1/CD47 checkpoint blockade is an encouraging new approach to further improve CD20 antibody therapy of lymphomas.

# **List of Figures**

Figure 1:	Indications for therapeutic antibodies	2
Figure 2:	Structure of an IgG1 molecule	5
Figure 3:	Overview of the development of antibodies with increasingly reduced murine moieties.	6
Figure 4:	Examples of formats of therapeutic antibodies or antibody-constructs	9
Figure 5:	Direct effector functions of therapeutic antibodies	. 11
Figure 6:	Indirect effector functions of therapeutic antibodies	. 12
Figure 7:	Structure of LILRB1 and LILRB2.	. 23
Figure 8:	Recognition of HLA molecules by KIR2DL3, LILRB1 and LILRB2	. 25
Figure 9:	Postulated effect of LILRB1 or LILRB2 antibody blockade on CD20 antibody-mediated ADCP of lymphoma cells	. 30
Figure 10:	Sensitivity of B-NHL cell lines to ADCP	. 55
Figure 11:	Surface antigen expression on B-NHL cell lines	. 56
Figure 12:	The expression ratio of CD20 to HLA-A,-B,-C molecules determines the sensitivity of B-NHL cell lines to ADCP mediated by rituximab plus CD47-IgGo	. 57
Figure 13:	Expression of LILRB1 and LILRB2 on M0 macrophages	
Figure 14:	Purification of LILRB2-IgGσ from the cell culture supernatant	
Figure 15:	Purity, integrity and homogeneity of LILRB1-lgGσ and LILRB2-lgGσ	. 60
Figure 16:	Binding of LILRB1-IgGσ and LILRB2-IgGσ to macrophages	. 61
Figure 17:	Antigen-specificity of LILRB1-IgGσ and LILRB2-IgGσ	. 62
Figure 18:	Disruption of receptor-ligand-interaction by LILRB1-IgGσ and LILRB2-IgGσ	. 63
Figure 19:	Impact of HLA receptor blockade on ADCP of Carnaval cells by M0 macrophages	. 64
Figure 20:	Antigen-specific enhancement of ADCP by LILRB1-IgGσ	. 65
Figure 21:	Enhanced ADCP of MEC2 and DG-75 cells by LILRB1-IgGo	
Figure 22:	Fold improvement in ADCP of B-NHL cell lines by LILRB1-IgGo	. 66
Figure 23:	Enhanced depletion of B-NHL cells by LILRB1-IgGσ	. 67
Figure 24:	Co-blockade of LILRB1 and CD47 promotes ADCP by IgA antibodies.	. 68
Figure 25:	Serial ADCP of B-NHL cells by M0 macrophages	. 69
Figure 26:	Kinetics of ADCP of DG-75 cells by M0 macrophages upon antibody treatment	. 70
Figure 27:	Dose-dependent enhancement of ADCP by LILRB1-IgGσ	. 71
Figure 28:	Further enhancement of ADCP by engineering the Fc domain of the CD20 antibody	. 72
Figure 29:	Expression of polarization marker antigens on M0, M1 and M2c macrophages.	
Figure 30:	Expression of the immune checkpoints LILRB1, LILRB2 and SIRPα on M0, M1 and M2c macrophages	
Figure 31:	Influence of macrophage activation on the expression of LILRB1 LILRB2 and SIRPG	75

## List of Figures

Figure 32:	Impact of HLA receptor blockade on ADCP by differentially polarized macrophages.	. 76
Figure 33:	Serial ADCP of B-NHL cells by polarized macrophages	. 77
Figure 34:	Influence of macrophage activation on ADCP of B-NHL cells upon antibody treatment.	. 78
Figure 35:	Kinetics of ADCP by polarized macrophages upon antibody treatment	. 79
Figure 36:	Fluorescence microscopy images of improved ADCP of CLL cells from patients by co-blockade of CD47 and LILRB1.	. 80
Figure 37:	Expression of cell surface antigens on patient-derived CLL and MCL cells.	. 81
Figure 38:	ADCP of individual patient-derived CLL cells upon CD47 and LILRB1 co-blockade.	. 82
Figure 39:	Sample group analysis of ADCP of patient-derived CLL cells	. 83
Figure 40:	Serial ADCP of patient-derived CLL cells.	. 83
Figure 41:	ADCP of MCL cells from patients upon CD47 and LILRB1 co-blockade.	. 84

## List of Tables

## **List of Tables**

Table 1:	Human FcγRs	. 14
Table 2:	Chemicals	. 31
Table 3:	Kits	. 32
Table 4:	Buffers, solutions and media.	. 33
Table 5:	Cell lines.	. 34
Table 6:	Culture media composition for cell lines.	. 35
Table 7:	Bacteria	. 35
Table 8:	Vectors	. 35
Table 9:	Primers.	. 36
Table 10:	Conjugated antibodies	. 36
Table 11:	Unconjugated antibodies.	. 37
Table 12:	Soluble, PE-conjugated HLA class I molecules used for binding studies	. 38
Table 13:	Consumables	. 38
Table 14:	Devices	. 40
Table 15:	Software	. 42
Table 16:	Composition of 10% and 12% SDS gels.	. 47

## **List of Abbreviations**

ADCP Antibody-dependent cellular phagocytosis

(Antikörperabhängige zelluläre Phagozytose)

A Absorbance

Ab Antibody

ADC Antibody-drug conjugate

ADCC Antibody-dependent cell-mediated cytotoxicity

Ag Antigen

ALL Acute lymphoblastic leukemia

AML Acute myeloid leukemia

APC Antigen presenting cell

APS Ammonium persulfate

ARC Antibody-radionuclide conjugate

B-ALL B-lineage acute lymphoblastic leukemia

B-NHL B-cell Non-Hodgkin lymphoma

BCMA B-cell maturation antigen

BCP-ALL B-cell precursor acute lymphoblastic leukemia

BiTE Bispecific T-cell engager

BSA Bovine serum albumin

BsAbs Bispecific antibodies

C1q Complement component 1q

CAR Chimeric antigen receptor

CD Cluster of differentiation

CDC Complement-dependent cytotoxicity

CDCC Complement-dependent cell-mediated cytotoxicity

CDCP Complement-dependent cell-mediated phagocytosis

CDR Complementarity determining regions

CFSE Carboxyfluorescein succinimidyl ester

C<sub>H</sub> Constant region of the antibody heavy chain

C<sub>L</sub> Constant region of the antibody light chain

CLL Chronic lymphocytic leukemia

CMV Cytomegalovirus

CTLA-4 Cytotoxic T-lymphocyte-associated protein 4

DAMP Damage-associated molecular pattern

DC Dendritic cell

dH<sub>2</sub>O Distilled water

DLBCL Diffuse large B-cell lymphoma

DMSO Dimethyl sulphoxide

DSMZ German Collection of Microorganisms and Cell Cultures

DTT DL-Dithiothreitol solution

E:T cell ratio Effector cell:target cell ratio

EGFR Epidermal growth factor receptor

EpCAM Epithelial cell adhesion molecule

ERK Extracellular-signal regulated kinase

Fab Fragment antigen binding

Fc Fragment crystallizable

FcR Fc region receptor

FCS Fetal calf serum

FcαR Immunoglobulin α Fc region receptor

FcyR Immunoglobulin y Fc region receptor

FITC Fluorescein isothiocyanate

GM-CSF Granulocyte-macrophage colony-stimulating factor

GPI Glycosylphosphatidylinositol

HC Heavy chain

HER Human epidermal growth factor receptor

HLA Human leukocyte antigen (Humanes Leukozytenantigen)

HRP Horseradish peroxidase

IFN Interferon

lg Immunoglobulin

IL Interleukin

ILT Immunoglobulin-like transcript

ITAM Immunoreceptor tyrosine-based activating motif

ITIM Immunoreceptor tyrosine-based inhibitory motif

KIR Killer cell immunoglobulin-like receptor

LAM Lymphoma-associated macrophage

LC Light chain

LILRB Leukocyte immunoglobulin-like receptor subfamily B

LIR Leukocyte immunoglobulin-like receptor

LPS Lipopolysaccharide

LRC Leukocyte receptor complex

LRP1 Prolow-density lipoprotein receptor-related protein 1

M-CSF Macrophage colony-stimulating factor

MAC Membrane attack complex

MAC1 Macrophage-1 antigen

MCL Mantle cell lymphoma

MIR Monocyte / macrophage lg-like receptor

MMAE Monomethyl auristatin E

MNC Mononuclear cell

MPO Myeloperoxidase

MW Molecular weight

N Amino

NA Neutrophil specific antigen

NET Neutrophil extracellular traps

NFkB Nuclear factor kappa-B

NK cells Natural killer cells

NKG2A Natural killer group 2 member A

ns Not significant

NSCLC Non-small cell lung cancer

PAA Polyacrylamide

PAMP Pathogen-associated molecular pattern

PBS Phosphate buffered saline

PD-1 Programmed cell death protein 1

PD-L1 Programmed cell death ligand 1

PE Phycoerythrin

Pen/Strep Penicillin / streptomycin

PirB Paired Ig-like receptor B

PRR Pathogen-recognition receptor

RBC Red blood cells

RCC Renal-cell carcinoma

RIFINs Repetitive interspersed families of polypeptides

ROS Reactive oxygen species

RTX Rituximab

SABC Specific antibody binding capacities

ScFv Single-chain variable fragment

SD Standard deviation

SDS Sodium dodecyl sulfate

SDS-PAGE Sodium dodecyl sulfate polyacrylamide gel electrophoresis

SEM Standard error of the mean

SHP SRC-homology 2 domain-containing phosphatase

Siglec Sialic acid-binding Ig-like lectin

SIRPα Signal regulatory protein α

SLAM Signaling lymphocytic activation molecule

SLAMF7 SLAM family member 7

STAT1 Signal transducer and activator of transcription 1

SYK Spleen tyrosine kinase

T-ALL T cell acute lymphoblastic leukemia

TAM Tumor-associated macrophage

TCR T cell receptor

T<sub>EM</sub> Effector memory T cell

TEMED Tetramethylenediamide

## List of Abbreviations

T<sub>EMRA</sub> Effector memory T cell re-expressing CD45RA

TGF Transforming growth factor

Th cell T helper cell

TLR Toll-like receptor

TME Tumor microenvironment

TNF Tumor necrosis factor

VEGF Vascular endothelial growth factor

V<sub>H</sub> Variable region of the antibody heavy chain

V<sub>L</sub> Variable region of the antibody light chain

w/o Without antibody

β2m β2 microglobulin

## 1. Introduction

## 1.1 Antibody-Based Immunotherapy of Cancer

The therapeutic potential of drugs to efficaciously and precisely attack pathogens or cancer cells has already been recognized around 1900 by Nobelist Paul Ehrlich. His theories evolved into what became known as the famous 'magic bullet concept': Targeted therapeutics, which bind selectively to their intended cell-structural targets, yet remain non-toxic in normal tissues (Ehrlich, 1900, Strebhardt and Ullrich, 2008). Furthermore, in an effort to explain the observation that in animals exposure to low doses of a toxin induced immunity against otherwise lethal doses of the same toxin Paul Ehrlich hypothesized that cells carry side chains on their surface, which specifically bind antigens and may be distributed more abundantly into the blood upon interaction with the antigen they are specific for. Such antitoxins, as detached side chains were termed by Paul Ehrlich, were later identified to be antibodies produced by activated B cells (Ehrlich, 1900, Strebhardt and Ullrich, 2008, Bjørneboe and Gormsen, 1943).

Their highly specific targeting properties render antibodies not only a pivotal component of the immune system, but also an ideal format to realize Paul Ehrlich's concept of a 'magic bullet'. Thus, since Georges J. F. Köhler and César Milstein described a technique to produce substantial amounts of monoclonal antibodies specific for a predetermined epitope in 1975, a discovery they later received the Nobel Prize for, monoclonal antibodies have revolutionized biomedical research, diagnostics and the therapeutic options in a broad spectrum of diseases (Kohler and Milstein, 1975). Henceforth, numerous biotechnological advances have enabled the elucidation of the detailed structure of antibody molecules, as well as the generation of less immunogenic and more effective antibodies and thus laid the foundation for the clinical application of antibodies as therapeutics. The range of antibody-based therapies has since then expanded remarkably and has been extended continuously to new antibody formats and therapeutic areas. To date, 224 antibody-based therapeutics have been granted approval or are in regulatory review and are applied in a variety of diseases. These include not only cancer, which is still the major indication for therapeutic antibodies, but also immune-mediated disorders, infectious diseases, as well as cardiovascular or neurological disorders (figure 1) (The Antibody Society, 2025).

A landmark success in the therapeutic use of antibodies was the marketing approval of the antibody rituximab, which binds cluster of differentiation (CD) 20, in 1997. Rituximab was the first antibody therapy to receive approval for a malignant disease and has revolutionized the treatment of various B-cell Non-Hodgkin lymphomas (B-NHL),

particularly when applied in combination with chemotherapy (Maloney et al., 1994, McLaughlin et al., 1998, Pavlasova and Mraz, 2020, Pierpont et al., 2018). Since then, a variety of target antigens in both solid and hematological cancers were identified, including human epidermal growth factor receptor (HER)2, epidermal growth factor receptor (EGFR), CD38 and CD19. The great success of antibodies as therapeutic agents traces back not least to the numerous advantages of antibody therapies. Antibodies are well-characterized molecules that can be produced easily and in consistently high quality and purity in recombinant systems. Furthermore, antibodies are characterized by enhanced tolerability and reduced toxicity compared to many conventional chemotherapy drugs, long plasma half-life and capability to mediate a broad spectrum of direct and indirect effector functions, which will be discussed in more detail later (Paul et al., 2024).

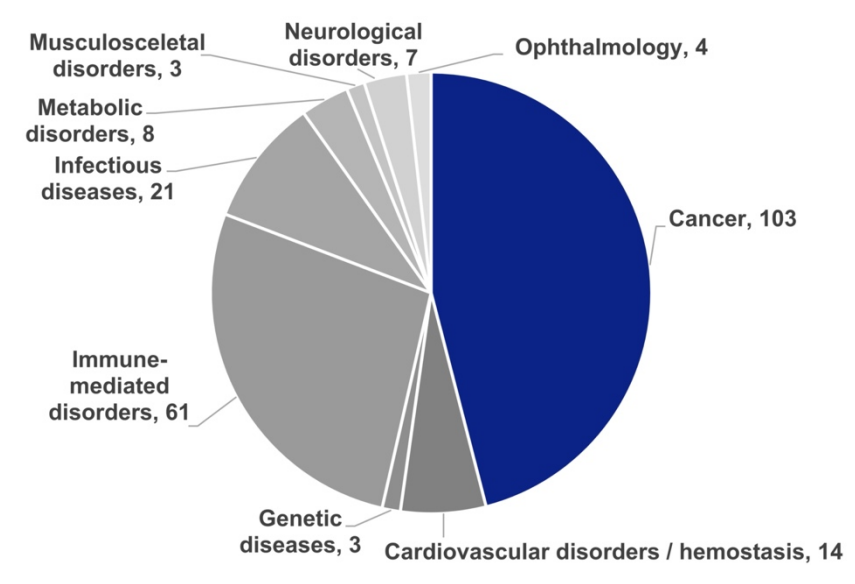


**Figure 1: Indications for therapeutic antibodies.** Indicated are the numbers of antibodies that have already been granted approval or are in regulatory review for treatment in the respective therapeutic area. Antibody products that have since been withdrawn from the market were included, biosimilar products not. The diagram was created using published data (The Antibody Society, 2025).

## 1.1.1 CD20 Antibody Therapy of B-Cell Non-Hodgkin Lymphoma

B-NHLs comprise a heterogeneous group of lymphoproliferative neoplasms, which commonly develop from B-cells in peripheral lymphoid tissue such as lymph nodes or the spleen, but can also affect the bone marrow or non-lymphoid tissues. According to histological and clinical features, B-NHLs are assigned to two prognostic groups. Thus, a distinction is made between acute, aggressive B-NHLs, which include for instance the diffuse large B-cell lymphoma (DLBCL) and Burkitt lymphoma, and less aggressive, indolent B-NHLs, to which among others the follicular lymphoma, mantle cell lymphoma (MCL) and chronic lymphocytic leukemia (CLL) are counted (Swerdlow et al., 2017).

Nearly all B-NHLs display CD20 at initial diagnosis. However, the biological function of this cell surface molecule is poorly understood (Pierpont et al., 2018). In normal B cells, display of CD20 is first detected in the early immature B cell stage. It is found on mature B cells at all stages of their development and its expression is downregulated upon differentiation into plasma cells (Pierpont et al., 2018). CD20 is not expressed in hematopoietic stem cells and in other normal tissues, except for weak expression in certain T cells (Hultin et al., 1993, Schuh et al., 2016). This expression pattern renders CD20 an attractive target antigen for antibody treatment of B-NHLs (Pierpont et al., 2018).

Treatment regimens for B-NHLs are chosen based on the disease subtype, stage and patient-related factors and include conventional approaches, such as chemotherapy or radiation therapy, stem cell transplantation and, with growing importance, targeted approaches such as tyrosine kinase inhibitors, therapeutic antibodies or chimeric antigen receptor (CAR) T cells (Wang et al., 2020a, Russler-Germain and Ghobadi, 2023). Within the therapeutic armamentarium, targeted therapies provide particularly great hope to further improve the therapeutic options, especially in the challenging situation of relapsed or refractory disease.

Despite the discovery of a plethora of target antigens for antibody therapies, CD20 remains to be a main target for the antibody treatment of malignant and non-malignant conditions to date (Delgado et al., 2024, Wang et al., 2020a). Thus, besides rituximab numerous CD20-targeting antibodies such as obinutuzumab, ofatumumab and ocrelizumab, bispecific anti-CD20/CD3 antibodies including epcoritamab, mosunetuzumab and glofitamab, as well as CD20 radioimmunoconjugates have emerged (Dabkowska et al., 2024, Chamarthy et al., 2011). Additionally, CD20 is currently investigated as a potential target for CAR T cells (Dabkowska et al., 2024).

## 1.1.2 Structure and Formats of Therapeutic Antibodies

Antibodies or immunoglobulins (Ig) are glycosylated proteins, which are naturally secreted by differentiated B cells, so-called plasma cells. Antibody secretion is initiated upon the recognition of a cognate immunogen by the B cell receptor, which contains a cell surface membrane Ig that has the identical binding domains as the secreted antibody molecule. Antibodies specifically bind to an individual epitope, a portion of the recognized antigen, and are the key component of the humoral branch of the adaptive immune response (Chaplin, 2010).

#### 1.1.2.1 Structure of Antibodies

In humans, the basic structure of an antibody typically consists of two pairs of identical heavy chains (HC) and light chains (LC). The chains are covalently linked through disulfide bridges (Padlan, 1994). Antibody LCs exist in two variants,  $\kappa$  and  $\lambda$ , of which only one variant is found in an individual antibody. The ratio of  $\kappa$  to  $\lambda$  variant varies between different species and is approximately two to one in human serum under physiological conditions (Mole et al., 1994). Antibody HCs occur in the five variants  $\alpha$ ,  $\delta$ ,  $\epsilon$ ,  $\gamma$  and  $\mu$  and allow to assign antibodies to one of the five different classes or isotypes, IgA, IgD, IgE, IgG and IgM, respectively. Antibodies of different isotypes differ in their structure, functions and the effector mechanisms they mediate. Since IgG is the predominant molecular format for therapeutic antibodies, the detailed structure will be explained based on this isotype.

Each of the four IgG polypeptide chains is composed of several Ig domains, for which a further distinction is made between variable and constant domains. The antibody LCs each comprise one variable region at their amino (N)-terminal end (V<sub>L</sub>) and one constant domain at their carboxylic acid end (C<sub>I</sub>) and have a molecular weight of about 25 kDa. The two antibody HCs are each composed of an N-terminal variable region (V<sub>H</sub>) accompanied by three constant domains (termed C<sub>H</sub>1, C<sub>H</sub>2 and C<sub>H</sub>3) and contain a flexible hinge region between C<sub>H</sub>1 and C<sub>H</sub>2 (figure 2). Each antibody HC has a molecular weight of approximately 50 kDa. In each arm of the antibody, V<sub>L</sub> and V<sub>H</sub> together with the C<sub>L</sub> and C<sub>H</sub>1 domains form the fragment antigen binding (Fab), which is responsible for the antibody binding to its epitope and thus determines the antibody's specificity. Consequently, each antibody molecule comprises two antigen binding sites. Located on the opposite side of the hinge region is the fragment crystallizable (Fc), which is formed by the C<sub>H</sub>2 and C<sub>H</sub>3 domains. Through the Fc region, antibodies interact with components of the immune system and thus mediate indirect effector functions (figure 2) (Padlan, 1994). According to minor differences in the HC constant domains, IgG molecules can further be categorized into the subclasses IgG1, IgG2, IgG3 and IgG4. Despite their great similarity, antibodies of different IgG subclasses vary in numerous aspects, such as complement activation or effector cell triggering (Vidarsson et al., 2014).

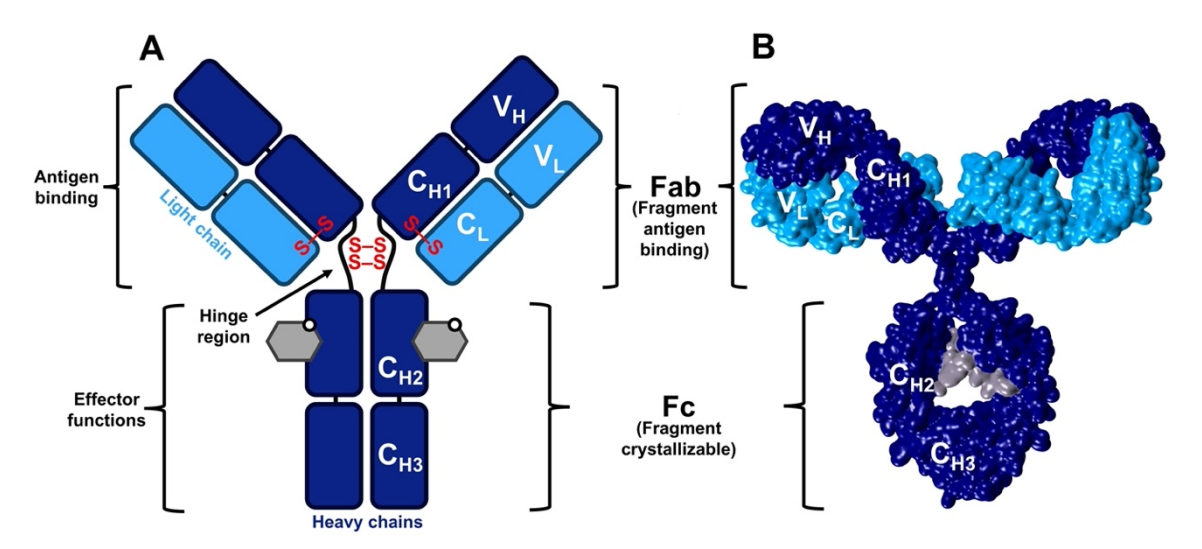


Figure 2: Structure of an IgG1 molecule. Displayed are the schematic (A) and crystal (B) structure of IgG1. Each IgG1 molecule comprises two identical light chains (LC; light blue) and heavy chains (HC; dark blue), which are bonded via disulfide bridges (red). The LC comprises one variable ( $V_L$ ) and one constant ( $C_L$ ) domain, the HC is composed of one variable ( $V_H$ ) and three constant ( $C_H1-C_H3$ ) domains. The variable regions of one LC and one HC, together with the  $C_L$  and  $C_{H1}$  domain form the two fragments antigen binding (Fab). The fragment crystallizable (Fc) is made up of the  $C_H2$  and  $C_H3$  domains. Additionally, IgG1 antibodies are gylcosylated at the conserved asparagine-297 in the  $C_H2$  region (grey). The pdb-file of an IgG1 molecule was kindly provided by M. Clark (Clark, 1997).

#### 1.1.2.2 Humanization of Antibodies

The first monoclonal antibodies applied clinically, such as the CD3 antibody muromonab-CD3 used for the treatment of acute glucocorticoid-resistant rejection of allogeneic transplants, were murine (Todd and Brogden, 1989). However, a major issue of murine antibodies applied in humans is the immunogenicity of the foreign protein, which can lead to adverse effects and decreased efficacy as a consequence of the formation of neutralizing antibodies (Hansel et al., 2010, Shawler et al., 1985). Various strategies were pursued to decrease the immunogenicity of therapeutic antibodies by reducing the murine moieties in antibody molecules (figure 3). Chimeric antibodies, such as rituximab, comprise the murine antibody's variable regions while the murine sequences of the constant regions are exchanged for the corresponding human sequences (Morrison et al., 1984, Boulianne et al., 1984, Reff et al., 1994). In humanized antibodies, such as the anti-HER2 antibody trastuzumab, also the framework regions of the murine variable domains are replaced by the respective human sequences and only the hypervariable complementarity determining regions (CDR), which are crucial for specific antigen recognition, remain of murine origin (figure 3) (Jones et al., 1986, Carter et al., 1992). Several new approaches have even enabled the production of completely human monoclonal antibodies, such as the anti-tumor necrosis factor (TNF)-α antibody adalimumab (figure 3). For example, phage display techniques were established to identify suitable sequences for the variable regions from human antibody phage display

libraries, which can subsequently be utilized to generate recombinant human antibodies (Alfaleh et al., 2020, Frenzel et al., 2016). Furthermore, the production of antibodies in transgenic mice, in which genes encoding for antibodies were replaced by the corresponding human sequences, as well as the immortalization and clonal expansion of human memory B cells have emerged as approaches to obtain fully human antibodies (Lonberg et al., 1994, Lanzavecchia et al., 2007).

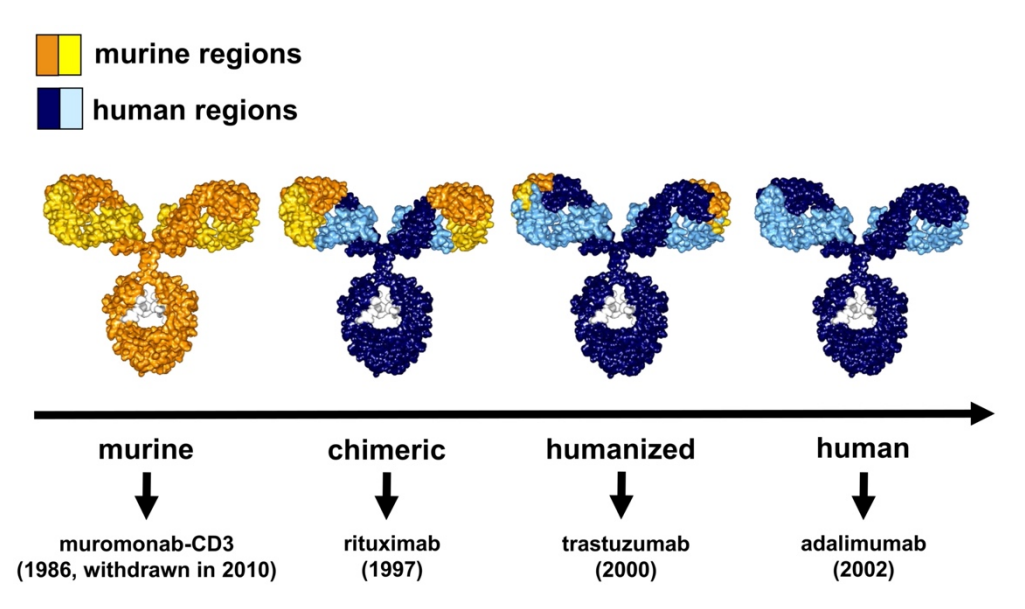


Figure 3: Overview of the development of antibodies with increasingly reduced murine moieties. The first therapeutic antibodies, such as muromonab-CD3, were murine antibodies. In chimeric antibody molecules, such as rituximab, murine variable regions are combined with the constant regions of human antibodies. In humanized antibodies, such as trastuzumab, only the hypervariable complementarity determining regions remain of murine origin. By now, also the generation of recombinant, fully human antibodies, such as adalimumab, has become possible. The pdb-file of an IgG1 molecule was kindly provided by M. Clark (Clark, 1997).

## 1.1.2.3 Formats of Therapeutic Antibodies

The above-described advances have opened the way for the development of a broad palette of therapeutic antibodies and antibody-derived constructs (Jin et al., 2022, Weiner, 2015). The simplest format of a therapeutic antibody is a monoclonal, monospecific, native antibody, which is specific for a soluble or cell-bound antigen (figure 4A). Even though other isotypes such as IgA are being evaluated, the vast majority of therapeutic antibodies are IgG (Leusen, 2015). Since the different IgG subclasses incorporate functional and structural differences, individual subclasses of IgG are chosen to achieve distinct therapeutic effects. For instance, IgG1 is the main format for therapeutic antibodies due to its high affinity for immunoglobulin  $\gamma$  Fc region receptors (Fc $\gamma$ R) and thus its high capability to activate Fc $\gamma$ R-carrying effector cells. In contrast, the notably lower affinity for Fc $\gamma$ R and for complement component 1q (C1q) of IgG4 antibodies renders them more suitable for applications, in which the engagement of immune cells or

the mediation of complement-dependent cytotoxicity play a subordinate role or is not desired. Examples herefore are the antibody blockade of inhibitory signaling receptors on effector cells or the specificity for an antigen that is found also on normal cells (Yu et al., 2020, Vidarsson et al., 2014).

Additionally, antibody constructs capable of recognizing more than one antigen have emerged as attractive therapeutic agents (figure 4B). Bispecific antibodies (BsAbs) are fusion proteins combining the antigen binding sites of two different antibodies in one molecule (Ma et al., 2021, Kontermann and Brinkmann, 2015). Particularly promising is the combination of the specificity for a tumor-expressed antigen with the specificity for a stimulatory receptor expressed on immune cells, such as CD3 on T cells. This enables BsAbs also to engage T cells, which do not express FcRs and thus do not recognize target cell-bound, conventionally structured antibodies (Staerz et al., 1985). Furthermore, combining the specificity for a broadly expressed antigen and the specificity for an antigen with a target cell-restricted expression pattern in a BsAb molecule may hold the potential to achieve enhanced binding selectivity to target cells and thus reduce on-target toxicity (Mazor et al., 2015). Since the first description of BsAbs in the 1960s, a broad spectrum of molecular platforms for their generation has been developed. These include for instance trifunctional antibodies, which comprise a functional Fc fragment and two different pairs of antibody HCs and LCs, each pair specific for an individual antigen (figure 4B). Moreover, numerous different antibody formats of non-lgG-like BsAbs lacking a functional Fc fragment have been developed. Fab domains or single-chain fragments variable (scFv), which consist of V<sub>H</sub> and V<sub>L</sub> domains linked by a short linker peptide, were used as binding domains (figure 4B) (Ma et al., 2021, Kellner et al., 2011, Kontermann and Brinkmann, 2015). A prominent example is the bispecific T-cell engager (BiTE) molecule blinatumomab, which is clinically applied in the therapy of B-cell precursor acute lymphoblastic leukemia (BCP-ALL) (Kantarjian et al., 2017). Blinatumomab consists of two peptide-linked scFvs, one targeting the T cell co-receptor CD3 and the other one CD19, which is found on B cells and B cell-derived lymphomas and leukemias. Blinatumomab thus brings T cells and target cells in close proximity, activates T cells and facilitates a T cell response against CD19-expressing tumor cells. This occurs irrespective of the recognition of antigens presented on human leukocyte antigen (HLA) molecules, which usually is necessary for T cell activation. Additionally, the small molecular weight of BiTEs of approximately only 55 kDa, compared to IgG molecules, which have a molecular weight of about 150 kDa, may contribute to improved penetration into cancerous tissue (Portell et al., 2013, Kontermann and Brinkmann, 2015).

Another promising approach is to engage antibodies or antibody fragments as vectors to precisely direct cytotoxic cargoes to malignant cells (figure 4C). Such therapeutic molecules commonly consist of a tumor-antigen-specific antibody, mostly of the IgG1 subclass due to its long serum half-life, covalently bound to a cytotoxic agent via a cleavable or a non-cleavable linker (Shastry et al., 2023, Fu et al., 2022). The toxic payload can be a chemotherapeutic agent, such as a microtubule inhibitor, a topoisomerase inhibitor or a mediator of DNA damage in antibody-drug conjugates (ADC), but also antibody-radionuclide conjugates (ARC) bearing a radioactive agent were developed (figure 4C) (Shastry et al., 2023, Steiner and Neri, 2011, Jin et al., 2022). An additional format are immunotoxins, which consist of an antibody domain fused to a protein toxin. An example is moxetumomab pasudotox, a fusion molecule of a CD22-specific variable fragment and *Pseudomonas* exotoxin A (Havaei et al., 2021).

Furthermore, fragments of antibody molecules can be used for the generation of genetically engineered CARs to enable lymphocytes, usually T cells, to recognize and eliminate target cells, which display a specific antigen (figure 4D) (Sterner and Sterner, 2021). CARs are modular receptors that consist of an extracellular antigen binding domain, classically an scFv specific for a cancer cell-expressed antigen, a hinge region, a transmembrane domain and one or more intracellular signaling domains (Sterner and Sterner, 2021). When T cells are genetically modified to carry CARs, the receptors enable the recognition of malignant cells and the subsequent activation of the T cells in a HLA-independent manner. Recently, CD19-specific CARs have demonstrated remarkable efficacy in relapsed and refractory B-lineage acute lymphoblastic leukemias (B-ALL) and B-NHLs (June and Sadelain, 2018, Brudno and Kochenderfer, 2018, Turtle et al., 2016). Moreover, CD22- and B-cell maturation antigen (BCMA)-directed CARs were effective in patients with refractory B-ALL and multiple myeloma, respectively (Fry et al., 2018, Brudno et al., 2018, Cohen et al., 2019).

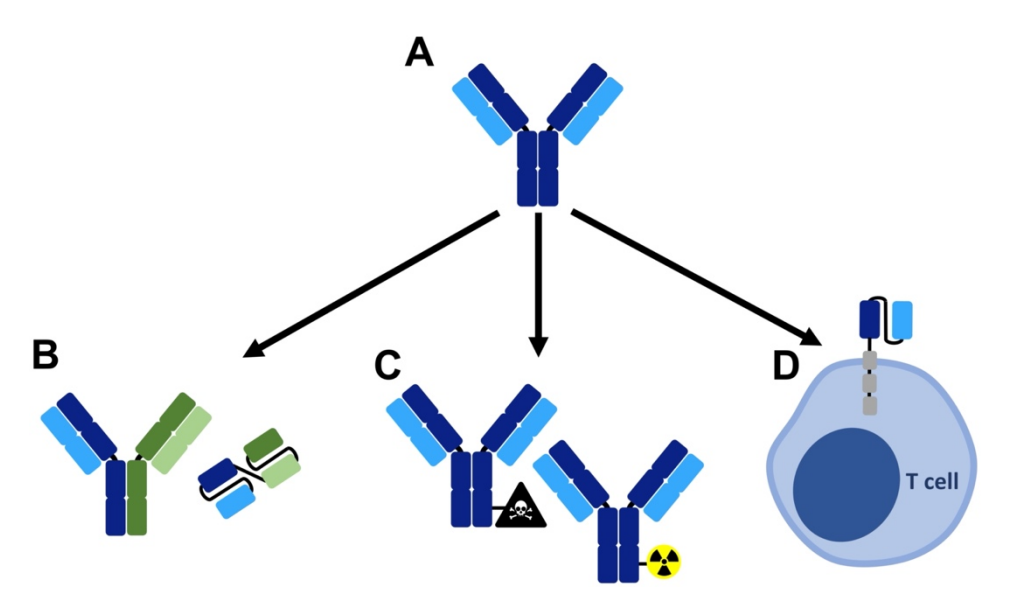


Figure 4: Examples of formats of therapeutic antibodies or antibody-constructs. (A) Numerous novel formats of therapeutic antibodies or antibody-constructs have emerged on the base of native antibody molecules. (B) Bispecific antibodies or antibody-constructs possess the ability to selectively bind two different antigens. They can be designed in an IgG-like format bearing an Fc-fragment (*left*) or as non-IgG-like fusion molecules containing single-chain fragments variable (scFv; *right*). (C) Antibodies can be employed as vehicles to precisely deliver cytotoxic payloads, such as drugs or radionuclides. (D) In T cell engineering, scFvs can be employed to generate the extracellular antigen recognition domain of chimeric antigen receptors (CAR) to allow T cells to recognize and kill cancer cells.

## 1.1.3 Effector Functions of Therapeutic Antibodies

Antibodies mediate their therapeutic effect through a diverse range of effector mechanisms. A general distinction can be made between direct effector functions, which only result from the interaction of the antibody with its epitope (figure 5), and indirect effector functions, such as the recruitment of effector cells or the complement system, which also involve the Fc domain (figure 6). Differences in the effector functions of different therapeutic antibodies not only result from their individual epitopes, but also depend on the antibody isotype, format and molecular modifications, such as Fc engineering to modulate the affinity for FcRs or complement factors (Redman et al., 2015, Weiner, 2015, Chan and Carter, 2010).

#### 1.1.3.1 Direct Effector Functions

Direct effector functions of therapeutic antibodies result from the interaction of the Fab domain with the antigen, which can either be membrane-bound or soluble. Antibodies or antibody fragments targeting soluble molecules can impede ligands, such as cytokines, from activating their cognate receptors (figure 5A). For instance, antibodies specific for the pro-inflammatory cytokine TNF- $\alpha$  such as adalimumab, golimumab or infliximab are clinically applied in the treatment of autoimmune diseases and chronic inflammatory bowel disease (Chan and Carter, 2010). On the other side, antibody blockade of cell

surface receptors or the competition for receptor binding between therapeutic antibodies and ligands can prevent receptor activation and thus disrupt signaling (figure 5B). In cancer immunotherapy, antibodies specific for cancer cell-expressed members of the ErbB receptor family such as the anti-HER2 antibody trastuzumab or the anti-EGFR antibodies cetuximab and panitumumab prevent receptor dimerization, disrupt proliferative signaling and thus induce cell cycle arrest or apoptosis (Harries and Smith, 2002, Martinelli et al., 2009). Impressive results were also achieved with therapeutic antibodies that abrogate co-inhibitory signaling in immune effector cells. Abrogation of the signaling of such receptors, which under physiological conditions contribute to the regulation of immune responses, can be exploited to initiate or modulate anti-cancer immunity (figure 5C). Particularly in malignant melanoma, blockade of inhibitory receptors in T cells by the anti-cytotoxic T-lymphocyte-associated protein 4 (CTLA-4) antibody ipilimumab or the anti-programmed cell death protein 1 (PD-1) antibody nivolumab is applied with great clinical success (Buchbinder and Desai, 2016). In contrast, binding of cell surface receptors such as HLA class II or Fas receptor (FasR) by therapeutic antibodies can also directly facilitate the activation of signaling cascades, leading to cell cycle arrest or apoptosis (figure 5D) (Dechant et al., 2003, Trauth et al., 1989). Furthermore, antibody binding of receptors or their ligands can result in receptor internalization or downregulation of cell surface expression and thus modulate the displayed amount of binding sites for a ligand, which is available for cellular activation (figure 5E) (Redman et al., 2015). The internalization of cell surface molecules upon antibody binding can additionally be harnessed to deliver cytotoxic or cytostatic agents intracellularly (figure 5F). Examples for this strategy are the above-mentioned ADCs, such as polatuzumab vedotin used in the treatment of lymphomas. It consists of the antimitotic agent monomethyl auristatin E (MMAE) linked to a monoclonal, recombinant, humanized IgG1 antibody specific for CD79b, a component of the B cell receptor. Upon target ligation, the molecule is internalized, the linker domain between the antibody and MMAE is cleaved by intracellular proteases and MMAE unfolds its anti-mitotic effect by interfering with the polymerization of tubulin (Dornan et al., 2009, Tilly et al., 2022).

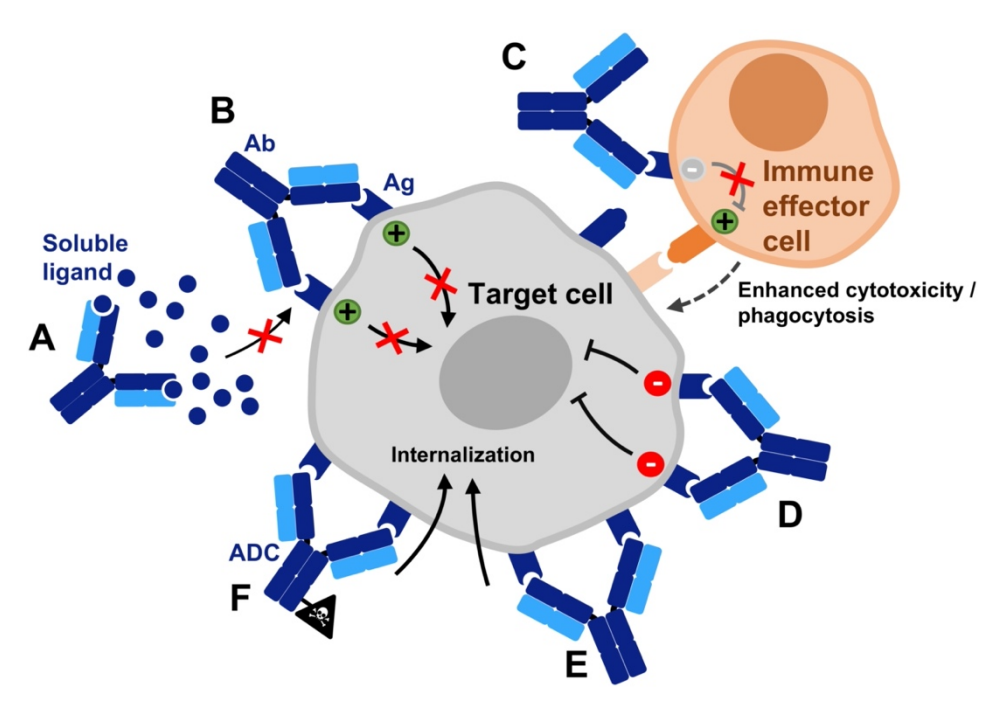
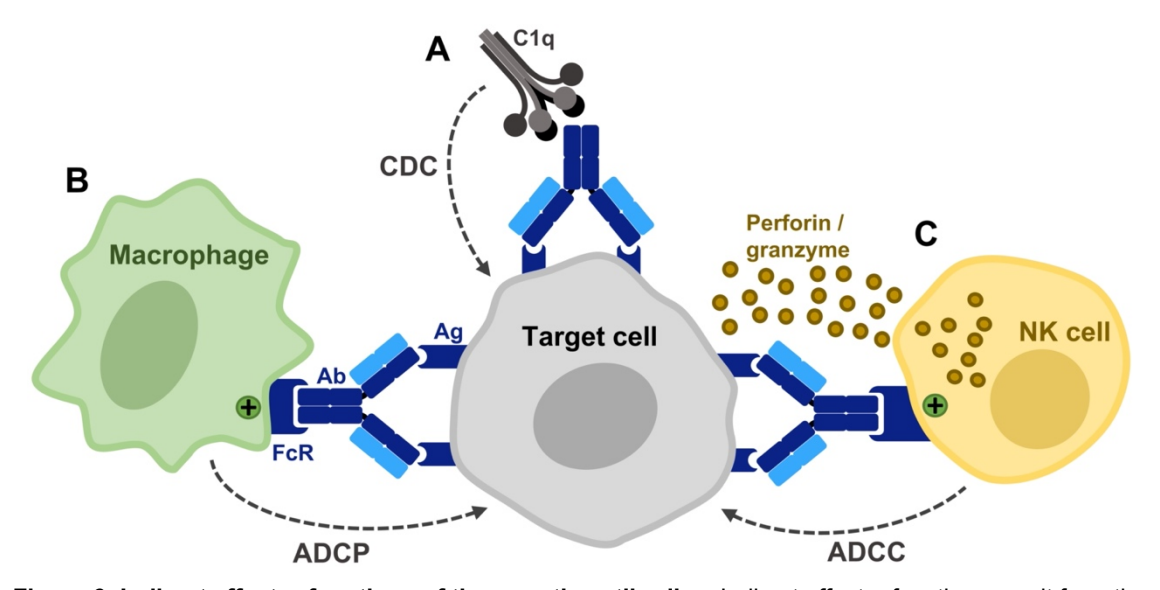


Figure 5: Direct effector functions of therapeutic antibodies. Direct effector functions result from the interaction of the antibody (Ab) Fab fragment with the antigen (Ag). (A) Antibodies can neutralize soluble ligands and thus prevent the activation of their cognate receptor. (B) Competitive binding of antibodies and cell-bound or soluble ligands to receptors can impede receptor activation. (C) Antibodies can abrogate inhibitory interactions between cells. The antibody blockade of co-inhibitory receptors in immune effector cells can enhance anti-tumor effector functions, such as cytotoxicity or phagocytosis. (D) Antibody binding of inhibitory receptors can activate suppressive intracellular downstream signaling cascades, resulting in cell cycle arrest or apoptosis. (E) Receptor ligation by antibodies can result in receptor internalization and thus modulate the amount of displayed binding sites for ligands. (F) Antibody-drug-conjugates (ADC) carrying toxic payloads, such as cytostatic drugs, can directly mediate cytotoxicity upon internalization.

#### 1.1.3.2 Indirect Effector Functions

In addition to effects mediated directly through antibody ligation of its epitope, therapeutic antibodies can activate components of the immune system. Such therapeutic effects, referred to as indirect effector functions, are conveyed through the interplay between the Fc fragment and effector cells or the complement system (figure 6).

Via the classical activation pathway of the complement system, binding of the C1q subunit of the complement complex C1 to the Fc fragment of cell-associated antibodies can result in the cleavage of the complement factors C2 and C4, leading to the formation of a membrane attack complex (MAC) and the lysis of the antibody-bound cell. This effector mechanism is referred to as complement-dependent cytotoxicity (CDC; figure 6A) (Dunkelberger and Song, 2010). Furthermore, the deposition of complement fragments such as the opsonin C3b on the cell surface provides an activating signal for immune effector cells and thus enables the elimination of target cells through complement-dependent cell-mediated phagocytosis (CDCP) by neutrophil granulocytes and macrophages (Vandendriessche et al., 2021) or complement-dependent cell-mediated cytotoxicity (CDCC) by NK cells and T cells (Lee et al., 2017). Cell surface-bound therapeutic antibodies are also capable of recruiting and activating immune effector cells. Through the engagement of FcRs on monocytes and macrophages, antibodies specific for a tumor-expressed antigen provide an activating signal to induce antibody-dependent cellular phagocytosis (ADCP) of malignant cells (figure 6B). Remarkably, the anti-cancer effect of an Fc-engineered CD19 antibody was abrogated upon the depletion of macrophages in a murine xenograft model of BCP-ALL, highlighting the importance of this effector mechanism during antibody treatment (Schewe et al., 2017). Expression of FcRs is not only found in macrophages, but also in other populations of immune effector cells, including natural killer (NK) cells and neutrophil granulocytes (Peipp et al., 2022, Behrens et al., 2023). NK cell recruitment and activation through FcR-engagement by cancer cell-bound therapeutic antibodies can result in the release of perforin and granzyme-containing lytic granula and thus facilitate the lysis of cancer cells, referred to as antibody-dependent cell-mediated cytotoxicity (ADCC; figure 6C) (Peipp et al., 2022). In neutrophil granulocytes, recognition of cancer cell-bound antibodies through FcRs promotes the formation of a cytotoxic synapse leading to cancer cell elimination through trogoptosis, as well as the initiation of apoptosis in malignant cells, for instance via the Fas-Fas-ligand pathway or via the ligation of death receptors by TNF-related apoptosis-inducing ligand (TRAIL) (Behrens et al., 2023).



**Figure 6: Indirect effector functions of therapeutic antibodies.** Indirect effector functions result from the interaction of the antibody (Ab) Fc domain with activating Fc receptors (FcR) on immune effector cells or the complement system. Ligation of the complement component 1q (C1q) can initiate the classical complement cascade and elimination of the target cell by complement-dependent cytotoxicity (CDC; (A)). The recognition of target cell-bound antibodies by immune effector cells through FcRs can result in effector cell activation and thus mediate antibody-dependent cellular phagocytosis (ADCP; (B)) by macrophages or antibody-dependent cell-mediated cytotoxicity (ADCC; (C)) by NK cells.

## 1.1.4 Immune Effector Cells for Therapeutic Antibodies

Numerous animal experiments identified the FcR-mediated recruitment and activation of immune effector cells to be a particularly important effector function of many therapeutic antibodies (Clynes et al., 2000, Weiskopf and Weissman, 2015, Wang et al., 2015, de Haij et al., 2010). In addition, observations from clinical studies clearly identified FcRengagement on immune effector cells to be critically involved in the response to treatment with therapeutic antibodies (Cartron et al., 2002, Weng and Levy, 2003). A range of FcRs for the different antibody isotypes exists in humans. FcRs differ in their expression pattern on immune cells, in the signaling pathways they induce, as well as in their affinity to the Fc fragment. For IgG, the repertoire expressed by effector cells includes the four activating FcyRs FcyRI (CD64), FcyRIIA (CD32a), FcyRIIC (CD32c) and FcyRIIIA (CD16a), the inhibitory receptor FcyRIIB (CD32b), and FcyRIIIB (CD16b) with a still unclear role (table 1). FcyRs belong to the Ig superfamily. Activating FcyRs are either composed of an α chain for Fc-binding and a γ chain dimer, which mediates signal-transduction (FcyRI, FcyRIIIA), or consist of a single α chain (FcyRIIA, FcyRIIC). They transduce activating signaling via immunoreceptor tyrosine-based activating motifs (ITAM). The inhibitory FcyRIIB comprises a single α chain and contains immunoreceptor tyrosine-based inhibitory motifs (ITIM) in its cytoplasmic domain (Ben Mkaddem et al., 2019, Nimmerjahn and Ravetch, 2008). FcyRIIIB has no intracellular domain and is linked to the cell membrane via a glycosyl-phosphatidylinositol (GPI) anchor. Only FcyRI binds Fc fragments with a high affinity, the affinity of all other FcyRs is lower (Nimmerjahn and Ravetch, 2008). Except for FcyRI, which is capable of binding monomeric IgG molecules due to an additional Ig-like portion in its extracellular domain, activation of all FcyRs requires the interaction with multiple IgG molecules within an immune complex (Harrison et al., 1994). In contrast to the broad spectrum of FcyRs, in humans only one FcR specific for the IgA Fc fragment is known (FcaRI / CD89) (Leusen, 2015).

Table 1: Human FcyRs.1

	Activating					Inhibitory
Name	FcγRI (CD64)	FcγRIIA (CD32a)	FcγRIIC (CD32c)	FcγRIIIA (CD16a)	FcγRIIIB (CD16b)	FcγRIIB (CD32b)
Affinity	High			Low to mediur	n	
Structure	Ligand- binding α chain and signal- transducing, ITAM-bearing γ chain-dimer	Single ITAM- bearing α chain	Single ITAM- bearing α chain	Ligand- binding α chain and signal- transducing, ITAM-bearing γ chain-dimer	Single glycosyl- phosphatidylinositol (GPI)-anchored α chain	Single ITAM- bearing α chain
Alleles	-	FcyRIIA <sup>131H</sup> FcyRIIA <sup>131R</sup>	-	FcγRIIIA <sup>158V</sup> FcγRIIIA <sup>158F</sup>	Neutrophil specific antigen (NA) 1, NA2	FcγRIIB <sup>232I</sup> FcγRIIB <sup>232T</sup>
Expression pattern	Monocytes, macrophages, neutrophils (inducible), mast cells (inducible), dendritic cells (DC)	Monocytes, macrophges, neutrophils, basophils, eosinophils, thromobocytes, DCs, CD4+ T cells (inducible)	Monocytes, macrophages, neutrophils, NK cells	Monocytes, macrophages, NK cells, γδ T cells	Neutrophils, basophils	Monocytes, macrophages, neutrophils, basophils DC, B cells, CD4+ T cells (inducible)

<sup>&</sup>lt;sup>1</sup> Modified from Nimmerjahn and Ravetch, 2008, and Ben Mkaddem et al., 2019.

#### 1.1.4.1 NK Cells

NK cells are cytotoxic lymphocytes of the innate immune system and contribute to the immunosurveillance of cancer (Morvan and Lanier, 2016). They lack antigen-specific receptors. Instead, a complex interplay of stimulating and inhibitory receptors allows them to distinguish between normal tissue and malignant or virus-infected cells. Activating NK cell receptors, such as natural killer group 2 member D (NKG2D), recognize germline-encoded, stress-inducible signal molecules expressed by malignant or virusinfected cells and, upon ligation, facilitate target cell lysis (Peipp et al., 2022). Inhibitory receptors, such as the HLA class I receptors killer cell immunoglobulin-like receptors (KIR) and the inhibitory subfamily B of leukocyte immunoglobulin-like receptors (LIR) sense the absence of constitutively expressed self molecules. The loss of self molecules, in particular HLA class I molecules, leads to diminished inhibitory signaling and reduces the NK cell activation threshold. This concept is also referred to as the 'missing self' hypothesis (Vivier et al., 2008, Ljunggren and Karre, 1990). Furthermore, CD56dim NK cells, the most abundant subtype of NK cells in the peripheral blood, carry FcyRIIIA, which allows them to detect antibody-coated target cells. Thus, they represent important effector cells in antibody-based cancer immunotherapies through mediating ADCC. In regard of the low affinity of FcyRIIIA to the antibody Fc domain, strategies to improve NK cell-mediated lysis of cancer cells include antibody Fc engineering to increase the Fc domains' affinity for FcyRIIIA, as for example in obinutuzumab, an Fc-glyco-engineered antibody specific for CD20, or bispecific antibodies bearing high affinity, FcγRIIIA-engaging Fab or scFv domains (Peipp et al., 2022).

## 1.1.4.2 T Cells

T cells are part of the adaptive immune system. They recognize foreign antigens and contribute to the generation and maintenance of immunologic memory for immune surveillance in infections and cancer. Thus, T cells are key effectors of adaptive cellmediated immunity (Raskov et al., 2021). To discriminate between normal cells and abnormal, virus-infected or malignant cells, CD8<sup>+</sup> T cells express T cell receptors (TCR). TCRs recognize peptides derived from cytoplasmic proteins degraded by the proteasome, which are presented by HLA class I molecules (Raskov et al., 2021). Upon TCRmediated recognition of a specific antigen and the presence of a co-stimulatory signal through the engagement of T cell-expressed CD28, activated CD8<sup>+</sup> T cells eliminate target cells through the formation of pores in the target cell membrane followed by the release of toxic granules containing granzymes, perforin, cathepsin C and granulysin, as well as the ingestion of granulysin, perforin and granzymes by target cells through endocytosis of cytotoxic T cell membranes. Additionally, CD8<sup>+</sup> T cells can trigger apoptosis by the expression of Fas-ligand for activation of the death receptor Fas in target cells (Raskov et al., 2021). Except for specific subsets, T cells do not carry FcyRs (Sandor and Lynch, 1993). Thus, T cells do not eliminate cancer cells through the recognition of cancer cell-bound therapeutic antibodies. Instead, targeting inhibitory T cell receptors such as PD-1 or its ligand (programmed cell death ligand 1, PD-L1), which mediate immune tolerance in T cells under physiological conditions, has been pursued with great success (Sharpe and Pauken, 2018, Robert et al., 2015, Motzer et al., 2015, Ansell, 2021). As mentioned above, other approaches to achieve T cell cytotoxicity in an HLA-independent manner include BsAbs bearing specificity for CD3 and a cancer cellexpressed antigen or the genetic modification of T cells to display antigen-specific CARs.

## 1.1.4.3 Neutrophil Granulocytes

Neutrophil granulocytes account for 50 – 70% of the circulating leukocytes and thus represent the major type of immune cell in humans. They are a component of the innate immune system and are critically involved especially in the initial immune reaction to bacterial and fungal infections (Behrens et al., 2023). Upon interaction with different pathogen-associated molecular patterns (PAMP) via pattern-recognition receptors (PRR) such as Toll-like receptors (TLR), they exert a broad variety of effector functions including degranulation and the release of toxic enzymes such as myeloperoxidase (MPO), the release of reactive oxygen species (ROS), the formation of neutrophil

extracellular traps (NET), trogocytosis, as well as phagocytosis. Particularly upon activation, neutrophil granulocytes express activating FcγRI and FcγRIIA (Wang and Jonsson, 2019). Thus, neutrophils have been demonstrated to function as effector cells in antibody-based cancer immunotherapies through neutrophil-mediated ADCC (Behrens et al., 2023, Burn et al., 2021). In humans, neutrophil granulocytes also express the GPI-anchored FcγRIIIB, which lacks an intracellular signaling domain and was suggested to function as a decoy receptor. The display of FcγRIIIB, as well as the expression of the inhibitory FcγRIIB in neutrophil granulocytes limits the potential of IgG-mediated ADCC (Chan et al., 2022, Treffers et al., 2018). However, neutrophil granulocytes express FcαRI, which enables them to interact with complexes of IgA. Interestingly, compared to IgG, therapeutic IgA molecules were demonstrated to induce more robust activation and stronger ITAM signaling in neutrophil granulocytes and thus may display an attractive alternative antibody isotype to optimize the involvement of neutrophil granulocytes during cancer immunotherapy (Chan et al., 2022).

## 1.1.4.4 Monocytes and Macrophages

Monocytes, together with macrophages and dendritic cells (DC), form the mononuclear phagocyte system. They make up 4-8 % of the peripheral blood leukocytes and possess the ability to differentiate into macrophages or DCs. Furthermore, monocytes express Fc $\gamma$ Rs and thus mediate effector functions such as ADCC and ADCP (Jakubzick et al., 2017).

Macrophages are mononuclear leukocytes with a wide distribution in lymphoid and non-lymphoid tissues. They are an essential element of innate immunity and critically contribute to the development, homeostasis and repair of tissues, as well as to inflammation and immune responses in infections and cancer (Wynn et al., 2013, Mantovani et al., 2022).

The extent of anatomical and functional plasticity of macrophages is unique among the hematopoietic system. Microenvironmental signals such as cytokines, microbial products, as well as autocrine and paracrine signaling profoundly influence the function of macrophages and facilitate their differentiation towards distinct phenotypes (Wynn et al., 2013). Particularly the exposure to either interferon (IFN)-γ, a cytokine secreted by T helper (Th) 1 cells or interleukin (IL)-4 released by Th2 cells influences the polarization of macrophages (Mills et al., 2000). Besides cytokines, TLR-engagement on macrophages by damage-associated molecular patterns (DAMP) or PAMPs as, for instance, the bacterial membrane component lipopolysaccharide (LPS) have significant impact on their state of polarization. Mirroring the nomenclature of the dichotomous

subdivision of Th cells into Th1 and Th2 cells, macrophages were roughly categorized into two subtypes according to their functional polarization. Differentially polarized macrophages differ in their expression of receptors, their production of cytokines, their effector functions and the chemokines they release (Mantovani et al., 2004). The presence of IFN-y and LPS facilitates differentiation towards the phenotype of classically activated, pro-inflammatory M1 macrophages. M1 macrophages are characterized by a high capacity of antigen presentation, enhanced pathogen killing abilities and elevated expression levels of CD80 and CD86, which bind CD28 and CTLA-4 on T cells and support the stimulation of T cell responses. M1 macrophages furthermore produce toxic intermediates such as ROS and release high levels of pro-inflammatory cytokines, including IL-12, IL-23 and TNF-α (Mantovani et al., 2004). In contrast, exposure in particular to IL-4 and IL-13 results in macrophage polarization towards an alternatively activated, anti-inflammatory M2 phenotype. M2 macrophages are defined by enhanced phagocytic capacity and display higher levels of CD163, a scavenger receptor specific for haptoglobin-hemoglobin-complexes. They release vascular endothelial growth factor (VEGF) and anti-inflammatory cytokines such as IL-10 and transforming growth factor (TGF)-β. M2 macrophages thus critically facilitate neoangiogenesis, cancer progression and the generation of an immunosuppressive milieu within the tumor microenvironment (TME) (Mantovani et al., 2004, Roszer, 2015, Mantovani et al., 2022). Yet, the presence of a broad spectrum of different microenvironmental signals leads to the acquisition of an M2 phenotype with high phenotypic heterogeneity and different functional properties. To take account of the different stimuli, the classification was subsequently expanded by categorizing M2 macrophages into M2a (stimuli: IL-4 + IL-13), M2b (immune complexes + TLR agonists), M2c (IL-10) and M2d (IL-6) subtypes (Mantovani et al., 2004, Hourani et al., 2021). However, macrophages are capable of high plasticity. Thus, M1 and M2 macrophages only represent the two extremes of a spectrum of macrophage activation with the possibility of intermediate subsets of phenotypes (Hourani et al., 2021). In cancer, macrophages play a dichotomous role. They are present at all stages of cancer development and progression (Nielsen and Schmid, 2017). Besides genetic alterations that lead to the activation of oncogenes or the inactivation of tumor-suppressor genes, inflammation substantially contributes to the malignant degeneration of cells and tumor progression (Coussens and Werb, 2002). In immunologically 'hot' tumors, which are characterized by pronounced infiltration by inflammatory cells such as macrophages, enhanced anti-tumor immune responses are observed. However, continually over-activated, inflammatory M1 macrophages contribute to the establishment and maintenance of 'smoldering' inflammation through the release of inflammatory cytokines (Balkwill and

Mantovani, 2001, Mantovani et al., 2008). Such chronic inflammation conversely promotes tumor development and progression. Progressive proliferation of tumors gives rise to the establishment of a TME, in which various cues such as the cytokine spectrum and interactions with tumor cells or the extracellular matrix facilitate the phenotype and functions of macrophages to markedly change from an immunologically active M1 state towards an anti-inflammatory M2-like phenotype. Such pro-tumorigenic tumorassociated macrophages (TAM) are among the most abundant cells within the TME and can ultimately account for almost 50% of the tumor mass in solid tumors. They contribute critically to the formation of an immunosuppressive environment and promote angiogenesis, proliferation, tissue invasion and metastasis (Qian and Pollard, 2010, Nielsen and Schmid, 2017). Consequently, it is not surprising that pronounced presence of TAMs is associated with a poor outcome in various cancer entities including Hodgkin's lymphoma, esophageal cancer and breast cancer (Steidl et al., 2010, Yagi et al., 2019, Larionova et al., 2020). However, there are exceptions and some studies also report a favorable role of macrophage infiltration, for instance in colon cancer (Larionova et al., 2020).

In contrast to their substantial role in cancer development and progression, numerous observations suggested macrophages to also be key effector cells for therapeutic antibodies such as rituximab (Marshall et al., 2017, Wynn et al., 2013, Feng et al., 2019, Uchida et al., 2004, Gong et al., 2005). Human macrophages express all three activating FcyRs and are capable of eliminating malignant cells directly through ADCP and ADCC during antibody therapy. Additionally, macrophages are antigen presenting cells (APC) and may thus even promote adaptive anti-cancer immunity by presenting cancer antigens to T cells (Gul and van Egmond, 2015, Feng et al., 2019). Of note, studies in B-NHL patients demonstrated a positive correlation between high contents of TAMs and improved survival when patients received treatment with rituximab. Thus, in these patients treatment with rituximab reversed the association between a high frequency of TAMs and adverse outcome (Canioni et al., 2008, Taskinen et al., 2007, Riihijarvi et al., 2015). Also, certain chemotherapeutic agents may hold the potential to further promote macrophage-mediated effector functions during antibody therapies. For instance, in a mouse model of BCP-ALL, cyclophosphamide enhanced the macrophage phagocytosis of leukemia cells by the CD52 antibody alemtuzumab (Pallasch et al., 2014).

## 1.2 Strategies to Improve Macrophage ADCP of Cancer Cells

Antibody-based therapies have fundamentally improved the treatment options in many cancer entities (Carter and Lazar, 2018). However, not all patients benefit and relapsed or refractory disease remains challenging. In consideration of the important role of macrophages, different approaches were pursued to optimize their recruitment and ADCP function. Particularly promising are strategies that aim to increase the antibody's affinity for activating FcγRs through antibody Fc engineering or the blockade of inhibitory receptors, which impede FcγR-mediated effector cell activation (Kellner et al., 2017, Feng et al., 2019).

### 1.2.1 Antibody Fc Engineering

Fc-mediated, indirect effector functions, such as ADCC, CDC and ADCP have been shown to be important effector mechanisms in antibody-based cancer immunotherapies (Kellner et al., 2017, Rogers et al., 2014, Schewe et al., 2017). Deeper insights into the mechanisms of action of therapeutic antibodies have laid the foundation for different strategies to modulate antibody effector functions by specific modifications of the Fc fragment. These approaches include the already mentioned modification of the Fc-linked glycan (Fc glyco-engineering), as well as modification of the amino acid sequence (Fc protein-engineering) (Kellner et al., 2017). Fc protein-engineering can be applied to enhance the affinity for activating FcyRs and thus improve the recruitment and activation of effector cells. For instance, modifying the C<sub>H</sub>2 domains of the tumor targeting antibodies trastuzumab or rituximab with the amino acid exchanges S239D and I332E augmented the antibodies' affinities for FcyRIIIA and FcyRIIA and thus enhanced ADCP of cancer cells relative to the corresponding native antibodies (Lazar et al., 2006). Remarkably, a surrogate of the Fc-engineered CD19 antibody tafasitamab was more effective in promoting ADCP than its non-engineered counterpart and prolonged survival in patient-derived xenograft models of pediatric BCP-ALL (Schewe et al., 2017). In contrast, genetic modification of the antibody Fc fragment also enables the generation of antibodies showing no detectable interaction with FcyRs or complement factors. Clinically, such non-immunostimulatory, Fc-silent antibodies may hold the potential to minimize on-target side effects as they avoid the activation of immune effector cells through FcyR-Fc interactions and provide pure receptor blockade, as desired for instance in the inhibition of immune checkpoints expressed on immune cells (Vafa et al., 2014, Tam et al., 2017).

### 1.2.2 Phagocytosis Checkpoints

Another attractive emerging approach to enhance ADCP of cancer cells by macrophages is the antibody masking of inhibitory checkpoints that hamper immune cell activation through FcγR-engagement. The phagocytosis of cancer cells is controlled by a complex interplay of activating and inhibitory signaling axes, which may represent viable targets for antibody therapeutics (Liu et al., 2023b).

Among the myeloid inhibitory receptors, signal regulatory protein (SIRP)  $\alpha$  is particularly well characterized. Upon recognition of its ligand CD47, a 'Don't Eat Me!' signal with a ubiquitous expression pattern in humans, SIRPα transduces an inhibitory signal in macrophages via the phosphorylation of intracellular ITIMs and, as a consequence, strongly hampers the phagocytosis of cancer cells (Barclay and Van den Berg, 2014). Thus, SIRPα signaling attenuates the efficacy of cancer cell-bound therapeutic antibodies to induce phagocytosis through the engagement of FcyRs on macrophages. Furthermore, elevated expression of CD47 is frequently found in a variety of cancers, rendering the CD47:SIRPα axis a potential immune escape mechanism. Antibodies masking either CD47 or SIRPα notably promoted macrophage phagocytosis in vitro and in tumor xenograft models (Barclay and Van den Berg, 2014, Logtenberg et al., 2020). For instance, under rituximab therapy, co-treatment with CD47-blocking antibodies promoted the uptake of lymphoma cells by macrophages in vitro and the antibody combination was effective in murine B-NHL models (Chao et al., 2010). Furthermore, concomitant treatment with the CD38 antibody daratumumab and CD47 inhibition was efficient in patient-derived xenograft models of T cell acute lymphoblastic leukemia (T-ALL) (Muller et al., 2022). Currently, various formats of therapeutic agents including monoclonal antibodies targeting CD47 or SIRPα, SIRPα-Fc fusion proteins and small molecule inhibitors are evaluated pre-clinically or clinically (Logtenberg et al., 2020, Yu et al., 2021, Sikic et al., 2019, Yang et al., 2021, Yu et al., 2022). In B-NHL patients, impressive effects were achieved when the CD47-directed IgG4 antibody magrolimab was combined with rituximab in a clinical phase lb study. In this study, 50% of the patients responded to the treatment combination and 36% of the patients experienced a complete response despite the inclusion only of patients that had relapsed or were refractory to at least two previous lines of therapy (Advani et al., 2018).

Emerging evidence indicates that also the PD-L1:PD-1 axis contributes to the regulation of macrophages. Expression of PD-1 was found especially in TAMs and was associated with reduced phagocytic capacity *in vivo*. Of note, the reduction of tumor growth achieved by anti-PD-1 antibodies or a PD-L1-blocking soluble fragment of the PD-1 ectodomain was abrogated by the depletion of TAMs in a xenograft model of colon cancer in mice

(Gordon et al., 2017). This finding highlights the critical contribution of macrophages to the therapeutic effect during inhibition of the PD-L1:PD-1 axis.

Sialic acid-binding Ig-like lectin (Siglec)-10 is another ITIM-bearing myeloid inhibitory receptor, which has gained increasing attention as a phagocytosis checkpoint. Expression of its ligand CD24, a sialylated cell surface antigen for which elevated expression levels are found in many cancer entities, has been shown to mediate protection from macrophage phagocytosis in malignant cells. Thus, monoclonal CD24 antibodies significantly promoted the clearance of mantle cell lymphoma (MCL) cells *in vitro* and of breast cancer cells *in vivo* by macrophages (Freile et al., 2022, Barkal et al., 2019).

The number of identified potential immune checkpoints in macrophages is steadily increasing. Recent findings imply that LIRs also may play an important role.

# 1.3 Leukocyte Immunoglobulin-Like Receptors as Targets for Immune Checkpoint Blockade

LIRs are a heterogeneous family of activating or inhibitory receptors expressed by a wide variety of immune and non-immune cells. The two best characterized LIRs, leukocyte immunoglobulin-like receptor subfamily B member 1 (LILRB1) and LILRB2 are inhibitory receptors for classical and non-classical HLA class I molecules. Both LILRB1 and LILRB2 have recently gained attention as promising potential target antigens for cancer immunotherapy (Zeller et al., 2023b, Chen et al., 2018).

LILRB1, also referred to as Ig-like transcript (ILT) 2, monocyte / macrophage Ig-like receptor (MIR) 7 or CD85j, is the most widely expressed LIR. LILRB1 is found on monocytes, macrophages, DCs, granulocytes, mast cell progenitors, osteoclast precursors, B cells and subpopulations of T cells and NK cells (Colonna et al., 1997, Mori et al., 2008, Carenza et al., 2019, Lewis Marffy and McCarthy, 2020, Tedla et al., 2008, Lesport et al., 2011, Zeller et al., 2023b). The receptor contributes to the regulation of various immune functions, such as differentiation, proliferation, cytokine release, antigen presentation and antibody production (Colonna et al., 1997, De Louche and Roghanian, 2022, Tenca et al., 2005, Young et al., 2008, Merlo et al., 2005, Naji et al., 2014). Engagement of LILRB1 has been demonstrated to hamper the cytotoxicity of LILRB1-expressing NK cells and T cells (Colonna et al., 1997, De Louche and Roghanian, 2022). Importantly, more recently regulatory checkpoint functions in phagocytosis through the recognition of HLA class I molecules have been shown for LILRB1 (Feng et al., 2019, Barkal et al., 2018). Thus, the abrogation of LILRB1 signaling may hold the potential to stimulate both innate and adaptive immunity.

LILRB2, also termed ILT4, MIR10 and CD85d, is mainly expressed in myeloid cells. However, it is also found in other cell populations, such as osteoclasts and mast cell progenitors (van der Touw et al., 2017, Colonna et al., 1998, Tedla et al., 2008). Interestingly, LILRB2 has been demonstrated to also be displayed on hematopoietic stem cells (Zheng et al., 2012). For LILRB2, an important role in the polarization of macrophages has been shown (Chen et al., 2018).

Both LILRB1 and LILRB2 have been demonstrated to be involved in various conditions, such as infections, autoimmune diseases, as well as cancer (De Louche and Roghanian, 2022, Abdallah et al., 2021, Deng et al., 2021, Hudson and Allen, 2016, Naji et al., 2014, Monsivais-Urenda et al., 2013, Doniz-Padilla et al., 2011, Kuroki et al., 2005, Li et al., 2020, Alaoui et al., 2018, Tedla et al., 2011).

#### 1.3.1 Genetics, Structure and Signaling of LILRB1 and LILRB2

LILRB1 and LILRB2 are members of the LIR gene family, which contains eleven proteinencoding genes and two pseudo genes (De Louche and Roghanian, 2022, Abdallah et al., 2021, Liu et al., 2000, Storm et al., 2021). The genes are clustered on chromosome 19q13.4 in the leukocyte receptor complex (LRC) and are located closely to the genes of a number of related receptors, such as KIRs. LIRs are divided into two subfamilies with opposing signaling characteristics (Abdallah et al., 2021, van der Touw et al., 2017, Brown et al., 2004). Subfamily A comprises the five cell surface molecules LILRA1, LILRA2 and LILRA4-6, which associate with the ITAM-containing FcR y chain and exert activating functions, and the soluble protein LILRA3. The inhibitory subfamily B includes the five type I transmembrane proteins LILRB1-5. LILRB have two to four Ig-like domains that mediate ligand-binding in their extracellular portion and contain two to four ITIMs for signal-transduction in their intracellular portion (De Louche and Roghanian, 2022, van der Touw et al., 2017, Deng et al., 2021). Expression of LILRBs is found exclusively in primates and humans. However, orthologs are known in other species, such as the murine paired Ig-like receptor B (PirB) 18 and gp49B1 (Storm et al., 2021, Deng et al., 2021). As the structurally related KIRs, LILRB receptors are polymorphic, yet to a smaller degree. However, LILRB1 and LILRB2 show noticeable allelic diversity (Brown et al., 2004, Liu et al., 2022, Oliveira et al., 2022).

LILRB1 is a 650 amino acid glycoprotein with an apparent molecular weight of approximately 110 – 120 kDa that comprises four extracellular Ig-like domains and a cytoplasmic tail with four ITIM or ITIM-like sequences (figure 7) (Cosman et al., 1997). LILRB2, a 597 amino acid glycoprotein of approximately 95 kDa also comprises four extracellular Ig-like domains. However, in contrast to LILRB1, LILRB2 contains only three

ITIM sequences in its intracellular portion (figure 7) (Colonna et al., 1998). For both receptors, variants were described that differ in their length.

Both LILRB1 and LILRB2 exert their inhibitory functions by interfering with the activity of intracellular kinases. Thus, ligand-binding results in the phosphorylation of tyrosines within the ITIMs and recruitment of the phosphatase SRC-homology 2 domain-containing phosphatase (SHP)-1 (Colonna et al., 1997, Cosman et al., 1997, Fanger et al., 1998, Kang et al., 2016). Additionally, recruitment of SHP-2 has been reported (Ketroussi et al., 2011, Shao et al., 2018). The activated phosphatases dephosphorylate ITAMs, as for instance in the cytoplasmic portion of FcRs, and impede major kinases involved in immune cell activation, such as spleen tyrosine kinase (SYK), SRC, zeta-chain associated protein kinase 70-kDa and phosphatidylinositol-4-phosphate 3-kinase (Kang et al., 2016).

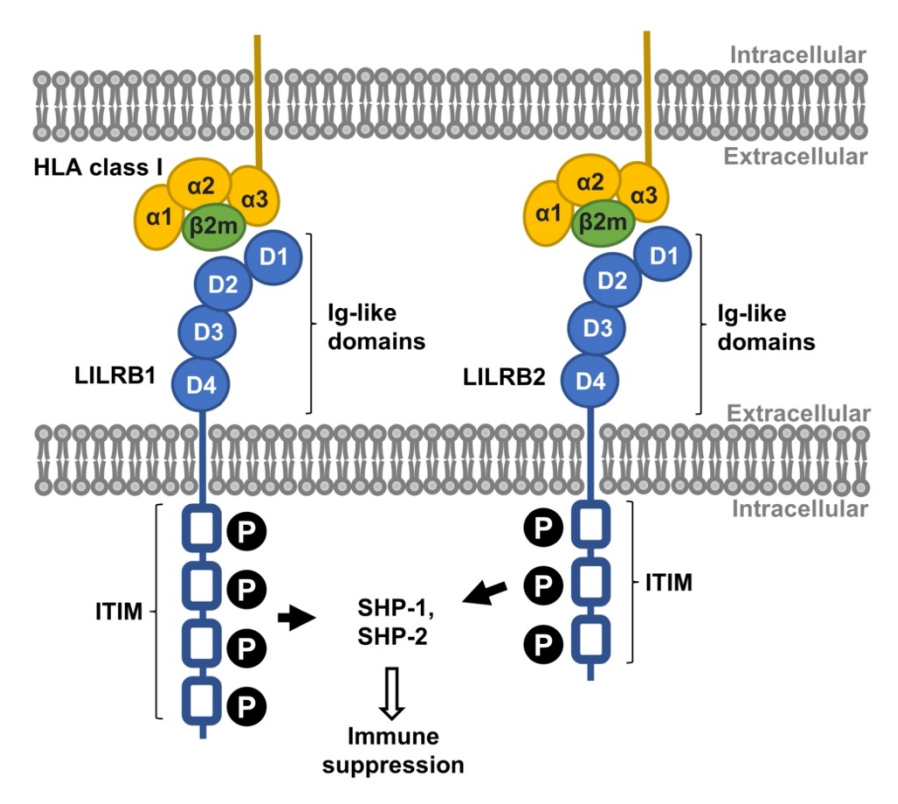


Figure 7: Structure of LILRB1 and LILRB2. LILRB1 and LILRB2 contain four extracellular Ig-like domains (D1-D4). Contact with HLA class I /  $\beta$ 2 microglobulin ( $\beta$ 2m) complexes locates to the D1 and D2 domains. Signal-transduction is mediated through four (LILRB1) or three (LILRB2) intracellular ITIM sequences. Upon receptor-engagement, tyrosine residues within the ITIM domains are phosphorylated and the receptors impair effector cell activation, for instance through SHP-1 and SHP-2. Parts of the figure were published in Zeller et al., 2023b.

#### 1.3.2 Broad Recognition of HLA Class I by LILRB1 and LILRB2

KIRs only recognize distinct allele variants of HLA class I. LILRB1 and LILRB2, however, interact with a variety of HLA class I molecules and recognize various alleles of classical HLA-A, HLA-B and HLA-C antigens, as well as the non-classical HLA molecules HLA-E,

HLA-F and HLA-G (Willcox et al., 2003a, Jones et al., 2011, Lepin et al., 2000, Navarro et al., 1999, Dulberger et al., 2017, Chapman et al., 1999, Shiroishi et al., 2006b, Allan et al., 1999). Yet, binding affinities vary between different HLA molecules. For instance, HLA-F and HLA-G were demonstrated to bind LILRB1 with a particularly high affinity. Interestingly, HLA-G exerts immune suppressive functions and thus plays an important role in cancer immune evasion. Of note, whereas LILRB1 only binds  $\beta$ 2 microglobulin ( $\beta$ 2m)-associated HLA class I molecules, LILRB2 also recognizes  $\beta$ 2m-free HLA molecules (Jones et al., 2011, Shiroishi et al., 2006b).

Crystal structure analysis of ligand-receptor complexes revealed that for both LILRB1 and LILRB2 the binding site for HLA molecules is confined to the apical D1-D2 region, which comprises two Ig-like domains (Willcox et al., 2003a, Chapman et al., 1999, Held and Mariuzza, 2008). In contrast, the D3-D4 regions do not contribute to binding (Nam et al., 2013, Wang et al., 2020b). The broad specificity for HLA class I molecules of LILRB1 and LILRB2 in contrast to KIRs is a consequence of the distinct site of interaction with the HLA/β2m complex. Crystallographic binding analyses with KIR2DL2 or KIR2DL3 and HLA-C revealed that KIRs mainly recognize the highly polymorphic helices of the α1 and  $\alpha$ 2 domains of HLA and interact with the C-terminal end of the peptide bound in the groove between them (figure 8A) (Parham and Moffett, 2013, Boyington and Sun, 2002, Boyington et al., 2000, Moradi et al., 2021). LILRB1, in contrast, binds the comparably low polymorphic HLA α3 domain with the apical D1 domain and the conserved β2m moiety predominantly with the D1-D2 interdomain hinge region (figure 8B) (Willcox et al., 2003a, Chapman et al., 1999, Held and Mariuzza, 2008). Yet, the binding affinity is also affected by LILRB1 polymorphisms, such as allele variants with differences in their D1-D2 regions, as well as polymorphisms in the HLA α3 domain (Liu et al., 2022, Jones et al., 2011). Compared to LILRB1, LILRB2 exhibits an overlapping, yet distinct mode of binding HLA molecules. Slight structural differences cause LILRB2 to predominantly bind to the α3 domain of HLA molecules (figure 8C) in contrast to LILRB1, which preferentially binds β2m (Shiroishi et al., 2006b). This results in the above-mentioned β2mindependent mode of HLA recognition by LILRB2 and the recognition also of open conformers lacking β2m and peptides (Jones et al., 2011, Shiroishi et al., 2006b).

Besides HLA molecules, LILRB1 and LILRB2 have several more ligands (De Louche and Roghanian, 2022, Deng et al., 2021, Kang et al., 2016). For instance, LILRB1 also interacts with the calcium-binding proteins S100A8 and S100A9 (Arnold et al., 2013) and recognizes several pathogen-derived ligands, including the human cytomegalovirus (CMV) gene product UL18 (Cosman et al., 1997, Yang and Bjorkman, 2008), dengue virus and bacterial antigens (Abdallah et al., 2021, Nakayama et al., 2007), along with

distinct *Plasmodium falciparum* repetitive interspersed families of polypeptides (RIFINs) (Saito et al., 2017). Among other ligands, LILRB2 also recognizes several angiopoietin-like proteins (Zheng et al., 2012),  $\beta$ -amyloid (Kim et al., 2013) and CD1d (Li et al., 2009). Interestingly, the murine PirB has been shown to also function as a receptor for several myelin inhibitors (e.g. Nogo66, MAG, OMgp) (Atwal et al., 2008).

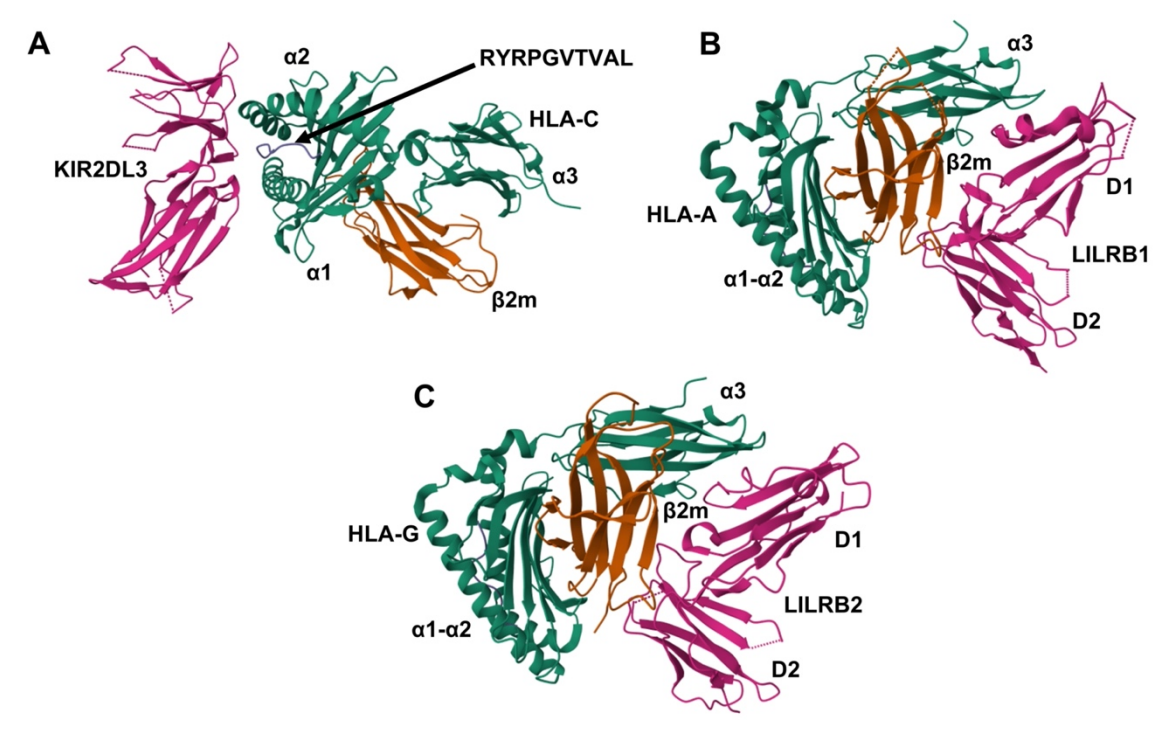


Figure 8: Recognition of HLA molecules by KIR2DL3, LILRB1 and LILRB2. (A) Killer immunoglobulin-like receptors (KIR), such as KIR2DL3 (magenta) mainly interact with the highly polymorphic  $\alpha 1$  and  $\alpha 2$  domains of human leukocyte antigen (HLA) molecules (green) and the peptide bound in the groove between them (blue; orange, β2m). The ribbon drawing of KIR2DL3 in complex with peptide (RYRPGVTVAL)-loaded HLA-C is derived from the pdb file 6PAG (Moradi et al., 2019, Moradi et al., 2021). (B) Leukocyte immunoglobulin-like receptor subfamily B member (LILRB) 1 (magenta) recognizes the comparably low polymorphic HLA  $\alpha 3$  domain (green) with the D1 domain and the conserved β2m moiety (orange) with the D1-D2 interdomain hinge region. The ribbon drawing of LILRB1 in complex with HLA-A2 is derived from pdb file 1P7Q (Willcox et al., 2003b, Willcox et al., 2003a). (C) Contact sites for LILRB2 (magenta) are also within the  $\alpha 3$  domain of HLA (green) and β2m (orange). In contrast to LILRB1, LILRB2 predominantly binds to the  $\alpha 3$  domain of HLA, resulting in a β2m-independent mode of HLA recognition. The ribbon drawing of LILRB2 complexed with HLA-G is derived from the pdb file 2DYP (Shiroishi et al., 2006a, Shiroishi et al., 2006b). All crystal structure images are sourced from the RCSB Protein Data Bank (RCSB.org) (Berman et al., 2000, Berman et al., 2003) and were created using Mol\* (Sehnal et al., 2021).

#### 1.3.3 LILRB1 and LILRB2 in the Regulation of Macrophages

Monocytes and macrophages carry all receptors of the inhibitory subfamily B of LIRs, including the HLA receptors LILRB1 and LILRB2 (van der Touw et al., 2017, Colonna et al., 1997, Barkal et al., 2018, Colonna et al., 1998). Cross-linking of LILRB1 in parallel to ligation of HLA-DR has been shown to result in downregulation of Ca<sup>2+</sup> mobilization in monocytes and macrophages (Colonna et al., 1997). Importantly, LILRB1- and LILRB2-engagement has been demonstrated to inhibit FcR-mediated tyrosine kinase-dependent

signaling in monocytes. Upon co-engagement of FcγRI and either LILRB1 or LILRB2, decreased tyrosine phosphorylation of the FcR γ-chain and SYK were observed. This led to a substantial decrease in FcγRI-mediated intracellular Ca²+ mobilization (Fanger et al., 1998). Thus, LILRB1 and LILRB2 signaling may also interfere with antibody effector functions conveyed through FcRs, such as ADCP. In fact, ligation of LILRB1 by HLA class I impaired phagocytosis by macrophages (Barkal et al., 2018). In a study aiming to elucidate inhibitory signaling pathways that limit macrophage phagocytosis of solid tumor cell lines upon CD47 antibody blockade, HLA class I molecules were found to be critical inhibitory regulators. Thus, gene knockout experiments identified LILRB1 as the major HLA class I receptor in macrophages responsible for this observation (Barkal et al., 2018). For LILRB2, a regulatory role in the phagocytosis of *E. coli* by macrophages has been suggested (Chen et al., 2018). Whether LILRB1 and LILRB2 are involved also in the regulation of macrophage phagocytosis of lymphoma cells is currently not known.

Apart from their function as regulators of phagocytosis, LILRB1 and LILRB2 may also contribute to the regulation of macrophage polarization. The abrogation of LILRB2 signaling has been demonstrated to facilitate the polarization of macrophages towards an inflammatory phenotype. Furthermore, stimulation of anti-LILRB2 antibody-treated macrophages with LPS augmented secretion of the pro-inflammatory cytokine TNF-α and favored inflammatory pathways, as indicated by increased phosphorylation of transcription factors such as nuclear factor kappa-B (NFκB), signal transducer and activator of transcription 1 (STAT1), extracellular-signal regulated kinases (ERK) 1/2, as well as p38 (Chen et al., 2018). A similar regulatory function has also been suggested for LILRB1. Thus, LILRB1 expression has been shown to be correlated with the expression of M2 macrophage-related antigens, such as CD163 or CD204, and gene knockout of LILRB1 in macrophages resulted in an increase of the proportion of immunophenotypical M1 macrophages *in vitro* (Zhang et al., 2021, Barkal et al., 2018).

#### 1.3.4 LILRB1 and LILRB2 in Cancer

Numerous studies have shown that LILRB receptors are involved in the evolution and progression of cancer and play a role during cancer treatments including immunotherapies (Kang et al., 2016, Carosella et al., 2021).

In various cancers, aberrant expression levels of LILRBs are found compared to adjacent healthy tissue (Liu et al., 2014, Garcia et al., 2020). Importantly, the expression of LILRBs and the immunosuppressive HLA-G correlated with poor differentiation and more ad-

vanced disease (Redondo-Garcia et al., 2023, Zou et al., 2023, Zhang et al., 2021, He et al., 2018).

Alterations in the expression of HLA class I are considered an important immune escape mechanism that is frequently observed in cancer. Whereas downmodulation of HLA class I allows cancer cells to avoid recognition by CD8<sup>+</sup> T cells, HLA class I also functions as a marker of self and mediates tolerance by NK cells. Thus, reduced or deficient display of HLA class I sensitizes cancer cells to attack by NK cells. Inhibition of NK cells upon recognition of HLA class I molecules mainly involves KIRs and natural killer group 2 member A (NKG2A) among other receptors. However, an inhibitory function has also been demonstrated for LILRB1. LILRB1 antibody blockade facilitated NK cell-mediated cytotoxicity against cancer cells, especially when combined with blocking anti-KIR or anti-NKG2A antibodies (Godal et al., 2010). Additionally, diminished display of HLA molecules may render cancer cells more susceptible to phagocytic uptake by macrophages. Besides cytotoxic lymphocytes, also macrophages are a critical effector cell population frequently found in the TME. Whereas M2-like pro-tumorigenic TAMs promote angiogenesis, cancer cell proliferation and the establishment of an immunosuppressive TME, macrophages are also capable of cancer cell phagocytosis and can even promote adaptive immune responses. Similar to the interaction of cancer cell-expressed CD47 with SIRPα on macrophages, HLA class I molecules on cancer cells function as 'Don't Eat Me!' signals through the engagement of LILRB1 on macrophages. In murine xenograft studies with human solid cancer cells carrying a mouse-human-chimeric β2m to enable interaction with mouse macrophages, display of HLA class I has been discovered to directly mediate protection of tumor cells from phagocytosis. In this study, gene-knockout of HLA class I consequently enhanced ADCP mediated by therapeutic antibodies targeting epithelial cell adhesion molecule (EpCAM) or EGFR (Barkal et al., 2018). Expression of LILRB1 and LILRB2 is found in a broad variety of cancers. Pronounced expression of LILRB1 has been detected in peripheral T cells and NK cells, as well as in the TME of patients with various solid tumors, including non-small cell lung cancer (NSCLC), RCC, head and neck cancer, esophagus and colon carcinoma. Subsequent analysis of cells in the TME revealed TAMs to be the immune cell population with the highest expression level of LILRB1 (Mandel et al., 2022). Studies in gastric cancer patients demonstrated that LILRB1<sup>+</sup> TAMs expressed an immunosuppressive M2-like phenotype (Zhang et al., 2021). However, besides TAMs also other immune cell populations in the TME, such as NK cells and certain CD8<sup>+</sup> T cells, carry LILRB1 (Mandel et al., 2022). In general, higher expression levels of LILRB1 were associated with worse outcome, as demonstrated for various cancers including gastric, prostate and ovarian cancer (Zhang et al., 2021, Vittrant et al., 2020, Xu et al., 2023). Expression of LILRB2 within the TME is also found in a number of different cancers, including breast cancer, colorectal cancer and RCC (Liu et al., 2014, Cai et al., 2019, Garcia et al., 2020). Further immuno-histochemical evaluation of breast cancer and RCC samples confirmed LILRB2 to also be expressed by immune cells within the TME, such as stromal macrophages (Liu et al., 2014, Garcia et al., 2020). Elevated levels of LILRB2 expression in tumors were associated with a worse prognosis (Redondo-Garcia et al., 2023). For instance, LILRB2 overexpression promoted tumor progression and angiogenesis in a murine colon cancer model (Liu et al., 2023a), an increased amount of LILRB2 mRNA went along with shorter progression-free survival in prostate cancer patients (Vittrant et al., 2020) and enhanced infiltration of pro-tumorigenic TAMs and impaired T cell proliferation and cytotoxicity were demonstrated for LILRB2-overexpressing NSCLC (Chen et al., 2021b). The discovery of the critical role of LILRBs in various cancers has raised the question about the potential of immune checkpoint inhibition of LILRB1 or LILRB2 for cancer immunotherapy. Barkal and colleagues reported enhanced ADCP of solid cancer cell lines displaying HLA class I by macrophages upon treatment with the murine hybridoma anti-LILRB1 IgG2b clone GHI/75. However, this antibody needed concomitant CD47 blockade by the IgG4 antibody magrolimab to exhibit its effect (Barkal et al., 2018). In contrast, the humanized, LILRB1-directed IgG4 antibody BND-22 not only promoted macrophage ADCP of solid cancer cells by the anti-EGFR antibody cetuximab, but proved efficient also as a single agent and induced the uptake of colon cancer cells by human macrophages in a murine xenograft model (Mandel et al., 2022). Various studies have confirmed that LILRB2 antibody blockade modulates the phenotype of TAMs ultimately leading to improved T cell activation (Chen et al., 2021b, Niu et al., 2022, Zuck et al., 2021). For instance, antagonistic murine hybridoma anti-LILRB2 antibodies shifted the polarization of tumor-infiltrating myeloid cells towards an inflammatory, M1-like phenotype and even promoted inflammation and adaptive immunity mediated by T cells (Chen et al., 2018). However, whether antibody blockade of LILRB1 or LILRB2 possesses the ability to increase the phagocytosis of lymphoma cells by macrophages is currently not known.

## 1.4 Aims and Objectives

Even though therapeutic antibodies have fundamentally improved the treatment options for cancer patients, relapsed or refractory disease is still a hurdle. Macrophages are key effector cells during antibody therapies, as they express all FcγRs in humans and are able to directly eliminate cancer cells through ADCP. An attractive approach to increase ADCP of cancer cells is immune checkpoint blockade to abrogate inhibitory signaling. In addition to CD47, HLA class I molecules were shown to impair phagocytosis in models of solid tumors, but a role for HLA class I and its receptors LILRB1 or LILRB2 in the regulation of CD20 antibody-mediated ADCP of lymphoma cells is still illusive. Here, it was thus hypothesized that LILRB1 or LILRB2 signaling in macrophages hampers ADCP of lymphoma cells and that their uptake can be enhanced by antibody blockade of the two receptors. Hence, the main objective of this thesis was to determine the influence of HLA class I expression on ADCP of lymphoma cells by CD20 antibodies and to evaluate the potential of LILRB1- or LILRB2-masking antibodies to enhance ADCP.

To determine the influence of HLA class I expression on ADCP by CD20 antibodies, the expression levels of HLA class I, CD47 and CD20 should be quantified and correlated to the sensitivity to ADCP mediated by the CD20 antibody rituximab with or without CD47 blockade. For antibody blockade, Fc-silent anti-LILRB1 and anti-LILRB2 antibodies (LILRB1-IgGσ and LILRB2-IgGσ, respectively) with abrogated FcγR binding should be generated, purified and characterized biochemically. The antibodies should be analyzed for antigen-specific binding and their ability to block the receptors' interaction with HLA molecules. Subsequently, the effect of HLA class I receptor blockade on ADCP of lymphoma cell lines should be determined. Monocytes should be isolated from the peripheral blood of healthy donors and differentiated to macrophages ex vivo. LILRB1-IgGσ or LILRB2-IgGσ should then be analyzed alone or in combination with the Fc-silent magrolimab variant CD47-IgGσ for their ability to increase the CD20 antibody-mediated phagocytosis of lymphoma cells in fluorescence microscopy-based experiments. To analyze also the kinetics of ADCP induced by therapeutic antibodies, the live cell imaging system IncuCyte® should be established and employed for automated phagocytosis assays. Also, a potential influence of the macrophage polarization state on ADCP of lymphoma cells should be analyzed. Hereto, monocytes should be differentiated towards macrophages with M0, M1 or M2 phenotypes to compare them as effector cells in ADCP assays. Finally, the findings obtained with cell lines should be confirmed with patient-derived lymphoma cells. Cancer cells should be enriched from the peripheral blood of lymphoma patients and the impact of LILRB1 or LILRB2 antibody masking on ADCP by CD20 antibodies with or without co-inhibition of CD47 should be evaluated.

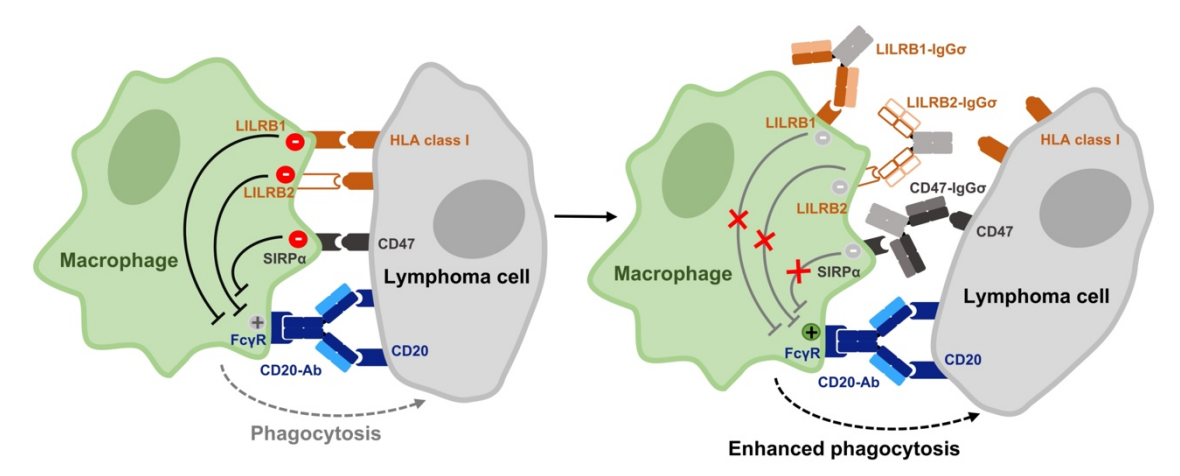


Figure 9: Postulated effect of LILRB1 or LILRB2 antibody blockade on CD20 antibody-mediated ADCP of lymphoma cells. Besides the CD47 receptor signal regulatory protein (SIRP)  $\alpha$ , the inhibitory receptors leukocyte immunoglobulin-like receptor subfamily B member (LILRB) 1 and LILRB2 for HLA class I interfere with Fc $\gamma$  receptor (Fc $\gamma$ R) signaling in macrophages. It was thus hypothesized that the blockade of LILRB1 or LILRB2 with Fc-silent antibodies with mutated Fc $\gamma$ R binding sites (i.e. LILRB1-IgG $\sigma$  and LILRB2-IgG $\sigma$ , respectively) may increase ADCP of lymphoma cells by macrophages. The ability of LILRB1 or LILRB2 immune checkpoint blockade to enhance the CD20 antibody (CD20-Ab)-mediated phagocytosis of lymphoma cells should be analyzed when applied alone or in combination with an Fc-silent version of the antibody magrolimab specific for CD47 (referred to as CD47-IgG $\sigma$ ).

# 2. Materials and Methods

## 2.1 Materials

## 2.1.1 Chemicals

Table 2: Chemicals.

Chemical	Manufacturer
Accutase	Thermo Fisher Scientific, Waltham, MA, USA
Acrylamide bisacrylamide (37.5 : 1) 30%	Carl Roth GmbH, Karlsruhe, Germany
Agarose Standard	Carl Roth GmbH, Karlsruhe, Germany
Albumin fraction V, biotin-free (BSA)	Carl Roth GmbH, Karlsruhe, Germany
Ammonium persulfate (APS)	Sigma-Aldrich, St. Louis, MO, USA
Ampicillin sodium salt	Sigma-Aldrich, St. Louis, MO, USA
Calcium chloride (CaCl <sub>2</sub> )	Carl Roth GmbH, Karlsruhe, Germany
CaptureSelect <sup>™</sup> IgG-C <sub>H</sub> 1 affinity matrix	Thermo Fisher Scientific, Waltham, MA, USA
CellBrite <sup>™</sup> Orange Cytoplasmic Membrane Labeling Dye	Biotium, Inc., Fremont, CA, USA
Chloroquine diphosphate salt	Sigma-Aldrich, St. Louis, MO, USA
CryoSure-DMSO	WAK-Chemie Medical GmbH, Steinbach, Germany
Distilled water (dH <sub>2</sub> O)	Thermo Fisher Scientific, Waltham, MA, USA
Ethanol ≥99,8 %	Carl Roth GmbH, Karlsruhe, Germany
Fetal calf serum (FCS)	Thermo Fisher Scientific, Waltham, MA, USA
Ficoll <sup>®</sup> Paque Plus	Cytiva, Marlborough, MA, USA
Gamunex <sup>®</sup> 10% 100 mg/ml	Grifols, Barcelona, Spain
Gel Loading Dye Purple (6 X)	New England BioLabs, Inc., Ipswich, MA, USA
Glycine	Carl Roth GmbH, Karlsruhe, Germany
Hydrochloric acid (HCI)	Carl Roth GmbH, Karlsruhe, Germany
Immobilon <sup>™</sup> Western Chemiluminescent HRP Substrate	Millipore Corporation, Billerica, MA, USA
Immersol <sup>™</sup> 518 F	Carl Zeiss AG, Jena, Germany
Isopropyl alcohol	Sigma-Aldrich, St. Louis, MO, USA
LB (Lysogeny broth) Agar (Lennox)	Carl Roth GmbH, Karlsruhe, Germany
LB (Lysogeny broth) Broth (Lennox)	Carl Roth GmbH, Karlsruhe, Germany

Lipopolysaccharide from <i>E. coli</i> O127:B8, BioXtra, γ-irradiated	Sigma-Aldrich, St. Louis, MO, USA
Methanol ≥99,9 %	Carl Roth GmbH, Karlsruhe, Germany
NucBlue™ Live ReadyProbes™ Reagent (Hoechst 33342)	Thermo Fisher Scientific, Waltham, MA, USA
PageRuler <sup>™</sup> Plus Prestained Protein Ladder	Thermo Fisher Scientific, Waltham, MA, USA
Pencillin 100 U/ml/streptomycin 100 µg/ml (Pen/Strep)	Lonza, Basel, Switzerland
Powdered milk	Carl Roth GmbH, Karlsruhe, Germany
Precision Plus Protein™ WesternC™ Blotting Standards	Bio-Rad Laboratories, Inc., Hercules, CA, USA
Quick-Load <sup>®</sup> 1 kb Plus DNA Ladder	New England BioLabs, Inc., Ipswich, MA, USA
Recombinant human GM-CSF	PeproTech, Cranbury, NJ, USA
Recombinant human IFN-γ	PeproTech, Cranbury, NJ, USA
Recombinant human IL-10	PeproTech, Cranbury, NJ, USA
Recombinant human M-CSF	PeproTech, Cranbury, NJ, USA
Roti <sup>®</sup> -Blue	Carl Roth GmbH, Karlsruhe, Germany
Sodium chloride (NaCl)	Carl Roth GmbH, Karlsruhe, Germany
Sodium dodecyl sulfate (SDS)	Carl Roth GmbH, Karlsruhe, Germany
SYBR™ Safe DNA Gel Stain	Thermo Fisher Scientific, Waltham, MA, USA
Tetramethylenediamine (TEMED)	Carl Roth GmbH, Karlsruhe, Germany
Tris(hydroxymethyl)aminomethan PUFFERAN®	Carl Roth GmbH, Karlsruhe, Germany
Triton X-100	Sigma-Aldrich, St. Louis, MO, USA
Trypan Blue solution	Sigma-Aldrich, St. Louis, MO, USA
TWEEN® 20	Carl Roth GmbH, Karlsruhe, Germany

## 2.1.2 Kits

Table 3: Kits.

Kit	Manufacturer
Agilent Protein 230 Kit	Agilent Technologies, Inc., Santa Clara, CA, USA
CFSE Cell Division Tracker Kit	BioLegend, San Diego, CA, USA
NucleoBond <sup>®</sup> Xtra Maxi	Macherey-Nagel, Dueren, Germany
NucleoSpin <sup>®</sup> Gel and PCR Clean-up	Macherey-Nagel, Dueren, Germany
NucleoSpin <sup>®</sup> Plasmid EasyPure	Macherey-Nagel, Dueren, Germany

pHrodo <sup>®</sup> Red Cell Labeling Kit for Incucyte <sup>®</sup> Phagocytosis Assays	Sartorius, Goettingen, Germany
Qifikit <sup>®</sup>	Dako, Glostrup, Denmark
Quick Ligation™ Kit	New England BioLabs, Inc., Ipswich, MA, USA

## 2.1.3 Buffers, Solutions and Media

Table 4: Buffers, solutions and media.

Buffer / Solution / Media	Composition / Manufacturer
Blocking solution (anti-human lg-kappa LC blot)	TBS, 3.2% (m/v) BSA, 2.0% powdered milk
Blocking solution (anti-human IgG-Fc blot)	TBS, 5.0% (m/v) powdered milk
Coomassie Blue staining solution	dH <sub>2</sub> O, 20% (v/v) methanol, 20% (v/v) Roti <sup>®</sup> -Blue
Cut Smart <sup>®</sup> Buffer	New England BioLabs, Inc., Ipswich, MA, USA
DL-Dithiothreitol solution (DTT)	Sigma-Aldrich, St. Louis, MO, USA
DMEM (1 X) + 4.5 g/L D-Glucose, L-Glutamine	Thermo Fisher Scientific, Waltham, MA, USA
Dulbecco's Phosphate Buffered Saline (1 X, PBS)	Thermo Fisher Scientific, Waltham, MA, USA
Dulbecco's Phosphate Buffered Saline (1 X, PBS)	Sigma-Aldrich, St. Louis, MO, USA
Dulbecco's Phosphate Buffered Saline (10 X, 10 X PBS)	Thermo Fisher Scientific, Waltham, MA, USA
Elution buffer (for C <sub>H</sub> 1-affinity matrix, pH 3.0)	0.1 M glycine
HBS buffer (2 X, pH 7.05)	50 mM HEPES, 280 mM NaCl, 1,5 mM Na <sub>2</sub> HPO <sub>4</sub>
Laemmli SDS sample buffer, non-reducing (6 X)	Thermo Fisher Scientific, Waltham, MA, USA
Laemmli SDS sample buffer, reducing (6 X)	Thermo Fisher Scientific, Waltham, MA, USA
Monocyte Attachment Medium	PromoCell GmbH, Heidelberg, Germany
Neutralization buffer (for C <sub>H</sub> 1-affinity matrix, pH 8.0)	1 M Tris
OptiMEM® I (1 X) + L-Glutamine, HEPES	Thermo Fisher Scientific, Waltham, MA, USA
PBA buffer (flow cytometry)	PBS, 1% (m/v) BSA

RPMI 1640 (1 X) + GlutaMAX <sup>™</sup> -I + 25mM HEPES + 3.024 g/L Sodium bicarbonate	Thermo Fisher Scientific, Waltham, MA, USA
S.O.C. media	Thermo Fisher Scientific, Waltham, MA, USA
SDS-PAGE running buffer (10 X)	25 mM Tris, 192 mM glycine, 0.1% (m/v) SDS
Staining solution (anti-human Ig-kappa LC blot)	TBS, 1.0% (m/v) BSA, 2% (m/v) powdered mild
TAE buffer (50X)	Carl Roth GmbH, Karlsruhe, Germany
TBST buffer	10 mM Tris, 150 mM NaCl, 0.05% (v/v) TWEEN® 20
Tris-buffered saline (TBS, pH 7.6)	10 mM Tris, 150 mM NaCl
Triton-Tween-TBS buffer	10 mM Tris, 150 mM NaCl, 0.05% (v/v) TWEEN® 20, 0.2% (v/v) Triton-X-100
IMDM (1 X) + GlutaMAX <sup>™</sup> -I + 25mM HEPES + 3.024 g/L Sodium bicarbonate	Thermo Fisher Scientific, Waltham, MA, USA
X-Vivo <sup>™</sup> 15	Lonza, Basel, Switzerland

## 2.1.4 Cell Lines

Table 5: Cell lines.

Cell Line	Cell Type	Source
Lenti-X <sup>™</sup> 293T	Subclone of the human embryonic kidney cell line HEK 293T	Clontech, Saint-Germain-en- Laye, France
CHO-K1	Chinese hamster ovary cells	German Collection of Microorganisms and Cell Cultures GmbH (DSMZ) Braunschweig, Germany (ACC 110)
Carnaval	DLBCL	DSMZ (ACC 724)
DG-75	Burkitt lymphoma	DSMZ (ACC 83)
MEC2	CLL	DSMZ (ACC 500)
SU-DHL-4	DLBCL	DSMZ (ACC 495)
Granta 519	MCL	DSMZ (ACC 342)

## 2.1.5 Cultivation of Cell Lines

Table 6: Culture media composition for cell lines.

Cell Lines	Culture Medium	Composition
Carnaval DG-75	R10 <sup>+</sup>	RPMI 1640 (1 X) + GlutaMAX <sup>TM</sup> -I + 25mM HEPES + 3.024 g/L Sodium bicarbonate
SU-DHL-4		10% FCS (v/v)
		1% Pen/Strep (v/v)
MEC-2	IMDM20 <sup>+</sup>	IMDM (1 X) + GlutaMAX <sup>™</sup> -I + 25mM HEPES + 3.024 g/L Sodium bicarbonate
		20% FCS (v/v)
		1% Pen/Strep (v/v)
Granta 519 Lenti-X <sup>™</sup> 293T CHO-K1	D10⁺	DMEM (1 X) + 4.5 g/L D-Glucose, L-Glutamine
		10% FCS (v/v)
0110-101		1% Pen/Strep (v/v)

## 2.1.6 Bacteria

Table 7: Bacteria.

Strain	Genotype	Source
Subcloning Efficiency™ DH5α Competent Cells	F <sup>-</sup> Φ80 <i>lac</i> ZΔM15 Δ( <i>lac</i> ZYA- <i>arg</i> F) U169 recA1 endA1 <i>hsd</i> R17(r <sub>k</sub> <sup>-</sup> , m <sub>k</sub> <sup>+</sup> ) phoA supE44 <i>thi</i> -1 gyrA96 relA1 λ <sup>-</sup>	Thermo Fisher Scientific, Waltham, MA, USA
One Shot™ TOP10 Chemically Competent E. coli	F-mcrA Δ(mrr-hsdRMS- mcrBC) Φ80LacZΔM15 Δ LacX74 recA1 araD139 Δ(araleu) 7697 galU galK rpsL (StrR) endA1 nupG	Thermo Fisher Scientific, Waltham, MA, USA

## 2.1.7 Vectors

Table 8: Vectors.

Vector	Manufacturer / Reference
pcDNA 3.1	Thermo Fisher Scientific, Waltham, MA, USA
pSecTag2-LC	Schewe et al., 2017
(Derivative of pSecTag2/Hygro C from Thermo Fisher Scientific, Waltham, MA, USA)	
pSecTag2-HC-IgG1σ	C Kellner, unpublished
(Derivative of pSecTag2/Hygro C)	

pSecTag2-GHI/75-LC	Zeller et al., 2022
(Derivative of pSecTag2/Hygro C)	
pSecTag2-GHI/75-HC-lgG2σ	Zeller et al., 2022
(Derivative of pSecTag2/Hygro C)	
pSecTag2-hu5F9-LC	Zeller et al., 2022
(Derivative of pSecTag2/Hygro C)	
pSecTag2-hu5F9-HC-lgG2σ	Zeller et al., 2022
(Derivative of pSecTag2/Hygro C)	

## 2.1.8 Primers

Table 9: Primers.

Primer	Sequence	Manufacturer
pSec-CMV (forward)	GGTAGGCGTGTACGGTGGGAGG	Thermo Fisher Scientific, Waltham, MA, USA
pSec-PolyA (reverse)	GGAAAGGACAGTGGGAGTGGCAC	Thermo Fisher Scientific, Waltham, MA, USA
pSec-CH1 (forward)	AGCTCAAGCCTCGGTACACAGACC	Thermo Fisher Scientific, Waltham, MA, USA

## 2.1.9 Antibodies

Table 10: Conjugated antibodies.

Antibody	Structure	Manufacturer
REA Control Antibody - APC	Human IgG1 clone REA293 APC-conjugated	Miltenyi Biotec B.V. & Co. KG, Bergisch Gladbach, Germany
REA Control Antibody (S)- PE	Human IgG1 clone REA293 PE-conjugated	Miltenyi Biotec Biotec B.V. & Co. KG, Bergisch Gladbach, Germany
CD3-APC	Human IgG1 clone REA613 APC-conjugated	Miltenyi Biotec Biotec B.V. & Co. KG, Bergisch Gladbach, Germany
CD14-PE	Human IgG1 clone REA 599 PE-conjugated	Miltenyi Biotec Biotec B.V. & Co. KG, Bergisch Gladbach, Germany
CD80-PE	Human IgG1 clone REA661 PE-conjugated	Miltenyi Biotec Biotec B.V. & Co. KG, Bergisch Gladbach, Germany
CD163-PE	Human IgG1 clone REA812 PE-conjugated	Miltenyi Biotec Biotec B.V. & Co. KG, Bergisch Gladbach, Germany

CD85j (ILT-2)-PE, anti- human	Human IgG1 clone REA998 PE-conjugated	Miltenyi Biotec Biotec B.V. & Co. KG, Bergisch Gladbach, Germany
CD85d (ILT4)-PE, anti- human	Human IgG1 clone REA184 PE-conjugated	Miltenyi Biotec Biotec B.V. & Co. KG, Bergisch Gladbach, Germany
F(ab') <sub>2</sub> Fragment of FITC- Conjugated Goat Anti- Mouse Immunoglobulins	Goat F(ab') <sub>2</sub> Fragment anti-mouse IgG FITC-conjugated	Dako, Glostrup, Denmark
Fluorescein (FITC)- conjugated AffiniPure F(ab') <sub>2</sub> Fragment Goat Anti-Mouse IgG, Fcγ Fragment specific	Goat F(ab <sup>'</sup> ) <sub>2</sub> Fragment anti-mouse IgG, Fcγ fragment specific polyclonal FITC-conjugated	Jackson ImmunoResearch Laboratories, Inc., West Grove, PA, USA
R-Phycoerythrin AffiniPure F(ab') <sub>2</sub> Fragment Goat Anti-Human IgG, Fcγ Fragment specific	Goat F(ab <sup>'</sup> ) <sub>2</sub> Fragment anti-human IgG, Fcγ fragment specific polyclonal PE-conjugated	Jackson ImmunoResearch Laboratories, Inc., West Grove, PA, USA
Anti-Human-IgG (Fc specific) – Peroxidase antibody produced in goat	Goat Ig anti-human-IgG, Fc specific polyclonal Peroxidase-conjugated	Sigma-Aldrich, St. Louis, MO, USA
Goat anti-human kappa light chain:HRP	Goat IgG anti-human kappa LC polyclonal HRP-conjugated	Bio-Rad Laboratories, Inc., Hercules, CA, USA

Table 11: Unconjugated antibodies.

Antibody	Structure	Manufacturer / Reference
Rituximab (MabThera®)	Chimeric, monoclonal anti-CD20 IgG1	Hoffmann-La Roche AG, Basel, Switzerland
Trastuzumab (Herceptin®)	Humanized, monoclonal anti-HER2 IgG1	Hoffmann-La Roche AG, Basel, Switzerland
IgG1 Isotype Control	Mouse, monoclonal IgG clone 11711	R&D Systems, Inc., Minneapolis, MN, USA
IgG2a Isotype Control	Mouse IgG2a clone MOPC-173	BioLegend, San Diego, CA, USA
CD20	Mouse IgG2a clone S1815E	BioLegend, San Diego, CA, USA
CD47	Mouse IgG1 clone B6H12	Thermo Fisher Scientific, Waltham, MA, USA

Anti-HLA-A,B,C	Mouse IgG2a clone W6/32	BioLegend, San Diego, CA, USA
Anti-HLA-G	Mouse IgG2a clone 87G	BioLegend, San Diego, CA, USA
Anti-human CD172a (SIRPα)	Mouse IgG2a clone 15-414	BioLegend, San Diego, CA, USA
Ultra-LEAF <sup>™</sup> purified anti- human CD85j (ILT2)	Mouse IgG2b clone GHI/75	BioLegend, San Diego, CA, USA
Anti-LILRB2/CD85j	Mouse, monoclonal IgG2a clone 287219	R&D Systems, Inc., Minneapolis, MN, USA

#### 2.1.10 Soluble HLA Molecules

Table 12: Soluble, PE-conjugated HLA class I molecules used for binding studies.

HLA subtype	Structure	Peptide origin	Peptide sequence	Manufacturer
A*0201	Dextramer PE-conjugated	CMV pp65	NLVPMVATV	Immudex, Kopenhagen, Denmark
B*0801	Dextramer PE-conjugated	EBV BZLF1	RAKFKQLL	Immudex, Kopenhagen, Denmark
C*0702	Pentamer PE-conjugated	CMV IE-1	CRVLCCYVL	ProImmune Ltd., Oxford, UK

## 2.1.11 Restriction Enzymes

The restriction enzymes *Nhe*I, *Ppu*MI, *Eco*O109I, *Hind*III, *Ale*I-v2, *Xcm*I, *Pme*I and *Bsr*GI, as well as the corresponding CutSmart® restriction enzyme buffer were obtained from New England BioLabs (Ipswich, MA, USA).

#### 2.1.12 Consumables

Table 13: Consumables.

Consumable	Manufacturer
Cellstar <sup>®</sup> 96 Well Cell Culture Plate (F-bottom)	Greiner Bio-One GmbH, Frickenhausen, Germany
Cellstar® 6 Well Cell Culture Plate	Greiner Bio-One GmbH, Frickenhausen, Germany
Combitips advanced® (2,5 ml/5 ml)	Eppendorf SE, Hamburg, Germany
μ-Slides 8 Well ibiTreat	Ibidi GmbH, Graefelfing, Germany
ZelluTrans regenerated cellulose dialysis tube (molecular weight cut-off: 6 – 8000)	Carl Roth GmbH, Karlsruhe, Germany

AESCULAP® Surgical Disposable Scalpel #10	B. Braun SE, Melsungen, Germany
Biosphere <sup>®</sup> Filter Tips 10 colourless (10 μl, 20 μl, 100 μl, 200 μl, 1000 μl)	Sarstedt, Nuembrecht, Germany
PS-Tube (5ml, for flow cytometry)	Greiner Bio-One GmbH, Frickenhausen, Germany
Serological pipettes (2 ml, 5 ml, 10 ml)	Sarstedt, Nuembrecht, Germany
Serological pipettes (25 ml, 50 ml)	Greiner Bio-One GmbH, Frickenhausen, Germany
Omnifix <sup>®</sup> -F syringes (1 ml)	B. Braun SE, Melsungen, Germany
Microlance <sup>™</sup> 3 26G ½" needles	Becton Dickinson, Franklin Lakes, NJ, USA
Steritop <sup>®</sup> 45 mm Neck Size Millipore Express <sup>®</sup> PLUS (0,22 µm)	Merck Millipore, Burlington, MA, USA
Millex <sup>®</sup> -LG Filter Unit (0,20 μm, 13 mm)	Merck Millipore, Burlington, MA, USA
SafeSeal reaction tube (0,5 ml, 1,5 ml, 2 ml)	Sarstedt, Nuembrecht, Germany
Cellstar <sup>®</sup> Screw cap tubes (50 ml)	Greiner Bio-One GmbH, Frickenhausen, Germany
Screw cap tubes (15 ml)	Sarstedt, Nuembrecht, Germany
Round bottom tubes (14 ml)	Thermo Fisher Scientific, Waltham, MA, USA
S-Monovette <sup>®</sup> Citrat 9NC 0.106 mol/l 3,2%	Sarstedt, Nuembrecht, Germany
Poly-Prep <sup>®</sup> Chromatography Columns	Bio-Rad Laboratories, Inc., Hercules, CA, USA
Vivaspin <sup>®</sup> 6 centrifugal concentrators	Sartorius, Goettingen, Germany
Cellstar <sup>®</sup> Cell culture dishes	Greiner Bio-One GmbH, Frickenhausen, Germany
Trans-Blot <sup>®</sup> Turbo <sup>™</sup> Transfer Pack	Bio-Rad Laboratories, Inc., Hercules, CA, USA
Cellstar <sup>®</sup> Cell culture flasks (25 cm <sup>2</sup> , 75 cm <sup>2</sup> , 175 cm <sup>2</sup> )	Greiner Bio-One GmbH, Frickenhausen, Germany
Nunc <sup>™</sup> EasYFlask <sup>™</sup> 75 cm² Nunclon <sup>™</sup> Delta Surface	Thermo Fisher Scientific, Waltham, MA, USA
Cell Scraper (Size M)	Sarstedt, Nuembrecht, Germany
Cryo.s <sup>™</sup> vials	Greiner Bio-One GmbH, Frickenhausen, Germany

## **2.1.13 Devices**

Table 14: Devices.

Device	Description	Manufacturer
2100 Bioanalyzer	Bioanalyzer	Agilent Technologies, Inc., Santa Clara, CA, USA
Accu-jet <sup>®</sup> pro	Pipette controller	Brand GmbH + Co. KG, Wertheim, Germany
AEKTA Pure	Protein purification system	Cytiva, Marlborough, MA, USA
Avanti J-26 XP	Ultra-centrifuge	Beckman Coulter, Pasadena, CA, USA
Axio Observer D1	Fluorescence microscope	Carl Zeiss AG, Jena, Germany
Axiocam 208 color	Microscope camera	Carl Zeiss AG, Jena, Germany
AxioCam MRm	Microscope camera	Carl Zeiss AG, Jena, Germany
BACS Innova 42	Incubator shaker	Eppendorf SE, Hamburg, Germany
Bio-Rad Power Pac 300	Power supply	Thermo Fisher Scientific, Waltham, MA, USA
Bizhub C3351	Multifunctional office printer	Konica Minolta, Inc., Tokyo, Japan
C1000 Touch	Thermal cycler	Bio-Rad Laboratories, Inc., Hercules, CA, USA
Combi-Spin FVL-2400N	Centrifuge and vortex combination	VWR International, Radnor, PA, USA
EnviroFalk evoqua	Water purification plant	EnviroFALK GmbH, Haimhausen, Germany
Eppendorf centrifuge 5424	Centrifuge	Eppendorf SE, Hamburg, Germany
ETG MBT 250	Heat block	ETG GmbH, Ilmenau, Germany
F9-C	Fraction collector	Cytiva, Marlborough, MA, USA
FACScalibur™	Flow cytometer	Becton Dickinson, Franklin Lakes, NJ, USA
Fusion SL	Western blot and chemiluminescence imaging system	Vilber Lourmat, Eberhardzell, Germany
GFL0815	Orbital shaker	LAUDA-GFL Gesellschaft fuer Labortechnik mbH, Burgwedel, Germany

HBO 100	Microscope illuminator	Carl Zeiss, Jena, Germany
HERAcell 240i	Incubator	Thermo Fisher Scientific, Waltham, MA, USA
Heraeus Fresco 21	Centrifuge	Thermo Fisher Scientific, Waltham, MA, USA
Heraeus Multifuge X3R	Centrifuge	Thermo Fisher Scientific, Waltham, MA, USA
HERAsafe 2030i	Biological safety cabinet	Thermo Fisher Scientific, Waltham, MA, USA
HERAtherm	Oven	Thermo Fisher Scientific, Waltham, MA, USA
IKA RH basic 2	Magnetic stirrer	IKA GmbH, Staufen, Germany
IncuCyte® SX1	Live cell analysis system	Sartorius, Goettingen, Germany
inoLab <sup>®</sup> pH 7110	pH meter	Xylem Analytics GmbH, Weilheim, Germany
Kendro Megafuge 1.0 R	Centrifuge	Thermo Fisher Scientific, Waltham, MA, USA
KF85	Flake ice maker	Ice line Migel, Milan, Italy
LABOPORT® N 816.3.KT.18	Vacuum pump	KNF DAC GmbH, Hamburg, Germany
LKB GPS 200/400	Electrophoresis power supply	Cytiva, Marlborough, MA, USA
Marienfeld Superior <sup>™</sup> Neubauer improved	Neubauer-improved counting chamber	Paul Marienfeld GmbH & Co. KG, Lauda- Koenigshofen, Germany
Memmert laboratory water bath	Water bath	Memmert, Buechenbach, Germany
Miele G7883	Laboratory dish washer	Miele & Cie. KG, Guetersloh, Germany
Mini-PROTEAN® Tetra Cell	Vertical gel electrophoresis cell	Bio-Rad Laboratories, Inc., Hercules, CA, USA
Multifuge X Pro Series	Centrifuge	Thermo Fisher Scientific, Waltham, MA, USA
Multipette® M4	Multi-dispenser pipette	Eppendorf SE, Hamburg, Germany
Nanodrop 2000c	Spectrophotometer	Thermo Fisher Scientific, Waltham, MA, USA
neoMag <sup>®</sup> D-6011	Magnetic stirrer	neoLab Migge GmbH, Heidelberg, Germany
neoVortex® D-6012	Vortex mixer	neoLab Migge GmbH, Heidelberg, Germany

Pico 21	Centrifuge	Thermo Fisher Scientific, Waltham, MA, USA
Quintix	Precision scales	Sartorius, Goettingen, Germany
Research <sup>®</sup> plus (0,1-2,5 µl / 0,5-10 µl / 2-20 µl / 5-100 µl / 20-200 µl / 100-1000 µl)	Piston-operated pipette	Eppendorf SE, Hamburg, Germany
Safe Imager™ 2.0 blue light transilluminator	Blue light transilluminator	Thermo Fisher Scientific, Waltham, MA, USA
Sharp R-5975	Microwave	Sharp, Sakai, Japan
Superdex <sup>™</sup> 200 Increase 10/300 GL column	Size exclusion chromatography column	Cytiva, Marlborough, MA, USA
Systec VX-150	Autoclave	Systec GmbH, Linden, Germany
Thermo HERAfreeze Basic	Freezer (-80°)	Thermo Fisher Scientific, Waltham, MA, USA
ThermoMixer C	Cooling and heating thermoshaker	Eppendorf SE, Hamburg, Germany
Trans-Blot <sup>®</sup> Turbo <sup>™</sup>	Protein transfer system	Bio-Rad Laboratories, Inc., Hercules, CA, USA
Wide Mini-Sub <sup>™</sup> Cell	Horizontal electrophoresis chamber	Bio-Rad Laboratories, Inc., Hercules, CA, USA
Zeiss Primovert	Inverted microscope	Carl Zeiss, Jena, Germany

## 2.1.14 Software

Table 15: Software.

Software	Manufacturer
Microsoft Office Professional Plus 2016	Microsoft Corporation, Redmond, WA, USA
IncuCyte 2020B	Sartorius, Goettingen, Germany
SerialCloner 2.6.1	Serial Basics, freeware (http://serialbasics.free.fr/Serial_Cloner.html)
Discovery Studio Visualizer 2017 R2	Biovia, San Diego, CA, USA
GeneStudio Pro 2.2.0.0	GeneStudio, Inc., Suwanee, GA, USA
Nanodrop 2000c v.1.6.198	Thermo Fisher Scientific, Waltham, MA, USA
CellQuest Pro v6.0	Becton Dickinson, Franklin Lakes, NJ, USA
FlowJo v10.6.2	Becton Dickinson, Franklin Lakes, NJ, USA
AxioVs 40 v4.8.20	Carl Zeiss, Jena, Germany

FusionCapt Advance 16.01	Vilber Lourmat, Eberhardzell, Germany
ZEN core v3.1.88.0000	Carl Zeiss, Jena, Germany
GraphPad Prism v8.0.2 and v10.1.1	GraphPad Software, La Jolla, CA, USA
Unicorn <sup>™</sup> 7.5	Cytiva, Marlborough, MA, USA
2100 Expert vB.02.10.SI764	Agilent Technologies, Inc., Santa Clara, CA, USA

### 2.2 Methods

## 2.2.1 Molecular Biology Techniques

#### 2.2.1.1 Enzymatic Restriction Digestion

Enzymatic restriction digestion was performed in CutSmart<sup>®</sup> buffer using 1  $\mu$ I of the indicated restriction enzymes according to the manufacturer's instructions. In a volume of 30  $\mu$ I, 1 – 2  $\mu$ g of plasmid DNA were digested for at least 2 h at 37° C in a heat block or a thermal cycler.

#### 2.2.1.2 Agarose Gel Electrophoresis

Agarose gel electrophoresis was performed to separate DNA fragments by size. In addition, DNA fragments of specific size were purified from the gel. Agarose gels were prepared by polymerizing 1% or 2% (m/v) Agarose Standard in TAE-buffer. DNA samples were stained with Gel Loading Dye Purple and loaded into the gel pockets. Electrophoresis was conducted in TAE buffer at 90 V for approximately 60 min. Quick-Load® 1 kb Plus DNA Ladder served as molecular weight reference. After completion, agarose gels were stained with SYBR™ Safe DNA Gel Stain (1:10⁴ dilution in TAE-buffer). DNA bands were visualized using the Fusion SL imaging system or a blue light transilluminator for documentation or gel extraction of individual DNA fragments, respectively.

#### 2.2.1.3 Purification of DNA from Agarose Gels

To purify DNA from the extracted gel fragments, NucleoSpin<sup>®</sup> Gel and PCR Clean-up kit was employed following the manufacturer's protocol. Elution of DNA from the column provided with the kit was carried out with 50  $\mu$ l of dH<sub>2</sub>O. The purified DNA was stored at -20° C until further use.

#### 2.2.1.4 Ligation of DNA Fragments

To ligate cohesive DNA ends, Quick Ligation<sup>™</sup> Kit was applied according to the manufacturer's instructions. In two separate preparations with a total volume of 20 µl

each, enzyme-digested insert DNA and recipient vector DNA were mixed for ligation in a molar ratio of 3:1 and 5:1 at room temperature for 15 min in the buffer system provided with the kit.

#### 2.2.1.5 DNA Sequencing

To verify correctness of the base sequence of plasmid DNA, Sanger sequencing was performed. For this purpose, 400-500 ng of the plasmid DNA were reacted with 5  $\mu$ l of a 5 pmol/ $\mu$ l solution of the appropriate sequencing primer (table 9) in a total volume of  $15-20~\mu$ l of dH<sub>2</sub>O. For plasmids encoding antibody HCs, the sequencing primers pSEC-CMV, pSEC-PolyA and pSEC-CH1 were used. For plasmids encoding antibody LCs, primers pSEC-CMV and pSEC-PolyA were employed. Sequencing of the samples was carried out by Eurofins Genomics Germany GmbH (Ebersberg, Germany). Results were analyzed using GeneStudio software.

#### 2.2.1.6 Transformation of Bacteria

For the transformation of Subcloning Efficiency<sup>TM</sup> DH5 $\alpha$  Competent Cells bacteria were reacted with 1 – 2 µg of plasmid DNA and set to rest on ice for 15 min. Subsequently, the bacteria were spread on an agar plate containing 50 µg/ml ampicillin using 100 µl of S.O.C. media. For the transformation of One Shot<sup>TM</sup> TOP10 Chemically Competent *E. coli*, 1.5 µl of plasmid DNA were added to the bacteria. The suspension was placed on ice for 30 min, followed by a heat shock at 42° C for 30 sec with subsequent transfer into 250 µl of S.O.C. media. After incubation in a shaking incubator at 37° C at 225 rpm for 1 h, the transformation mixtures were spread on agar plates supplemented with 50 µg/ml of ampicillin. Agar plates were incubated at 37° C until the next day and subsequently stored at 4°C.

#### 2.2.1.7 Amplification of Plasmid DNA in Bacteria

For the amplification of plasmids in *E. coli*, single colonies of plasmid-transformed bacteria were transferred into round-bottom tubes containing 3 ml of LB media supplemented with 50  $\mu$ g/ml of ampicillin (referred to as mini-culture). The cultures were then incubated at 225 rpm in a shaking incubator at 37° C overnight. For larger scale preparations, mini-cultures were transferred to Erlenmeyer flasks with baffle containing 300 ml of LB media supplemented with 50  $\mu$ g/ml of ampicillin after 6 – 8 h of incubation at 37° C (referred to as maxi-culture). Incubation was subsequently carried out at 225 rpm in a shaking incubator at 37° C overnight.

#### 2.2.1.8 Isolation of Plasmid DNA from Bacteria

For the isolation of plasmid DNA from  $E.\ coli$  expanded in mini-cultures, NucleoSpin® Plasmid EasyPure kit was employed following the manufacturer's protocol. Isolation of plasmid DNA from  $E.\ coli$  expanded in maxi-cultures was performed using NucleoBond® Xtra Maxi kit according to the manufacturer's instructions. In deviation from the manufacturer's protocol, plasmid DNA was eluted in 500 - 600  $\mu$ l of dH<sub>2</sub>O. Purified plasmid DNA was stored at -20° C.

#### 2.2.1.9 Spectrophotometric Analysis

The concentration and the purity of plasmids, as well as the concentration of purified antibodies was analyzed with the spectrophotometer Nanodrop 2000c. In case of plasmid DNA, 1  $\mu$ I of the probes was loaded and the concentration was determined by measuring the absorbance (A) at 260 nm and 280 nm. The ratios of A<sub>260 nm</sub>/A<sub>280 nm</sub> and A<sub>260 nm</sub>/A<sub>230 nm</sub> were used to determine the purity of the plasmid DNA and were expected to show readings of 1.8 – 2.0 and > 2, respectively. To estimate the concentration of fractions of eluted antibodies, 2  $\mu$ I of the samples were loaded and measured at A<sub>280 nm</sub>. For all measurements the respective solvent was used as reference.

#### 2.2.1.10 Purification of Antibodies

Recombinant antibodies were purified from the cell culture supernatant by affinity chromatography. For this purpose, CaptureSelect<sup>TM</sup> IgG-C<sub>H</sub>1 affinity matrix was stirred into the collected cell culture supernatant at  $4^{\circ}$  C overnight in a ratio of 1:1000 according to the manufacturer's instructions. The following day, the antibody-bound matrix particles were concentrated by centrifugation to a volume of 5-10 ml and loaded on a Poly-Prep<sup>®</sup> Chromatography Column. The matrix was rinsed twice with 10 ml of PBS. Antibodies were then eluted by adding elution buffer (0.1 M glycine, pH 3) to the column, using 1 ml each to collect 10 fractions. To restore the pH of 7.4, the elution buffer was immediately neutralized with 250  $\mu$ l of neutralization buffer (1 M Tris, pH 8). The concentration of protein in each individual elution fraction was then estimated spectrophotometrically. Depending on the concentration of the protein, fractions were transferred either individually or combined into ZelluTrans regenerated cellulose dialysis tubes and dialyzed against at least  $10^5$  times the volume of PBS at  $4^{\circ}$  C. After 48-72 h, the purified antibodies were removed from the dialysis tubes, sterile filtered with syringe driven 0.2  $\mu$ m filter units and stored at  $4^{\circ}$ C until further use.

#### 2.2.1.11 Concentration and Purity of Antibody Preparations

The concentration of recombinant antibodies was determined by capillary electrophoresis. To this, the 2100 Bioanalyzer and the corresponding Agilent Protein 230 Kit were used following the manufacturer's recommendations. Samples were applied to the protein chip in a reduced and a non-reduced formulation. Reduction of the antibodies was achieved with the buffers provided with the kit and using DTT as reduction agent. Concentrations of antibody preparations were then determined from the capillary electrophoresis of the reduced sample and purity was defined as the proportion of the antibody HCs and LCs to the total amount of protein.

#### 2.2.1.12 Sodium Dodecyl Sulfate Polyacrylamide Gel Electrophoresis

Sodium dodecyl sulfate (SDS) gels were prepared according to published methods (table 16) (Sambrook and Russell, 2000). Reducing or non-reducing Laemmli SDS sample buffer was added to each of the proteins to be analyzed. Probes were denatured (5 min, 95° C) and, after brief centrifugation, loaded into the gel pockets. The discontinuous gel used for reduced proteins consisted of a stacking gel for concentration of the applied samples and a resolving gel with a polyacrylamide (PAA) content of 10% or 12% for separation of the proteins. For electrophoresis of non-reduced proteins, 4 - 15% Mini-PROTEAN® TGX™ PAA gels were used. Precision Plus Protein™ WesternC™ Blotting Standards or PageRuler<sup>™</sup> Plus Prestained Protein Ladder functioned as molecular weight reference. Electrophoresis was conducted in Mini-PROTEAN® Tetra Cells at initially 80 V until the dye front reached the resolving gel, then at 140 V for 60 – 90 min. Gels were subsequently used for western transfer experiments or Coomassie Blue staining was performed. Therefore, gels were soaked in Coomassie Blue staining solution (table 4) overnight on an orbital shaker at room temperature. On the next day, gels were decolorized with dH2O and the visualized protein bands were documented using a bizhub C3351 scanner.

Table 16: Composition of 10% and 12% SDS gels.1

Solution	Stacking gel	Resolving gel 10%	Resolving gel 12%
dH₂O	2.7 ml	4.0 ml	3.3 ml
Acrylamide / bisacrylamide 30%	670 μl	3.3 ml	4.0 ml
1.5 M Tris (pH 8.8)	-	2.5 ml	2.5 ml
1.0 M Tris (pH 6.8)	500 µl	-	-
SDS 10%	40 µl	100 μΙ	100 µl
APS 10%	40 µl	100 µl	100 μΙ
TEMED	4 µl	4 μΙ	4 μl

<sup>&</sup>lt;sup>1</sup> Quantities for two gels, modified from Sambrook and Russell, 2000.

#### 2.2.1.13 Western Transfer Experiments

Western transfer experiments were performed to detect specific proteins separated by SDS-PAGE. After completion of the gel run, protein bands were transferred from SDS gels to 0.2 µm nitrocellulose membranes at 1.0 A and 25 V for 30 min using the Trans-Blot<sup>®</sup> Turbo<sup>™</sup> Transfer Pack and the corresponding Trans-Blot<sup>®</sup> Turbo<sup>™</sup> transfer system according to the manufacturer's instructions. Free binding sites were saturated by incubating the membrane in blocking solution (anti-human IgG-Fc blot; table 4) overnight on an orbital shaker. Horseradish peroxidase (HRP)-conjugated antibodies were then applied to specifically detect antibody HCs or LCs. To detect the antibody HCs, goatanti-human IgG-HRP antibodies (Fc specific) were added at a dilution of 1:5000. Membranes were then incubated on an orbital shaker for 1 h at room temperature, washed three times for 10 min with TBST buffer (table 4) and were subsequently available for visualization. To detect the antibody LCs, membranes were washed tree times with TBST buffer for 10 min each and subsequently set to rest in staining solution (anti-human Ig-kappa LC blot; table 4) supplement with 1:2500 of goat anti-human kappa light chain:HRP for 1 h at room temperature on an orbital shaker. The membrane was then washed three times for 10 min each with TBST, then once for 10 min with TBS and was subsequently available for visualization.

To visualize the stained proteins by chemiluminescence, Immobilon<sup>™</sup> Western Chemiluminescent HRP Substrate was applied and a digital image was generated immediately with the Fusion SL imaging system.

#### 2.2.1.14 Size Exclusion Chromatography

To verify the absence of multimers and aggregates of the generated recombinant antibodies,  $100 - 400 \,\mu g$  of the antibody preparations were loaded on a Superdex<sup>TM</sup> 200 Increase 10/300 GL column in an AEKTApure protein purification system. Analysis was performed at a flow speed of 75 ml/min and PBS was used as running buffer. Due to the differences in the proteins' retention time depending on their molecular weight, their elution from the column occurs in ascending order of size. For analysis of the molecular weight of proteins,  $UV_{280 \, nm}$  absorption was subsequently plotted against the elution volume using the Unicorn<sup>TM</sup> 7.5 software. Following the same procedure, thyroglobulin (669 kDa), ferritin (440 kDa), conalbumin (75 kDa), ovalbumin (43 kDa) and trastuzumab (145 kDa) were analyzed as molecular weight controls.

#### 2.2.2 Cell Biology Techniques

#### 2.2.2.1 Cell Culture

Cell lines were cultivated in  $25 \text{ cm}^2 - 175 \text{ cm}^2$  sterile cell culture flasks in a humidified atmosphere at  $37 \,^{\circ}$  C and  $6\% \, \text{CO}_2$  (standard conditions) in the corresponding cell culture media (table 6). Depending on their confluence, cells were passaged two to three times per week. Suspension cells were passaged in a ratio of 1:1 - 1:5, adherent cells were treated with Accutase and subsequently passaged in a ratio of 1:5 - 1:20. After staining dead cells with Trypan blue solution, the concentration of cells was determined using a Neubauer-improved counting chamber and calculated according to the following formula:

Concentration of cells 
$$\left(\frac{cells}{ml}\right) = \frac{\sum cells\ counted}{\sum quadrants\ counted} \times dilution\ factor \times 10^4$$

#### 2.2.2.2 Transfection of Mammalian Cells

#### 2.2.2.1 Calcium Phosphate Transfection

For the generation of recombinant antibodies, Lenti-X<sup>TM</sup> 293T cells (referred to as Lenti-X cells) were transfected by calcium phosphate transfection with chloroquine as published (Sambrook and Russell, 2000). In brief,  $3 \times 10^6$  Lenti-X cells were seeded in 10 cm cell culture plates and allowed to settle at standard conditions overnight. On the following day, cells were co-transfected with 10  $\mu$ g each of the expression vectors encoding the antibody HC and LC in 1 ml of HBS buffer (table 4) containing 100  $\mu$ l of CaCl<sub>2</sub> and 5  $\mu$ l of chloroquine. After 9 – 10 h of incubation at standard conditions, the cell culture medium was changed to fresh D10<sup>+</sup> medium and cells were incubated for further 48 h at standard conditions. Subsequently, the cell culture supernatant containing

the antibodies expressed by transfected Lenti-X cells was collected every 24 h for six days, stored at 4° C and sterile filtered until purification of the antibodies was performed.

## 2.2.2.2 Lipofectamine Transfection

To achieve transient expression of cell surface antigens, transfection of CHO-K1 cells was performed with Lipofectamine  $^{\otimes}$  & PLUS<sup>TM</sup> Reagent. Five hundred thousand CHO-K1 cells were plated out on 6 well cell culture plates in 3 ml of D10 $^{+}$  medium and incubated at standard conditions for 24 h. On the following day, the cell culture medium was changed to 2 ml of fresh D10 $^{+}$  medium. Per well, 500 µl of OPTI-MEM $^{\otimes}$  I medium were mixed with 2.5 µg of plasmid DNA and 2.5 µl PLUS reagent and incubated for 5 min at room temperature. Then, 6.25 µl of Lipofectamine were added and the solution was incubated at room temperature for further 30 min. The transfection mix was then applied to the CHO-K1 cells and the plates were set to rest for 48 – 72 h at standard conditions before cells were harvested for subsequent experiments.

#### 2.2.2.3 Flow Cytometry

Flow cytometry experiments were performed on a FACScalibur<sup>TM</sup> device. CellQuest Pro and FlowJo were used to analyze the results. Dead cells, debris or cell conjugates were excluded by applying appropriate scatter gates and  $1 \times 10^5$  events were counted.

#### 2.2.2.3.1 Cell Surface Antigen Expression

To analyze the display of cell surface antigens, cells were treated with antibodies coupled to a fluorescent dye. The antibodies were diluted as recommended in 50 µl of PBA buffer, cells were stained for 1 h at 4° C in the dark. Subsequently, cells were washed, resuspended in PBA buffer and analyzed in the flow cytometer. To quantify the amount of cell surface antigens, Qifikit was used following the manufacturer's guidelines. For this purpose, cells were incubated with 20 µg/ml of non-conjugated murine antibodies specific for the antigen of interest in 50 µl of PBA buffer containing 1 mg/ml of pooled human Ig (Gamunex 10%, 100 mg/ml) for 1 h at 4° C. Subsequently, samples were washed with PBA buffer and the cells, as well as the calibration beads provided with the kit, were incubated in 50 µl of a 1:50 dilution of fluorescein isothiocyanate (FITC)-coupled secondary antibodies in PBA buffer containing 1 mg/ml of pooled human Ig (Gamunex 10%, 100 mg/ml) for 30 min at 4° C in the dark. The samples were then washed with PBA buffer, resuspended in PBA buffer and analyzed for binding by flow cytometry. Specific antibody binding capacities (SABC) were calculated following the manufacturer's instructions using Microsoft Excel 2016.

#### 2.2.2.3.2 Binding of Recombinant Antibodies

Binding of antibodies was evaluated in indirect immunofluorescence assays. To this, cells were reacted with 50  $\mu$ g/ml of antibodies in 50  $\mu$ l of PBA buffer for 60 min at 4° C. Cells were washed with PBA buffer and incubated in 30  $\mu$ l of a 1:20 dilution of F(ab')<sub>2</sub> fragments of goat anti-human IgG, Fc $\gamma$  fragment specific antibodies in PBA buffer for 30 min at 4° C in the dark. Cells were then washed, resuspended in PBA buffer and flow cytometry analysis was performed.

#### 2.2.2.3.3 Binding of Soluble HLA Molecules

To analyze the binding of HLA molecules, cells were stained with fluorescence-conjugated, soluble HLA class I molecules (table 12) following the recommendations by the manufacturers, washed with PBA and analyzed for binding using flow cytometry. To analyze the ability of antibodies produced in house to impede receptor ligation by HLA class I molecules, cells were pre-treated with 50 µg/ml of the respective antibodies in 20 µl of PBA buffer for 1 h at 4° C, before 3 µl of phycoerythrin (PE)-conjugated MHC I Dextramer® of CMV pp65 peptide (NLVPMVATV)-loaded HLA-A\*0201 (table 12) were added. Cells were incubated in the dark at 4° C for 30 min, washed with PBA and analyzed for binding by flow cytometry. Mean fluorescence intensity (MFI) values obtained with a control antibody were set to 100% and relative binding of the HLA dextramer was determined.

## 2.2.2.4 Isolation of Mononuclear Cells from Peripheral Blood

Experiments were performed with permission of the Ethics Committee of the faculty of medicine, LMU Munich (18-821, 21-0816) after receiving written informed consent of study participants. Leukoreduction system chambers or citrate-buffered peripheral blood samples were used as a source of mononuclear cells (MNC) from healthy individuals or lymphoma patients, respectively. Samples were either diluted with PBS or used undiluted and 9 – 10 ml were slowly stacked on 6 – 20 ml of Ficoll® Paque Plus. MNCs were subsequently separated by density gradient centrifugation from erythrocytes and granulocytes (20 min, 20 °C, 1460 g). MNCs were collected and washed with PBS for three times. Hypotonic lysis of remaining erythrocytes was carried out, if necessary, by resuspending cells in 45 ml of ice cold dH<sub>2</sub>O for 30 sec. The lysis was terminated by adding 5 ml of 10 X PBS. Cells were then washed with PBS for one more time and the cell count per ml was determined.

#### 2.2.2.5 Generation of Macrophages

To generate human macrophages,  $60 \times 10^6$  MNCs isolated from leukocyte reduction systems were seeded in 75 cm<sup>2</sup> Nunc EasYFlask cell culture flasks in 5 ml of monocyte attachment medium and incubated at standard conditions for 10 min to isolate monocytes by plastic adherence. Attached cells were then washed intensively with PBS for three times to remove non-adherent cells and cultured in X-Vivo<sup>™</sup> 15 medium supplemented with 0.5% Pen/Strep (v/v) at standard conditions. The next day, cells were washed again with PBS for three times and cultured in X-Vivo<sup>TM</sup> 15 medium containing 0.5% Pen/Strep (v/v) and cytokines. For the generation of non-polarized M0 macrophages, monocytes were kept in X-Vivo<sup>™</sup> 15 medium containing 0.5% Pen/Strep and, unless stated otherwise, 50 ng/ml of macrophage colony-stimulating factor (M-CSF) for seven days. In individual assays, 10 ng/ml of granulocyte-macrophage colonystimulating factor (GM-CSF) were applied instead of M-CSF. Unless otherwise indicated, polarization towards an M1 phenotype was achieved by exposing monocytes to GM-CSF (10 ng/ml) for six days, followed by activation with IFN-γ (10 ng/ml) and LPS (100 ng/ml) for additional 48 h. To obtain M2 macrophages (M2c subtype), monocytes were cultured in X-Vivo<sup>™</sup> 15 medium containing 0.5% Pen/Strep and 50 ng/ml of M-CSF. After six days, 10 ng/ml of IL-10 were added for further 48 h.

Macrophages were detached by treatment with Accutase as recommended by the manufacturer.

#### 2.2.2.6 Analysis of Antibody-Dependent Cellular Phagocytosis

#### 2.2.2.6.1 Fluorescence Microscopy

Twenty thousand macrophages were seeded on μ-Slides in 300 μl of X-Vivo 15<sup>TM</sup> medium containing 0.5% Pen/Strep (v/v) and the respective cytokines used for the polarization of the individual macrophage phenotype. Cells were allowed to settle for at least 1 h at standard conditions. One hundred microliters of the medium were removed and 10 μg/ml of each of the indicated antibodies were applied. Forty thousand lymphoma cells, labeled with carboxyfluorescein succinimidyl ester (CFSE) as per the manufacturer's instructions, were added to the macrophages in 100 μl of X-Vivo 15<sup>TM</sup> medium supplemented with 0.5% Pen/Strep (v/v). Cells were co-incubated for 2 h at standard conditions. Subsequently, non-phagocytozed lymphoma cells were cleared away by changing the supernatant to 300 μl of fresh X-Vivo 15<sup>TM</sup> medium supplemented with 0.5% Pen/Strep (v/v). Phagocytosis was then quantified by inspecting 50 – 100 randomly selected macrophages for engulfed green fluorescenting lymphoma cells by

fluorescence microscopy (1000x magnification, immersion oil). Phagocytic index values were determined according to the following formula:

$$Phagocytic\ index\ =\ \frac{\sum engulfed\ lymphoma\ cells}{\sum inspected\ macrophages}\ \times\ 100$$

In some experiments, macrophages were labeled with CellBrite Orange Cytoplasmic Membrane Labeling Dye and nuclei were stained with Hoechst 33342 NucBlue Live ReadyProbes. Cells were either stained in a two-step approach starting with staining in 100 µl of X-Vivo 15<sup>TM</sup> medium containing 0.5% Pen/Strep (v/v) and 0.5% CellBrite Orange Cytoplasmic Membrane Labeling Dye for 10 min at standard conditions, before washing the cells twice with X-Vivo 15<sup>TM</sup> medium containing 0.5% Pen/Strep (v/v) and staining in 100 µl of X-Vivo 15<sup>TM</sup> medium containing 0.5% Pen/Strep (v/v) and two drops per ml of Hoechst 33342 NucBlue Live ReadyProbes for 20 min at room temperature. Alternatively, cells were stained in a one-step approach in 150 µl of X-Vivo 15<sup>TM</sup> medium containing 0.5% Pen/Strep (v/v), 0.5% CellBrite Orange Cytoplasmic Membrane Labeling Dye and two drops per ml of Hoechst 33342 NucBlue Live ReadyProbes for 15 min at standard conditions. Subsequently, the medium was changed to X-Vivo 15<sup>TM</sup> medium supplemented with 0.5% Pen/Strep (v/v).

Analysis for target cell engulfment and photography of the cells were performed on an Axio Observer D1 fluorescence microscope. Photography was performed using the AxioCam MRm camera and AxioVs 40 software.

#### 2.2.2.6.2 Live Cell Imaging

Forty thousand human macrophages were plated on 96 well cell culture plates in 50 μl of X-Vivo 15<sup>TM</sup> medium containing 0.5% Pen/Strep (v/v) and the respective cytokines used for the polarization of the individual macrophage phenotype. Cells were set to rest at room temperature for 30 min to ensure equal distribution and subsequently incubated for at least 1 h at standard conditions to achieve attachment of macrophages. Antibodies were then applied as indicated. The pH-sensitive cell labeling dye pHrodo® Red provided with the pHrodo® Red Cell Labeling Kit for Incucyte® Phagocytosis Assays was applied to lymphoma cells at a concentration of 500 ng/ml before target cells were incubated at standard conditions for 1 h as recommended by the manufacturer. Lymphoma cells were then washed once with the respective cell culture medium before 8 × 10<sup>4</sup> lymphoma cells were seeded per well in 50 μl of X-Vivo 15<sup>TM</sup> medium containing 0.5% Pen/Strep (v/v) to the macrophages. After removal of all air bubbles, four images were generated per well every 30 min over a period of four to eight hours with the IncuCyte® live cell imaging system. The red fluorescence intensity of the PHrodo® Red cell labeling dye increases

upon phagocytosis, which allows discrimination of phagocytozed cells from cells in the supernatant. The Incucyte 2020B software was used to determine the red object count per image and the settings were adjusted to exclude non-phagocytozed lymphoma cells in the supernatant.

To determine macrophage-mediated cancer cell depletion from the supernatant, lymphoma cells labeled with CFSE were co-incubated with macrophages and the indicated antibodies in 8 well μ-slides for 2 h as explained earlier. The supernatant was then removed carefully avoiding disturbance of the adherent macrophages and 100 μl of the supernatant were transferred to each of two wells of a 96-well plate. Cells were pelleted by centrifugation and quantified by analysis of nine images per well with the lncuCyte® system. Mean values were calculated, relative residual numbers of lymphoma cells were calculated by normalizing data to the control assay without antibody treatment and the extent of target cell depletion was determined.

#### 2.2.2.7 Statistical and Graphical Analysis

GraphPad Prism 8.0.2 and 10.1.1 software were used for graphical and statistical analysis. To detect statistically significant differences, two-sided Student's t-test, one-way or two-way ANOVA with Šidàk´s, Tukey's or Fisher's post-test were used as indicated. The Pearsons correlation test was employed to assess the correlation between the ratio of cell surface antigen expression and sensitivity to ADCP of lymphoma cells. P-values  $\leq$  0.05 were regarded statistically significant and standard deviation (SD) or standard error of the mean (SEM) are indicated.

## 3. Results

The receptors for HLA class I LILRB1 and LILRB2 are promising emerging targets for immune checkpoint therapy of cancer. However, whether LILRB1 and LILRB2 contribute to the regulation of CD20 antibody-mediated ADCP of lymphoma cells by macrophages is currently not known and was thus investigated in this thesis. To this, expression vectors for light and heavy chains of an Fc-silent anti-LILRB2 antibody with abrogated FcγR binding were cloned. This antibody and an IgGσ antibody against LILRB1, for which expression vectors were already available in the working group, were expressed, purified and analyzed for their binding specificity and ability to block receptor ligation. The generated anti-LILRB1 and anti-LILRB2 antibodies were then analyzed alone or in combination with an Fc-silent CD47 antibody derived from magrolimab for their potential to enhance the CD20 antibody-mediated macrophage phagocytosis of lymphoma cell lines and of freshly isolated CLL or MCL cells from patients.

# 3.1 Influence of HLA Class I Expression on ADCP of Lymphoma Cells

## 3.1.1 Sensitivity of Different Lymphoma Cell Lines to ADCP

Intending to identify key determinants of the phagocytosis of lymphoma cells, the sensitivity of different B-NHL cell lines to ADCP by macrophages was analyzed. Monocytes were isolated from the peripheral blood of healthy donors, differentiated to non-polarized M0 macrophages and co-incubated with the lymphoma cell lines Carnaval (DLBCL), SU-DHL-4 (DLBCL), DG-75 (Burkitt lymphoma) or MEC2 (CLL). To trigger phagocytosis, the CD20 antibody rituximab was applied to the cells at the saturating concentration of 10 µg/ml and the phagocytosis was determined by fluorescence microscopy (figure 10). The cell line Granta 519 (MCL) had been analyzed previously and data were kindly provided for the analysis. With the exception of DG-75 cells, rituximab triggered ADCP of all lymphoma cell lines. However, a substantial discrepancy in efficacy was observed. Whereas SU-DHL-4 was the most susceptible cell line to ADCP by rituximab, Granta 519, MEC2 and Carnaval cells were notably less sensitive. Engagement of the myeloid inhibitory receptor SIRPa by the 'Don't Eat Me!' signal CD47 mediates an inhibitory signal in macrophages. To abrogate inhibitory signaling and thus to enhance phagocytosis, an Fc-silent version of the CD47-directed antibody magrolimab (referred to as CD47-IgGσ) with abrogated FcyR binding was generated. To this, the expression vectors pSecTag2hu5F9-HC-lgG2σ and pSecTag2-hu5F9-LC (Zeller et al., 2022) were co-transfected into Lenti-X cells and the antibody was purified from the supernatant by affinity

chromatography. Subsequently, purity, integrity and binding selectivity were verified (data not shown). CD47-IgGσ, which was unable to induce phagocytosis as a single agent, significantly enhanced ADCP of Granta 519, MEC2 and Carnaval cells by macrophages at its saturating concentration of 10 μg/ml when combined with rituximab (figure 10). No significant enhancement of ADCP was found in experiments with DG-75 or SU-DHL-4 cells. The anti-HER2 antibody trastuzumab used as IgG1 isotype control antibody was unable to trigger ADCP in all analyzed cell lines, which did not express HER2 (figure 10).

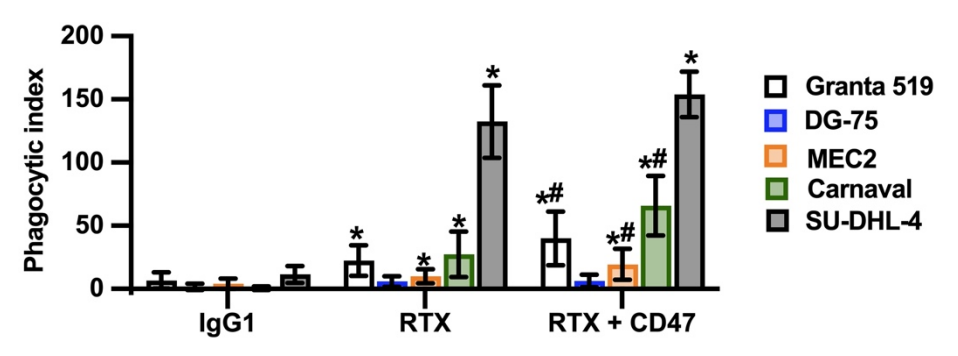


Figure 10: Sensitivity of B-NHL cell lines to ADCP. Monocytes were enriched from peripheral blood and differentiated to M0 macrophages with M-CSF. Macrophages were co-cultured with CFSE-labeled Granta 519, DG-75, MEC2, Carnaval or SU-DHL-4 cells (E:T cell ratio: 1:2) under treatment with rituximab (RTX) or co-treatment with RTX and CD47-lgG $\sigma$  (CD47). Trastuzumab (lgG1) served as control. All antibodies were tested at the saturating concentration of 10  $\mu$ g/ml. ADCP was determined by fluorescence microscopy after 2 h and phagocytic index values were calculated. Bars indicate mean values  $\pm$  SD of 8 (Granta 519), 6 (DG-75), 10 (MEC2), 11 (Carnaval) or 4 (SU-DHL-4) individual experiments. Statistically significant differences (P  $\leq$  0.05) in ADCP compared to treatment with lgG1 (\*) or RTX (#) are indicated (Two-way ANOVA with Tukey's multiple comparisons test). Results were published (Zeller et al., 2022).

### 3.1.2 Expression of CD20, CD47 and HLA Class I by Lymphoma Cells

Besides the expression level of the target antigen recognized by the FcyR-activating antibody also the expression of 'Don't Eat Me!' signals may play a role in determining the susceptibility of target cells to ADCP. Similar to CD47, a function as a 'Don't Eat Me!' signal has been reported for HLA class I molecules expressed on solid cancer cells. It was thus hypothesized that the display of HLA molecules may also hamper the phagocytosis of lymphoma cells, in particular under CD47 blockade, and may contribute to the observed differences in the sensitivity of the panel of the B-NHL cell lines to ADCP in this study. Therefore, the expression levels of the rituximab antigen CD20, the 'Don't Eat Me!' molecule CD47, classical HLA class I molecules, as well as of the non-classical HLA-G were determined for the cell lines Carnaval, DG-75, MEC2 and SU-DHL-4 by calibrated flow cytometry (figure 11). Data for Granta 519 cells were already available and included in the analysis. Expression levels of these antigens differed notably between the analyzed cell lines. Particularly high variability was observed in the

expression of CD20, which was significantly lower expressed by DG-75 cells, and the classical HLA class I molecules HLA-A, HLA-B and HLA-C, for which significantly lower expression levels were found in Carnaval and SU-DHL-4 cells relative to the other cell lines. Only minor differences were detected in the expression of CD47. Expression of HLA-G was, except for Granta 519 cells (mean value of SABC: 18292.1), barely found in DG-75 (1036.11), MEC2 (1941.28), Carnaval (625.292) and SU-DHL-4 (759.001) cells.

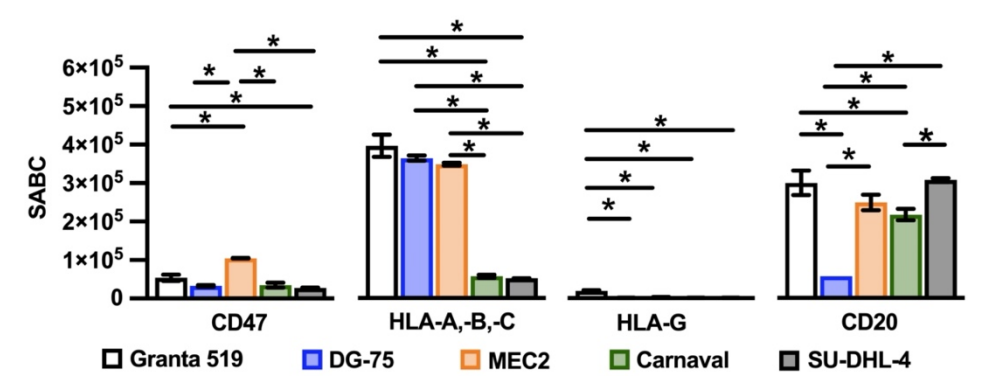


Figure 11: Surface antigen expression on B-NHL cell lines. Expression of the cell surface antigens CD47, HLA-A,-B,-C, HLA-G and CD20 on B-NHL cell lines was analyzed. B-NHL cells were immunolabeled with antibodies against the indicated antigens and specific antibody binding capacities (SABC) were quantified via flow cytometry. Bars show mean values  $\pm$  SEM of three independent experiments. Statistically significant differences are indicated (\*, P  $\leq$  0.05; one-way ANOVA with Tukey's *post hoc* test). Results were published (Zeller et al., 2022).

#### 3.1.3 Correlation Between Antigen Expression and ADCP

To analyze the influence of surface antigen expression on the sensitivity of lymphoma cells to ADCP by rituximab with concomitant CD47 blockade, correlation analysis was performed. Although no correlation was found between the sensitivity of lymphoma cells to phagocytosis mediated by the co-treatment with rituximab and CD47-IgG $\sigma$  and either the amount of displayed classical HLA class I (p = 0.087, R² = 0.6772; data not shown) or CD20 (p = 0.292, R² = 0.350; data not shown), a positive correlation was found for the ratio of CD20 to classical HLA class I expression levels (figure 12). It was thus concluded that both the quantity of CD20 molecules per cell as targets for rituximab, as well as the amount of displayed classical HLA molecules contribute to defining the sensitivity of lymphoma cells to macrophage ADCP. Thus, in this lymphoma cell line model higher amounts of CD20 in relation to lower amounts of HLA class I on lymphoma cells were associated with higher susceptibility to phagocytosis by macrophages.

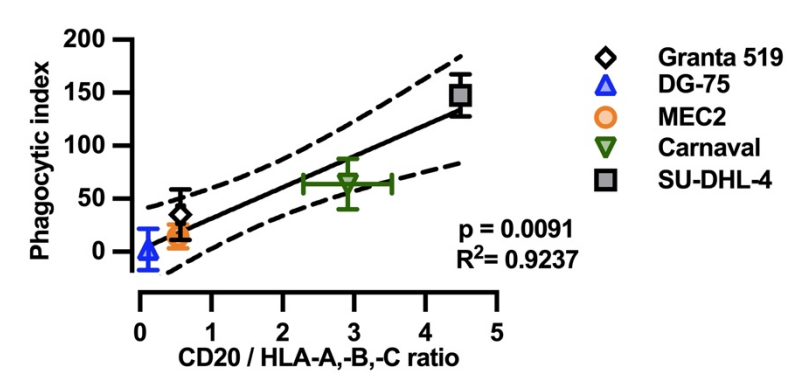


Figure 12: The expression ratio of CD20 to HLA-A,-B,-C molecules determines the sensitivity of B-NHL cell lines to ADCP mediated by rituximab plus CD47-IgGσ. For each lymphoma cell line, the mean phagocytic index value (determined from the data in figure 10) upon co-treatment with rituximab and CD47-IgGσ (vertical axis) was plotted against the expression ratio of CD20 to HLA-A,-B,-C on the cells (horizontal axis; values from figure 11). Indicated is the best-fit curve (solid line) with the 95% confidence interval (dashed lines), error bars indicate SD. Results were published (Zeller et al., 2022).

### 3.1.4 LILRB1 and LILRB2 Expression on M0 Macrophages

Besides the CD47 receptor SIRPα, macrophages carry the inhibitory receptors for HLA class I LILRB1 and LILRB2 (figure 13). Non-polarized M0 macrophages were differentiated from monocytes and the expression of antigens was determined by flow cytometry. Given the influence of HLA class I expression levels on the sensitivity of B-NHL cells to ADCP that was found, the interaction of HLA class I molecules with the inhibitory receptors LILRB1 and LILRB2 on macrophages may limit the efficacy of therapeutic antibodies to induce ADCP of lymphoma cells. It was thus hypothesized that blocking antibodies specific for LILRB1 or LILRB2 may hold the potential to further improve the phagocytosis of lymphoma cells mediated by CD20 antibodies.

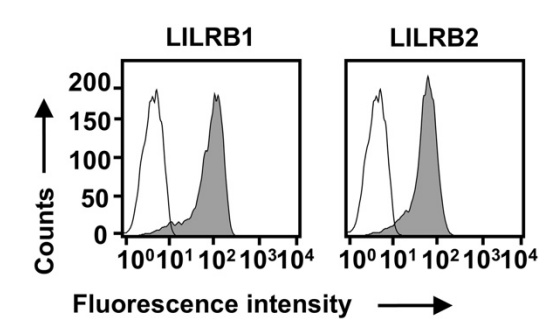


Figure 13: Expression of LILRB1 and LILRB2 on M0 macrophages. Monocytes were differentiated to M0 macrophages with M-CSF and incubated with either murine anti-LILRB1 or anti-LILRB2 antibodies (grey shaded peaks) or an isotype control antibody (black outlined peaks). To detect binding, secondary FITC-coupled antibodies specific for the murine Fc domain were applied and cells were analyzed by flow cytometry. Results from one representative experiment out of seven experiments are shown. Results were published (Zeller et al., 2022).

## 3.2 Generation of Fc-silent anti-LILRB1 and anti-LILRB2 Antibodies

To analyze the influence of HLA class I receptor blockade on the phagocytosis of lymphoma cells, monoclonal, Fc-silent antibodies specific for either LILRB1 or LILRB2 (referred to as LILRB1-IgG $\sigma$  and LILRB2-IgG $\sigma$ , respectively) with abrogated binding to Fc $\gamma$ Rs were generated.

### 3.2.1 Cloning of Expression Vectors

PSecTag2/Hygro C-derived vectors for the expression of an Fc-silent anti-LILRB1 anti-body (referred to as LILRB1-IgG $\sigma$ ) were already available in the research group. The vectors (i.e. pSecTag2-GHI/75-LC and pSecTag2-GHI/75-HC-IgG2 $\sigma$ ) contained sequences of the V<sub>L</sub> and V<sub>H</sub> domains of the antibody GHI/75 (Pulford et al., 1991, Maute et al., 2019), which were fused to constant human  $\kappa$  LC and IgG2 $\sigma$  HC regions (amino acid substitutions: V234A/G237A/P238S/H268A/V309L/A330S/P331S (Vafa et al., 2014)), respectively.

To generate expression vectors for an Fc-silent version of the LILRB2-directed antibody 19.h1 (referred to as LILRB2-IgG $\sigma$ ), DNA fragments encoding the V<sub>L</sub> and V<sub>H</sub> regions were generated *de novo* (Themo Fisher Scientific) according to published sequences (Cohen et al., 2020) and inserted into the expression vectors pSecTag2-LC (Schewe et al., 2017) and pSecTag2-HC-IgG1 $\sigma$  (C Kellner, unpublished) bearing the amino acid substitutions L234A/L235A/G237A/P238S/H268A/A330S/P331S (Tam et al., 2017) using *Nhel/Hind*III and *Nhel/Ppu*MI restriction sites, respectively.

### 3.2.2 Expression and Purification of LILRB1-IgG $\sigma$ and LILRB2-IgG $\sigma$

For the expression of Fc-silent anti-LILRB1 and anti-LILRB2 antibodies, plasmids encoding the respective antibody HC and LC were co-transfected into Lenti-X cells and affinity chromatography was performed to purify the antibodies from the supernatant. To visualize successful purification from the cell culture supernatant, SDS-PAGE was performed under reducing conditions, as exemplified for LILRB2-IgGσ in figure 14. Various bands of different electrophoretic mobility indicated that the untreated cell culture supernatant (lane 1) and the first wash fraction (lane 2) with PBS of the column holding the antibody-bound matrix particles contained multiple proteins of different molecular weights. The decrease in protein bands in the second PBS wash fraction of the column (lane 3) indicates the successful removal of unwanted protein contaminations from the column before the elution of LILRB2-IgGσ from the matrix particles. The antibody was

then eluted from the matrix particles and consecutive elution fractions were collected. Whereas the first and the second antibody elution fractions (lane 5 and 6, respectively) did not contain relevant amounts of protein, the lanes of the elution fractions three, four and five (lane 7, 8 and 9, respectively) showed two distinct protein bands at 50 kDa and 25 kDa, which were in line with the expected molecular weights of the separated antibody HCs and LCs, respectively. Similar results were obtained for LILRB1-IgG $\sigma$ . For subsequent analysis, the antibody preparations were extensively dialyzed against PBS.

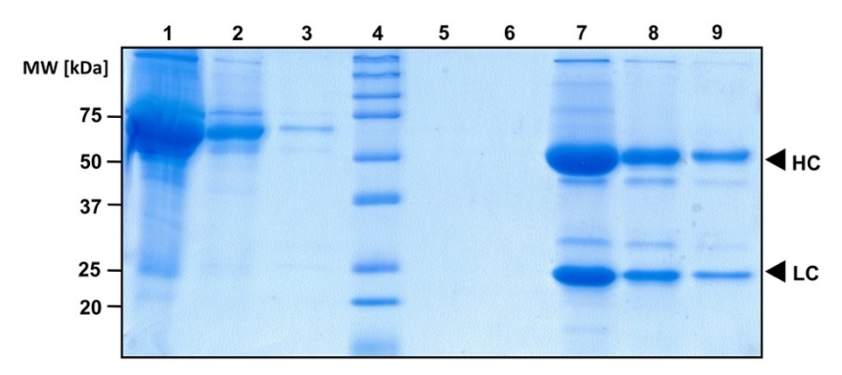


Figure 14: Purification of LILRB2-IgG $\sigma$  from the cell culture supernatant. The Fc-silent anti-LILRB2 antibody LILRB2-IgG $\sigma$  was purified from the cell culture supernatant of transfected Lenti-X cells employing the CaptureSelect<sup>TM</sup> IgG-C<sub>H</sub>1 affinity matrix. Consecutive elution fractions were collected. Aliquots of 15  $\mu$ I of the cell culture supernatant, the wash fractions and the elution fractions were transferred to a 12% PAA gel and analyzed by SDS-PAGE under reducing conditions. Proteins were visualized by staining with Coomassie blue. According to apparent molecular weights (MW), distinct protein bands of approx. 50 kDa and 25 kDa were assigned to the separated antibody heavy (HC) and light chains (LC), respectively. Assignment of the lanes: (1) cell culture supernatant, (2) wash fraction 1, (3) wash fraction 2, (4) MW standard, (5) antibody elution fraction 1, (6) antibody elution fraction 2, (7) antibody elution fraction 3, (8) antibody elution fraction 4, (9) antibody elution fraction 5.

### 3.2.3 Biochemical Characterization of LILRB1-IgGσ and LILRB2-IgGσ

To confirm purity and integrity of LILRB1-IgGσ and LILRB2-IgGσ, microfluid-based chip electrophoresis was performed (figure 15A). Under non-reducing conditions, both samples showed a distinct band of a 150 kDa polypeptide, which is in line with the molecular weight of an IgG molecule composed of two HCs and two LCs. Under reducing conditions, disulfide bonds were broken up, resulting in the separation of the antibody chains. As expected, electrophoresis of each LILRB1-IgGσ and LILRB2-IgGσ revealed two distinct bands of polypeptides with molecular weights of 25 kDa and 50 kDa, which represented the antibodies' LCs and HCs, respectively. The absence of additional bands of polypeptides indicates high purity of both antibody preparations, which exceeded 97% in both cases, as calculated using 2100 Expert software.

To specifically identify the antibody HCs and LCs, western transfer experiments were performed with LILRB1-IgGσ and LILRB2-IgGσ (figure 15B). SDS-PAGE was conducted under non-reducing or reducing conditions, proteins were blotted to membranes and HCs

and LCs were detected using HRP-conjugated antibodies specific for human HCs or LCs. Under reducing conditions, protein bands of the separated antibody HCs and LCs were observed at the expected molecular weights of 50 kDa and 25 kDa, respectively, (figure 15B) in both LILRB1-IgGσ and LILRB2-IgGσ preparations. Under non-reducing conditions, in both antibody preparations a sole protein band at 150 kDa was detected with both anti-HC and anti-LC antibodies, which is in line with the molecular weight of an assembled IgG molecule (data not shown).

Gel filtration analysis of both antibody preparations was performed to detect potentially occurring multimers or aggregates (figure 15C). The adsorption of proteins was analyzed by photometry and the molecular weight was determined based on the elution volume. Analysis revealed a sole, narrow peak for both antibody constructs at the expected molecular weight of 150 kDa. Thus, LILRB1-IgG $\sigma$  and LILRB2-IgG $\sigma$  were monomeric in solution.

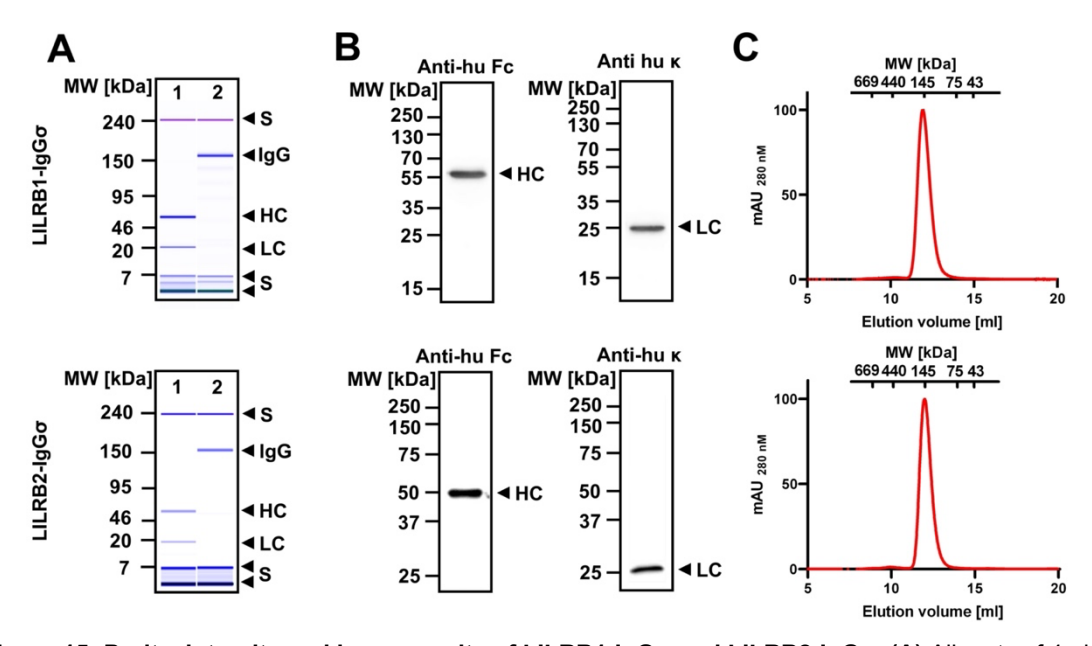
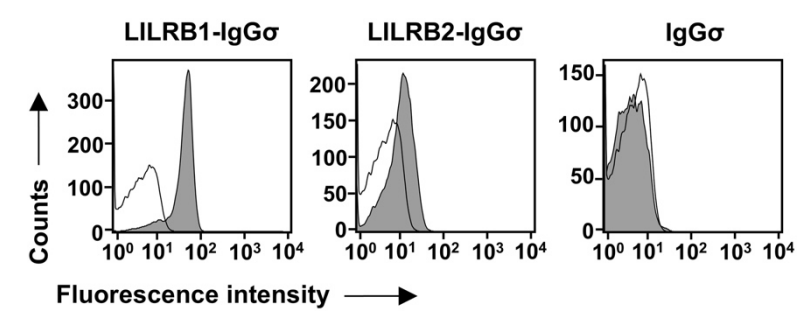


Figure 15: Purity, integrity and homogeneity of LILRB1-IgGσ and LILRB2-IgGσ. (A) Aliquots of 4  $\mu$ l of the purified antibodies were assessed by microfluid-based chip electrophoresis under reducing (lane 1) or non-reducing (lane 2) conditions. According to apparent molecular weights (MW), protein bands were allocated to separated antibody heavy (HC) or light chains (LC) or disulfide-bonded IgG molecules. (S, system peaks) (B) For western transfer assays under reducing conditions, 1  $\mu$ g of the purified antibody preparations was loaded on 12% (LILRB1-IgGσ) or 10% (LILRB2-IgGσ) PAA gels. Proteins were separated by SDS-PAGE and transferred to nitrocellulose membranes. Antibody HCs and LCs were specifically visualized using horseradish-peroxidase-conjugated Fc-specific goat anti-human-IgG (anti-hu Fc) and goat anti-human  $\kappa$  light chain (anti-hu  $\kappa$ ) antibodies, respectively. (C) LILRB1-IgGσ and LILRB2-IgGσ were analyzed by gel filtration. One hundred to 400  $\mu$ g of proteins were injected. Thyroglobulin (669 kDa), ferritin (440 kDa), conalbumin (75 kDa), ovalbumin (43 kDa) and trastuzumab (145 kDa) served as molecular weight references. Results were published (Zeller et al., 2022).

### 3.3 Binding Properties of LILRB1-IgGσ and LILRB2-IgGσ

### 3.3.1 Binding of LILRB1-IgG $\sigma$ and LILRB2-IgG $\sigma$ to Macrophages

Initially, the interaction of LILRB1-IgG $\sigma$  and LILRB2-IgG $\sigma$  with macrophages was analyzed. M0 macrophages, which express significant amounts of both LILRB1 and LILRB2 (figure 13), were treated with LILRB1-IgG $\sigma$  or LILRB2-IgG $\sigma$  and antibody binding was analyzed by flow cytometry (figure 16). As a result, both antibodies bound to macrophages, yet a greater shift in fluorescence intensity was detected in experiments with LILRB1-IgG $\sigma$ . This observation could indicate a higher affinity of the antibody for its target antigen or be due to lower expression levels of LILRB2. An in-house produced Fc-silent variant of trastuzumab specific for HER2, which is not expressed by macrophages, was used as an isotype control and did not bind to the cells.



**Figure 16: Binding of LILRB1-IgGσ and LILRB2-IgGσ to macrophages.** M0 macrophages were incubated with PBS (black outlined peaks) or 50  $\mu$ g/ml of LILRB1-IgGσ or LILRB2-IgGσ (grey shaded peaks). An Fc-silent version of trastuzumab (IgGσ) served as control. PE-conjugated F(ab')<sub>2</sub> fragments of goat antihuman Fcγ region antibodies were applied and antibody binding was analyzed by flow cytometry. Results from one representative experiment are shown (n = 3). Results were published (Zeller et al., 2022).

### 3.3.2 Antigen-Specific Binding of LILRB1-lgGσ and LILRB2-lgGσ

Specific recognition of the respective target antigen by LILRB1-IgG $\sigma$  and LILRB2-IgG $\sigma$  is essential to determine the individual impact of LILRB1 or LILRB2 antibody blockade on the phagocytosis of lymphoma cells. CHO-K1 cells, which normally do not express LILRB1 and LILRB2, were transfected with LILRB1 or LILRB2 cDNA expression vectors for transient expression of either LILRB1 or LILRB2 (referred to as CHO-LILRB1 and CHO-LILRB2 cells, respectively). The transfected cells were then employed in antibody binding studies (figure 17). Staining of CHO-LILRB1 and CHO-LILRB2 cells with commercially available, PE-conjugated antibodies specific for LILRB1 or LILRB2 confirmed successful transfection and sufficient antigen expression. CHO-LILRB1 and CHO-LILRB2 cells were then treated with LILRB1-IgG $\sigma$  or LILRB2-IgG $\sigma$  and binding was determined by flow cytometry. The experiments revealed antigen-specific binding of LILRB1-IgG $\sigma$  only to CHO-LILRB1 cells, but not to CHO-LILRB2 cells. LILRB2-IgG $\sigma$  mainly bound to CHO-LILRB2 cells, yet a minor shift in fluorescence intensity was also

detected in experiments with CHO-LILRB1 cells. This finding may indicate weak cross-reactivity of LILRB2-IgG $\sigma$  with LILRB1. An Fc-silent variant of trastuzumab, which was used as an isotype control, neither bound to CHO-LILRB1 cells nor to CHO-LILRB2 cells. None of the antibodies reacted with mock transfected CHO-K1 control cells.

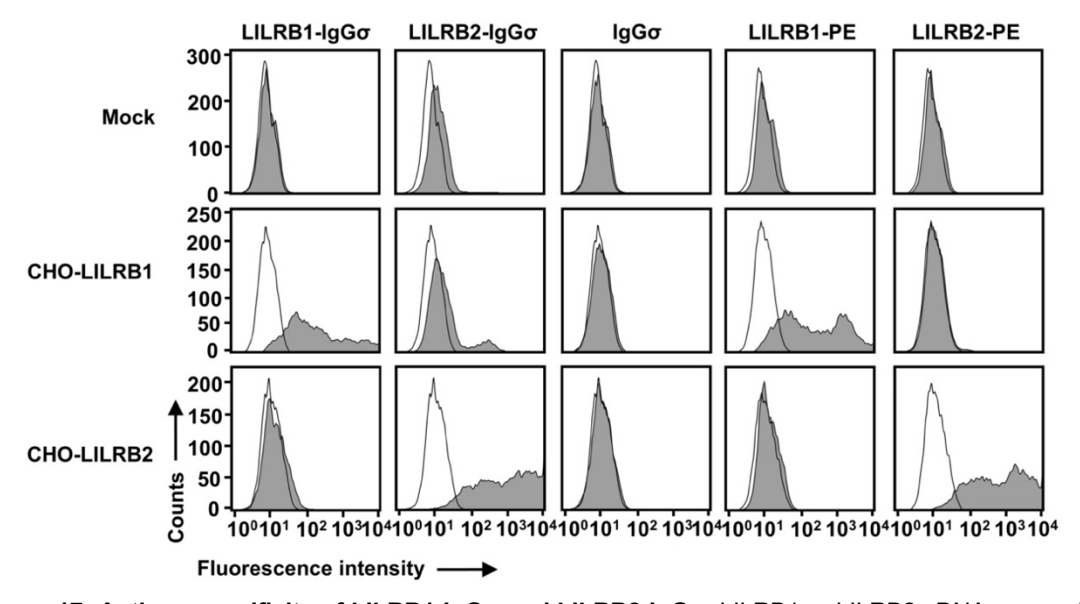


Figure 17: Antigen-specificity of LILRB1-IgGσ and LILRB2-IgGσ. LILRB1 or LILRB2 cDNA expression constructs were transfected into CHO-K1 cells to achieve transient expression of either LILRB1 or LILRB2 (referred to as CHO-LILRB1 and CHO-LILRB2 cells, respectively). CHO-LILRB1 cells, CHO-LILRB2 cells and mock transfected CHO-K1 cells (treated with transfection reagent only; Mock) were incubated with either PBS (black outlined peaks) or with 50 μg/ml of LILRB1-IgGσ, LILRB2-IgGσ or an Fc-silent version of trastuzumab (IgGσ; grey shaded peaks). Detection of antibody binding was performed with secondary PE-conjugated F(ab')₂ fragments of goat anti-human Fcγ region antibodies. To ensure sufficient cell surface expression of LILRB1 and LILRB2, commercially available, PE-conjugated anti-LILRB1 (LILRB1-PE) and anti-LILRB2 (LILRB2-PE) antibodies were employed. Cells were analyzed by flow cytometry. Representative results from one out of three performed experiments are shown. Results were published (Zeller et al., 2022).

### 3.4 Receptor Blocking by LILRB1-IgGσ and LILRB2-IgGσ

LILRB1 and LILRB2 bind different HLA class I molecules with varying affinities (Shiroishi et al., 2006b). To find a suitable reagent for blocking studies with LILRB1-IgGσ and LILRB2-IgGσ, binding of different soluble, PE-conjugated, viral peptide-loaded pentamers or dextramers of HLA-A, HLA-B and HLA-C molecules (table 12) to CHO-LILRB1 and CHO-LILRB2 cells was analyzed. CHO-LILRB1 or CHO-LILRB2 cells were stained with the soluble HLA molecules and binding was determined via flow cytometry (data not shown). All three HLA molecules bound to CHO-LILRB1 cells. The highest fluorescence intensity was detected in experiments with a PE-conjugated pentamer of HLA-C\*0702 carrying a CMV IE-1 peptide. In contrast, substantially lower fluorescence intensities were observed with CHO-LILRB2 cells. Whereas in experiments with HLA-B\*0801 and HLA-C\*0702 weak binding to CHO-LILRB2 cells was detected, a dextramer of HLA-

A\*0201 loaded with the CMV pp65 NLVPMVATV peptide efficiently bound to CHO-LILRB2 cells. Yet, the detected fluorescence intensity was lower than in experiments with CHO-LILRB1 cells. No interaction of soluble HLA peptide multimers with mock transfected CHO-K1 cells was observed, indicating that LILRB1 and LILRB2 were responsible for the binding of the HLA multimers to CHO-LILRB1 and CHO-LILRB2 cells, respectively. Since CMV pp65 peptide-loaded HLA-A\*0201 displayed binding to CHO-LILRB1 as well as to CHO-LILRB2 cells, this molecule was chosen to analyze the ability of LILRB1-IgGσ and LILRB2-IgGσ to interfere with LILRB1 and LILRB2 ligation by HLA class I, respectively. To mask receptors, CHO-LILRB1 and CHO-LILRB2 cells were pretreated with LILRB1-IgGo and LILRB2-IgGo, respectively. Cells were then reacted with HLA-A\*0201-CMV pp65 (NLVPMVATV) dextramers. Binding of the dextramers was analyzed by flow cytometry and residual binding to the cells pre-treated with LILRB1-IgGσ and LILRB2-IgGσ was determined relative to the interaction with control cells that were pre-treated with HER2-IgGσ (figure 18). LILRB1-IgGσ and LILRB2-IgGσ effectively inhibited binding of the HLA-A\*0201 dextramer to CHO-K1 cells expressing LILRB1 and LILRB2, respectively, and only minor residual binding was detectable upon antibody blockade. Thus, LILRB1-lgGσ and LILRB2-lgGσ are suitable reagents to mask LILRB1 and LILRB2, respectively.

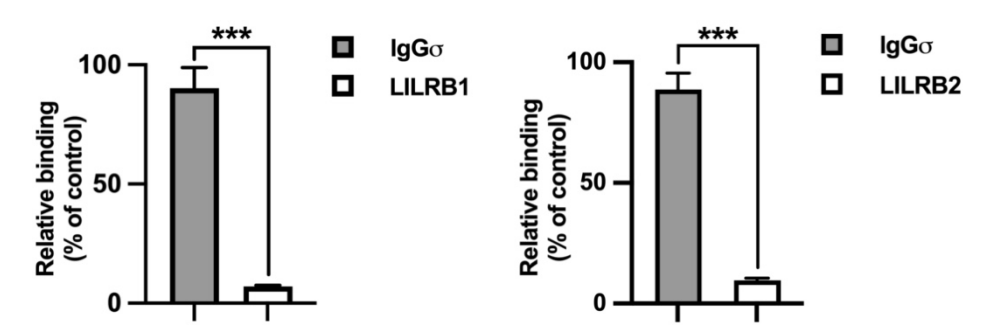


Figure 18: Disruption of receptor-ligand-interaction by LILRB1-IgGσ and LILRB2-IgGσ. CHO-K1 cells were transfected with expression constructs for either LILRB1 ( $left\ graph$ ) or LILRB2 ( $right\ graph$ ) to achieve transient display of the receptors. Cells were then incubated with 50 μg/ml of either LILRB1-IgGσ (LILRB1) or LILRB2-IgGσ (LILRB2), respectively, to block LILRB receptors. HER2-IgGσ (IgGσ) served as control antibody. To analyze the residual interaction of HLA molecules with LILRB receptors, PE-labeled MHC I Dextramer® of NLVPMVATV-peptide-loaded HLA-A\*0201 molecules were applied to the cells. Using flow cytometry, mean fluorescence intensity values were determined and residual ligation of CHO-LILRB1 and CHO-LILRB2 cells by HLA molecules relative to cells treated with the control antibody was calculated. Bars indicate mean values ± SEM of three independent experiments (\*\*\*\*, P ≤ 0.001; Student's t test). Results were published (Zeller et al., 2022).

## 3.5 Analysis of the Impact of LILRB1 or LILRB2 Blockade on ADCP in Lymphoma Cell Line Models

### 3.5.1 ADCP of Lymphoma Cell Lines upon HLA Receptor Blockade

The impact of LILRB1 or LILRB2 antibody blockade on the phagocytosis of lymphoma cells was initially analyzed with Carnaval DLBCL cells. Monocytes were differentiated to M0 macrophages, incubated with Carnaval cells in the presence of antibodies and phagocytosis was determined via fluorescence microscopy (figure 19). LILRB1-lgGσ or LILRB2-lgGσ were applied alone, together with rituximab, or with both rituximab and the CD47-lgσ antibody for concomitant CD47 blockade. When applied alone, neither LILRB1-lgGσ nor LILRB2-lgGσ induced ADCP. Also, when used in combination with rituximab, the two antibodies did not enhance ADCP significantly, although enhanced ADCP was observed in some experiments with individual macrophage preparations. However, when used together with rituximab and CD47-lgGσ, LILRB1-lgGσ, but not LILRB2-lgGσ, significantly further enhanced the uptake of Carnaval cells.

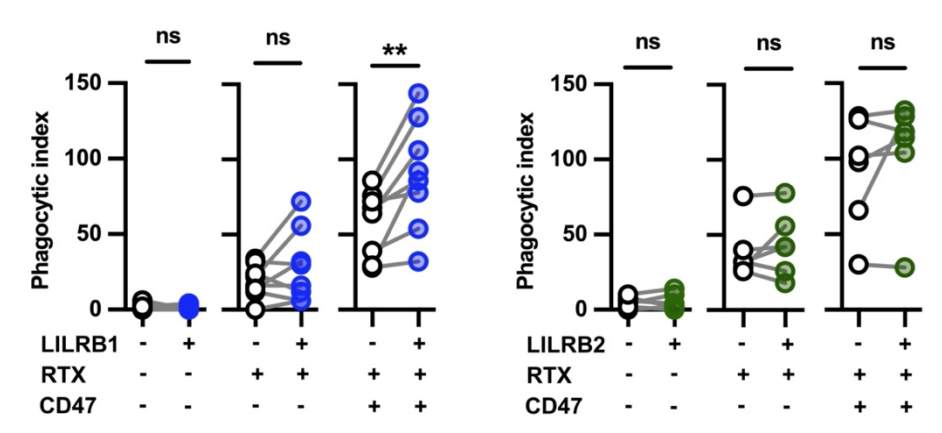
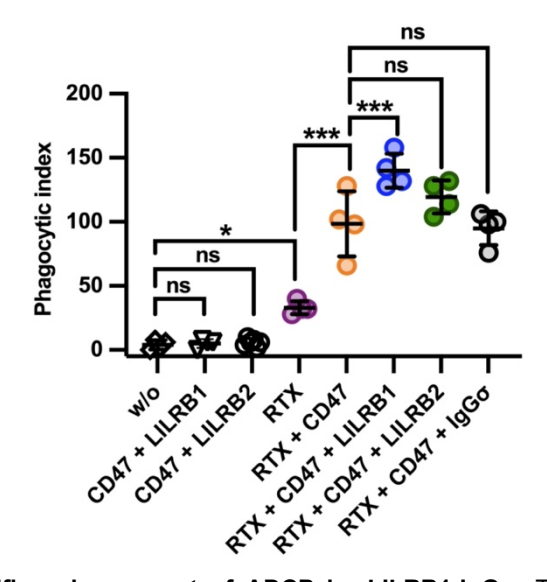


Figure 19: Impact of HLA receptor blockade on ADCP of Carnaval cells by M0 macrophages. LILRB1-IgGσ (LILRB1; *left*) and LILRB2-IgGσ (LILRB2; *right*) were tested for their impact on the phagocytosis of CFSE-labeled Carnaval cells by M0 macrophages (E:T cell ratio: 1:2). The antibodies (10 μg/ml each) were either used as a single agent, combined with rituximab (RTX) or with RTX and CD47-IgGσ (CD47). Phagocytosis was determined via fluorescence microscopy after 2 h and phagocytic index values were calculated. Data points show results obtained with individual preparations of macrophages from eight (LILRB1-IgGσ) or six (LILRB2-IgGσ) different donors (\*\*, P ≤ 0.01; ns, not significant; one-way ANOVA with Šidàk s multiple comparisons test). Results were published (Zeller et al., 2022).

To confirm an antigen-specific mechanism of action of LILRB1-IgG $\sigma$  in enhancing ADCP, an Fc-silent variant of trastuzumab (referred to as HER2-IgG $\sigma$ ) was compared to LILRB1-IgG $\sigma$  in fluorescence microscopy-based ADCP experiments with Carnaval cells and M0 macrophages (figure 20). When applied alongside with rituximab and CD47-IgG $\sigma$ , LILRB1-IgG $\sigma$  again significantly further enhanced ADCP, whereas the Fc-silent control antibody did not promote phagocytosis. Some effects were observed by adding LILRB2-IgG $\sigma$  to rituximab and CD47-IgG $\sigma$  in individual experiments, but overall statisti-

cal significance was not reached. Interestingly, ADCP of Carnaval cells was also not initiated when rituximab containing a functional Fc region was not added and only combinations of CD47-IgG $\sigma$  with LILRB1-IgG $\sigma$  or LILRB2-IgG $\sigma$  were applied. This finding indicates that even disruption of inhibitory signaling of both SIRP $\alpha$  and LILRB1 in macrophages was not sufficient to initiate the phagocytosis of lymphoma cells in the absence of Fc $\gamma$ R-engagement, which provides an activating signal.



**Figure 20: Antigen-specific enhancement of ADCP by LILRB1-IgGσ.** To verify antigen-specificity, LILRB1-IgGσ was compared to an Fc-silent variant of trastuzumab (IgGσ). Carnaval cells labeled with CFSE were co-cultured with M0 macrophages (E:T cell ratio: 1:2) without antibody treatment (w/o) or under treatment with 10 μg/ml of each of the indicated antibodies. Phagocytosis was determined by fluorescence microscopy after 2 h and phagocytic index values were calculated. Data points represent results obtained with individual preparations of macrophages from four different donors. Horizontal lines represent mean values, the error bars indicate SD (\*, P ≤ 0.05; \*\*\*\*, P ≤ 0.001; ns, not significant; one-way ANOVA with Šidàk´s multiple comparisons test). Results were published (Zeller et al., 2022).

To analyze, whether the enhancement of ADCP by LILRB1-IgGσ when added to treatment with rituximab and CD47-IgGσ is applicable also to other lymphoma cell lines, fluorescence microscopy-based ADCP experiments were performed with DG-75 Burkitt lymphoma and MEC2 CLL cells (figure 21). As observed in experiments with Carnaval cells as targets, the antibody combination of LILRB1-IgGσ, rituximab and CD47-IgGσ significantly promoted the phagocytosis of MEC2 cells compared to dual application of rituximab and CD47-IgGσ only. Of note, upon treatment with the triple antibody combination decent phagocytosis of DG-75 cells was observed. These cells hardly were engulfed even when rituximab was paired with CD47-IgGσ. Again, when an Fc-silent control antibody or LILRB2-IgGσ were applied together with rituximab and CD47-IgGσ, no improvement in phagocytosis was observed. Also, CD47 and LILRB1 or LILRB2 immune checkpoint co-blockade did not translate into the initiation of phagocytosis of MEC2 or DG-75 cells without rituximab treatment.

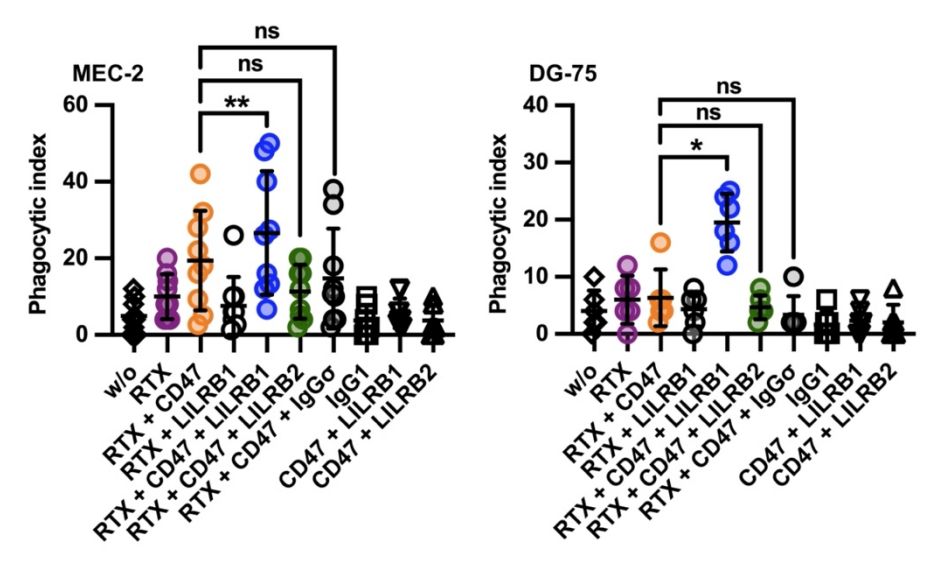


Figure 21: Enhanced ADCP of MEC2 and DG-75 cells by LILRB1-IgG $\sigma$ . MEC2 and DG-75 cells were labeled with CFSE and co-incubated with M0 macrophages (E:T cell ratio: 1:2) under treatment with the indicated antibodies or antibody combinations (10 µg/ml each; w/o, without antibody treatment) for 2 h. Fluorescence microscopy was used to determine the phagocytic index for each treatment. Trastuzumab (IgG1) and an Fc-silent version of it (IgG $\sigma$ ) were employed as controls. Data points represent results obtained with individual preparations of macrophages from ten (MEC2) or six (DG-75) different donors. Horizontal lines indicate mean values  $\pm$  SD (\*, P  $\leq$  0.05; \*\*, P  $\leq$  0.01; ns, not significant; one-way ANOVA with Šidàk s multiple comparisons test). Results were published (Zeller et al., 2022).

Similar results were observed when Granta 519 MCL cells were employed as target cells, whereas no significant improvements in ADCP were found with SU-DHL-4 DLBCL cells, which are highly susceptible to ADCP by rituximab (data not shown; experiments were performed by Dr. Sebastian Lutz in collaboration) (Zeller et al., 2022). Comparing the analyzed lymphoma cell lines, the largest fold increase in ADCP by combining rituximab and CD47-IgG $\sigma$  with LILRB1-IgG $\sigma$  was observed in experiments with DG-75 cells (figure 22). Interestingly, among the analyzed cell lines DG-75 cells had the lowest expression level of CD20 (figure 11).

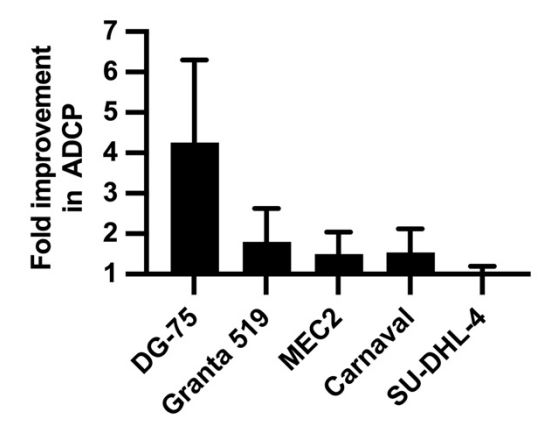
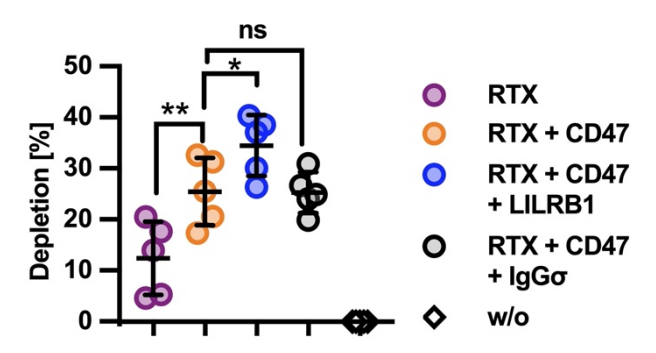


Figure 22: Fold improvement in ADCP of B-NHL cell lines by LILRB1-IgG $\sigma$ . Phagocytic index values from ADCP assays with DG-75, MEC2 and Carnaval cells (figures 20 and 21) were used to determine the increase in phagocytosis by concomitant treatment with LILRB1-IgG $\sigma$  in addition to rituximab plus CD47-IgG $\sigma$  relative to the extent of phagocytosis by rituximab and CD47-IgG $\sigma$  only. Assays with SU-DHL-4 and Granta 519 cells were performed by Dr. Sebastian Lutz in collaboration and data were kindly provided for this analysis. Bars indicate mean values  $\pm$  SD. Results were published (Zeller et al., 2022).

### 3.5.2 Depletion of Lymphoma Cells upon HLA Receptor Blockade

In fluorescence microscopy-based ADCP experiments, LILRB1-IgG $\sigma$  demonstrated efficacy to enhance the CD20 antibody-mediated macrophage phagocytosis of lymphoma cells when combined with concomitant CD47 blockade, whereas LILRB2-IgG $\sigma$  was not efficient. Next, the results obtained with LILRB1-IgG $\sigma$  should be confirmed by analyzing the depletion of lymphoma cells from the supernatant. Therefore, the IncuCyte® live cell imaging technology was newly established and employed to determine the residual remaining lymphoma cells in the supernatant after co-incubation with macrophages and treatment with antibodies (figure 23). In accordance with the previous findings, treatment with LILRB1-IgG $\sigma$  led to significantly improved depletion of Carnaval cells by M0 macrophages when applied together with rituximab and CD47-IgG $\sigma$ .



**Figure 23: Enhanced depletion of B-NHL cells by LILRB1-IgGσ**. CFSE-labeled Carnaval cells were incubated with M0 macrophages (E:T cell ratio: 1:2) and the indicated antibodies (10 μg/ml each) for 2 h. Then, the supernatant was removed, residual Carnaval cells were quantified by live cell imaging and the percentage of residual cells compared to the control assay without antibody treatment (w/o) was determined. Horizontal lines show mean values, error bars represent SD of five individual experiments (\*, P ≤ 0.05; \*\*, P ≤ 0.01; ns, not significant; one-way ANOVA with Šidàk´s multiple comparisons test; RTX, rituximab; CD47, CD47-IgGσ; LILRB1, LILRB1-IgGσ; IgGσ, HER2-IgGσ). Results were published (Zeller et al., 2022).

#### 3.5.3 Impact of LILRB1-IgGσ on IgA Antibody-Mediated ADCP

Phagocytosis experiments with Carnaval, MEC2 and DG-75 cells revealed that an activating signal in form of FcγR-engagement by rituximab is crucial for the co-inhibition of LILRB1 and CD47 to become effective. Whereas the majority of therapeutic antibodies are IgG molecules, also the IgA isotype may hold promise. CD20-directed IgA antibodies have been demonstrated to induce macrophage ADCP of lymphoma cells and the effect was further enhanced, when the antibodies were combined with CD47 blockade (Evers et al., 2021). To investigate, whether also LILRB1 blockade enhances IgA antibodymediated phagocytosis, LILRB1-IgGσ was combined with an IgA2 version of rituximab (referred to as RTX-IgA2) (figure 24). As observed with the parental antibody rituximab, RTX-IgA2 induced the phagocytosis of Carnaval cells by M0 macrophages and ADCP was further enhanced, when RTX-IgA2 was combined with CD47-IgGσ.

Again, LILRB1-IgGσ demonstrated efficacy and further boosted phagocytosis when applied together with RTX-IgA2 and CD47-IgGσ. An IgA2 version of the anti-EGFR antibody cetuximab was employed as a control and did not mediate ADCP.

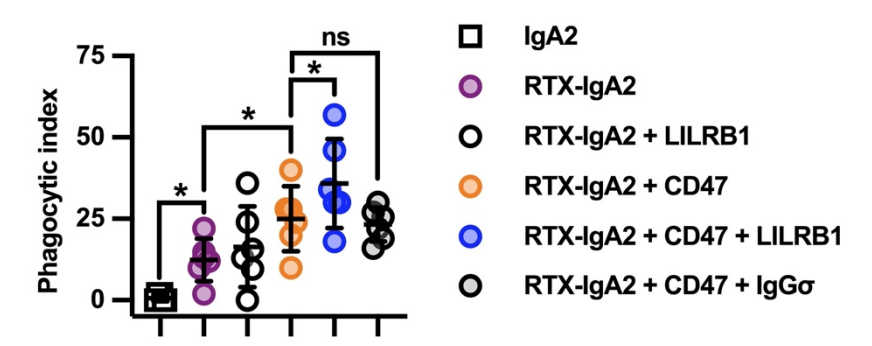


Figure 24: Co-blockade of LILRB1 and CD47 promotes ADCP by IgA antibodies. CFSE-labeled Carnaval cells were incubated with M0 macrophages (E:T cell ratio: 1:2) and an IgA2 version of rituximab (RTX-IgA2) applied as single agent or together with CD47-IgGσ and/or LILRB1-IgGσ (each antibody applied at 10 μg/ml) for 2 h. Phagocytosis was determined via fluorescence microscopy. An IgA2 version of the anti-EGFR antibody cetuximab (IgA2) and an Fc-silent version of trastuzumab (IgGσ) were employed as control. Horizontal lines represent mean phagocytic index values ± SD of six individual experiments (\*, P ≤ 0.05; ns, not significant; one-way ANOVA with Šidàk´s multiple comparisons test; LILRB1, LILRB1-IgGσ; CD47, CD47-IgGσ). Results were published (Zeller et al., 2022).

## 3.5.4 Serial Phagocytosis of Lymphoma Cell Lines upon HLA Receptor Blockade

In fluorescence microscopy-based ADCP experiments, individual M0 macrophages demonstrated the ability to engulf multiple lymphoma cells (figure 25). Particularly when rituximab was paired with both CD47-lgGσ and LILRB1-lgGσ, multiple cell ADCP by individual macrophages occurred in assays with Carnaval, Granta 519 and MEC2 cells. With DG-75 cells as targets serial phagocytosis was also observed, but to a notably lesser extent and only upon triple treatment with rituximab, CD47-lgGσ and LILRB1-lgGσ. To evaluate the relative contribution of single and multiple lymphoma cell ADCP, the analyzed phagocytic events were allocated to engulfment of the first target cell (initial phagocytosis) or to uptake of further target cells (serial phagocytosis) (figure 25). Of note, in experiments with Carnaval cells, enhancement of rituximab-mediated ADCP by immune checkpoint co-inhibition of CD47 and LILRB1 was particularly achieved by serial phagocytosis and multiple lymphoma cell uptake by individual macrophages. However, also the absolute number of macrophages, which had engulfed lymphoma cells, increased upon blockade of both immune checkpoints.

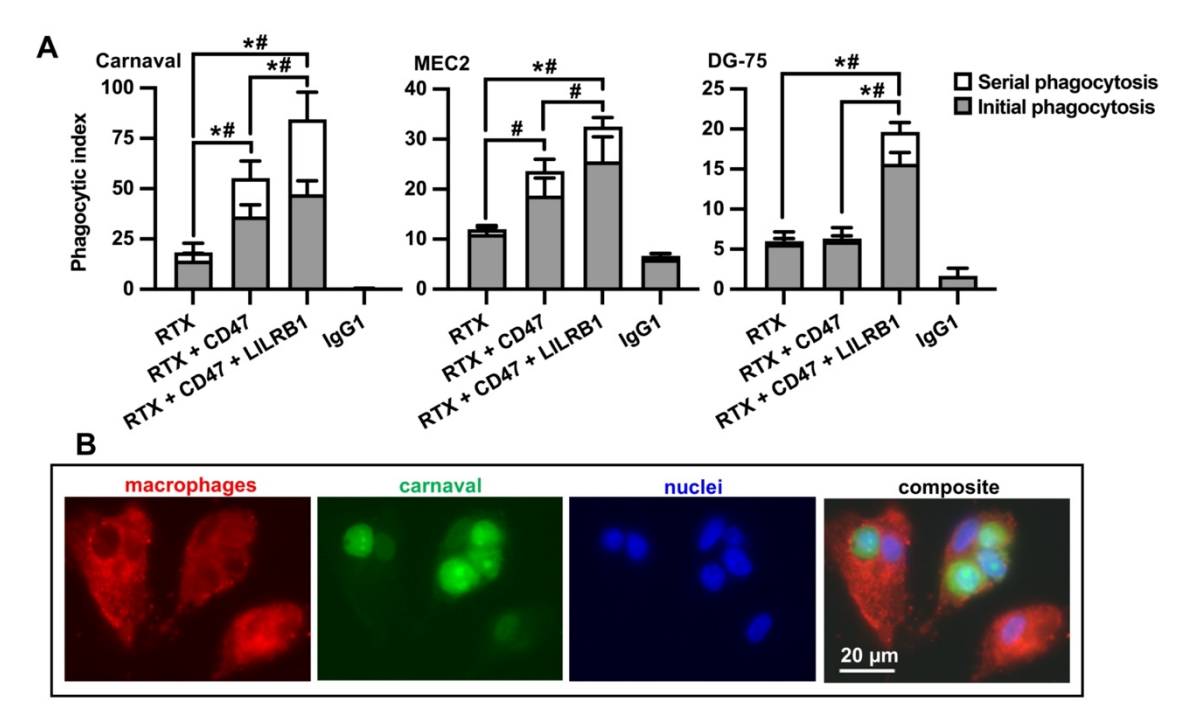


Figure 25: Serial ADCP of B-NHL cells by M0 macrophages. (A) The engulfment of multiple Carnaval (n = 9), MEC2 (n = 6) or DG-75 (n = 6) cells by individual M0 macrophages is promoted by LILRB1 and CD47 antibody co-blockade. Phagocytoses mediated by rituximab (RTX), RTX and CD47-IgGσ (CD47) or RTX, CD47-IgGσ and LILRB1-IgGσ (LILRB1) were categorized as either the initial engulfment of a lymphoma cell (initial phagocytosis) or the uptake of further lymphoma cells (serial phagocytosis) and are shown as proportions of phagocytic index values. Bars indicate mean values ± SEM. Statistically significant differences in initial (\*) and serial (#) phagocytosis event values are marked (P ≤ 0.05; two-way ANOVA with Tukey's post hoc test). (B) Carnaval cells labeled with CSFE were co-cultured with Cell Brite<sup>TM</sup> Orange-labeled M0 macrophages (E:T cell ratio: 1:2) under treatment with rituximab, CD47-IgGσ and LILRB1-IgGσ (10 μg/ml each). Images show three macrophages (red), having phagocytozed one (left macrophage), three (middle macrophage) or no (right macrophage) Carnaval cells (green). NucBlue<sup>TM</sup> was employed for the staining of nuclei (blue). Image four is a microscope composite image combining the red (first image), green (second image) and blue (third image) channel images. Results were published (Zeller et al., 2022).

### 3.5.5 Kinetics of ADCP upon HLA Receptor Blockade

The analysis of phagocytosis by fluorescence microscopy only allows for investigation at one distinct time point. To also analyze the kinetics of the initiation of ADCP by antibodies, real time, live cell imaging of macrophage phagocytosis of lymphoma cells via the IncuCyte® live cell imaging device was established. DG-75 cells were stained with the pH-sensitive dye pHrodo® Red, which is nonfluorescent at a neutral pH, and co-cultured with M0 macrophages under antibody/antibody combination treatment. When target cells are engulfed, the acidic pH in the phagolysosome causes an increase in red fluorescence of pHrodo® Red-stained cells. Red object counts per microscope image were quantified as a measure of phagocytosis and repetitive analysis of the phagocytosis was performed (figure 26). As observed in previous experiments, DG-75 cells were barely phagocytozed when rituximab or the combination of rituximab and CD47-IgGo were applied. In accordance with the findings in fluorescence microscopy-based

phagocytosis assays, LILRB1-IgGσ again significantly potentiated ADCP of DG-75 cells in live cell imaging experiments when paired with rituximab and CD47-IgGσ. Phagocytosis of DG-75 cells occurred rapidly. ADCP by LILRB1-IgGσ was already detected after 30 min and peaked after 2 h with a subsequent decrease in red object count per image. Treatment with LILRB2-IgGσ or an Fc-silent control antibody did not mediate an effect on ADCP at any time point.

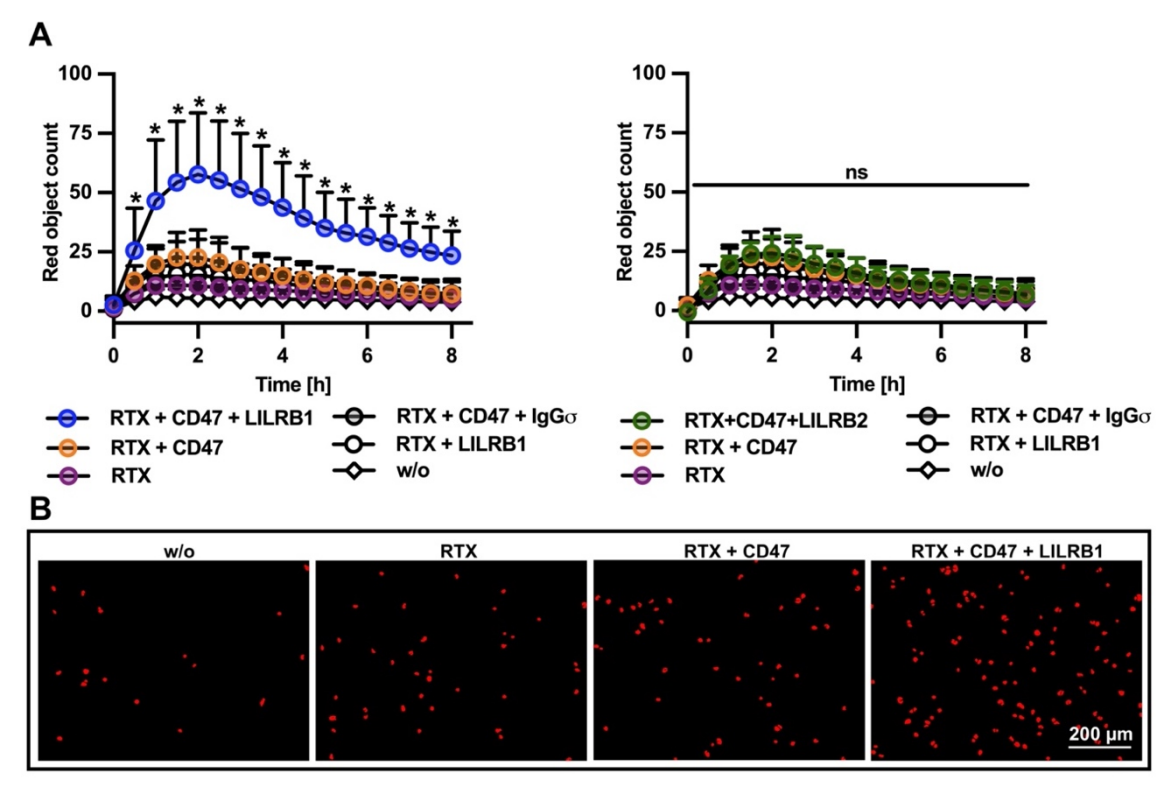


Figure 26: Kinetics of ADCP of DG-75 cells by M0 macrophages upon antibody treatment. Live cell imaging was established to determine the kinetics of ADCP induced by antibody treatment. (A) Rituximab (RTX), CD47-IgGσ (CD47) and LILRB1-IgGσ (LILRB1; *left diagram*) or LILRB2-IgGσ (LILRB2; *right diagram*) were applied alone or in combination (each at a concentration of 10 μg/ml; w/o, without added antibody) to DG-75 cells labeled with pHrodo® Red and M0 macrophages (E:T cell ratio: 1:2) from different donors (n = 9). HER2-IgGσ (IgGσ) served as control. Phagocytosis was analyzed repetitively by live cell imaging. Data points indicate means ± SD of red object count per image. Statistically significant (P ≤ 0.05) differences between the treatment groups RTX/CD47-IgGσ vs. RTX/CD47-IgGσ/LILRB1-IgGσ are indicated (\*), comparison of the treatment groups RTX/CD47-IgGσ vs. RTX/CD47-IgGσ/LILRB2-IgGσ revealed no statistically significant differences (ns; two-way ANOVA with Fisher's LSD test). (B) Shown are representative live cell imaging results of increased fluorescence of pHrodo® Red-labeled DG-75 cells engulfed by M0 macrophages upon antibody treatment. Images were taken after 1.5 h and show the control assay devoid of antibodies (*first image*), treatment with RTX (*second image*), RTX and CD47-IgGσ (*third image*) and RTX plus concomitant application of CD47-IgGσ and LILRB1-IgGσ (*fourth image*; n = 9). Results were published (Zeller et al., 2022).

#### 3.5.6 Dose-Dependent Enhancement of ADCP by LILRB1-IgGσ

To explore the dose-dependent enhancement of the phagocytosis of lymphoma cells by LILRB1-IGσ, live cell imaging phagocytosis assays were performed, in which treatment with rituximab plus CD47-IgGσ was combined with ascending concentrations of either

LILRB1-IgG $\sigma$  or HER2-IgG $\sigma$  as a control (figure 27). DG-75 cells and M0 macrophages were employed as target and effector cells, respectively. Analysis revealed that higher concentrations of LILRB1-IgG $\sigma$  led to higher rates of ADCP. When rituximab and CD47-IgG $\sigma$  were combined with 2 µg/ml or 10 µg/ml of LILRB1-IgG $\sigma$ , significantly elevated levels of ADCP were observed after 1 h of application, with 50 µg/ml of LILRB1-IgG $\sigma$  already after 30 min. Again, a peak was reached after 2 h with a subsequent decrease in red object counts. LILRB1-IgG $\sigma$  applied at 0.4 µg/ml or HER2-IgG $\sigma$  applied at any concentration were unable to enhance ADCP of DG-75 cells, which were only phagocytozed when both CD47 and LILRB1 were blocked efficiently, in agreement with previous observations.

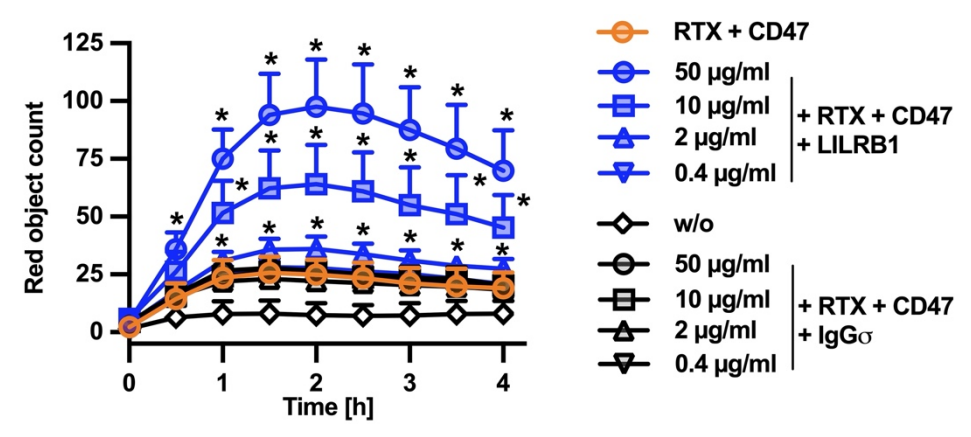


Figure 27: Dose-dependent enhancement of ADCP by LILRB1-IgGσ. DG-75 cells were labeled with pHrodo® Red and co-cultured with human M0 macrophages (E:T cell ratio: 1:2) from four different donors under treatment with rituximab (RTX) and CD47-IgGσ (CD47; each at a fixed concentration of 10 μg/ml). Either LILRB1-IgGσ (LILRB1) or the control antibody HER2-IgGσ (IgGσ) were added at corresponding ascending concentrations from 0.4 μg/ml to 50 μg/ml. Phagocytosis was determined repetitively via live cell imaging for 4 h. Data points represent means ± SD of red object count per image. Statistically significant differences between treatment groups containing LILRB1-IgGσ and HER2-IgGσ at corresponding concentrations are indicated (\*, P ≤ 0.05; two-way ANOVA with Fisher's LSD test). Results were published (Zeller et al., 2022).

## 3.5.7 Impact of Enhanced FcyR Activation on ADCP under LILRB1 and CD47 Dual Immune Checkpoint Blockade

Improvement of FcγR-engagement through antibody Fc engineering has been demonstrated to increase ADCP (Schewe et al., 2017). Therefore, it was analyzed, whether further enhancement of ADCP was achievable by combining anti-LILRB1 and CD47 antibodies with an in-house produced, Fc-engineered version of rituximab with improved affinity for FcγRs (referred to as RTX-DE) by the amino acid exchanges S239D and I332E. Phagocytosis of DG-75 cells by M0 macrophages was determined in live cell imaging phagocytosis assays under treatment with either rituximab or RTX-DE alone or together with CD47-IgGσ or CD47-IgGσ and LILRB1-IgGσ (figure 28). When rituximab or RTX-DE were combined with CD47-IgGσ, ADCP was potentiated. Importantly, dual

LILRB1/CD47 checkpoint inhibition significantly further improved both RTX-DE- and rituximab-mediated phagocytosis. Of note, 2 h after application of the antibodies, the treatment combination of RTX-DE, CD47-IgGσ and LILRB1-IgGσ was significantly more potent than CD47 and LILRB1 co-blockade combined with the native rituximab. These findings indicate that enhancement of the phagocytosis of lymphoma cells through the co-inhibition of LILRB1 and CD47 can even further be promoted by additionally optimizing effector cell recruitment through raising the affinity of the cancer cell-directed antibody for activating FcγRs.

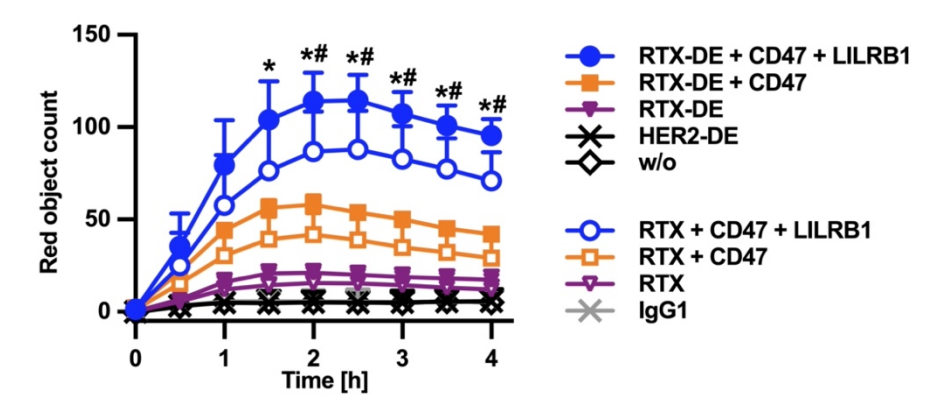


Figure 28: Further enhancement of ADCP by engineering the Fc domain of the CD20 antibody. Induction of ADCP by rituximab (RTX) or an Fc-engineered version of RTX with improved FcγR affinity (RTX-DE) was determined in four-hour live cell imaging phagocytosis experiments with pHrodo® Red-labeled DG-75 cells and M0 macrophages (E:T cell ratio: 1:2). Cells were incubated with RTX or RTX-DE alone or together with CD47-IgGσ, LILRB1-IgGσ or both (each applied at a concentration of 10 μg/ml). Trastuzumab (IgG1) and its Fc-engineered derivate HER2-DE were used in control reactions. Data points represent mean red object counts  $\pm$  SD of four individual experiments (\*, statistically significant differences between RTX-DE/CD47-IgGσ/LILRB1-IgGσ and RTX-DE/CD47-IgGσ/LILRB1-IgGσ; #, statistically significant differences between RTX-DE/CD47-IgGσ/LILRB1-IgGσ and RTX/CD47-IgGσ/LILRB1-IgGσ; P ≤ 0.05; two-way ANOVA with Fisher's LSD test). Results were published (Zeller et al., 2022).

# 3.6 Evaluation of LILRB1 or LILRB2 Blockade in Differentially Polarized Macrophages

When paired with rituximab and CD47 inhibition, LILRB1-IgG $\sigma$  enhanced the phagocytosis of different lymphoma cell lines by non-polarized M0 macrophages differentiated with M-CSF. However, macrophages are highly plastic cells that exist in a wide range of functional polarizations. To analyze the influence of LILRB1 and LILRB2 on the phagocytosis activity of polarized macrophages, monocytes were cultured in the presence of cytokines or their combinations with other stimuli to generate differentially polarized macrophages. The polarization state was verified by expression analysis of polarization marker antigens. Expression of SIRP $\alpha$ , LILRB1 and LILRB2 was analyzed and the differentially polarized macrophages were compared as effector cells in phagocytosis assays.

## 3.6.1 Expression of M1 and M2c Marker Antigens by Polarized Macrophages

Monocytes were enriched from the peripheral blood of healthy volunteers, differentiated in the presence of GM-CSF and activated with IFN-γ and LPS to generate classically activated, pro-inflammatory M1 macrophages. In parallel, monocytes were polarized with M-CSF and IL-10 to generate alternatively activated, anti-inflammatory M2c macrophages. Non-polarized M0 macrophages, obtained by the culture of monocytes from the same donor under exposure to M-CSF only, were employed as a control. M1, M2c and M0 macrophages were immunolabeled with PE-conjugated antibodies against CD14, which is a non-specific marker antigen for monocytes and macrophages, the M2 marker antigen CD163 or the M1 marker antigen CD80 (figure 29). Analysis by flow cytometry revealed prominent expression of CD14 in all three subgroups of macrophages. As expected, CD163 expression was strong in M2c macrophages and comparably low CD163 levels were detected in M1 macrophages. CD80 expression, on the other hand, was prominent in M1 macrophages, but barely detectable in M0 or M2c macrophages. These findings confirmed that the cytokine and stimuli combinations mentioned above were effective in inducing either an M1 or M2c phenotype in macrophages.

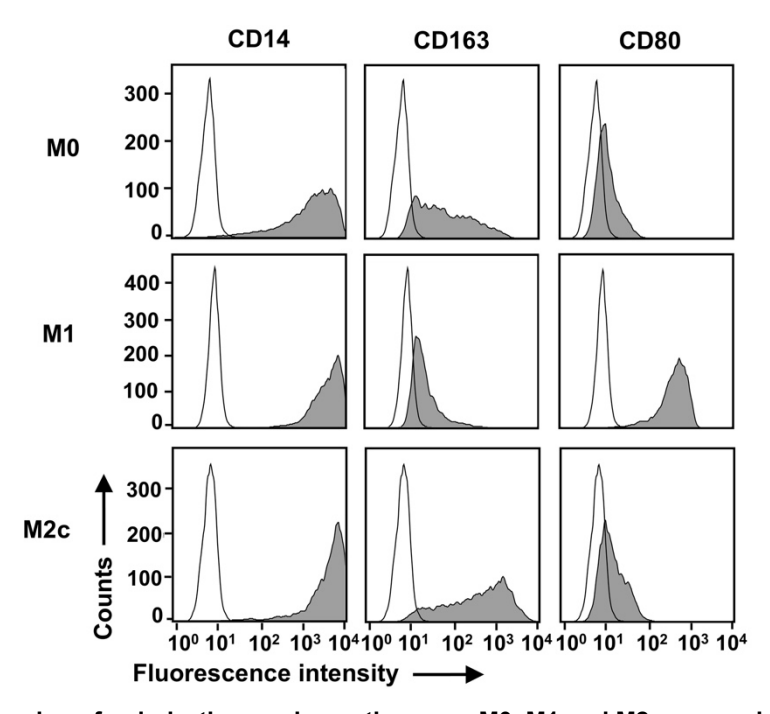


Figure 29: Expression of polarization marker antigens on M0, M1 and M2c macrophages. Monocytes were differentiated towards non-polarized M0 macrophages or polarized towards an M1 or M2c phenotype in parallel. To determine surface antigen expression, cells were incubated with PE-conjugated antibodies against CD14, CD163 and CD80 (grey shaded peaks) or a PE-conjugated control antibody (black outlined peaks). Antibody binding was determined via flow cytometry. Histograms from one representative experiment out of three experiments are shown. Results were published (Zeller et al., 2022).

## 3.6.2 Expression of Immune Checkpoint Molecules on Polarized Macrophages

Expression of the immune checkpoint molecules LILRB1, LILRB2 and SIRPα in differentially polarized macrophages was quantified to evaluate their availability for immune checkpoint blockade. Peripheral blood monocytes were differentiated towards M1 or M2c macrophages in parallel. Non-polarized M0 macrophages derived from monocytes from the same donor were employed as a control. Cell surface expression of antigens was determined by calibrated flow cytometry (figure 30). Compared to M0 macrophages, similar amounts of LILRB1 and LILRB2 were detected on M1 and M2c macrophages. Expression analysis of SIRPα revealed similar expression levels in M0 and M2c macrophages. Interestingly, decreased expression was found in M1 macrophages.

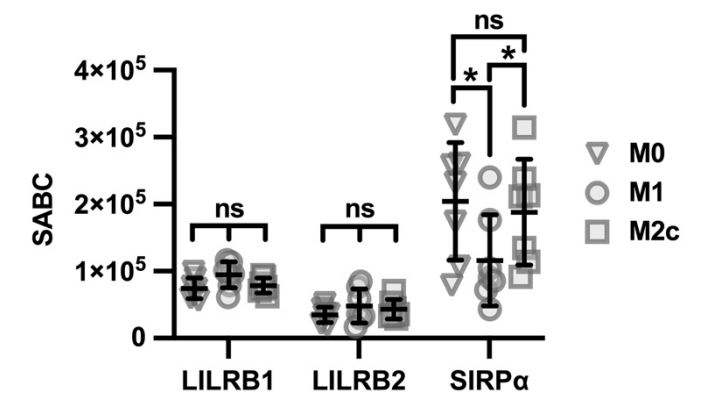


Figure 30: Expression of the immune checkpoints LILRB1, LILRB2 and SIRPα on M0, M1 and M2c macrophages. M0, M1 or M2c macrophages derived from monocytes from the same donor were immunolabeled with anti-LILRB1, anti-LILRB2 or anti-SIRPα antibodies and binding was analyzed via calibrated flow cytometry. Data points represent the calculated specific antibody binding capacities (SABC) for macrophages derived from seven individual donors. Bars indicate mean values  $\pm$  SD and statistically significant differences are indicated (\*, P ≤ 0.05; ns, not significant; two-way ANOVA with Tukey's *post hoc* test). Results were published (Zeller et al., 2022).

## 3.6.3 Influence of Macrophage Activation by LPS and IFN-γ on the Expression of LILRB1, LILRB2 and SIRPα

The activation of macrophages by activating stimuli, such as IFN-γ and LPS, is crucial to obtain polarization towards a classically activated, pro-inflammatory M1 phenotype. To analyze the impact of exposure to cytokines and activating stimuli on the expression of immune checkpoint molecules, peripheral blood monocytes were differentiated to M0 macrophages under exposure to either M-CSF or GM-CSF. Subsequently, cells were either activated with IFN-γ and LPS to adopt an M1 phenotype or left untreated. Thus generated macrophage subpopulations were assessed for expression levels of the immune checkpoint molecules LILRB1, LILRB2 and SIRPα by calibrated flow cytometry (figure 31). Interestingly, exposure to IFN-γ and LPS led to notably higher expression

levels of LILRB1 and LILRB2 in both M-CSF- and GM-CSF-treated macrophage populations. Contrary to the display of HLA receptors, macrophage activation with IFN- γ and LPS resulted in significantly reduced SIRPα expression levels.

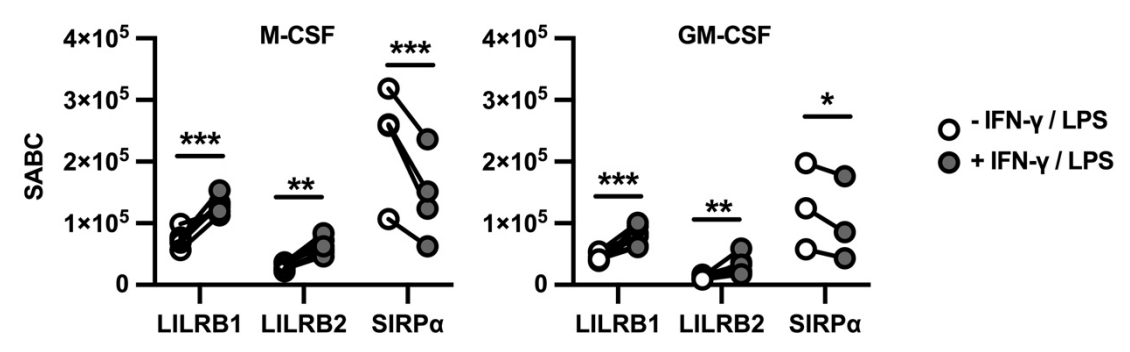


Figure 31: Influence of macrophage activation on the expression of LILRB1, LILRB2 and SIRPα. Monocytes were differentiated to macrophages with either M-CSF (*left graph*) or GM-CSF (*right graph*). After six days, macrophages were either activated by additional treatment with IFN- $\gamma$  and LPS for 48 h or left untreated. Cells were stained with antibodies specific for LILRB1, LILRB2 or SIRPα and binding was analyzed via calibrated flow cytometry. Data points mark the calculated specific antibody binding capacities (SABC) for macrophages derived from four (M-CSF) or three (GM-CSF) individual donors. Statistically significant differences between cells activated with IFN- $\gamma$  and LPS and cells left untreated are highlighted (\*, P ≤ 0.05; \*\*, P ≤ 0.01; \*\*\*\*, P ≤ 0.001; two-way ANOVA with Fisher s LSD test). Results were published (Zeller et al., 2022).

### 3.6.4 Phagocytosis of Lymphoma Cells by Polarized Macrophages

The impact of HLA receptor antibody blockade was analyzed in phagocytosis assays with polarized macrophages as effector cells. Macrophages differentiated towards an M1 or M2c phenotype were incubated with Carnaval cells under treatment with rituximab, CD47-lgGσ, LILRB1-lgGσ, LILRB2-lgGσ or antibody combinations and phagocytosis was determined by fluorescence microscopy (figure 32). Rituximab was effective in inducing the phagocytosis by all the analyzed macrophage populations. ADCP by macrophages of an M0 or M2c phenotype was significantly further enhanced when rituximab was accompanied by CD47-lgGσ. A similar, yet not statistically significant, trend was observed in experiments with M1 macrophages as effector cells. Remarkably, as seen in phagocytosis assays with M0 macrophages, LILRB1-lgGσ significantly further potentiated the phagocytosis of lymphoma cells by both M2c and M1 macrophages when applied alongside rituximab and CD47 blockade. In accordance with previous findings for M0 macrophages, LILRB2-lgGσ did not mediate an effect on ADCP by M1 or M2c macrophages.

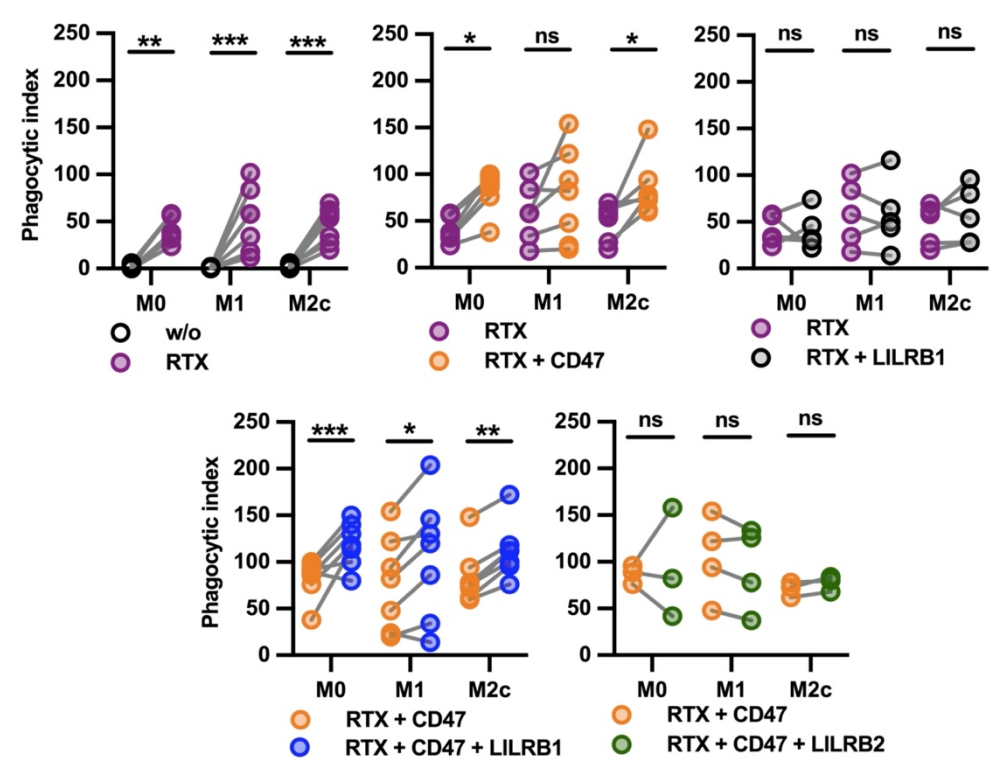


Figure 32: Impact of HLA receptor blockade on ADCP by differentially polarized macrophages. M0, M1 or M2c macrophages differentiated from monocytes from the same donors (n = 6) were analyzed via fluorescence microscopy for their capability to engulf CFSE-labeled Carnaval cells (E:T cell ratio: 1:2) when treated with the indicated antibodies (10 µg/ml each). Cells were analyzed after 2 h and phagocytic index values were determined. Induction of ADCP was assessed for treatment with rituximab (RTX) vs. the control reaction devoid of antibodies (w/o;  $upper\ left\ graph$ ), RTX/CD47-lgG $\sigma$  (CD47) vs. RTX ( $upper\ middle\ graph$ ), RTX/LILRB1-lgG $\sigma$  (LILRB1) vs. RTX ( $upper\ middle\ graph$ ), RTX/CD47-lgG $\sigma$ /LILRB1-lgG $\sigma$  vs. RTX/CD47-lgG $\sigma$ (lower left graph) and RTX/CD47-lgG $\sigma$ /LILRB2-lgG $\sigma$  (LILRB2) vs. RTX/CD47-lgG $\sigma$  (lower right graph). Statistically significant differences are marked (\*, P  $\leq$  0.05; \*\*, P  $\leq$  0.01; \*\*\*, P  $\leq$  0.001; ns, not significant; two-way ANOVA with Šidàk s multiple comparisons test). Results were published (Zeller et al., 2022).

### 3.6.5 Serial Phagocytosis of Lymphoma Cells by Polarized Macrophages

As observed in experiments with M0 macrophages as effector cells, individual M1 and M2c macrophages demonstrated the ability to engulf multiple lymphoma cells. Again, phagocytic events were categorized into initial ADCP, i.e. the primary uptake of a target cell, and serial ADCP, i.e. the uptake of further target cells, and the relative contribution of single and multiple cell phagocytosis to the overall phagocytic index values achieved by the application of the indicated antibodies was determined (figure 33). Again, particularly LILRB1/CD47 antibody co-inhibition facilitated the uptake of multiple Carnaval cells. In both M1 and M2c macrophages, the increase in phagocytosis upon combination of rituximab with CD47-lgGσ or CD47-lgGσ plus LILRB1-lgGσ mainly resulted from the serial uptake of target cells by individual macrophages.

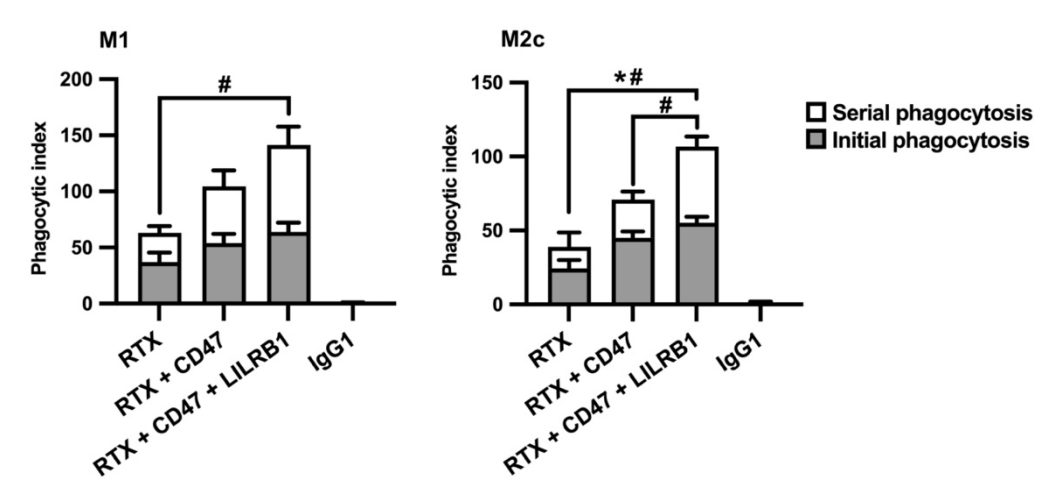


Figure 33: Serial ADCP of B-NHL cells by polarized macrophages. Dual inhibition of LILRB1 and CD47 promoted multiple cell ADCP of Carnaval cells by M1 (*left diagram*) or M2c (*right diagram*) macrophages. Phagocytic events from fluorescence microscopy phagocytosis experiments (figure 32) were grouped into primary ADCP of a target cell (initial phagocytosis) and the uptake of further target cells (serial phagocytosis) and are plotted as proportions of overall phagocytic index values. Bars represent mean values  $\pm$  SEM. Statistically significant differences between the treatment groups in initial (\*) and serial (#) phagocytosis event values are marked (P  $\leq$  0.05; two-way ANOVA with Tukey's *post hoc* test).

## 3.6.6 Influence of Macrophage Activation by LPS and IFN-γ on the Phagocytosis of Lymphoma Cells

Next, the influence of macrophage activation on the phagocytosis of lymphoma cells upon antibody treatment was determined. Macrophages pre-treated with either M-CSF or GM-CSF were activated with IFN-γ and LPS or left untreated and co-incubated with Carnaval cells. Rituximab, CD47-IgGσ, LILRB1-IgGσ or combinations of antibodies were applied, phagocytosis was quantified via fluorescence microscopy and compared between the different effector cell populations (figure 34). As a result, non-activated, GM-CSF-differentiated macrophages were incapable of ADCP in contrast to their counterparts differentiated with M-CSF. Activation with IFN-γ and LPS enhanced the phagocytic capacity of GM-CSF-differentiated macrophages, particularly when cells were treated with rituximab plus LILRB1 and CD47 co-blockade. Enhancement of phagocytosis upon exposure to IFN-γ and LPS was also observed in M-CSF-treated macrophages, which were in general superior to the macrophage populations differentiated with GM-CSF. Importantly, irrespective of M-CSF or GM-CSF pre-treatment, the highest phagocytic index values were achieved when LILRB1-IgGσ, CD47-IgGσ and rituximab were applied together.

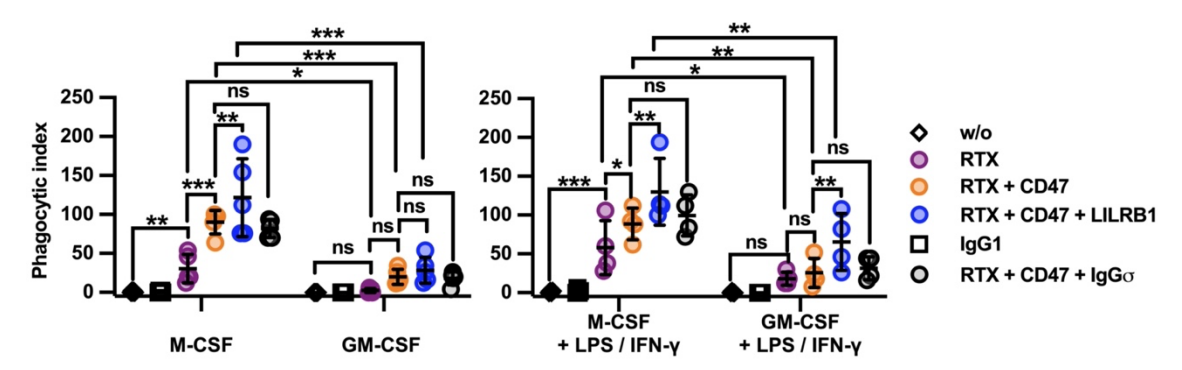


Figure 34: Influence of macrophage activation on ADCP of B-NHL cells upon antibody treatment. Monocytes were differentiated to macrophages under exposure to either M-CSF or GM-CSF for six days. Cells then either remained untreated to become M0 macrophages (*left graph*; n = 5) or were activated with IFN-γ and LPS to acquire an M1 phenotype (*right graph*; n = 4). The different macrophage preparations were then employed as effector cells in two-hour fluorescence microscopy phagocytosis experiments with CFSE-labeled Carnaval cells (E:T cell ratio: 1:2) under treatment with the indicated antibodies/antibody combinations (each antibody applied at 10 μg/ml). Data points represent the calculated phagocytic index values for macrophage preparations derived from different donors. Horizonal lines indicate mean values ± SD (\*, P ≤ 0.05; \*\*, P ≤ 0.01; \*\*\*, P ≤ 0.001; ns, not significant; two-way ANOVA and Fisher s LSD test; w/o, without antibody; RTX, rituximab; CD47, CD47-IgGσ; LILRB1, LILRB1-IgGσ; IgG1, trastuzumab; IgGσ, HER2-IgGσ). Results were published (Zeller et al., 2022).

## 3.6.7 Kinetics of ADCP of Lymphoma Cells by Differentially Polarized Macrophages

Furthermore, the beneficial effect of LILRB1 antibody blockade on the phagocytosis by M1 or M2c macrophages was confirmed in live cell imaging phagocytosis assays with DG-75 cells (figure 35). Experiments revealed slightly enhanced phagocytosis by M2c and M0 macrophages upon the dual treatment with rituximab and CD47-IgGσ in comparison to the control group. A similar trend was observed with M1 macrophages, however, statistical significance was not reached. Importantly, in line with the findings in fluorescence microscopy-based phagocytosis assays, the presence of LILRB1-IgGo alongside CD47-IgGo and rituximab significantly enhanced the engulfment of DG-75 cells regardless of the macrophage polarization state. Interestingly, the kinetics of phagocytosis differed between differentially polarized macrophages. ADCP by M2c or M0 macrophages occurred quickly and peaked after 2 h (M0) or 2.5 h (M2c). In contrast, ADCP in experiments with M1 macrophages increased slower and reached the maximum value after 3 h. In general, the maximum red object count per image upon treatment with rituximab plus LILRB1/CD47 co-inhibition was detected in experiments with M2c macrophages as effector cells. In accordance with previous results, rituximab combined with LILRB1-IgGo alone, as well as treatment with LILRB2-IgGo did not enhance ADCP.

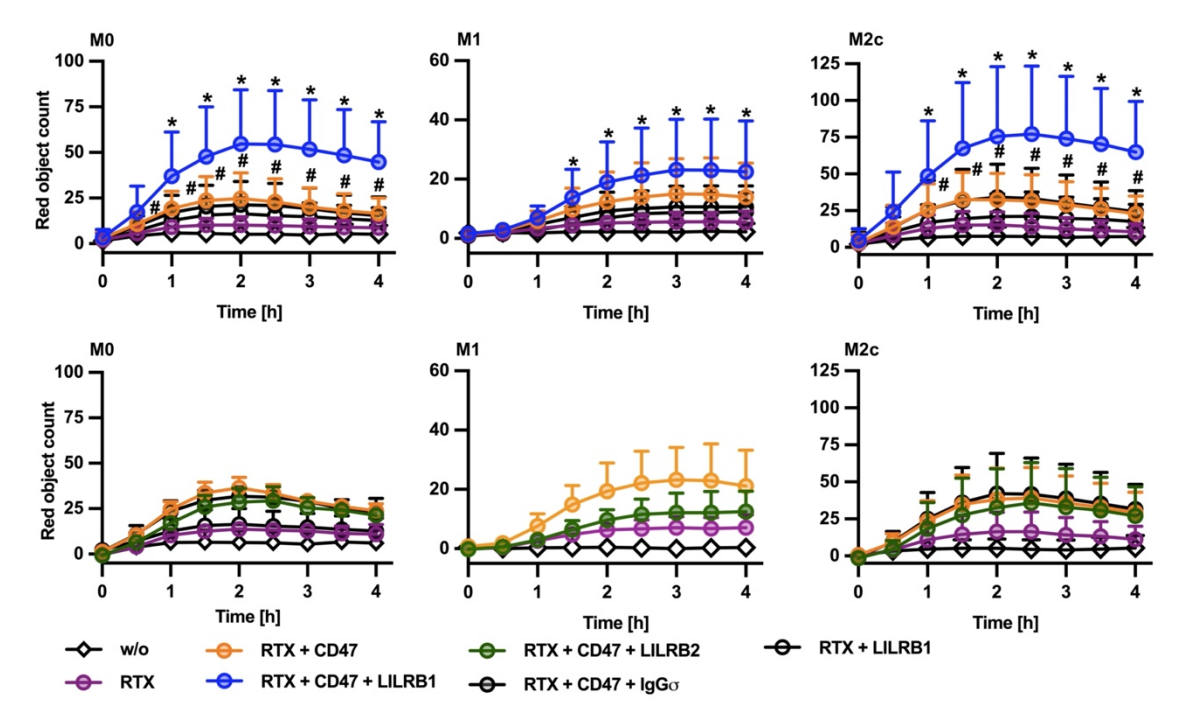


Figure 35: Kinetics of ADCP by polarized macrophages upon antibody treatment. Monocytes were differentiated to M0, M1 and M2c macrophages in parallel (n=6) and employed as effector cells in live cell imaging assays with pHrodo® Red-labeled DG-75 cells as targets (E:T cell ratio: 1:2). Cells were co-incubated under antibody treatment (each applied at 10 µg/ml) with rituximab (RTX), CD47-lgG $\sigma$  (CD47) or both together combined with LILRB1-lgG $\sigma$  (LILRB1;  $top\ row$ ) or LILRB2-lgG $\sigma$  (LILRB2;  $top\ row$ ). HER2-lgG $\sigma$  (lgG $\sigma$ ) served as control. Data points show mean values  $top\ SD$  of red object count per image of individual experiments (w/o, without antibody). Statistically significant differences (P  $top\ SD$  0.05) between the treatment groups RTX vs. RTX/CD47-lgG $\sigma$  (#) and RTX/CD47-lgG $\sigma$ /LILRB1-lgG $\sigma$  vs. RTX/CD47-lgG $\sigma$  (\*) are marked (two-way ANOVA and Fisher's LSD test). Results were published (Zeller et al., 2022).

# 3.7 Efficacy of LILRB1-IgGσ and LILRB2-IgGσ in Enhancing ADCP of Patient-Derived Lymphoma Cells

LILRB1-IgGσ was found to enhance the phagocytosis of various lymphoma cell lines by non-polarized and by polarized macrophages, as well as to promote the serial engulfment of lymphoma cells by individual macrophages. Yet, cell lines do not adequately mirror the complex functional and morphological characteristics of the disease in patients. To address the greater complexity and clinical heterogeneity in patients, cancer cells were prepared from peripheral blood samples of MCL or CLL patients. In an initial experiment using CLL cells from one randomly selected patient, enhanced rituximab-mediated ADCP under LILRB1/CD47 co-blockade was observed (figure 36). The patient-derived CLL and MCL cells were then analyzed for surface antigen expression and employed as target cells in further ADCP experiments to determine the effect of HLA class I receptor antibody blockade.

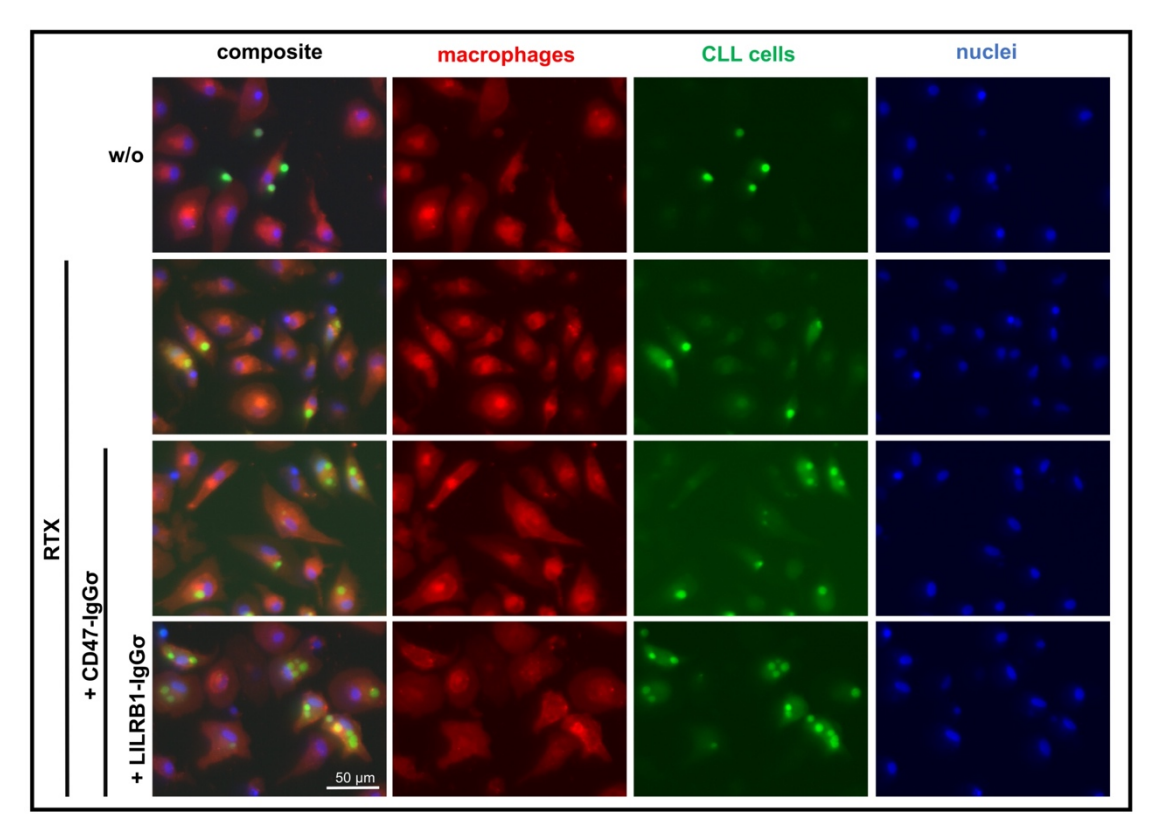


Figure 36: Fluorescence microscopy images of improved ADCP of CLL cells from patients by coblockade of CD47 and LILRB1. Patient-derived CLL cells (sample CLL\_05) were labeled with CFSE and co-cultured with M0 macrophages stained with Cell Brite<sup>TM</sup> Orange cytoplasmic membrane dye in an E:T cell ratio of 1:2 and 10 μg/ml of rituximab (RTX) alone, RTX plus CD47-lgGσ (CD47) or RTX plus both CD47-lgGσ and LILRB1-lgGσ (LILRB1; w/o, without antibody treatment). Nuclei were stained with NucBlue<sup>TM</sup>. Phagocytosis was assessed via fluorescence microscopy after 2h and cells were imaged. The left panel column shows microscope composite images of the red, green and blue channels. The second, third and fourth panel columns show the same section of the slide in the red, green and blue channels, respectively. Results were published (Zeller et al., 2022).

## 3.7.1 Expression of CD20, CD47 and HLA Class I by Patient-Derived Lymphoma Cells

The patient-derived CLL and MCL cells were immunolabeled with antibodies against CD47, classical HLA class I molecules, HLA-G and CD20 (figure 37A). Antigen expression level analysis by calibrated flow cytometry revealed that all twelve CLL samples expressed the rituximab target CD20 and the SIRPα ligand CD47 at comparable levels (figure 37B). Higher expression levels and greater heterogeneity were found for the display of classical HLA-A, -B and -C molecules among the analyzed CLL samples. HLA-G was hardly detectable. Similar results were found for the expression of CD47 and classical HLA-A, -B and -C molecules, as well as the non-classical HLA-G in the two analyzed patient-derived MCL samples (figure 37A). Interestingly, the expression levels of CD20 differed between the two MCL samples. Whereas MCL\_01 displayed a similar amount of CD20 (SABC ≈ 24,000) as found in patient-derived CLL samples, notably higher CD20 expression was detected on MCL\_02 cells (SABC ≈ 160,000).

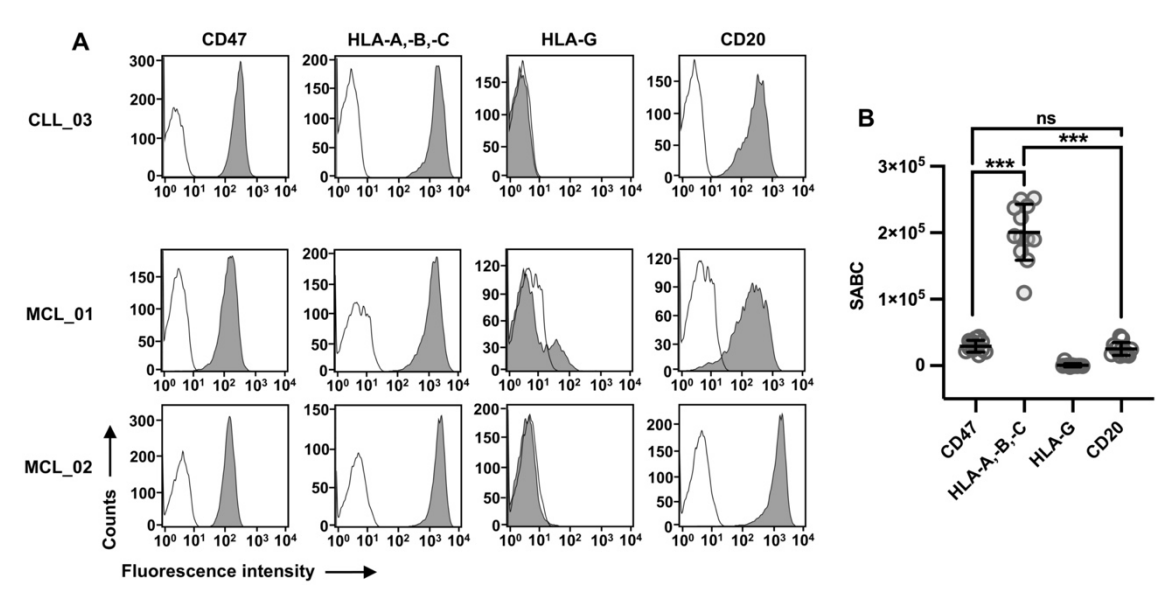


Figure 37: Expression of cell surface antigens on patient-derived CLL and MCL cells. The extent of CD47, HLA-A,-B,-C, HLA-G and CD20 expression on patient-derived cancer cells was determined by staining the cells with PE-conjugated antibodies specific for the indicated antigen (grey shaded peaks) or an isotype control antibody (black outlined peaks). Antibody binding was measured by flow cytometry. (A) Shown are representative results for one patient-derived CLL sample (CLL\_03; *upper row*) and the two patient-derived MCL samples MCL\_01 (*middle row*) and MCL\_02 (*lower row*). (B) Additionally, for the patient-derived CLL samples specific antibody binding capacities (SABC) were determined via calibrated flow cytometry. Data points represent the SABCs for individual CLL patient samples. Horizonal lines indicate mean SABC  $\pm$  SD (\*\*\*\*, P  $\leq$  0.001; ns, not significant; one-way ANOVA with Tukey's multiple comparison test). Results were published (Zeller et al., 2022).

### 3.7.2 ADCP of Patient-Derived Chronic Lymphocytic Leukemia Cells

To determine, whether the abrogation of LILRB1 or LILRB2 signaling in macrophages is effective to also promote the engulfment of patient-derived lymphoma cells, antibody treatment combinations of rituximab, CD47-IgGσ, LILRB1-IgGσ and LILRB2-IgGσ were applied to CLL cells enriched from the peripheral blood of patients and M0 macrophages and the phagocytosis was determined via fluorescence microscopy (figure 38). Combining rituximab with CD47-IgGσ led to enhanced phagocytosis of CLL cells in the majority of the analyzed patient samples. However, in individual patient samples, such as CLL\_04 and CLL\_10, antibody blockade of CD47 was insufficient to improve phagocytosis, even though reasonable expression of CD20 and CD47 in both samples was confirmed in earlier experiments (figure 37). Remarkably, in all analyzed CLL patient samples the highest phagocytic index values were achieved when rituximab and CD47-IgGσ treatment was combined with LILRB1-IgGσ, even in CLL samples in which CD47-IgGσ was not effective to enhance rituximab-mediated phagocytosis when applied alone.

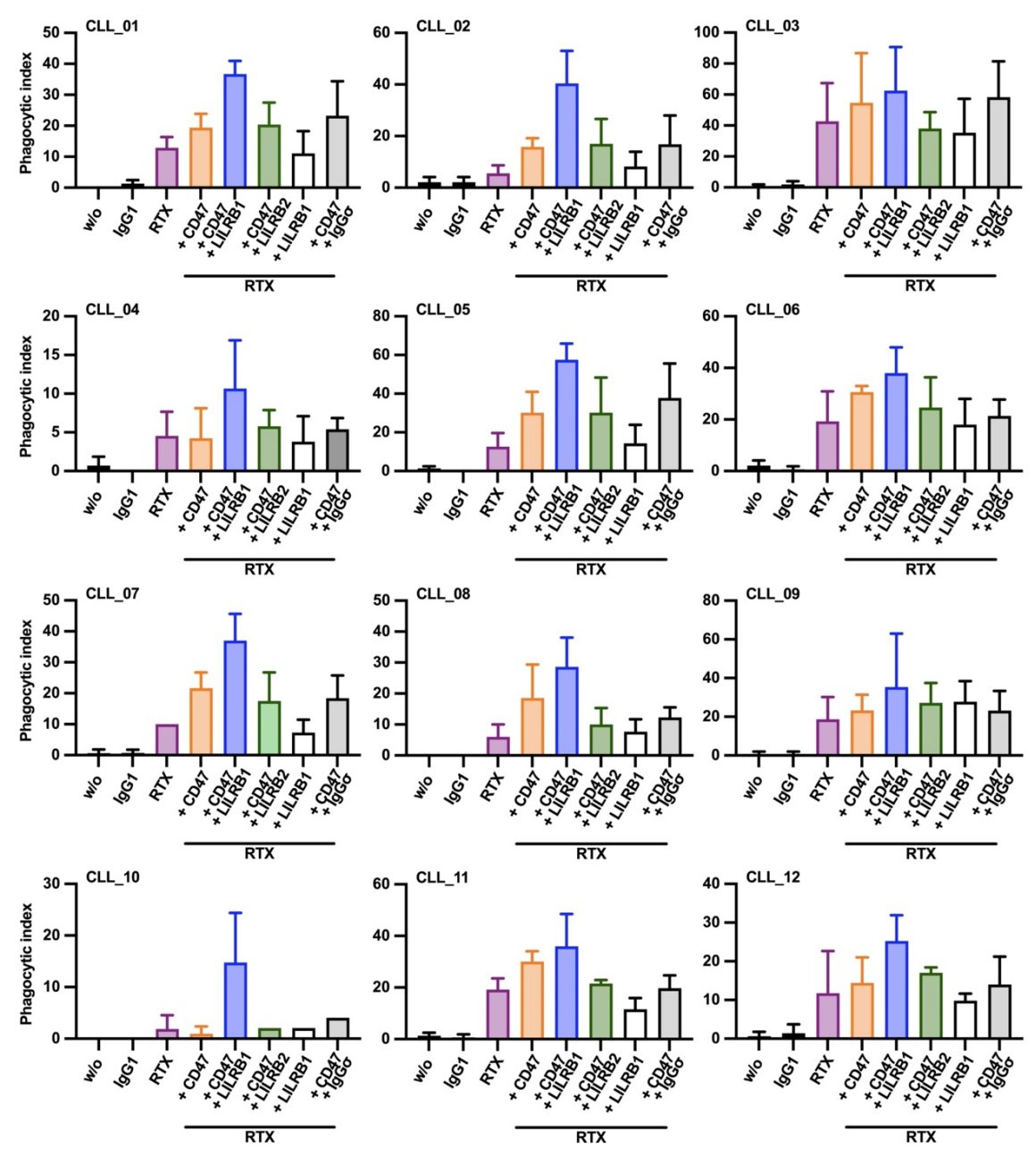
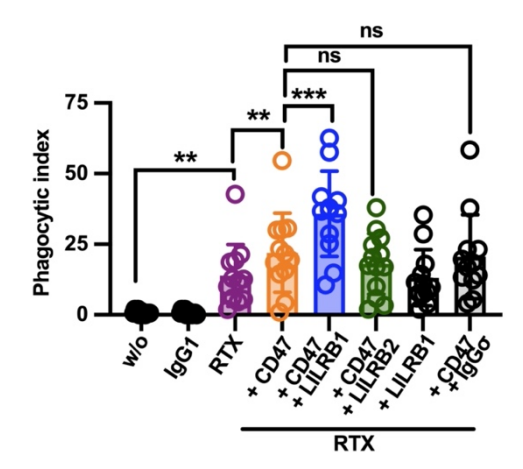


Figure 38: ADCP of individual patient-derived CLL cells upon CD47 and LILRB1 co-blockade. CFSE-labeled, patient-derived CLL cells were analyzed as target cells for M0 macrophages (E:T cell ratio: 1:2) in ADCP assays under treatment with 10  $\mu$ g/ml of rituximab (RTX), CD47-lgG $\sigma$  (CD47), LILRB1-lgG $\sigma$  (LILRB1), LILRB2-lgG $\sigma$  (LILRB2) or their combinations (w/o, without antibody treatment). Trastuzumab (lgG1) and HER2-lgG $\sigma$  (lgG $\sigma$ ) served as controls. Phagocytosis was determined after 2 h via fluorescence microscopy and phagocytic index values were calculated. Bars show mean phagocytic index values  $\pm$  SD from two (CLL\_10) or three (all other samples) independent experiments with individual preparations of macrophages. Results were published (Zeller et al., 2022).

To confirm statistical significance between the results achieved with different antibodies/antibody combinations, sample group analysis was performed (figure 39). In line with the previous findings, LILRB1-IgG $\sigma$  further enhanced the rituximab-mediated phagocytosis of patient-derived CLL cells when combined with CD47-IgG $\sigma$ . Treatment with LILRB2-IgG $\sigma$  was not effective.



**Figure 39: Sample group analysis of ADCP of patient-derived CLL cells.** Shown is the group analysis of phagocytosis experiments with cancer cells derived from 12 individual CLL patients and M0 macrophages. Data points represent mean phagocytic index values calculated from the results of ADCP experiments with the individual patient samples shown in figure 38. Bars represent overall mean phagocytic index values  $\pm$  SD (\*\*, P ≤ 0.01; \*\*\*, P ≤ 0.001; ns, not significant; one-way ANOVA with Šidàk´s multiple comparisons test; w/o, without added antibody; IgG1, trastuzumab; RTX, rituximab; CD47, CD47-IgGσ; LILRB1, LILRB1-IgGσ; LILRB2, LILRB2-IgGσ, HER2-IgGσ). Results were published (Zeller et al., 2022).

## 3.7.3 Serial Phagocytosis of Patient-Derived Chronic Lymphocytic Leukemia Cells

Further analysis revealed that serial engulfment of cancer cells by individual macrophages also occurred in experiments with patient-derived CLL cells. Again, engulfment of target cells upon treatment with different antibodies or their combinations was categorized into initial and serial phagocytosis as described above (figure 40). In agreement with the previous results, particularly treatment with rituximab plus LILRB1 and CD47 coblockade resulted in an increased frequency of serial phagocytosis events.

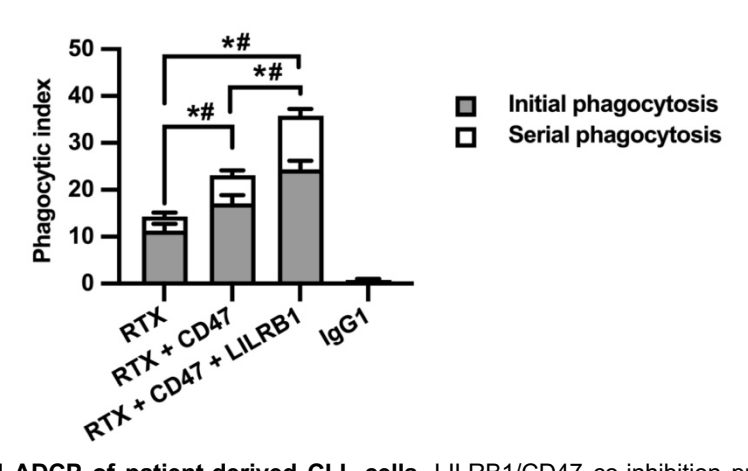


Figure 40: Serial ADCP of patient-derived CLL cells. LILRB1/CD47 co-inhibition promoted the serial uptake of CLL cells by individual M0 macrophages. Phagocytic events (figure 38) were grouped into uptake of the first lymphoma cell (initial phagocytosis) or of further lymphoma cells (serial phagocytosis) and are plotted as proportions of the total phagocytic index values. Bars represent mean values  $\pm$  SEM. Statistically significant differences in initial (\*) and serial (#) phagocytosis event values are marked (P  $\leq$  0.05; two-way ANOVA with Tukey's *post hoc* test). Results were published (Zeller et al., 2022).

### 3.7.4 ADCP of Patient-Derived Mantle Cell Lymphoma Cells

In addition to patient-derived CLL cells, the potential of LILRB1-IgGσ to promote the phagocytosis of MCL cells derived from the peripheral blood of two individual patients was evaluated (figure 41). As revealed by fluorescence microscopy, rituximab induced ADCP of both MCL samples by M0 macrophages. In experiments with MCL\_01 cells as targets, phagocytosis was enhanced significantly when rituximab was combined with CD47-IgGσ, whereas CD47-IgGσ was not effective with MCL\_02 cells as targets. Importantly, despite the resistance of MCL\_2 cells to CD47 inhibition, dual LILRB1/CD47 checkpoint inhibition significantly further promoted the rituximab-mediated phagocytosis of both patient-derived MCL samples.

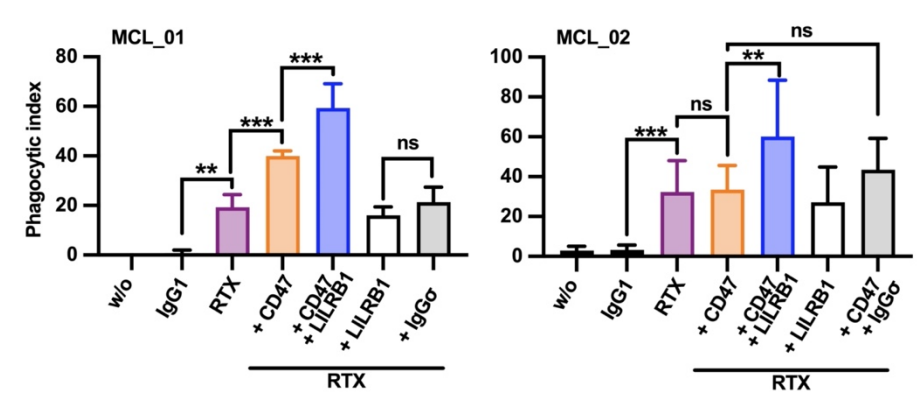


Figure 41: ADCP of MCL cells from patients upon CD47 and LILRB1 co-blockade. CFSE-labeled MCL cells derived from two patients (MCL\_01, n = 3; and MCL\_02, n = 6) were analyzed for phagocytosis by M0 macrophages (E:T cell ratio: 1:2) via fluorescence microscopy when no antibodies (w/o), rituximab (RTX), CD47-lgG $\sigma$  (CD47), LILRB1-lgG $\sigma$  (LILRB1) or combinations of antibodies were present (antibodies applied at 10  $\mu$ g/ml each). Phagocytosis was determined after 2 h and phagocytic index values were calculated. Trastuzumab (lgG1) and HER2-lgG $\sigma$  (lgG $\sigma$ ) were employed as controls. Bars represent mean phagocytic index values  $\pm$  SD determined for preparations of macrophages from individual donors. Statistically significant differences are marked (\*\*, P ≤0.01; \*\*\*\*, P ≤ 0.001; ns, not significant; one-way ANOVA with Fisher`s LSD test). Results were published (Zeller et al., 2022).

### 4. Discussion

Investigations in a B-NHL cell line system for the sensitivity to macrophage phagocytosis revealed a positive correlation between the CD20-to-HLA class I expression ratio and the magnitude of ADCP induced by rituximab and an Fc-silent variant of the CD47 antibody magrolimab. To determine the effect of masking the HLA class I receptors LILRB1 and LILRB2 on the ADCP of B-NHL cells by macrophages, Fc-silent antibodies against either LILRB1 or LILRB2 with abrogated FcyR binding were generated, characterized for purity, integrity, binding selectivity and their ability to block ligand interaction. The antibodies were then evaluated for their potential to promote the CD20 antibodymediated ADCP of B-NHL cells with or without co-application of CD47-IgGo. Whereas LILRB2-IgGσ was ineffective, LILRB1-IgGσ notably promoted the ADCP of B-NHL cells, yet strictly needed the co-inhibition of CD47 and the co-application of a tumor targeting CD20 antibody bearing a functional Fc domain to unfold its effect. Thus, immune checkpoint co-inhibition of LILRB1 and CD47 potentiated the phagocytosis when combined with different CD20-directed antibodies including rituximab, a variant of rituximab Fc-engineered for improved affinity for activating FcyR, as well as an IgA2 isotype switch variant of rituximab. In addition, LILRB1-lgGσ promoted the serial uptake of cancer cells by individual macrophages. Importantly, LILRB1 antibody blockade demonstrated efficacy not only in B-NHL cell lines, but also considerably enhanced the phagocytosis of freshly isolated CLL and MCL cells from patients.

Antibody blockade of adaptive immune checkpoints, such as PD-1, its ligand PD-L1 or CTLA-4, to establish T cell immunity has become an indispensable element of cancer immunotherapy (Wei et al., 2018, Chen and Mellman, 2013). Promising responses were observed particularly in solid cancers, including malignant melanoma, RCC and NSCLC (Seidel et al., 2018). However, in the treatment of B-lineage lymphomas the clinical benefit of disrupting the PD-1:PD-L1 axis differs substantially by the lymphoma subtype. Encouraging results were obtained in classical Hodgkin's lymphoma, in which response rates exceeded 70% (Ansell, 2021, Ansell et al., 2015). Unfortunately, the response rates to T cell-directed immune checkpoint therapies do not translate to most entities of B-NHLs, as demonstrated for DLBCL, follicular lymphoma and CLL (Ansell, 2021, Armand et al., 2021). Application of the anti-PD-1 antibody nivolumab, for instance, was not efficient in relapsed or refractory DLBCL leading to response rates of only 10% in a phase II trial (Ansell et al., 2019). Also, even though some clinical activity of the anti-PD-1 antibody pembrolizumab was observed in patients with CLL and Richter transformation, the antibody was not efficient in patients with relapsed CLL (Ding et al., 2017). Limitations arise particularly when an immunosuppressive microenvironment that promotes tumor progression evolves within tumors and reprograms immune cells into pro-tumorigenic states or when cancer cells lack immunogenicity. In this regard, immune checkpoint inhibition in macrophages, which are critically involved in the formation and maintenance of the immune hostile TME, yet also possess the ability to recognize cancer cells and eliminate them directly through phagocytosis, may display an interesting alternative (Lentz et al., 2021, Demaria et al., 2019). For instance, impressive clinical results were obtained in B-NHL patients by combining rituximab treatment with antibody blockade of CD47, the ligand of the myeloid inhibitory receptor SIRPα (Advani et al., 2018).

### 4.1 Further Critical Factors Affecting ADCP

As revealed in this thesis, the application of blocking anti-LILRB1 antibodies along with CD47 inhibition holds the potential to further promote macrophage ADCP of B-NHL cells by CD20 antibodies. Interestingly, even upon blocking both immune checkpoints reasonable differences in the efficacy of this antibody combination were noticed between different B-NHL cell lines. In Carnaval and MEC2 cells, concomitant LILRB1 antibody blockade mediated an approx. 1.5-fold improvement in ADCP compared to treatment with rituximab and CD47 blockade only, whereas DG-75 cells were found to be notably more resistant to rituximab-induced ADCP. Even upon blockade of CD47 ADCP was comparably low. However, in these cells LILRB1-IgGσ potentiated the phagocytosis by more than a factor of four (figure 21, figure 22).

Additionally, the different cell lines analyzed in this study varied remarkably in the overall phagocytosis rates achieved by LILRB1 and CD47 co-blockade. The mean phagocytic index values ranged from around 20 (DG-75 cells) to nearly 150 (Carnaval cells). Of note, considerable variation in the overall magnitude of mean phagocytic index values, as well as in the fold improvement of ADCP mediated by LILRB1-IgGσ, was also found between individual patient-derived CLL cell samples. These observations may mirror the sophisticated regulation of phagocytosis, which is subject to the cooperation of numerous stimulatory and inhibitory receptors. Besides CD47 and HLA class I, several cancer cellexpressed antigens have been demonstrated to confer protection from phagocytosis. For instance, roles as 'Don't Eat Me!' signals were unraveled for PD-L1, CD24, adipocyte plasma membrane-associated protein and signaling lymphocytic activation molecule (SLAM) family members. On the other side, inhibitory checkpoint functions in macrophages were unraveled for PD-1, multiple Siglecs and SLAM family receptors (Feng et al., 2019, Barkal et al., 2019, Kamber et al., 2021, Li et al., 2022). Such receptors on macrophages may cooperate with SIRPα and LILRB1 in the inhibition of the phagocytosis of lymphoma cells and differences in the expression levels of their

ligands may contribute to reduce the susceptibility of individual phenotypes of lymphoma cells for ADCP, as observed for instance for DG-75 cells or cell samples of individual CLL patients. Interference with these signaling pathways may thus hold the potential to achieve additional improvements. Moreover, the expression of ,Eat Me!' signals in cancer cells, such as calreticulin or SLAM family member 7 (SLAMF7), and the activation of the cognate pro-phagocytic molecules on macrophages including prolow-density lipoprotein receptor-related protein 1 (LRP1) and macrophage-1 antigen (MAC1), as well as the activating macrophage receptors CD137 and CD11b may play a role in the regulation of the phagocytosis of lymphoma cells (Feng et al., 2019, Stoll et al., 2021, Chen et al., 2017). However, the involvement of SLAMF7 in the phagocytosis of malignant cells is currently discussed controversially and conflicting data exists concerning the impact of its expression on CD47 antibody-mediated phagocytosis (Chen et al., 2017, He et al., 2019). Moreover, also cellular attributes of the target cells, such as their size, shape or rigidity may influence the susceptibility to macrophage phagocytosis (Sosale et al., 2015).

# 4.2 Requirement of CD47 Co-Blockade and the Presence of FcyR Activation for the Efficacy of Anti-LILRB1 Antibodies

It was observed that LILRB1-IgGσ required the concurrent disruption of the SIRPα:CD47 axis to enhance CD20 antibody-mediated ADCP. This finding suggests that inhibitory SIRPα signaling holds a dominant role in the regulation of phagocytosis. SIRPα and LILRB1 share several similarities in their overall structure. They both recognize their ligands through Ig-like domains in their extracellular portions and upon ligation transduce an inhibitory signal via the phosphorylation of ITIMs in their intracellular domains, which results in the recruitment and activation of the SH2-domain-containing protein tyrosine phosphatases SHP-1 and SHP-2 (Fanger et al., 1998, Ketroussi et al., 2011, Logtenberg et al., 2020). SIRP $\alpha$  signaling hampers phagocytosis by interfering with the interaction of macrophages and target cells. Non-ligated SIRPα is excluded from the phagocytic synapse, the contact zone between phagocyte receptors and their target structure. CD47 ligation re-localizes SIRPa to the phagocytic synapse and its activation inhibits the activation of integrins, which are necessary for efficient cell spreading and engulfment (Morrissey et al., 2020). SIRPα signaling furthermore impairs cytoskeletal remodeling through the dephosphorylation of myosin IIA. Moreover, SIRPα has been demonstrated to counteract activating signals in myeloid cells, for instance through the dephosphorylation of ITAMs and thus the inactivation of FcRs (Tsai and Discher, 2008, Suter et al., 2021, Logtenberg et al., 2020). Particularly the latter finding may explain the

direct inhibitory influence of CD47 during therapy with tumor targeting antibodies. Coligation of LILRB1 and the activating Fc $\gamma$ RI has been demonstrated to reduce the mobilization of intracellular Ca<sup>2+</sup>, however, the distinct molecular mechanism by which LILRB1 signaling interferes with the phagocytosis of cancer cells by macrophages remains to be elucidated (Fanger et al., 1998). Also, whether differences between the signaling pathways of SIRP $\alpha$  and LILRB1 exist that result in the inhibition of the phagocytosis process at different phases and thus contribute to the dominant role of SIRP $\alpha$  has not yet been clarified.

Importantly, even the simultaneous application of both CD47-IgG $\sigma$  and LILRB1-IgG $\sigma$  did not induce phagocytosis in the absence of the cancer cell-binding CD20 antibody with a competent Fc domain *in vitro*. Consequently, upon the use of an Fc-silent antibody format for dual LILRB1/CD47 immune checkpoint inhibition, the specificity for the elimination of target cells is not only maintained, but may precisely be pre-defined by the specificity of the FcR-engaging, tumor targeting antibody. This antibody is needed to provide an activating signal by FcR stimulation. As indicated by the obtained experimental results, the combination partner can be a native IgG1 antibody, an Fc-engineered IgG1-derivative or an IgA2 antibody. Likely, also other antibody isotypes or bispecific antibodies engaging FcR may be suitable.

The dependency of LILRB1 and CD47 co-blockade on FcR-engagement to promote phagocytosis may be related to different reasons. Since the macrophage phagocytosis of malignant cells is regulated by an equilibrium of pro- and anti-phagocytic signaling, even the abrogation of both SIRPα and LILRB1 signaling may be insufficient to shift the balance towards pro-phagocytic signaling to induce the engulfment of lymphoma cells. However, an IgG4 version of the antibody clone used for the generation of CD47-IgGσ bearing a functional Fc domain has been demonstrated to induce macrophage phagocytosis as a single agent and when combined with LILRB1-blocking antibodies without requiring further activating signals to become effective (Liu et al., 2015a, Barkal et al., 2018). It thus appears more likely that the abrogation of FcγR binding in CD47-IgGσ is responsible for the observed dependency on FcR-engagement by a tumor targeting antibody in the approach pursued here. Interestingly, improving FcγR activation by pairing CD47-IgGσ and LILRB1-IgGσ with an optimized rituximab variant resulted in further enhanced phagocytosis (figure 28).

For immune checkpoint blockade, Fc-silent antibodies, which lack the ability to recruit immune effector cells, may furthermore hold the potential to reduce on-target toxicity. Indeed, the regulatory role of CD47 was initially discovered, when red blood cells (RBC) of CD47-/- mice lacking CD47 expression were found to be rapidly cleared from the

bloodstream through phagocytosis by macrophages when transferred to wild-type mice, whereas normal CD47-expressing RBC were spared (Oldenborg et al., 2000). Since CD47 expression in RBC gradually decreases with their age, it is considered an important cell surface marker of RBC turnover. The involvement of CD47 in the regulation of homeostatic clearance of aging RBC, as well as its ubiquitous expression also in healthy tissues remains a serious concern in CD47-directed therapies. Even upon the use of antibody formats with decreased ability to mediate Fc-dependent effector mechanisms, such as the IgG4 antibody magrolimab, blocking CD47 may lead to increased RBC clearance and hemolysis (Advani et al., 2018). Concerning this issue, CD47 antibodies unable to interact with FcγRs, such as CD47-IgGσ, may represent a superior alternative antibody format, as they provide pure receptor blockade without mediating indirect cytotoxic or phagocytic effects towards the target cell on their own. Instead, they rely on an additional activating stimulus, such as fully functional tumor targeting antibodies, to initiate target cell elimination by macrophages.

The engagement of FcRs during CD47 antibody therapy may also be of clinical relevance. It was recently announced that the clinical trials exploring the efficacy of magrolimab combined with azacitidine in myelodysplastic syndrome (MDS) patients or together with azacitidine and venetoclax in AML patients have been discontinued due to futility and increased risk of death. However, when combined with rituximab, magrolimab showed promising activity in B-NHL patients (Advani et al., 2018). Since in human macrophages Fc-FcγR interactions have been demonstrated to be necessary for CD47 antibodies to become effective, CD47 blockade may require the additional engagement of FcRs to become effective in patients, for instance through combination with tumor targeting antibodies for enhanced effector cell recruitment (Jain et al., 2019). However, in the treatment of AML conventional IgG1 antibodies have still not been approved and therefore combination studies are difficult to realize.

### 4.3 Inability of LILRB2-IgGσ to Promote Phagocytosis

In contrast to the antibody blockade of LILRB1, LILRB2-IgGσ did not enhance the phagocytosis of lymphoma cells, even when combined with CD47 co-blockade and CD20 antibodies. Although both LILRB1 and LILRB2 are closely related in many aspects, differences exist between the two receptors and different roles in immunity have been described. Both LILRB1 and LILRB2 interact with HLA class I molecules on cancer cells and mediate inhibitory signaling through ITIMs in their intracellular portions. However, structural differences between the receptors exist concerning the binding of HLA molecules. Thus, LILRB1 recognizes only HLA class I complexed with β2m, whereas LILRB2

binds β2m-free variants as well (Jones et al., 2011, Shiroishi et al., 2006b). Additionally, different affinities of LILRB1 and LILRB2 to individual HLA alleles have been described (Shiroishi et al., 2006b). Indeed, in own experiments weaker binding of randomly chosen soluble HLA molecules to LILRB2-transfected CHO-K1 cells was detected in comparison to the LILRB1-expressing counterparts, which may reflect the previously reported differences in affinity. Furthermore, inhibitory signaling by LILRB1 and LILRB2 differs in that LILRB1 possesses four intracellular ITIM or ITIM-like sequences, whereas LILRB2 contains only three. This difference may result in reduced potency of LILRB2 to suppress effector cell functions and thus the receptor may play an inferior role. Yet, engagement of LILRB2, similar to LILRB1 ligation, has been demonstrated to inhibit FcyR signaling and thus to contribute to the down-modulation of effector cell activation (Fanger et al., 1998). Yet, the abrogation of LILRB2 signaling has been suggested not to influence phagocytosis of solid cancer cell lines by macrophages (Barkal et al., 2018). However, in this individual study considerably lower expression levels of LILRB2 compared to LILRB1 were detected in human macrophages. In contrast, other studies reported similar expression levels of LILRB1 and LILRB2 for peripheral monocytes (Fanger et al., 1998) and in flow cytometry assays performed in the context of this thesis, macrophages generated ex vivo from peripheral blood monocytes displayed LILRB2 at similar levels as LILRB1 (figure 13). Concerning the individual anti-LILRB2 antibody employed here, LILRB2-IgGo was monomeric in solution, displayed a selective mode of binding to LILRB2 and effectively blocked receptor interaction with HLA class I molecules, which is consistent with previous results for the antibody clone the sequences were derived from (Cohen et al., 2020). The observed differences between LILRB1-IgGo and LILRB2-IgGo in the ability to enhance the phagocytosis of lymphoma cells may thus be related to the quality of receptor-ligand interaction, differing affinities for HLA class I and the potency of the respective receptor's intracellular signaling. Furthermore, it has not been ruled out with certainty that the particular anti-LILRB2 antibody used here may also function in an agonistic way and facilitated the activation of LILRB2 downstream pathways concurrently to the prevention of ligand-binding. It also is conceivable that in the situation of LILRB1 and LILRB2 competing for binding to HLA class I, LILRB2 antibody blockade shifted the balance towards LILRB1-engagement and thus the effect of disrupting inhibitory LILRB2 signaling was abrogated by the more dominant suppressive influence of LILRB1.

# 4.4 Anti-Cancer Effects of LILRB Blockade in Different Immune Effector Cells

Antibody co-masking of LILRB1 and CD47 has demonstrated efficacy to promote ADCP in combination with different CD20-specific IgG antibodies. Thus, enhanced phagocytosis of lymphoma cells was found for combinations with the native IgG1 antibody rituximab, its Fc protein-engineered variant RTX-DE and when applied with the Fc glycoengineered obinutuzumab (Zeller et al., 2022). Moreover, LILRB1/CD47 co-inhibition enhanced the phagocytosis when combined with an IgA2 version of rituximab (figure 24). Although most therapeutic antibodies are IgG, the IgA isotype may reflect a promising alternative format for cancer immunotherapeutics. Therapeutic IgG molecules are chosen mainly for their high capability to recruit NK cells, macrophages and to trigger CDC. However, through the activation of FcαRI IgA antibodies are also capable of engaging myeloid effector cells, including monocytes, macrophages and neutrophil granulocytes. Additionally, employing IgA antibodies circumvents activation of inhibitory FcγRIIB expressed by myeloid cells, which dampens stimulatory signaling by activating FcγR. In neutrophils, IgA antibodies are even more effective than IgG antibodies (Evers et al., 2020).

Macrophage ADCP of lymphoma cells, as well as ADCC of lymphoma cells by neutrophil granulocytes mediated by CD20 IgA antibodies can significantly be enhanced by the cognate presence of CD47 blocking antibodies (Evers et al., 2021). As revealed here, the additional co-inhibition of LILRB1 demonstrated efficacy to further promote the IgA antibody-mediated phagocytosis of lymphoma cells. Hence, it can be concluded that also LILRB1 interferes with FcαRI signaling in macrophages.

Of note, co-application of LILRB1-IgGσ and CD47-IgGσ also improved ADCP by tumor targeting antibodies specific for other antigens than CD20. It has recently been demonstrated that the antibody combination enhances the phagocytosis of T-ALL cells mediated by the CD38 antibody daratumumab *in vitro* (Zeller et al., 2023a, Zeller et al., 2024). Thus, the approach of LILRB1/CD47 co-inhibition may be efficient also in further types of cancer.

In addition to enhancing macrophage phagocytosis of solid cancer and lymphoma cells, LILRB1-directed antibodies may mediate further effector functions. Both gene knockout of LILRB1 and treatment with anti-LILRB2 antibodies were found to alter the polarization state of macrophages towards an inflammatory, M1-like phenotype (Barkal et al., 2018, Chen et al., 2018). Thus, also anti-LILRB1 antibodies may exert this effect and the antibody blockade of LILRB1 may modulate TAMs or myeloid derived suppressor cells and contribute to revert immune suppression in the TME. Furthermore, besides dendritic

cells and B cells macrophages are professional antigen-presenting cells. The optimization of the phagocytosis of cancer cells may result in increased presentation of tumor antigens and thus initiate T cell anti-cancer immunity (Feng et al., 2019). In murine models of colon cancer and B cell lymphoma, treatment with CD47-specific antibodies resulted in tumor antigen-specific T cell responses (Liu et al., 2015b). However, whether also LILRB1 blockade holds the potential to promote adaptive T cell immunity is currently not known and will require further studies.

Like *ex vivo* generated macrophages, also lymphoma-associated macrophages (LAM) isolated from the bone marrow (BM) of DLBCL patients with BM infiltration were found to pronouncedly express LILRB1 (Zeller et al., 2022). Interestingly, when LILRB1 expression levels were compared to macrophages derived from the BM of DLBCL patients without BM infiltration, a tendency towards enhanced expression of LILRB1 in LAMs was observed. However, statistical significance for this observation was not reached. Importantly, LILRB1 blockade was also efficient in LAMs and significantly enhanced the phagocytosis of lymphoma cells when combined with CD47 antibodies and rituximab (Zeller et al., 2022).

Expression of the HLA receptors LILRB1 and LILRB2 is found also in other populations of immune cells. For instance, certain CD8<sup>+</sup> T cells, as well as certain NK cells carry LILRB1. LILRB1 expression in NK cells varies substantially between individuals and is elevated in peripheral blood CD56<sup>dim</sup> NK cells, which also express FcyRIIIA, compared to CD56<sup>bright</sup> NK cells, which do not express FcyRIIIA (Colonna et al., 1997, Morandi et al., 2011). Moreover, LILRB1 is found on terminally differentiated NK cells and virusinduced, adaptive NK cells (Freud et al., 2017, Beziat et al., 2010, Peppa et al., 2018, Muntasell et al., 2016). In NK cells, LILRB1 blockade has been revealed to enhance both natural cytotoxicity and ADCC. Thus, antibody blockade of LILRB1 promoted NK cell cytotoxicity towards CLL cells, especially when paired with the immunomodulator lenalidomide (Villa-Alvarez et al., 2018). Also, anti-LILRB1 antibodies potentiated NK cell-mediated killing of glioblastoma cells and this effect was further enhanced in the presence of the cytostatic drug temozolomide (Lorenzo-Herrero et al., 2023). LILRB1 has furthermore been demonstrated to interfere with cetuximab-mediated ADCC by NK cells (Roberti et al., 2015). Thus, LILRB1 antibody blockade promoted lysis and restored the deficient ADCC of triple-negative breast cancer cells by cetuximab. Since activated NK cells were shown to also express SIRPα upon stimulation with IL-2, LILRB1/CD47 co-inhibition may allow to further promote NK cell-mediated ADCC (Deuse et al., 2021). Among CD8<sup>+</sup> T cells, LILRB1 is predominantly found on terminally differentiated effector memory T cells re-expressing CD45RA (T<sub>EMRA</sub>), which exert high cytotoxicity and are of great relevance as effector cells for CD3 bispecific antibodies, as well as on certain effector memory T cells ( $T_{EM}$ ) (Kim et al., 2019). Antibody blockade of LILRB1 augmented T cell activation and promoted T cell cytotoxicity by a bispecific [anti-MART-1 × CD3] antibody towards malignant melanoma cells through interfering with the recognition of HLA-G by LILRB1 (Mandel et al., 2022, Kim et al., 2019). Thus, LILRB1-blocking antibodies not only enhance phagocytosis by macrophages, but also promote cancer cell lysis by cytotoxic lymphocytes.

Investigations for the expression of LILRB1 in neutrophil granulocytes revealed contradictory results. While some LILRB1-directed antibody clones displayed binding to neutrophil granulocytes, other antibody clones, including the clone GHI/75 LILRB1-IgG $\sigma$  was derived from, did not (Tedla et al., 2003, Pulford et al., 1991). However, several studies have confirmed LILRB2 to be expressed on neutrophil granulocytes (Baudhuin et al., 2013, Bankey et al., 2010). Furthermore, disruption of the CD47:SIRP $\alpha$  axis enhanced ADCC and trogoptosis by neutrophil granulocytes (Matlung et al., 2018). Thus, although LILRB2-IgG $\sigma$  was not efficient in macrophages to enhance the phagocytosis of lymphoma cells, it may be worth evaluating LILRB2 blockade or even the co-inhibition of LILRB2 and CD47 in neutrophil granulocytes.

# 4.5 Challenges in the Development of LILRB1-Directed Antibodies and Potential Pitfalls in their Application

The further investigation of LILRB1 and CD47 co-blockade towards clinical application will require studies in animal models. However, several aspects make the evaluation of this approach a challenging issue in mice. The expression of LILRB1 is restricted to humans and primates (Storm et al., 2021). Analogous to LILRB1 in humans, the murine receptor orthologue PirB binds major histocompatibility complex class I molecules with a broad specificity and also interacts with β2m, suggesting an involvement of β2m as a contact site between receptor and ligand (Nakamura et al., 2004, Takai, 2005). However, PirB does not recognize human complexes of HLA and β2m. The species-specific mode of binding has been suggested to be mediated by differences between murine and human β2m (Barkal et al., 2018). Since murine β2m has proven incapable of forming stable complexes with HLA α-chains, the generation of chimeric β2m, in which the human β2m is modified by replacing the human sequences against the corresponding murine amino acid sequence only within the LILRB1 contact site has been suggested as a potential solution (Barkal et al., 2018). Another potential opportunity could be the generation of LILRB1 transgenic mice. LILRB1 knock-in mice with sufficient LILRB1 expression levels have already been described, yet, immune competent mice were used

in this study (Belkin et al., 2003). However, to study the role of LILRB1 in the phagocytosis of lymphoma cells, engraftment of human cancer cells is necessary, which requires immune deficient mice. A further solution to overcome species-specific recognition of cancer cell-expressed HLA molecules could be the use of humanized mice, in which human CD34<sup>+</sup> progenitor cells are transplanted to establish human leukocytes (Stripecke et al., 2020). Yet, the recognition of human cancer cells by human leukocytes may interfere with the co-engraftment of cancer cells in such mice, which may make partial matching of HLA alleles necessary. Furthermore, the differences between co-existing human and murine macrophages may be challenging. Human macrophages are responsive to both CD47 and LILRB1 antibody blockade. In contrast, murine macrophages lack expression of LILRB1. Thus, due to the ligation of human CD47 by murine SIRPα, only CD47-, but not LILRB1-directed antibodies will exert effects (Barkal et al., 2018). Moreover, murine macrophages are more susceptible to CD47 antibody blockade. Whereas here, Fc-silent, LILRB1- or CD47-specific antibodies strictly required the presence of an activating signal to become effective, Fc-silent CD47 antibodies were found to prolong survival in murine xenograft models of T-ALL and BCP-ALL already when applied as monotherapy (Muller et al., 2022, Vogiatzi et al., 2020, Schewe et al., 2024). In vitro, CD47 blockade by Fab fragments was shown to be sufficient to induce ADCP by murine macrophages, but not by human macrophages, which required FcyR activation (Jain et al., 2019). These differences may distort results and the differentiation between effects mediated by human or murine macrophages may only be possible upon depletion of murine macrophages.

Furthermore, various different hematological and solid cancers express LILRB1 (Kang et al., 2016) including AML (Kang et al., 2015), certain entities of T cell lymphomas (Urosevic et al., 2004, Nikolova et al., 2002, Kamarashev et al., 2001), B-lineage lymphomas and leukemias (Harly et al., 2011, Naji et al., 2012, Lozano et al., 2018), ovarian cancer (Xu et al., 2023), gastric cancer (Zhang et al., 2012) and RCC (Tronik-Le Roux et al., 2020). Interestingly, the display of LILRB1 on cancer cells may mediate opposing effects. For instance, in cutaneous T-cell lymphoma cells, LILRB1 expression has been demonstrated to confer protection against cell death inducted by CD3/TCR-mediated activation (Urosevic et al., 2004). On the other hand, several studies revealed a beneficial role for the expression of LILRB1 in certain types of cancer. For instance, in neoplastic B cells, LILRB1 signaling impaired cancer cell proliferation and resulted in cell cycle arrest (Naji et al., 2012). Furthermore, expression of LILRB1 may even sensitize cancer cells for elimination by immune cells. Display of LILRB1 on multiple myeloma cells resulted in enhanced NK cell- and T cell-mediated antitumor activity. Immune

escape mediated by the loss of LILRB1 expression in multiple myeloma cells was, among other factors, suggested to be related to engagement of the LILRB1 ligand S100A9 on NK cells, since the blockade of S100A9 partially abrogated the effect of LILRB1 overexpression on cytotoxicity (Lozano et al., 2018). Additionally, through the recognition of HLA molecules on  $\gamma\delta$  T cells, LILRB1 expression in lymphoma cells has been demonstrated to exert a co-stimulatory function and thus increased the sensitivity for lysis by certain  $\gamma\delta$  T cells (Harly et al., 2011). Thus, further investigations will be needed to determine under which circumstances and in which types of cancer the antibody blockade of LILRB1 is beneficial.

# 4.6 Perspectives of Immune Checkpoint Co-Blockade in Cancer Immunotherapy

Durable response rates were observed upon antibody immune checkpoint blockade of PD-1 or CTLA-4 in T cells. However, single agent application was found to be effective only in a fraction of patients (Rotte, 2019). Various approaches are being pursued to enhance efficacy and to overcome resistance, including combination strategies with tumor targeting antibodies, chemotherapy or the co-blockade of different immune checkpoints. Particularly the concurrent masking of PD-1 and CTLA-4 resulted in an impressive increase in response rates and median survival times in malignant melanoma (Rotte, 2019). The emerging field of immune checkpoint inhibition in innate immune cells raises the question about novel potential combination strategies, which may even hold the potential to stimulate both innate and adaptive immunity simultaneously. For instance, encouraging pre-clinical results were achieved by combining disruption of the CD47:SIRPα axis with immune checkpoint blockade in T cells. Thus, the co-treatment with anti-PD-L1 and CD47 antibodies or a bispecific heterodimer fusion protein of an anti-PD-L1 antibody and SIRPα inhibited tumor growth of colon carcinoma cells in vivo (Chen et al., 2021a, Liu et al., 2018). Additionally, bispecific anti-CD47-PD-L1 antibodies and the anti-PD-L1-SIRPα fusion protein displayed enhanced binding selectivity to PD-L1<sup>+</sup> CD47<sup>+</sup> cancer cells and notably reduced binding to CD47-expressing RBC when compared to CD47 antibodies and SIRPα-Fc-fusion proteins, respectively (Chen et al., 2021a, Liu et al., 2018). Regarding LILRB1, elevated expression has been suggested to function as a possible mechanism of resistance in PD-1 immune checkpoint therapy, since upregulation of LILRB1 protein was found in 48% of malignant melanoma patients following nivolumab therapy (Mandel et al., 2022). Moreover, as mentioned above, LILRB1 has not only been found to be a macrophage phagocytosis checkpoint impairing the engulfment of cancer cells, but also to interfere with the cellular cytotoxicity of certain

CD8<sup>+</sup> T cells. Of note, a nonoverlapping expression pattern of LILRB1 and PD-1 was described across CD8<sup>+</sup> T<sub>EMRA</sub> and T<sub>EM</sub> cells and the co-blockade of both receptors may thus hold the potential to harness both subsets. The analysis of intratumoral CD8<sup>+</sup> T cells revealed that in individual RCC patients PD-1<sup>+</sup> LILRB1<sup>-</sup> and PD-1<sup>-</sup> LILRB1<sup>+</sup> T cells were present in comparable proportions and the cytotoxic functions of PD-1<sup>-</sup> LILRB1<sup>+</sup> T cells were specifically inhibited by the engagement of HLA-G, rendering them a so far unexploited population of effector cells in the tumor microenvironment (Barkal et al., 2018, Mandel et al., 2022, Dumont et al., 2019). Indeed, the release of TNF-α by autologous MNCs co-cultured with colon cancer cells was promoted synergistically when anti-PD1 antibodies were combined with anti-LILRB1 antibodies (Mandel et al., 2022). Furthermore, as demonstrated here for the co-inhibition of LILRB1 and CD47, combination strategies of immune checkpoint inhibitors in myeloid cells could display a promising approach. For instance, a synergistic ADCP-enhancing effect has been reported for the co-blockade of CD47 and CD24. Masking of both receptors notably further promoted the phagocytosis of MCL cells by M2-like TAMs compared to single agent application of CD47 or CD24 antibodies in vitro (Aroldi et al., 2022). Even further enhancement of ADCP was achieved in this study when the CD47/CD24 co-blockade was combined with rituximab. Moreover, even though LILRB2-IgGσ was not effective in promoting ADCP of lymphoma cells here, the cognate blockade of LILRB2 in addition to LILRB1 may be beneficial, as it may allow to relieve immunosuppression in the TME by modulating TAMs and thus promote the anti-tumor functions of various effector cell populations.

A potential pitfall in CD47 antibody therapy may originate from antigen sink as a consequence of the ubiquitous expression of the molecule. However, also anti-SIRPα antibodies demonstrated efficacy in mediating anti-tumor immunity and may display an attractive alternative (Abe et al., 2018, Gauttier et al., 2020). Since the simultaneous inhibition of the SIRPα:CD47 and the LILRB1:HLA axis was effective in enhancing ADCP of lymphoma cells here, the abrogation of both signaling pathways in macrophages through bispecific anti-SIRPα-LILRB1 antibodies may be a promising further approach. The encouraging pre-clinical findings on the effect of LILRB1 blockade have laid the foundation for first clinical evaluations of LILRB1-targeting agents. Different formats of therapeutic antibodies or fusion proteins specific for either LILRB1, LILRB1 and LILRB2 or LILRB1, LILRB2 and the KIR KIR3DL1 are currently being evaluated alone or together with anti-EGFR, anti-PD-1 or anti-CTLA-4 antibodies (Mandel et al., 2022, Udartseva et al., 2022, Mondal et al., 2021, Belaunzaran et al., 2021). Early findings have been released for the dose escalation of the single agent application of the antibody clone

NGM707, which recognizes both LILRB1 and LILRB2, and its combination with pembrolizumab. As a result, NGM707 was well tolerated when applied alone or in combination with pembrolizumab and early signs of efficacy were observed (Naing et al., 2022, Wang et al., 2024). However, current clinical studies are only conducted in patients with solid tumors.

In conclusion, the pre-clinical results presented in this thesis provide substantial evidence for *in vitro* efficacy of the combination of CD20 antibodies with LILRB1 and CD47 co-inhibition. Masking of the HLA class I receptor LILRB1 complemented the blockade of CD47 and the concomitant checkpoint inhibition of LILRB1 and CD47 may hold the potential to further ameliorate the CD20 antibody therapy of lymphomas. Consequently, combining tumor targeting antibodies with LILRB1 blockade and CD47-or SIRPα-directed antibodies is worth further evaluation *in vivo* in appropriate mouse xenograft models and development towards clinical application.

## 5. Bibliography

- Abdallah, F., Coindre, S., Gardet, M., Meurisse, F., Naji, A., Suganuma, N., Abi-Rached, L., Lambotte, O. & Favier, B. 2021. Leukocyte Immunoglobulin-Like Receptors in Regulating the Immune Response in Infectious Diseases: A Window of Opportunity to Pathogen Persistence and a Sound Target in Therapeutics. *Front Immunol*, 12, 717998.
- Abe, T., Tanaka, Y., Piao, J., Tanimine, N., Oue, N., Hinoi, T., Garcia, N. V., Miyasaka, M., Matozaki, T., Yasui, W. & Ohdan, H. 2018. Signal regulatory protein alpha blockade potentiates tumoricidal effects of macrophages on gastroenterological neoplastic cells in syngeneic immunocompetent mice. *Ann Gastroenterol Surg*, 2, 451-462.
- Advani, R., Flinn, I., Popplewell, L., Forero, A., Bartlett, N. L., Ghosh, N., Kline, J., Roschewski, M., LaCasce, A., Collins, G. P., Tran, T., Lynn, J., Chen, J. Y., Volkmer, J. P., Agoram, B., Huang, J., Majeti, R., Weissman, I. L., Takimoto, C. H., Chao, M. P. & Smith, S. M. 2018. CD47 Blockade by Hu5F9-G4 and Rituximab in Non-Hodgkin's Lymphoma. *N Engl J Med*, 379, 1711-1721.
- Alaoui, L., Palomino, G., Zurawski, S., Zurawski, G., Coindre, S., Dereuddre-Bosquet, N., Lecuroux, C., Goujard, C., Vaslin, B., Bourgeois, C., Roques, P., Le Grand, R., Lambotte, O. & Favier, B. 2018. Early SIV and HIV infection promotes the LILRB2/MHC-I inhibitory axis in cDCs. *Cell Mol Life Sci*, 75, 1871-1887.
- Alfaleh, M. A., Alsaab, H. O., Mahmoud, A. B., Alkayyal, A. A., Jones, M. L., Mahler, S. M. & Hashem, A. M. 2020. Phage Display Derived Monoclonal Antibodies: From Bench to Bedside. *Front Immunol*, 11, 1986.
- Allan, D. S., Colonna, M., Lanier, L. L., Churakova, T. D., Abrams, J. S., Ellis, S. A., McMichael, A. J. & Braud, V. M. 1999. Tetrameric complexes of human histocompatibility leukocyte antigen (HLA)-G bind to peripheral blood myelomonocytic cells. *J Exp Med*, 189, 1149-56.
- Ansell, S. M. 2021. Checkpoint Blockade in Lymphoma. J Clin Oncol, 39, 525-533.
- Ansell, S. M., Lesokhin, A. M., Borrello, I., Halwani, A., Scott, E. C., Gutierrez, M., Schuster, S. J., Millenson, M. M., Cattry, D., Freeman, G. J., Rodig, S. J., Chapuy, B., Ligon, A. H., Zhu, L., Grosso, J. F., Kim, S. Y., Timmerman, J. M., Shipp, M. A. & Armand, P. 2015. PD-1 blockade with nivolumab in relapsed or refractory Hodgkin's lymphoma. *N Engl J Med*, 372, 311-9.
- Ansell, S. M., Minnema, M. C., Johnson, P., Timmerman, J. M., Armand, P., Shipp, M. A., Rodig, S. J., Ligon, A. H., Roemer, M. G. M., Reddy, N., Cohen, J. B., Assouline, S., Poon, M., Sharma, M., Kato, K., Samakoglu, S., Sumbul, A. & Grigg, A. 2019. Nivolumab for Relapsed/Refractory Diffuse Large B-Cell Lymphoma in Patients Ineligible for or Having Failed Autologous Transplantation: A Single-Arm, Phase II Study. *J Clin Oncol*, 37, 481-489.
- Armand, P., Janssens, A., Gritti, G., Radford, J., Timmerman, J., Pinto, A., Mercadal Vilchez, S., Johnson, P., Cunningham, D., Leonard, J. P., Rodig, S. J., Martin-Regueira, P., Sumbul, A., Samakoglu, S., Tang, H. & Ansell, S. M. 2021. Efficacy and safety results from CheckMate 140, a phase 2 study of nivolumab for relapsed/refractory follicular lymphoma. *Blood*, 137, 637-645.
- Arnold, V., Cummings, J. S., Moreno-Nieves, U. Y., Didier, C., Gilbert, A., Barre-Sinoussi, F. & Scott-Algara, D. 2013. S100A9 protein is a novel ligand for the CD85j receptor and its interaction is implicated in the control of HIV-1 replication by NK cells. *Retrovirology*, 10, 122.

- Aroldi, A., Mauri, M., Villa, M., Malighetti, F., Cocito, F., Voena, C., Chiarle, R., Mologni, L., Piazza, R. & Gambacorti-Passerini, C. 2022. Effects of CD24 "Don't Eat Me" Signal Blockade in Combination with Anti-CD47 and Rituximab in Mantle-Cell Lymphoma. *Blood*, 140 (Supplement 1), 3136-3138.
- Atwal, J. K., Pinkston-Gosse, J., Syken, J., Stawicki, S., Wu, Y., Shatz, C. & Tessier-Lavigne, M. 2008. PirB is a functional receptor for myelin inhibitors of axonal regeneration. *Science*, 322, 967-70.
- Balkwill, F. & Mantovani, A. 2001. Inflammation and cancer: back to Virchow? *Lancet*, 357, 539-45.
- Bankey, P. E., Banerjee, S., Zucchiatti, A., De, M., Sleem, R. W., Lin, C. F., Miller-Graziano, C. L. & De, A. K. 2010. Cytokine induced expression of programmed death ligands in human neutrophils. *Immunol Lett*, 129, 100-7.
- Barclay, A. N. & Van den Berg, T. K. 2014. The interaction between signal regulatory protein alpha (SIRPalpha) and CD47: structure, function, and therapeutic target. *Annu Rev Immunol*, 32, 25-50.
- Barkal, A. A., Brewer, R. E., Markovic, M., Kowarsky, M., Barkal, S. A., Zaro, B. W., Krishnan, V., Hatakeyama, J., Dorigo, O., Barkal, L. J. & Weissman, I. L. 2019. CD24 signalling through macrophage Siglec-10 is a target for cancer immunotherapy. *Nature*, 572, 392-396.
- Barkal, A. A., Weiskopf, K., Kao, K. S., Gordon, S. R., Rosental, B., Yiu, Y. Y., George, B. M., Markovic, M., Ring, N. G., Tsai, J. M., McKenna, K. M., Ho, P. Y., Cheng, R. Z., Chen, J. Y., Barkal, L. J., Ring, A. M., Weissman, I. L. & Maute, R. L. 2018. Engagement of MHC class I by the inhibitory receptor LILRB1 suppresses macrophages and is a target of cancer immunotherapy. *Nat Immunol*, 19, 76-84.
- Baudhuin, J., Migraine, J., Faivre, V., Loumagne, L., Lukaszewicz, A. C., Payen, D. & Favier, B. 2013. Exocytosis acts as a modulator of the ILT4-mediated inhibition of neutrophil functions. *Proc Natl Acad Sci U S A*, 110, 17957-62.
- Behrens, L. M., van Egmond, M. & van den Berg, T. K. 2023. Neutrophils as immune effector cells in antibody therapy in cancer. *Immunol Rev*, 314, 280-301.
- Belaunzaran, O. M., Rafiei, A., Kumar, A., Gualandi, M., Westphal, M., Vogt, L., Smith, S., Curran, M. & Renner, C. 2021. IosH2 exerts potent anti-tumor activity by blocking LILRB1/2 and KIR3DL1 receptor signaling. *J Immunother Cancer*, 9 (Supplement 2), A906.
- Belkin, D., Torkar, M., Chang, C., Barten, R., Tolaini, M., Haude, A., Allen, R., Wilson, M. J., Kioussis, D. & Trowsdale, J. 2003. Killer cell Ig-like receptor and leukocyte Ig-like receptor transgenic mice exhibit tissue- and cell-specific transgene expression. *J Immunol*, 171, 3056-63.
- Ben Mkaddem, S., Benhamou, M. & Monteiro, R. C. 2019. Understanding Fc Receptor Involvement in Inflammatory Diseases: From Mechanisms to New Therapeutic Tools. *Front Immunol*, 10, 811.
- Berman, H., Henrick, K. & Nakamura, H. 2003. Announcing the worldwide Protein Data Bank. *Nat Struct Biol*, 10, 980.
- Berman, H. M., Westbrook, J., Feng, Z., Gilliland, G., Bhat, T. N., Weissig, H., Shindyalov, I. N. & Bourne, P. E. 2000. The Protein Data Bank. *Nucleic Acids Res*, 28, 235-42.

- Beziat, V., Descours, B., Parizot, C., Debre, P. & Vieillard, V. 2010. NK cell terminal differentiation: correlated stepwise decrease of NKG2A and acquisition of KIRs. *PLoS One*, 5, e11966.
- Bjørneboe, M. & Gormsen, H. 1943. Experimental studies on the role of plasma cells as antibody producers. *APMIS*, 20, 649-662.
- Boulianne, G. L., Hozumi, N. & Shulman, M. J. 1984. Production of functional chimaeric mouse/human antibody. *Nature*, 312, 643-6.
- Boyington, J. C., Motyka, S. A., Schuck, P., Brooks, A. G. & Sun, P. D. 2000. Crystal structure of an NK cell immunoglobulin-like receptor in complex with its class I MHC ligand. *Nature*, 405, 537-43.
- Boyington, J. C. & Sun, P. D. 2002. A structural perspective on MHC class I recognition by killer cell immunoglobulin-like receptors. *Mol Immunol*, 38, 1007-21.
- Brown, D., Trowsdale, J. & Allen, R. 2004. The LILR family: modulators of innate and adaptive immune pathways in health and disease. *Tissue Antigens*, 64, 215-25.
- Brudno, J. N. & Kochenderfer, J. N. 2018. Chimeric antigen receptor T-cell therapies for lymphoma. *Nat Rev Clin Oncol*, 15, 31-46.
- Brudno, J. N., Maric, I., Hartman, S. D., Rose, J. J., Wang, M., Lam, N., Stetler-Stevenson, M., Salem, D., Yuan, C., Pavletic, S., Kanakry, J. A., Ali, S. A., Mikkilineni, L., Feldman, S. A., Stroncek, D. F., Hansen, B. G., Lawrence, J., Patel, R., Hakim, F., Gress, R. E. & Kochenderfer, J. N. 2018. T Cells Genetically Modified to Express an Anti-B-Cell Maturation Antigen Chimeric Antigen Receptor Cause Remissions of Poor-Prognosis Relapsed Multiple Myeloma. *J Clin Oncol*, 36, 2267-2280.
- Buchbinder, E. I. & Desai, A. 2016. CTLA-4 and PD-1 Pathways: Similarities, Differences, and Implications of Their Inhibition. *Am J Clin Oncol*, 39, 98-106.
- Burn, G. L., Foti, A., Marsman, G., Patel, D. F. & Zychlinsky, A. 2021. The Neutrophil. *Immunity*, 54, 1377-1391.
- Cai, Z., Wang, L., Han, Y., Gao, W., Wei, X., Gong, R., Zhu, M., Sun, Y. & Yu, S. 2019. Immunoglobulin-like transcript 4 and human leukocyte antigen-G interaction promotes the progression of human colorectal cancer. *Int J Oncol*, 54, 1943-1954.
- Canioni, D., Salles, G., Mounier, N., Brousse, N., Keuppens, M., Morchhauser, F., Lamy, T., Sonet, A., Rousselet, M. C., Foussard, C. & Xerri, L. 2008. High numbers of tumor-associated macrophages have an adverse prognostic value that can be circumvented by rituximab in patients with follicular lymphoma enrolled onto the GELA-GOELAMS FL-2000 trial. *J Clin Oncol*, 26, 440-6.
- Carenza, C., Calcaterra, F., Oriolo, F., Di Vito, C., Ubezio, M., Della Porta, M. G., Mavilio, D. & Della Bella, S. 2019. Costimulatory Molecules and Immune Checkpoints Are Differentially Expressed on Different Subsets of Dendritic Cells. Front Immunol, 10, 1325.
- Carosella, E. D., Gregori, S. & Tronik-Le Roux, D. 2021. HLA-G/LILRBs: A Cancer Immunotherapy Challenge. *Trends Cancer*, 7, 389-392.
- Carter, P., Presta, L., Gorman, C. M., Ridgway, J. B., Henner, D., Wong, W. L., Rowland, A. M., Kotts, C., Carver, M. E. & Shepard, H. M. 1992. Humanization of an anti-p185HER2 antibody for human cancer therapy. *Proc Natl Acad Sci U S A*, 89, 4285-9.

- Carter, P. J. & Lazar, G. A. 2018. Next generation antibody drugs: pursuit of the 'high-hanging fruit'. *Nat Rev Drug Discov*, 17, 197-223.
- Cartron, G., Dacheux, L., Salles, G., Solal-Celigny, P., Bardos, P., Colombat, P. & Watier, H. 2002. Therapeutic activity of humanized anti-CD20 monoclonal antibody and polymorphism in IgG Fc receptor FcgammaRIIIa gene. *Blood*, 99, 754-8.
- Chamarthy, M. R., Williams, S. C. & Moadel, R. M. 2011. Radioimmunotherapy of non-Hodgkin's lymphoma: from the 'magic bullets' to 'radioactive magic bullets'. *Yale J Biol Med*, 84, 391-407.
- Chan, A. C. & Carter, P. J. 2010. Therapeutic antibodies for autoimmunity and inflammation. *Nat Rev Immunol*, 10, 301-16.
- Chan, C., Lustig, M., Baumann, N., Valerius, T., van Tetering, G. & Leusen, J. H. W. 2022. Targeting Myeloid Checkpoint Molecules in Combination With Antibody Therapy: A Novel Anti-Cancer Strategy With IgA Antibodies? *Front Immunol*, 13, 932155.
- Chao, M. P., Alizadeh, A. A., Tang, C., Myklebust, J. H., Varghese, B., Gill, S., Jan, M., Cha, A. C., Chan, C. K., Tan, B. T., Park, C. Y., Zhao, F., Kohrt, H. E., Malumbres, R., Briones, J., Gascoyne, R. D., Lossos, I. S., Levy, R., Weissman, I. L. & Majeti, R. 2010. Anti-CD47 antibody synergizes with rituximab to promote phagocytosis and eradicate non-Hodgkin lymphoma. *Cell*, 142, 699-713.
- Chaplin, D. D. 2010. Overview of the immune response. *J Allergy Clin Immunol*, 125, S3-23.
- Chapman, T. L., Heikeman, A. P. & Bjorkman, P. J. 1999. The inhibitory receptor LIR-1 uses a common binding interaction to recognize class I MHC molecules and the viral homolog UL18. *Immunity*, 11, 603-13.
- Chen, D. S. & Mellman, I. 2013. Oncology meets immunology: the cancer-immunity cycle. *Immunity*, 39, 1-10.
- Chen, H. M., van der Touw, W., Wang, Y. S., Kang, K., Mai, S., Zhang, J., Alsina-Beauchamp, D., Duty, J. A., Mungamuri, S. K., Zhang, B., Moran, T., Flavell, R., Aaronson, S., Hu, H. M., Arase, H., Ramanathan, S., Flores, R., Pan, P. Y. & Chen, S. H. 2018. Blocking immunoinhibitory receptor LILRB2 reprograms tumor-associated myeloid cells and promotes antitumor immunity. *J Clin Invest*, 128, 5647-5662.
- Chen, J., Zhong, M. C., Guo, H., Davidson, D., Mishel, S., Lu, Y., Rhee, I., Perez-Quintero, L. A., Zhang, S., Cruz-Munoz, M. E., Wu, N., Vinh, D. C., Sinha, M., Calderon, V., Lowell, C. A., Danska, J. S. & Veillette, A. 2017. SLAMF7 is critical for phagocytosis of haematopoietic tumour cells via Mac-1 integrin. *Nature*, 544, 493-497.
- Chen, S. H., Dominik, P. K., Stanfield, J., Ding, S., Yang, W., Kurd, N., Llewellyn, R., Heyen, J., Wang, C., Melton, Z., Van Blarcom, T., Lindquist, K. C., Chaparro-Riggers, J. & Salek-Ardakani, S. 2021a. Dual checkpoint blockade of CD47 and PD-L1 using an affinity-tuned bispecific antibody maximizes antitumor immunity. *J Immunother Cancer*, 9.
- Chen, X., Gao, A., Zhang, F., Yang, Z., Wang, S., Fang, Y., Li, J., Wang, J., Shi, W., Wang, L., Zheng, Y. & Sun, Y. 2021b. ILT4 inhibition prevents TAM- and dysfunctional T cell-mediated immunosuppression and enhances the efficacy of anti-PD-L1 therapy in NSCLC with EGFR activation. *Theranostics*, 11, 3392-3416.

- Clark, M. R. 1997. IgG effector mechanisms. Chem Immunol, 65, 88-110.
- Clynes, R. A., Towers, T. L., Presta, L. G. & Ravetch, J. V. 2000. Inhibitory Fc receptors modulate in vivo cytotoxicity against tumor targets. *Nat Med*, 6, 443-6.
- Cohen, A. D., Garfall, A. L., Stadtmauer, E. A., Melenhorst, J. J., Lacey, S. F., Lancaster, E., Vogl, D. T., Weiss, B. M., Dengel, K., Nelson, A., Plesa, G., Chen, F., Davis, M. M., Hwang, W. T., Young, R. M., Brogdon, J. L., Isaacs, R., Pruteanu-Malinici, I., Siegel, D. L., Levine, B. L., June, C. H. & Milone, M. C. 2019. B cell maturation antigen-specific CAR T cells are clinically active in multiple myeloma. *J Clin Invest*, 129, 2210-2221.
- Cohen, H. B., Mackenzie, L. P., Shaffer, D. R., Ramsay, Y. & Smith, J. Y.-F. 2020.

  Antibodies to LILRB2. U.S. patent Nr. 10,723,789. Washington, DC: U.S. Patent and Trademark Office.
- Colonna, M., Navarro, F., Bellon, T., Llano, M., Garcia, P., Samaridis, J., Angman, L., Cella, M. & Lopez-Botet, M. 1997. A common inhibitory receptor for major histocompatibility complex class I molecules on human lymphoid and myelomonocytic cells. *J Exp Med.* 186, 1809-18.
- Colonna, M., Samaridis, J., Cella, M., Angman, L., Allen, R. L., O'Callaghan, C. A., Dunbar, R., Ogg, G. S., Cerundolo, V. & Rolink, A. 1998. Human myelomonocytic cells express an inhibitory receptor for classical and nonclassical MHC class I molecules. *J Immunol.* 160, 3096-100.
- Cosman, D., Fanger, N., Borges, L., Kubin, M., Chin, W., Peterson, L. & Hsu, M. L. 1997. A novel immunoglobulin superfamily receptor for cellular and viral MHC class I molecules. *Immunity*, 7, 273-82.
- Coussens, L. M. & Werb, Z. 2002. Inflammation and cancer. Nature, 420, 860-7.
- Dabkowska, A., Domka, K. & Firczuk, M. 2024. Advancements in cancer immunotherapies targeting CD20: from pioneering monoclonal antibodies to chimeric antigen receptor-modified T cells. *Front Immunol*, 15, 1363102.
- de Haij, S., Jansen, J. H., Boross, P., Beurskens, F. J., Bakema, J. E., Bos, D. L., Martens, A., Verbeek, J. S., Parren, P. W., van de Winkel, J. G. & Leusen, J. H. 2010. In vivo cytotoxicity of type I CD20 antibodies critically depends on Fc receptor ITAM signaling. *Cancer Res*, 70, 3209-17.
- De Louche, C. D. & Roghanian, A. 2022. Human inhibitory leukocyte Ig-like receptors: from immunotolerance to immunotherapy. *JCI Insight*, 7.
- Dechant, M., Bruenke, J. & Valerius, T. 2003. HLA class II antibodies in the treatment of hematologic malignancies. *Semin Oncol*, 30, 465-75.
- Delgado, S. R., Faissner, S., Linker, R. A. & Rammohan, K. 2024. Key characteristics of anti-CD20 monoclonal antibodies and clinical implications for multiple sclerosis treatment. *J Neurol*, 271, 1515-1535.
- Demaria, O., Cornen, S., Daeron, M., Morel, Y., Medzhitov, R. & Vivier, E. 2019. Harnessing innate immunity in cancer therapy. *Nature*, 574, 45-56.
- Deng, M., Chen, H., Liu, X., Huang, R., He, Y., Yoo, B., Xie, J., John, S., Zhang, N., An, Z. & Zhang, C. C. 2021. Leukocyte immunoglobulin-like receptor subfamily B: therapeutic targets in cancer. *Antib Ther,* 4, 16-33.
- Deuse, T., Hu, X., Agbor-Enoh, S., Jang, M. K., Alawi, M., Saygi, C., Gravina, A., Tediashvili, G., Nguyen, V. Q., Liu, Y., Valantine, H., Lanier, L. L. & Schrepfer, S. 2021. The SIRPalpha-CD47 immune checkpoint in NK cells. *J Exp Med*, 218.

- Ding, W., LaPlant, B. R., Call, T. G., Parikh, S. A., Leis, J. F., He, R., Shanafelt, T. D., Sinha, S., Le-Rademacher, J., Feldman, A. L., Habermann, T. M., Witzig, T. E., Wiseman, G. A., Lin, Y., Asmus, E., Nowakowski, G. S., Conte, M. J., Bowen, D. A., Aitken, C. N., Van Dyke, D. L., Greipp, P. T., Liu, X., Wu, X., Zhang, H., Secreto, C. R., Tian, S., Braggio, E., Wellik, L. E., Micallef, I., Viswanatha, D. S., Yan, H., Chanan-Khan, A. A., Kay, N. E., Dong, H. & Ansell, S. M. 2017. Pembrolizumab in patients with CLL and Richter transformation or with relapsed CLL. Blood, 129, 3419-3427.
- Doniz-Padilla, L., Paniagua, A. E., Sandoval-Correa, P., Monsivais-Urenda, A., Leskela, S., Marazuela, M. & Gonzalez-Amaro, R. 2011. Analysis of expression and function of the inhibitory receptor ILT2 in lymphocytes from patients with autoimmune thyroid disease. *Eur J Endocrinol*, 165, 129-36.
- Dornan, D., Bennett, F., Chen, Y., Dennis, M., Eaton, D., Elkins, K., French, D., Go, M. A., Jack, A., Junutula, J. R., Koeppen, H., Lau, J., McBride, J., Rawstron, A., Shi, X., Yu, N., Yu, S. F., Yue, P., Zheng, B., Ebens, A. & Polson, A. G. 2009. Therapeutic potential of an anti-CD79b antibody-drug conjugate, anti-CD79b-vc-MMAE, for the treatment of non-Hodgkin lymphoma. *Blood*, 114, 2721-9.
- Dulberger, C. L., McMurtrey, C. P., Holzemer, A., Neu, K. E., Liu, V., Steinbach, A. M., Garcia-Beltran, W. F., Sulak, M., Jabri, B., Lynch, V. J., Altfeld, M., Hildebrand, W. H. & Adams, E. J. 2017. Human Leukocyte Antigen F Presents Peptides and Regulates Immunity through Interactions with NK Cell Receptors. *Immunity*, 46, 1018-1029 e7.
- Dumont, C., Jacquier, A., Verine, J., Noel, F., Goujon, A., Wu, C. L., Hung, T. M., Desgrandchamps, F., Culine, S., Carosella, E. D., Rouas-Freiss, N. & LeMaoult, J. 2019. CD8(+)PD-1(-)ILT2(+) T Cells Are an Intratumoral Cytotoxic Population Selectively Inhibited by the Immune-Checkpoint HLA-G. *Cancer Immunol Res*, 7, 1619-1632.
- Dunkelberger, J. R. & Song, W. C. 2010. Complement and its role in innate and adaptive immune responses. *Cell Res*, 20, 34-50.
- Ehrlich, P. 1900. Croonian lecture: on immunity with special reference to cell life. *Proc R Soc Lond*, 66, 424-448.
- Evers, M., Rosner, T., Dunkel, A., Jansen, J. H. M., Baumann, N., Ten Broeke, T., Nederend, M., Eichholz, K., Klausz, K., Reiding, K., Schewe, D. M., Kellner, C., Peipp, M., Leusen, J. H. W. & Valerius, T. 2021. The selection of variable regions affects effector mechanisms of IgA antibodies against CD20. *Blood Adv*, 5, 3807-3820.
- Evers, M., Ten Broeke, T., Jansen, J. H. M., Nederend, M., Hamdan, F., Reiding, K. R., Meyer, S., Moerer, P., Brinkman, I., Rosner, T., Lebbink, R. J., Valerius, T. & Leusen, J. H. W. 2020. Novel chimerized IgA CD20 antibodies: Improving neutrophil activation against CD20-positive malignancies. *MAbs*, 12, 1795505.
- Fanger, N. A., Cosman, D., Peterson, L., Braddy, S. C., Maliszewski, C. R. & Borges, L. 1998. The MHC class I binding proteins LIR-1 and LIR-2 inhibit Fc receptormediated signaling in monocytes. *Eur J Immunol*, 28, 3423-34.
- Feng, M., Jiang, W., Kim, B. Y. S., Zhang, C. C., Fu, Y. X. & Weissman, I. L. 2019. Phagocytosis checkpoints as new targets for cancer immunotherapy. *Nat Rev Cancer*, 19, 568-586.
- Freile, J. A., Ustyanovska Avtenyuk, N., Corrales, M. G., Lourens, H. J., Huls, G., van Meerten, T., Cendrowicz, E. & Bremer, E. 2022. CD24 Is a Potential Immunotherapeutic Target for Mantle Cell Lymphoma. *Biomedicines*, 10.

- Frenzel, A., Schirrmann, T. & Hust, M. 2016. Phage display-derived human antibodies in clinical development and therapy. *MAbs*, 8, 1177-1194.
- Freud, A. G., Mundy-Bosse, B. L., Yu, J. & Caligiuri, M. A. 2017. The Broad Spectrum of Human Natural Killer Cell Diversity. *Immunity*, 47, 820-833.
- Fry, T. J., Shah, N. N., Orentas, R. J., Stetler-Stevenson, M., Yuan, C. M., Ramakrishna, S., Wolters, P., Martin, S., Delbrook, C., Yates, B., Shalabi, H., Fountaine, T. J., Shern, J. F., Majzner, R. G., Stroncek, D. F., Sabatino, M., Feng, Y., Dimitrov, D. S., Zhang, L., Nguyen, S., Qin, H., Dropulic, B., Lee, D. W. & Mackall, C. L. 2018. CD22-targeted CAR T cells induce remission in B-ALL that is naive or resistant to CD19-targeted CAR immunotherapy. *Nat Med*, 24, 20-28.
- Fu, Z., Li, S., Han, S., Shi, C. & Zhang, Y. 2022. Antibody drug conjugate: the "biological missile" for targeted cancer therapy. *Signal Transduct Target Ther*, 7, 93.
- Garcia, M., Palma, M. B., Verine, J., Miriuka, S., Inda, A. M., Errecalde, A. L., Desgrandchamps, F., Carosella, E. D. & Tronik-Le Roux, D. 2020. The immune-checkpoint HLA-G/ILT4 is involved in the regulation of VEGF expression in clear cell renal cell carcinoma. *BMC Cancer*, 20, 624.
- Gauttier, V., Pengam, S., Durand, J., Biteau, K., Mary, C., Morello, A., Neel, M., Porto, G., Teppaz, G., Thepenier, V., Danger, R., Vince, N., Wilhelm, E., Girault, I., Abes, R., Ruiz, C., Trilleaud, C., Ralph, K., Trombetta, E. S., Garcia, A., Vignard, V., Martinet, B., Glemain, A., Bruneau, S., Haspot, F., Dehmani, S., Duplouye, P., Miyasaka, M., Labarriere, N., Laplaud, D., Le Bas-Bernardet, S., Blanquart, C., Catros, V., Gouraud, P. A., Archambeaud, I., Auble, H., Metairie, S., Mosnier, J. F., Costantini, D., Blancho, G., Conchon, S., Vanhove, B. & Poirier, N. 2020. Selective SIRPalpha blockade reverses tumor T cell exclusion and overcomes cancer immunotherapy resistance. *J Clin Invest*, 130, 6109-6123.
- Godal, R., Bachanova, V., Gleason, M., McCullar, V., Yun, G. H., Cooley, S., Verneris, M. R., McGlave, P. B. & Miller, J. S. 2010. Natural killer cell killing of acute myelogenous leukemia and acute lymphoblastic leukemia blasts by killer cell immunoglobulin-like receptor-negative natural killer cells after NKG2A and LIR-1 blockade. *Biol Blood Marrow Transplant*, 16, 612-21.
- Gong, Q., Ou, Q., Ye, S., Lee, W. P., Cornelius, J., Diehl, L., Lin, W. Y., Hu, Z., Lu, Y., Chen, Y., Wu, Y., Meng, Y. G., Gribling, P., Lin, Z., Nguyen, K., Tran, T., Zhang, Y., Rosen, H., Martin, F. & Chan, A. C. 2005. Importance of cellular microenvironment and circulatory dynamics in B cell immunotherapy. *J Immunol*, 174, 817-26.
- Gordon, S. R., Maute, R. L., Dulken, B. W., Hutter, G., George, B. M., McCracken, M. N., Gupta, R., Tsai, J. M., Sinha, R., Corey, D., Ring, A. M., Connolly, A. J. & Weissman, I. L. 2017. PD-1 expression by tumour-associated macrophages inhibits phagocytosis and tumour immunity. *Nature*, 545, 495-499.
- Gul, N. & van Egmond, M. 2015. Antibody-Dependent Phagocytosis of Tumor Cells by Macrophages: A Potent Effector Mechanism of Monoclonal Antibody Therapy of Cancer. *Cancer Res.* 75, 5008-13.
- Hansel, T. T., Kropshofer, H., Singer, T., Mitchell, J. A. & George, A. J. 2010. The safety and side effects of monoclonal antibodies. *Nat Rev Drug Discov*, 9, 325-38.

- Harly, C., Peyrat, M. A., Netzer, S., Dechanet-Merville, J., Bonneville, M. & Scotet, E. 2011. Up-regulation of cytolytic functions of human Vdelta2-gamma T lymphocytes through engagement of ILT2 expressed by tumor target cells. *Blood*, 117, 2864-73.
- Harries, M. & Smith, I. 2002. The development and clinical use of trastuzumab (Herceptin). *Endocr Relat Cancer*, 9, 75-85.
- Harrison, P. T., Davis, W., Norman, J. C., Hockaday, A. R. & Allen, J. M. 1994. Binding of monomeric immunoglobulin G triggers Fc gamma RI-mediated endocytosis. *J Biol Chem*, 269, 24396-402.
- Havaei, S. M., Aucoin, M. G. & Jahanian-Najafabadi, A. 2021. Pseudomonas Exotoxin-Based Immunotoxins: Over Three Decades of Efforts on Targeting Cancer Cells With the Toxin. *Front Oncol*, 11, 781800.
- He, J., Xu, J., Yu, X., Zhu, H., Zeng, Y., Fan, D. & Yi, X. 2018. Overexpression of ANGPTL2 and LILRB2 as predictive and therapeutic biomarkers for metastasis and prognosis in colorectal cancer. *Int J Clin Exp Pathol*, 11, 2281-2294.
- He, Y., Bouwstra, R., Wiersma, V. R., de Jong, M., Jan Lourens, H., Fehrmann, R., de Bruyn, M., Ammatuna, E., Huls, G., van Meerten, T. & Bremer, E. 2019. Cancer cell-expressed SLAMF7 is not required for CD47-mediated phagocytosis. *Nat Commun*, 10, 533.
- Held, W. & Mariuzza, R. A. 2008. Cis interactions of immunoreceptors with MHC and non-MHC ligands. *Nat Rev Immunol*, 8, 269-78.
- Hourani, T., Holden, J. A., Li, W., Lenzo, J. C., Hadjigol, S. & O'Brien-Simpson, N. M. 2021. Tumor Associated Macrophages: Origin, Recruitment, Phenotypic Diversity, and Targeting. *Front Oncol*, 11, 788365.
- Hudson, L. E. & Allen, R. L. 2016. Leukocyte Ig-Like Receptors A Model for MHC Class I Disease Associations. *Front Immunol*, 7, 281.
- Hultin, L. E., Hausner, M. A., Hultin, P. M. & Giorgi, J. V. 1993. CD20 (pan-B cell) antigen is expressed at a low level on a subpopulation of human T lymphocytes. *Cytometry,* 14, 196-204.
- Jain, S., Van Scoyk, A., Morgan, E. A., Matthews, A., Stevenson, K., Newton, G., Powers, F., Autio, A., Louissaint, A., Pontini, G., Aster, J. C., Luscinskas, F. W. & Weinstock, D. M. 2019. Targeted inhibition of CD47-SIRPalpha requires Fc-FcgammaR interactions to maximize activity in T-cell lymphomas. *Blood*, 134, 1430-1440.
- Jakubzick, C. V., Randolph, G. J. & Henson, P. M. 2017. Monocyte differentiation and antigen-presenting functions. *Nat Rev Immunol*, 17, 349-362.
- Jin, S., Sun, Y., Liang, X., Gu, X., Ning, J., Xu, Y., Chen, S. & Pan, L. 2022. Emerging new therapeutic antibody derivatives for cancer treatment. Signal Transduct Target Ther, 7, 39.
- Jones, D. C., Kosmoliaptsis, V., Apps, R., Lapaque, N., Smith, I., Kono, A., Chang, C., Boyle, L. H., Taylor, C. J., Trowsdale, J. & Allen, R. L. 2011. HLA class I allelic sequence and conformation regulate leukocyte Ig-like receptor binding. *J Immunol*, 186, 2990-7.
- Jones, P. T., Dear, P. H., Foote, J., Neuberger, M. S. & Winter, G. 1986. Replacing the complementarity-determining regions in a human antibody with those from a mouse. *Nature*, 321, 522-5.

- June, C. H. & Sadelain, M. 2018. Chimeric Antigen Receptor Therapy. *N Engl J Med*, 379, 64-73.
- Kamarashev, J., Burg, G., Mingari, M. C., Kempf, W., Hofbauer, G. & Dummer, R. 2001. Differential expression of cytotoxic molecules and killer cell inhibitory receptors in CD8+ and CD56+ cutaneous lymphomas. *Am J Pathol*, 158, 1593-8.
- Kamber, R. A., Nishiga, Y., Morton, B., Banuelos, A. M., Barkal, A. A., Vences-Catalan, F., Gu, M., Fernandez, D., Seoane, J. A., Yao, D., Liu, K., Lin, S., Spees, K., Curtis, C., Jerby-Arnon, L., Weissman, I. L., Sage, J. & Bassik, M. C. 2021. Inter-cellular CRISPR screens reveal regulators of cancer cell phagocytosis. *Nature*, 597, 549-554.
- Kang, X., Kim, J., Deng, M., John, S., Chen, H., Wu, G., Phan, H. & Zhang, C. C. 2016. Inhibitory leukocyte immunoglobulin-like receptors: Immune checkpoint proteins and tumor sustaining factors. *Cell Cycle*, 15, 25-40.
- Kang, X., Lu, Z., Cui, C., Deng, M., Fan, Y., Dong, B., Han, X., Xie, F., Tyner, J. W., Coligan, J. E., Collins, R. H., Xiao, X., You, M. J. & Zhang, C. C. 2015. The ITIM-containing receptor LAIR1 is essential for acute myeloid leukaemia development. *Nat Cell Biol*, 17, 665-77.
- Kantarjian, H., Stein, A., Gokbuget, N., Fielding, A. K., Schuh, A. C., Ribera, J. M., Wei, A., Dombret, H., Foa, R., Bassan, R., Arslan, O., Sanz, M. A., Bergeron, J., Demirkan, F., Lech-Maranda, E., Rambaldi, A., Thomas, X., Horst, H. A., Bruggemann, M., Klapper, W., Wood, B. L., Fleishman, A., Nagorsen, D., Holland, C., Zimmerman, Z. & Topp, M. S. 2017. Blinatumomab versus Chemotherapy for Advanced Acute Lymphoblastic Leukemia. *N Engl J Med*, 376, 836-847.
- Kellner, C., Bruenke, J., Horner, H., Schubert, J., Schwenkert, M., Mentz, K., Barbin, K., Stein, C., Peipp, M., Stockmeyer, B. & Fey, G. H. 2011. Heterodimeric bispecific antibody-derivatives against CD19 and CD16 induce effective antibody-dependent cellular cytotoxicity against B-lymphoid tumor cells. *Cancer Lett.* 303, 128-39.
- Kellner, C., Otte, A., Cappuzzello, E., Klausz, K. & Peipp, M. 2017. Modulating Cytotoxic Effector Functions by Fc Engineering to Improve Cancer Therapy. *Transfus Med Hemother*, 44, 327-336.
- Ketroussi, F., Giuliani, M., Bahri, R., Azzarone, B., Charpentier, B. & Durrbach, A. 2011. Lymphocyte cell-cycle inhibition by HLA-G is mediated by phosphatase SHP-2 and acts on the mTOR pathway. *PLoS One*, 6, e22776.
- Kim, A., Han, C. J., Driver, I., Olow, A., Sewell, A. K., Zhang, Z., Ouyang, W., Egen, J. G. & Yu, X. 2019. LILRB1 Blockade Enhances Bispecific T Cell Engager Antibody-Induced Tumor Cell Killing by Effector CD8(+) T Cells. *J Immunol*, 203, 1076-1087.
- Kim, T., Vidal, G. S., Djurisic, M., William, C. M., Birnbaum, M. E., Garcia, K. C., Hyman, B. T. & Shatz, C. J. 2013. Human LilrB2 is a beta-amyloid receptor and its murine homolog PirB regulates synaptic plasticity in an Alzheimer's model. *Science*, 341, 1399-404.
- Kohler, G. & Milstein, C. 1975. Continuous cultures of fused cells secreting antibody of predefined specificity. *Nature*, 256, 495-7.
- Kontermann, R. E. & Brinkmann, U. 2015. Bispecific antibodies. *Drug Discov Today*, 20, 838-47.

- Kuroki, K., Tsuchiya, N., Shiroishi, M., Rasubala, L., Yamashita, Y., Matsuta, K., Fukazawa, T., Kusaoi, M., Murakami, Y., Takiguchi, M., Juji, T., Hashimoto, H., Kohda, D., Maenaka, K. & Tokunaga, K. 2005. Extensive polymorphisms of LILRB1 (ILT2, LIR1) and their association with HLA-DRB1 shared epitope negative rheumatoid arthritis. *Hum Mol Genet*, 14, 2469-80.
- Lanzavecchia, A., Corti, D. & Sallusto, F. 2007. Human monoclonal antibodies by immortalization of memory B cells. *Curr Opin Biotechnol*, 18, 523-8.
- Larionova, I., Tuguzbaeva, G., Ponomaryova, A., Stakheyeva, M., Cherdyntseva, N., Pavlov, V., Choinzonov, E. & Kzhyshkowska, J. 2020. Tumor-Associated Macrophages in Human Breast, Colorectal, Lung, Ovarian and Prostate Cancers. *Front Oncol.* 10, 566511.
- Lazar, G. A., Dang, W., Karki, S., Vafa, O., Peng, J. S., Hyun, L., Chan, C., Chung, H. S., Eivazi, A., Yoder, S. C., Vielmetter, J., Carmichael, D. F., Hayes, R. J. & Dahiyat, B. I. 2006. Engineered antibody Fc variants with enhanced effector function. *Proc Natl Acad Sci U S A*, 103, 4005-10.
- Lee, C. H., Romain, G., Yan, W., Watanabe, M., Charab, W., Todorova, B., Lee, J., Triplett, K., Donkor, M., Lungu, O. I., Lux, A., Marshall, N., Lindorfer, M. A., Goff, O. R., Balbino, B., Kang, T. H., Tanno, H., Delidakis, G., Alford, C., Taylor, R. P., Nimmerjahn, F., Varadarajan, N., Bruhns, P., Zhang, Y. J. & Georgiou, G. 2017. IgG Fc domains that bind C1q but not effector Fcgamma receptors delineate the importance of complement-mediated effector functions. *Nat Immunol*, 18, 889-898.
- Lentz, R. W., Colton, M. D., Mitra, S. S. & Messersmith, W. A. 2021. Innate Immune Checkpoint Inhibitors: The Next Breakthrough in Medical Oncology? *Mol Cancer Ther*, 20, 961-974.
- Lepin, E. J., Bastin, J. M., Allan, D. S., Roncador, G., Braud, V. M., Mason, D. Y., van der Merwe, P. A., McMichael, A. J., Bell, J. I., Powis, S. H. & O'Callaghan, C. A. 2000. Functional characterization of HLA-F and binding of HLA-F tetramers to ILT2 and ILT4 receptors. *Eur J Immunol*, 30, 3552-61.
- Lesport, E., Baudhuin, J., Sousa, S., LeMaoult, J., Zamborlini, A., Rouas-Freiss, N., Carosella, E. D. & Favier, B. 2011. Inhibition of human gamma delta [corrected] T-cell antitumoral activity through HLA-G: implications for immunotherapy of cancer. *Cell Mol Life Sci*, 68, 3385-99.
- Leusen, J. H. 2015. IgA as therapeutic antibody. Mol Immunol, 68, 35-9.
- Lewis Marffy, A. L. & McCarthy, A. J. 2020. Leukocyte Immunoglobulin-Like Receptors (LILRs) on Human Neutrophils: Modulators of Infection and Immunity. *Front Immunol*, 11, 857.
- Li, D., Wang, L., Yu, L., Freundt, E. C., Jin, B., Screaton, G. R. & Xu, X. N. 2009. Ig-like transcript 4 inhibits lipid antigen presentation through direct CD1d interaction. *J Immunol*, 182, 1033-40.
- Li, D., Xiong, W., Wang, Y., Feng, J., He, Y., Du, J., Wang, J., Yang, M., Zeng, H., Yang, Y. G., Wu, N., Chen, S. & Dong, Z. 2022. SLAMF3 and SLAMF4 are immune checkpoints that constrain macrophage phagocytosis of hematopoietic tumors. *Sci Immunol*, 7, eabj5501.
- Li, Q., Li, J., Wang, S., Wang, J., Chen, X., Zhou, D., Fang, Y., Gao, A. & Sun, Y. 2020. Overexpressed immunoglobulin-like transcript (ILT) 4 in lung adenocarcinoma is correlated with immunosuppressive T cell subset infiltration and poor patient outcomes. *Biomark Res*, 8, 11.

- Liu, F., Cocker, A. T. H., Pugh, J. L., Djaoud, Z., Parham, P. & Guethlein, L. A. 2022. Natural LILRB1 D1-D2 variants show frequency differences in populations and bind to HLA class I with various avidities. *Immunogenetics*, 74, 513-525.
- Liu, J., Wang, L., Gao, W., Li, L., Cui, X., Yang, H., Lin, W., Dang, Q., Zhang, N. & Sun, Y. 2014. Inhibitory receptor immunoglobulin-like transcript 4 was highly expressed in primary ductal and lobular breast cancer and significantly correlated with IL-10. *Diagn Pathol*, 9, 85.
- Liu, J., Wang, L., Zhao, F., Tseng, S., Narayanan, C., Shura, L., Willingham, S., Howard, M., Prohaska, S., Volkmer, J., Chao, M., Weissman, I. L. & Majeti, R. 2015a. Pre-Clinical Development of a Humanized Anti-CD47 Antibody with Anti-Cancer Therapeutic Potential. *PLoS One*, 10, e0137345.
- Liu, J., Zhang, F., He, J., Wang, S., Wang, L., Li, J., Shi, W., Han, Y., Gao, A. & Sun, Y. 2023a. Tumor-derived Immunoglobulin-like transcript 4 facilitates angiogenesis of colorectal cancer. *Am J Cancer Res*, 13, 419-435.
- Liu, W. R., Kim, J., Nwankwo, C., Ashworth, L. K. & Arm, J. P. 2000. Genomic organization of the human leukocyte immunoglobulin-like receptors within the leukocyte receptor complex on chromosome 19q13.4. *Immunogenetics*, 51, 659-69.
- Liu, X., Liu, L., Ren, Z., Yang, K., Xu, H., Luan, Y., Fu, K., Guo, J., Peng, H., Zhu, M. & Fu, Y. X. 2018. Dual Targeting of Innate and Adaptive Checkpoints on Tumor Cells Limits Immune Evasion. *Cell Rep*, 24, 2101-2111.
- Liu, X., Pu, Y., Cron, K., Deng, L., Kline, J., Frazier, W. A., Xu, H., Peng, H., Fu, Y. X. & Xu, M. M. 2015b. CD47 blockade triggers T cell-mediated destruction of immunogenic tumors. *Nat Med*, 21, 1209-15.
- Liu, Y., Wang, Y., Yang, Y., Weng, L., Wu, Q., Zhang, J., Zhao, P., Fang, L., Shi, Y. & Wang, P. 2023b. Emerging phagocytosis checkpoints in cancer immunotherapy. *Signal Transduct Target Ther*, 8, 104.
- Ljunggren, H. G. & Karre, K. 1990. In search of the 'missing self': MHC molecules and NK cell recognition. *Immunol Today*, 11, 237-44.
- Logtenberg, M. E. W., Scheeren, F. A. & Schumacher, T. N. 2020. The CD47-SIRPalpha Immune Checkpoint. *Immunity*, 52, 742-752.
- Lonberg, N., Taylor, L. D., Harding, F. A., Trounstine, M., Higgins, K. M., Schramm, S. R., Kuo, C. C., Mashayekh, R., Wymore, K., McCabe, J. G. & et al. 1994. Antigen-specific human antibodies from mice comprising four distinct genetic modifications. *Nature*, 368, 856-9.
- Lorenzo-Herrero, S., Sordo-Bahamonde, C., Martinez-Perez, A., Corte-Torres, M. D., Fernandez-Vega, I., Solis-Hernandez, M. P. & Gonzalez, S. 2023. Immunoglobulin-like transcript 2 blockade restores antitumor immune responses in glioblastoma. *Cancer Sci*, 114, 48-62.
- Lozano, E., Diaz, T., Mena, M. P., Sune, G., Calvo, X., Calderon, M., Perez-Amill, L., Rodriguez, V., Perez-Galan, P., Roue, G., Cibeira, M. T., Rosinol, L., Isola, I., Rodriguez-Lobato, L. G., Martin-Antonio, B., Blade, J. & Fernandez de Larrea, C. 2018. Loss of the Immune Checkpoint CD85j/LILRB1 on Malignant Plasma Cells Contributes to Immune Escape in Multiple Myeloma. *J Immunol*, 200, 2581-2591.
- Ma, J., Mo, Y., Tang, M., Shen, J., Qi, Y., Zhao, W., Huang, Y., Xu, Y. & Qian, C. 2021. Bispecific Antibodies: From Research to Clinical Application. *Front Immunol*, 12, 626616.

- Maloney, D. G., Liles, T. M., Czerwinski, D. K., Waldichuk, C., Rosenberg, J., Grillo-Lopez, A. & Levy, R. 1994. Phase I clinical trial using escalating single-dose infusion of chimeric anti-CD20 monoclonal antibody (IDEC-C2B8) in patients with recurrent B-cell lymphoma. *Blood*, 84, 2457-66.
- Mandel, I., Haves Ziv, D., Goldshtein, I., Peretz, T., Alishekevitz, D., Fridman Dror, A., Hakim, M., Hashmueli, S., Friedman, I., Sapir, Y., Greco, R., Qu, H., Nestle, F., Wiederschain, D., Pao, L., Sharma, S. & Ben Moshe, T. 2022. BND-22, a first-in-class humanized ILT2-blocking antibody, promotes antitumor immunity and tumor regression. *J Immunother Cancer*, 10.
- Mantovani, A., Allavena, P., Marchesi, F. & Garlanda, C. 2022. Macrophages as tools and targets in cancer therapy. *Nat Rev Drug Discov*, 21, 799-820.
- Mantovani, A., Allavena, P., Sica, A. & Balkwill, F. 2008. Cancer-related inflammation. *Nature*, 454, 436-44.
- Mantovani, A., Sica, A., Sozzani, S., Allavena, P., Vecchi, A. & Locati, M. 2004. The chemokine system in diverse forms of macrophage activation and polarization. *Trends Immunol.* 25, 677-86.
- Marshall, M. J. E., Stopforth, R. J. & Cragg, M. S. 2017. Therapeutic Antibodies: What Have We Learnt from Targeting CD20 and Where Are We Going? *Front Immunol*, 8, 1245.
- Martinelli, E., De Palma, R., Orditura, M., De Vita, F. & Ciardiello, F. 2009. Antiepidermal growth factor receptor monoclonal antibodies in cancer therapy. *Clin Exp Immunol*, 158, 1-9.
- Matlung, H. L., Babes, L., Zhao, X. W., van Houdt, M., Treffers, L. W., van Rees, D. J., Franke, K., Schornagel, K., Verkuijlen, P., Janssen, H., Halonen, P., Lieftink, C., Beijersbergen, R. L., Leusen, J. H. W., Boelens, J. J., Kuhnle, I., van der Werff Ten Bosch, J., Seeger, K., Rutella, S., Pagliara, D., Matozaki, T., Suzuki, E., Menke-van der Houven van Oordt, C. W., van Bruggen, R., Roos, D., van Lier, R. A. W., Kuijpers, T. W., Kubes, P. & van den Berg, T. K. 2018. Neutrophils Kill Antibody-Opsonized Cancer Cells by Trogoptosis. Cell Rep, 23, 3946-3959 e6.
- Maute, R. L., Weiskopf, K. A., Ring, A. M. & Weissman, I. L. 2019. Composition and methods for inducing phagocytosis of MHC class I positive cells and counteracting anti-CD47/ SIRPA resistance. U.S. patent Nr. 10,316,094. Washington, DC: U.S. Patent and Trademark Office.
- Mazor, Y., Hansen, A., Yang, C., Chowdhury, P. S., Wang, J., Stephens, G., Wu, H. & Dall'Acqua, W. F. 2015. Insights into the molecular basis of a bispecific antibody's target selectivity. *MAbs*, 7, 461-9.
- McLaughlin, P., Grillo-Lopez, A. J., Link, B. K., Levy, R., Czuczman, M. S., Williams, M. E., Heyman, M. R., Bence-Bruckler, I., White, C. A., Cabanillas, F., Jain, V., Ho, A. D., Lister, J., Wey, K., Shen, D. & Dallaire, B. K. 1998. Rituximab chimeric anti-CD20 monoclonal antibody therapy for relapsed indolent lymphoma: half of patients respond to a four-dose treatment program. *J Clin Oncol*, 16, 2825-33.
- Merlo, A., Tenca, C., Fais, F., Battini, L., Ciccone, E., Grossi, C. E. & Saverino, D. 2005. Inhibitory receptors CD85j, LAIR-1, and CD152 down-regulate immunoglobulin and cytokine production by human B lymphocytes. *Clin Diagn Lab Immunol*, 12, 705-12.
- Mills, C. D., Kincaid, K., Alt, J. M., Heilman, M. J. & Hill, A. M. 2000. M-1/M-2 macrophages and the Th1/Th2 paradigm. *J Immunol*, 164, 6166-73.

- Mole, C. M., Bene, M. C., Montagne, P. M., Seilles, E. & Faure, G. C. 1994. Light chains of immunoglobulins in human secretions. *Clin Chim Acta*, 224, 191-7.
- Mondal, K., Song, C., Tian, J., Ho, C., Rivera, L. B., Huang, J., Chen, P., Crawley, S., Lin, V. Y., Sitrin, J., Roda, J. M., Shen, D., Tian, H., Wang, Y., Kutach, A., Kim, J., Sissons, J., Kaplan, D. D. & Stone, G. W. 2021. Preclinical evaluation of NGM707, a novel anti-ILT2/anti-ILT4 dual antagonist monoclonal antibody. *Cancer Res*, 81 (13 Supplement), LB156.
- Monsivais-Urenda, A., Gomez-Martin, D., Santana-de-Anda, K., Cruz-Martinez, J., Alcocer-Varela, J. & Gonzalez-Amaro, R. 2013. Defective expression and function of the ILT2/CD85j regulatory receptor in dendritic cells from patients with systemic lupus erythematosus. *Hum Immunol*, 74, 1088-96.
- Moradi, S., Rossjohn, J. & Vivian, J. P. 2019. Killer cell immunoglobulin-like receptor 2DL3 in complex with HLA-C\*07:02. https://doi.org/10.2210/pdb6PAG/pdb.
- Moradi, S., Stankovic, S., O'Connor, G. M., Pymm, P., MacLachlan, B. J., Faoro, C., Retiere, C., Sullivan, L. C., Saunders, P. M., Widjaja, J., Cox-Livingstone, S., Rossjohn, J., Brooks, A. G. & Vivian, J. P. 2021. Structural plasticity of KIR2DL2 and KIR2DL3 enables altered docking geometries atop HLA-C. *Nat Commun*, 12, 2173.
- Morandi, F., Ferretti, E., Castriconi, R., Dondero, A., Petretto, A., Bottino, C. & Pistoia, V. 2011. Soluble HLA-G dampens CD94/NKG2A expression and function and differentially modulates chemotaxis and cytokine and chemokine secretion in CD56bright and CD56dim NK cells. *Blood*, 118, 5840-50.
- Mori, Y., Tsuji, S., Inui, M., Sakamoto, Y., Endo, S., Ito, Y., Fujimura, S., Koga, T., Nakamura, A., Takayanagi, H., Itoi, E. & Takai, T. 2008. Inhibitory immunoglobulin-like receptors LILRB and PIR-B negatively regulate osteoclast development. *J Immunol*, 181, 4742-51.
- Morrison, S. L., Johnson, M. J., Herzenberg, L. A. & Oi, V. T. 1984. Chimeric human antibody molecules: mouse antigen-binding domains with human constant region domains. *Proc Natl Acad Sci U S A*, 81, 6851-5.
- Morrissey, M. A., Kern, N. & Vale, R. D. 2020. CD47 Ligation Repositions the Inhibitory Receptor SIRPA to Suppress Integrin Activation and Phagocytosis. *Immunity*, 53, 290-302 e6.
- Morvan, M. G. & Lanier, L. L. 2016. NK cells and cancer: you can teach innate cells new tricks. *Nat Rev Cancer*, 16, 7-19.
- Motzer, R. J., Escudier, B., McDermott, D. F., George, S., Hammers, H. J., Srinivas, S., Tykodi, S. S., Sosman, J. A., Procopio, G., Plimack, E. R., Castellano, D., Choueiri, T. K., Gurney, H., Donskov, F., Bono, P., Wagstaff, J., Gauler, T. C., Ueda, T., Tomita, Y., Schutz, F. A., Kollmannsberger, C., Larkin, J., Ravaud, A., Simon, J. S., Xu, L. A., Waxman, I. M., Sharma, P. & CheckMate, I. 2015. Nivolumab versus Everolimus in Advanced Renal-Cell Carcinoma. N Engl J Med, 373, 1803-13.
- Muller, K., Vogiatzi, F., Winterberg, D., Rosner, T., Lenk, L., Bastian, L., Gehlert, C. L., Autenrieb, M. P., Bruggemann, M., Cario, G., Schrappe, M., Kulozik, A. E., Eckert, C., Bergmann, A. K., Bornhauser, B., Bourquin, J. P., Valerius, T., Peipp, M., Kellner, C. & Schewe, D. M. 2022. Combining daratumumab with CD47 blockade prolongs survival in preclinical models of pediatric T-ALL. *Blood*, 140, 45-57.
- Muntasell, A., Pupuleku, A., Cisneros, E., Vera, A., Moraru, M., Vilches, C. & Lopez-Botet, M. 2016. Relationship of NKG2C Copy Number with the Distribution of

- Distinct Cytomegalovirus-Induced Adaptive NK Cell Subsets. *J Immunol*, 196, 3818-27.
- Naing, A., Wang, J. S., Sharma, M. R., Sommerhalder, D., Gandhi, L., Oh, D.-Y., Jiang, Y., Michalski, J., Lee, J., Zhou, K., Taylor, N., Yan, L., Roda, J. M., Blum, L., Ling, L., Mikaelian, I., Depaoli, A. M., Hanes, V., Kaplan, D. D. & Lieu, H. D. 2022. First-in-human study of NGM707, an ILT2/ILT4 dual antagonist antibody in advanced or metastatic solid tumors: Preliminary monotherapy dose escalation data. *Immunooncol Technol*, 16 (Supplement 1), 29.
- Naji, A., Menier, C., Maki, G., Carosella, E. D. & Rouas-Freiss, N. 2012. Neoplastic B-cell growth is impaired by HLA-G/ILT2 interaction. *Leukemia*, 26, 1889-92.
- Naji, A., Menier, C., Morandi, F., Agaugue, S., Maki, G., Ferretti, E., Bruel, S., Pistoia, V., Carosella, E. D. & Rouas-Freiss, N. 2014. Binding of HLA-G to ITIM-bearing Ig-like transcript 2 receptor suppresses B cell responses. *J Immunol*, 192, 1536-46.
- Nakamura, A., Kobayashi, E. & Takai, T. 2004. Exacerbated graft-versus-host disease in Pirb-/- mice. *Nat Immunol*, 5, 623-9.
- Nakayama, M., Underhill, D. M., Petersen, T. W., Li, B., Kitamura, T., Takai, T. & Aderem, A. 2007. Paired Ig-like receptors bind to bacteria and shape TLR-mediated cytokine production. *J Immunol*, 178, 4250-9.
- Nam, G., Shi, Y., Ryu, M., Wang, Q., Song, H., Liu, J., Yan, J., Qi, J. & Gao, G. F. 2013. Crystal structures of the two membrane-proximal lg-like domains (D3D4) of LILRB1/B2: alternative models for their involvement in peptide-HLA binding. *Protein Cell*, 4, 761-70.
- Navarro, F., Llano, M., Bellon, T., Colonna, M., Geraghty, D. E. & Lopez-Botet, M. 1999. The ILT2(LIR1) and CD94/NKG2A NK cell receptors respectively recognize HLA-G1 and HLA-E molecules co-expressed on target cells. *Eur J Immunol*, 29, 277-83.
- Nielsen, S. R. & Schmid, M. C. 2017. Macrophages as Key Drivers of Cancer Progression and Metastasis. *Mediators Inflamm*, 2017, 9624760.
- Nikolova, M., Musette, P., Bagot, M., Boumsell, L. & Bensussan, A. 2002. Engagement of ILT2/CD85j in Sezary syndrome cells inhibits their CD3/TCR signaling. *Blood*, 100, 1019-25.
- Nimmerjahn, F. & Ravetch, J. V. 2008. Fcgamma receptors as regulators of immune responses. *Nat Rev Immunol*, 8, 34-47.
- Niu, X., Wang, C., Zhao, J., Hu, J., Sun, J., Zheng, X., Qiu, Y., Wu, Z., Qiu, Y., Qiu, Q. & Lu, H. 2022. ES009, a LILRB2-specific blocking antibody, reprograms myeloid cells into pro-inflammation phenotype and potentiates T cell activation. *J ImmunoTher Cancer*, 10 (Supplement 2), A1102.
- Oldenborg, P. A., Zheleznyak, A., Fang, Y. F., Lagenaur, C. F., Gresham, H. D. & Lindberg, F. P. 2000. Role of CD47 as a marker of self on red blood cells. *Science*, 288, 2051-4.
- Oliveira, M. L. G., Castelli, E. C., Veiga-Castelli, L. C., Pereira, A. L. E., Marcorin, L., Carratto, T. M. T., Souza, A. S., Andrade, H. S., Simoes, A. L., Donadi, E. A., Courtin, D., Sabbagh, A., Giuliatti, S. & Mendes-Junior, C. T. 2022. Genetic diversity of the LILRB1 and LILRB2 coding regions in an admixed Brazilian population sample. *HLA*, 100, 325-348.
- Padlan, E. A. 1994. Anatomy of the antibody molecule. *Mol Immunol*, 31, 169-217.

- Pallasch, C. P., Leskov, I., Braun, C. J., Vorholt, D., Drake, A., Soto-Feliciano, Y. M., Bent, E. H., Schwamb, J., Iliopoulou, B., Kutsch, N., van Rooijen, N., Frenzel, L. P., Wendtner, C. M., Heukamp, L., Kreuzer, K. A., Hallek, M., Chen, J. & Hemann, M. T. 2014. Sensitizing protective tumor microenvironments to antibody-mediated therapy. *Cell*, 156, 590-602.
- Parham, P. & Moffett, A. 2013. Variable NK cell receptors and their MHC class I ligands in immunity, reproduction and human evolution. *Nat Rev Immunol*, 13, 133-44.
- Paul, S., Konig, M. F., Pardoll, D. M., Bettegowda, C., Papadopoulos, N., Wright, K. M., Gabelli, S. B., Ho, M., van Elsas, A. & Zhou, S. 2024. Cancer therapy with antibodies. *Nat Rev Cancer*, 24, 399-426.
- Pavlasova, G. & Mraz, M. 2020. The regulation and function of CD20: an "enigma" of B-cell biology and targeted therapy. *Haematologica*, 105, 1494-1506.
- Peipp, M., Klausz, K., Boje, A. S., Zeller, T., Zielonka, S. & Kellner, C. 2022. Immunotherapeutic targeting of activating natural killer cell receptors and their ligands in cancer. *Clin Exp Immunol*, 209, 22-32.
- Peppa, D., Pedroza-Pacheco, I., Pellegrino, P., Williams, I., Maini, M. K. & Borrow, P. 2018. Adaptive Reconfiguration of Natural Killer Cells in HIV-1 Infection. *Front Immunol*, 9, 474.
- Pierpont, T. M., Limper, C. B. & Richards, K. L. 2018. Past, Present, and Future of Rituximab-The World's First Oncology Monoclonal Antibody Therapy. *Front Oncol*, 8, 163.
- Portell, C. A., Wenzell, C. M. & Advani, A. S. 2013. Clinical and pharmacologic aspects of blinatumomab in the treatment of B-cell acute lymphoblastic leukemia. *Clin Pharmacol*, 5, 5-11.
- Pulford, K., Micklem, K., Thomas, J., Jones, M. & Mason, D. Y. 1991. A 72-kD B cell-associated surface glycoprotein expressed at high levels in hairy cell leukaemia and plasma cell neoplasms. *Clin Exp Immunol*, 85, 429-35.
- Qian, B. Z. & Pollard, J. W. 2010. Macrophage diversity enhances tumor progression and metastasis. *Cell.* 141, 39-51.
- Raskov, H., Orhan, A., Christensen, J. P. & Gogenur, I. 2021. Cytotoxic CD8(+) T cells in cancer and cancer immunotherapy. *Br J Cancer*, 124, 359-367.
- Redman, J. M., Hill, E. M., AlDeghaither, D. & Weiner, L. M. 2015. Mechanisms of action of therapeutic antibodies for cancer. *Mol Immunol*, 67, 28-45.
- Redondo-Garcia, S., Barritt, C., Papagregoriou, C., Yeboah, M., Frendeus, B., Cragg, M. S. & Roghanian, A. 2023. Human leukocyte immunoglobulin-like receptors in health and disease. *Front Immunol*, 14, 1282874.
- Reff, M. E., Carner, K., Chambers, K. S., Chinn, P. C., Leonard, J. E., Raab, R., Newman, R. A., Hanna, N. & Anderson, D. R. 1994. Depletion of B cells in vivo by a chimeric mouse human monoclonal antibody to CD20. *Blood*, 83, 435-45.
- Riihijarvi, S., Fiskvik, I., Taskinen, M., Vajavaara, H., Tikkala, M., Yri, O., Karjalainen-Lindsberg, M. L., Delabie, J., Smeland, E., Holte, H. & Leppa, S. 2015.

  Prognostic influence of macrophages in patients with diffuse large B-cell lymphoma: a correlative study from a Nordic phase II trial. *Haematologica*, 100, 238-45.
- Robert, C., Long, G. V., Brady, B., Dutriaux, C., Maio, M., Mortier, L., Hassel, J. C., Rutkowski, P., McNeil, C., Kalinka-Warzocha, E., Savage, K. J., Hernberg, M.

- M., Lebbe, C., Charles, J., Mihalcioiu, C., Chiarion-Sileni, V., Mauch, C., Cognetti, F., Arance, A., Schmidt, H., Schadendorf, D., Gogas, H., Lundgren-Eriksson, L., Horak, C., Sharkey, B., Waxman, I. M., Atkinson, V. & Ascierto, P. A. 2015. Nivolumab in previously untreated melanoma without BRAF mutation. *N Engl J Med*, 372, 320-30.
- Roberti, M. P., Julia, E. P., Rocca, Y. S., Amat, M., Bravo, A. I., Loza, J., Colo, F., Loza, C. M., Fabiano, V., Maino, M., Podhorzer, A., Fainboim, L., Barrio, M. M., Mordoh, J. & Levy, E. M. 2015. Overexpression of CD85j in TNBC patients inhibits Cetuximab-mediated NK-cell ADCC but can be restored with CD85j functional blockade. *Eur J Immunol*, 45, 1560-9.
- Rogers, L. M., Veeramani, S. & Weiner, G. J. 2014. Complement in monoclonal antibody therapy of cancer. *Immunol Res*, 59, 203-10.
- Roszer, T. 2015. Understanding the Mysterious M2 Macrophage through Activation Markers and Effector Mechanisms. *Mediators Inflamm*, 2015, 816460.
- Rotte, A. 2019. Combination of CTLA-4 and PD-1 blockers for treatment of cancer. *J Exp Clin Cancer Res*, 38, 255.
- Russler-Germain, D. A. & Ghobadi, A. 2023. T-cell redirecting therapies for B-cell non-Hodgkin lymphoma: recent progress and future directions. *Front Oncol*, 13, 1168622.
- Saito, F., Hirayasu, K., Satoh, T., Wang, C. W., Lusingu, J., Arimori, T., Shida, K., Palacpac, N. M. Q., Itagaki, S., Iwanaga, S., Takashima, E., Tsuboi, T., Kohyama, M., Suenaga, T., Colonna, M., Takagi, J., Lavstsen, T., Horii, T. & Arase, H. 2017. Immune evasion of Plasmodium falciparum by RIFIN via inhibitory receptors. *Nature*, 552, 101-105.
- Sambrook, J. & Russell, D. W. 2000. *Molecular Cloning: A Laboratory Manual*, Cold Spring Harbour Laboratory Press.
- Sandor, M. & Lynch, R. G. 1993. Lymphocyte Fc receptors: the special case of T cells. *Immunol Today*, 14, 227-31.
- Schewe, D. M., Alsadeq, A., Sattler, C., Lenk, L., Vogiatzi, F., Cario, G., Vieth, S., Valerius, T., Rosskopf, S., Meyersieck, F., Alten, J., Schrappe, M., Gramatzki, M., Peipp, M. & Kellner, C. 2017. An Fc-engineered CD19 antibody eradicates MRD in patient-derived MLL-rearranged acute lymphoblastic leukemia xenografts. *Blood*, 130, 1543-1552.
- Schewe, D. M., Vogiatzi, F., Munnich, I. A., Zeller, T., Windisch, R., Wichmann, C., Muller, K., Bhat, H., Felix, E., Mougiakakos, D., Bruns, H., Lenk, L., Valerius, T., Humpe, A., Peipp, M. & Kellner, C. 2024. Enhanced potency of immunotherapy against B-cell precursor acute lymphoblastic leukemia by combination of an Fcengineered CD19 antibody and CD47 blockade. *Hemasphere*, 8, e48.
- Schuh, E., Berer, K., Mulazzani, M., Feil, K., Meinl, I., Lahm, H., Krane, M., Lange, R., Pfannes, K., Subklewe, M., Gurkov, R., Bradl, M., Hohlfeld, R., Kumpfel, T., Meinl, E. & Krumbholz, M. 2016. Features of Human CD3+CD20+ T Cells. *J Immunol*, 197, 1111-7.
- Sehnal, D., Bittrich, S., Deshpande, M., Svobodova, R., Berka, K., Bazgier, V., Velankar, S., Burley, S. K., Koca, J. & Rose, A. S. 2021. Mol\* Viewer: modern web app for 3D visualization and analysis of large biomolecular structures. *Nucleic Acids Res*, 49, W431-W437.
- Seidel, J. A., Otsuka, A. & Kabashima, K. 2018. Anti-PD-1 and Anti-CTLA-4 Therapies in Cancer: Mechanisms of Action, Efficacy, and Limitations. *Front Oncol*, 8, 86.

- Shao, H., Ma, L., Jin, F., Zhou, Y., Tao, M. & Teng, Y. 2018. Immune inhibitory receptor LILRB2 is critical for the endometrial cancer progression. *Biochem Biophys Res Commun*, 506, 243-250.
- Sharpe, A. H. & Pauken, K. E. 2018. The diverse functions of the PD1 inhibitory pathway. *Nat Rev Immunol*, 18, 153-167.
- Shastry, M., Gupta, A., Chandarlapaty, S., Young, M., Powles, T. & Hamilton, E. 2023. Rise of Antibody-Drug Conjugates: The Present and Future. *Am Soc Clin Oncol Educ Book*, 43, e390094.
- Shawler, D. L., Bartholomew, R. M., Smith, L. M. & Dillman, R. O. 1985. Human immune response to multiple injections of murine monoclonal IgG. *J Immunol*, 135, 1530-5.
- Shiroishi, M., Kuroki, K., Rasubala, L., Kohda, D. & Maenaka, K. 2006a. Crystal Structure of LILRB2(LIR2/ILT4/CD85d) complexed with HLA-G. https://doi.org/10.2210/pdb2DYP/pdb.
- Shiroishi, M., Kuroki, K., Rasubala, L., Tsumoto, K., Kumagai, I., Kurimoto, E., Kato, K., Kohda, D. & Maenaka, K. 2006b. Structural basis for recognition of the nonclassical MHC molecule HLA-G by the leukocyte Ig-like receptor B2 (LILRB2/LIR2/ILT4/CD85d). Proc Natl Acad Sci U S A, 103, 16412-7.
- Sikic, B. I., Lakhani, N., Patnaik, A., Shah, S. A., Chandana, S. R., Rasco, D., Colevas, A. D., O'Rourke, T., Narayanan, S., Papadopoulos, K., Fisher, G. A., Villalobos, V., Prohaska, S. S., Howard, M., Beeram, M., Chao, M. P., Agoram, B., Chen, J. Y., Huang, J., Axt, M., Liu, J., Volkmer, J. P., Majeti, R., Weissman, I. L., Takimoto, C. H., Supan, D., Wakelee, H. A., Aoki, R., Pegram, M. D. & Padda, S. K. 2019. First-in-Human, First-in-Class Phase I Trial of the Anti-CD47 Antibody Hu5F9-G4 in Patients With Advanced Cancers. *J Clin Oncol*, 37, 946-953.
- Sosale, N. G., Rouhiparkouhi, T., Bradshaw, A. M., Dimova, R., Lipowsky, R. & Discher, D. E. 2015. Cell rigidity and shape override CD47's "self"-signaling in phagocytosis by hyperactivating myosin-II. *Blood*, 125, 542-52.
- Staerz, U. D., Kanagawa, O. & Bevan, M. J. 1985. Hybrid antibodies can target sites for attack by T cells. *Nature*, 314, 628-31.
- Steidl, C., Lee, T., Shah, S. P., Farinha, P., Han, G., Nayar, T., Delaney, A., Jones, S. J., Iqbal, J., Weisenburger, D. D., Bast, M. A., Rosenwald, A., Muller-Hermelink, H. K., Rimsza, L. M., Campo, E., Delabie, J., Braziel, R. M., Cook, J. R., Tubbs, R. R., Jaffe, E. S., Lenz, G., Connors, J. M., Staudt, L. M., Chan, W. C. & Gascoyne, R. D. 2010. Tumor-associated macrophages and survival in classic Hodgkin's lymphoma. N Engl J Med, 362, 875-85.
- Steiner, M. & Neri, D. 2011. Antibody-radionuclide conjugates for cancer therapy: historical considerations and new trends. *Clin Cancer Res*, 17, 6406-16.
- Sterner, R. C. & Sterner, R. M. 2021. CAR-T cell therapy: current limitations and potential strategies. *Blood Cancer J*, 11, 69.
- Stoll, A., Bruns, H., Fuchs, M., Volkl, S., Nimmerjahn, F., Kunz, M., Peipp, M., Mackensen, A. & Mougiakakos, D. 2021. CD137 (4-1BB) stimulation leads to metabolic and functional reprogramming of human monocytes/macrophages enhancing their tumoricidal activity. *Leukemia*, 35, 3482-3496.
- Storm, L., Bruijnesteijn, J., de Groot, N. G. & Bontrop, R. E. 2021. The Genomic Organization of the LILR Region Remained Largely Conserved Throughout

- Primate Evolution: Implications for Health And Disease. *Front Immunol*, 12, 716289.
- Strebhardt, K. & Ullrich, A. 2008. Paul Ehrlich's magic bullet concept: 100 years of progress. *Nat Rev Cancer*, 8, 473-80.
- Stripecke, R., Munz, C., Schuringa, J. J., Bissig, K. D., Soper, B., Meeham, T., Yao, L. C., Di Santo, J. P., Brehm, M., Rodriguez, E., Wege, A. K., Bonnet, D., Guionaud, S., Howard, K. E., Kitchen, S., Klein, F., Saeb-Parsy, K., Sam, J., Sharma, A. D., Trumpp, A., Trusolino, L., Bult, C. & Shultz, L. 2020. Innovations, challenges, and minimal information for standardization of humanized mice. *EMBO Mol Med*, 12, e8662.
- Suter, E. C., Schmid, E. M., Harris, A. R., Voets, E., Francica, B. & Fletcher, D. A. 2021. Antibody:CD47 ratio regulates macrophage phagocytosis through competitive receptor phosphorylation. *Cell Rep.*, 36, 109587.
- Swerdlow, S. H., Campo, E., Harris, N. L., Jaffe, E. S., Pileri, S. A., Stein, H. & Thiele, J. 2017. WHO Classification of Tumours of Haematopoietic and Lymphoid Tissues, International Agency for Research of Cancer, Lyon.
- Takai, T. 2005. Paired immunoglobulin-like receptors and their MHC class I recognition. *Immunology*, 115, 433-40.
- Tam, S. H., McCarthy, S. G., Armstrong, A. A., Somani, S., Wu, S. J., Liu, X., Gervais, A., Ernst, R., Saro, D., Decker, R., Luo, J., Gilliland, G. L., Chiu, M. L. & Scallon, B. J. 2017. Functional, Biophysical, and Structural Characterization of Human IgG1 and IgG4 Fc Variants with Ablated Immune Functionality. *Antibodies (Basel)*, 6.
- Taskinen, M., Karjalainen-Lindsberg, M. L., Nyman, H., Eerola, L. M. & Leppa, S. 2007. A high tumor-associated macrophage content predicts favorable outcome in follicular lymphoma patients treated with rituximab and cyclophosphamidedoxorubicin-vincristine-prednisone. *Clin Cancer Res*, 13, 5784-9.
- Tedla, N., An, H., Borges, L., Vollmer-Conna, U., Bryant, K., Geczy, C. & McNeil, H. P. 2011. Expression of activating and inhibitory leukocyte immunoglobulin-like receptors in rheumatoid synovium: correlations to disease activity. *Tissue Antigens*, 77, 305-16.
- Tedla, N., Bandeira-Melo, C., Tassinari, P., Sloane, D. E., Samplaski, M., Cosman, D., Borges, L., Weller, P. F. & Arm, J. P. 2003. Activation of human eosinophils through leukocyte immunoglobulin-like receptor 7. *Proc Natl Acad Sci U S A*, 100, 1174-9.
- Tedla, N., Lee, C. W., Borges, L., Geczy, C. L. & Arm, J. P. 2008. Differential expression of leukocyte immunoglobulin-like receptors on cord-blood-derived human mast cell progenitors and mature mast cells. *J Leukoc Biol*, 83, 334-43.
- Tenca, C., Merlo, A., Merck, E., Bates, E. E., Saverino, D., Simone, R., Zarcone, D., Trinchieri, G., Grossi, C. E. & Ciccone, E. 2005. CD85j (leukocyte lg-like receptor-1/lg-like transcript 2) inhibits human osteoclast-associated receptor-mediated activation of human dendritic cells. *J Immunol*, 174, 6757-63.
- The Antibody Society 2025. Therapeutic monoclonal antibodies approved or in regulatory review. (05.01.2025); www.antibodysociety.org/antibody-therapeutics-product-data.
- Tilly, H., Morschhauser, F., Sehn, L. H., Friedberg, J. W., Trneny, M., Sharman, J. P., Herbaux, C., Burke, J. M., Matasar, M., Rai, S., Izutsu, K., Mehta-Shah, N., Oberic, L., Chauchet, A., Jurczak, W., Song, Y., Greil, R., Mykhalska, L.,

- Bergua-Burgues, J. M., Cheung, M. C., Pinto, A., Shin, H. J., Hapgood, G., Munhoz, E., Abrisqueta, P., Gau, J. P., Hirata, J., Jiang, Y., Yan, M., Lee, C., Flowers, C. R. & Salles, G. 2022. Polatuzumab Vedotin in Previously Untreated Diffuse Large B-Cell Lymphoma. *N Engl J Med*, 386, 351-363.
- Todd, P. A. & Brogden, R. N. 1989. Muromonab CD3. A review of its pharmacology and therapeutic potential. *Drugs*, 37, 871-99.
- Trauth, B. C., Klas, C., Peters, A. M., Matzku, S., Moller, P., Falk, W., Debatin, K. M. & Krammer, P. H. 1989. Monoclonal antibody-mediated tumor regression by induction of apoptosis. *Science*, 245, 301-5.
- Treffers, L. W., van Houdt, M., Bruggeman, C. W., Heineke, M. H., Zhao, X. W., van der Heijden, J., Nagelkerke, S. Q., Verkuijlen, P., Geissler, J., Lissenberg-Thunnissen, S., Valerius, T., Peipp, M., Franke, K., van Bruggen, R., Kuijpers, T. W., van Egmond, M., Vidarsson, G., Matlung, H. L. & van den Berg, T. K. 2018. FcgammaRIIIb Restricts Antibody-Dependent Destruction of Cancer Cells by Human Neutrophils. *Front Immunol.* 9, 3124.
- Tronik-Le Roux, D., Sautreuil, M., Bentriou, M., Verine, J., Palma, M. B., Daouya, M., Bouhidel, F., Lemler, S., LeMaoult, J., Desgrandchamps, F., Cournede, P. H. & Carosella, E. D. 2020. Comprehensive landscape of immune-checkpoints uncovered in clear cell renal cell carcinoma reveals new and emerging therapeutic targets. *Cancer Immunol Immunother*, 69, 1237-1252.
- Tsai, R. K. & Discher, D. E. 2008. Inhibition of "self" engulfment through deactivation of myosin-II at the phagocytic synapse between human cells. *J Cell Biol*, 180, 989-1003.
- Turtle, C. J., Hanafi, L. A., Berger, C., Gooley, T. A., Cherian, S., Hudecek, M., Sommermeyer, D., Melville, K., Pender, B., Budiarto, T. M., Robinson, E., Steevens, N. N., Chaney, C., Soma, L., Chen, X., Yeung, C., Wood, B., Li, D., Cao, J., Heimfeld, S., Jensen, M. C., Riddell, S. R. & Maloney, D. G. 2016. CD19 CAR-T cells of defined CD4+:CD8+ composition in adult B cell ALL patients. *J Clin Invest*, 126, 2123-38.
- Uchida, J., Hamaguchi, Y., Oliver, J. A., Ravetch, J. V., Poe, J. C., Haas, K. M. & Tedder, T. F. 2004. The innate mononuclear phagocyte network depletes B lymphocytes through Fc receptor-dependent mechanisms during anti-CD20 antibody immunotherapy. *J Exp Med*, 199, 1659-69.
- Udartseva, O., Pupecka-Swider, M., Garcia-Broncano, P., Guo, N., Campbell, S., Klakus, E., Ward, R., Iyer, P., Brittsan, C., Wensley, B., Morin, B., Slee, A., Chand, D., Galand, C., Ignatovich, O., Briend, E. & Savitsky, D. 2022. AGEN1571 is a novel high-affinity ILT2 antagonist antibody that promotes adaptive and innate immune responses. *Cancer Res*, 82 (12\_Supplement), 2906.
- Urosevic, M., Kamarashev, J., Burg, G. & Dummer, R. 2004. Primary cutaneous CD8+ and CD56+ T-cell lymphomas express HLA-G and killer-cell inhibitory ligand, ILT2. *Blood*, 103, 1796-8.
- Vafa, O., Gilliland, G. L., Brezski, R. J., Strake, B., Wilkinson, T., Lacy, E. R., Scallon, B., Teplyakov, A., Malia, T. J. & Strohl, W. R. 2014. An engineered Fc variant of an IgG eliminates all immune effector functions via structural perturbations. *Methods*, 65, 114-26.
- van der Touw, W., Chen, H. M., Pan, P. Y. & Chen, S. H. 2017. LILRB receptor-mediated regulation of myeloid cell maturation and function. *Cancer Immunol Immunother*, 66, 1079-1087.

- Vandendriessche, S., Cambier, S., Proost, P. & Marques, P. E. 2021. Complement Receptors and Their Role in Leukocyte Recruitment and Phagocytosis. *Front Cell Dev Biol*, 9, 624025.
- Vidarsson, G., Dekkers, G. & Rispens, T. 2014. IgG subclasses and allotypes: from structure to effector functions. *Front Immunol*, 5, 520.
- Villa-Alvarez, M., Sordo-Bahamonde, C., Lorenzo-Herrero, S., Gonzalez-Rodriguez, A. P., Payer, A. R., Gonzalez-Garcia, E., Villa-Alvarez, M. C., Lopez-Soto, A. & Gonzalez, S. 2018. Ig-Like Transcript 2 (ILT2) Blockade and Lenalidomide Restore NK Cell Function in Chronic Lymphocytic Leukemia. *Front Immunol*, 9, 2917.
- Vittrant, B., Bergeron, A., Molina, O. E., Leclercq, M., Legare, X. P., Hovington, H., Picard, V., Martin-Magniette, M. L., Livingstone, J., Boutros, P. C., Collins, C., Fradet, Y. & Droit, A. 2020. Immune-focused multi-omics analysis of prostate cancer: leukocyte Ig-Like receptors are associated with disease progression. *Oncoimmunology*, 9, 1851950.
- Vivier, E., Tomasello, E., Baratin, M., Walzer, T. & Ugolini, S. 2008. Functions of natural killer cells. *Nat Immunol*, 9, 503-10.
- Vogiatzi, F., Muller, K., Winterberg, D., Rosner, T., Lenk, L., Cario, G., Schrappe, M., Kulozik, A. E., Bornhauser, B., Bourquin, J. P., Valerius, T., Peipp, M., Kellner, C. & Schewe, D. M. 2020. Co-Targeting of CD38 and CD47 in T Cell Acute Lymphoblastic Leukemia. *Blood*, 136 (Supplement 1), 39-40.
- Wang, J. S., Sommerhalder, D., Manish, S., Edenfield, W. J., Sehgal, K., Oh, D.-Y., Jiang, Y., Michalski, J., Lee, J., Hammers, H. J., Bai, L.-Y., Hsu, C.-H., Dampier, B. A. P., Zhou, K., Blum, L. K., Lancaster, J. S., Abhyankar, D. J., Lieu, H. D., Hanes, V. & Naing, A. 2024. Phase 1/2 study of NGM707, an ILT2/ILT4 dual antagonist antibody, in advanced solid tumors: Interim results from dose-escalation. *JCO*, 42 (16\_suppl), 2582-2582.
- Wang, L., Qin, W., Huo, Y. J., Li, X., Shi, Q., Rasko, J. E. J., Janin, A. & Zhao, W. L. 2020a. Advances in targeted therapy for malignant lymphoma. *Signal Transduct Target Ther*, 5, 15.
- Wang, Q., Song, H., Cheng, H., Qi, J., Nam, G., Tan, S., Wang, J., Fang, M., Shi, Y., Tian, Z., Cao, X., An, Z., Yan, J. & Gao, G. F. 2020b. Structures of the four Iglike domain LILRB2 and the four-domain LILRB1 and HLA-G1 complex. *Cell Mol Immunol*, 17, 966-975.
- Wang, W., Erbe, A. K., Hank, J. A., Morris, Z. S. & Sondel, P. M. 2015. NK Cell-Mediated Antibody-Dependent Cellular Cytotoxicity in Cancer Immunotherapy. *Front Immunol*, 6, 368.
- Wang, Y. & Jonsson, F. 2019. Expression, Role, and Regulation of Neutrophil Fcgamma Receptors. *Front Immunol*, 10, 1958.
- Wei, S. C., Duffy, C. R. & Allison, J. P. 2018. Fundamental Mechanisms of Immune Checkpoint Blockade Therapy. *Cancer Discov*, 8, 1069-1086.
- Weiner, G. J. 2015. Building better monoclonal antibody-based therapeutics. *Nat Rev Cancer*, 15, 361-70.
- Weiskopf, K. & Weissman, I. L. 2015. Macrophages are critical effectors of antibody therapies for cancer. *MAbs*, 7, 303-10.
- Weng, W. K. & Levy, R. 2003. Two immunoglobulin G fragment C receptor polymorphisms independently predict response to rituximab in patients with follicular lymphoma. *J Clin Oncol*, 21, 3940-7.

- Willcox, B. E., Thomas, L. M. & Bjorkman, P. J. 2003a. Crystal structure of HLA-A2 bound to LIR-1, a host and viral major histocompatibility complex receptor. *Nat Immunol*, 4, 913-9.
- Willcox, B. E., Thomas, L. M. & Bjorkman, P. J. 2003b. Crystal Structure of HLA-A2 Bound to LIR-1, a Host and Viral MHC Receptor. https://doi.org/10.2210/pdb1P7Q/pdb.
- Wynn, T. A., Chawla, A. & Pollard, J. W. 2013. Macrophage biology in development, homeostasis and disease. *Nature*, 496, 445-55.
- Xu, X., Yin, S., Wang, Y., Zhu, Q., Zheng, G., Lu, Y., Li, T. & Zhu, C. 2023. LILRB1(+) immune cell infiltration identifies immunosuppressive microenvironment and dismal outcomes of patients with ovarian cancer. *Int Immunopharmacol*, 119, 110162.
- Yagi, T., Baba, Y., Okadome, K., Kiyozumi, Y., Hiyoshi, Y., Ishimoto, T., Iwatsuki, M., Miyamoto, Y., Yoshida, N., Watanabe, M., Komohara, Y. & Baba, H. 2019. Tumour-associated macrophages are associated with poor prognosis and programmed death ligand 1 expression in oesophageal cancer. *Eur J Cancer*, 111, 38-49.
- Yang, Y., Yang, Z. & Yang, Y. 2021. Potential Role of CD47-Directed Bispecific Antibodies in Cancer Immunotherapy. *Front Immunol*, 12, 686031.
- Yang, Z. & Bjorkman, P. J. 2008. Structure of UL18, a peptide-binding viral MHC mimic, bound to a host inhibitory receptor. *Proc Natl Acad Sci U S A*, 105, 10095-100.
- Young, N. T., Waller, E. C., Patel, R., Roghanian, A., Austyn, J. M. & Trowsdale, J. 2008. The inhibitory receptor LILRB1 modulates the differentiation and regulatory potential of human dendritic cells. *Blood*, 111, 3090-6.
- Yu, J., Li, S., Chen, D., Liu, D., Guo, H., Yang, C., Zhang, W., Zhang, L., Zhao, G., Tu, X., Peng, L., Liu, S., Bai, X., Song, Y., Jiang, Z., Zhang, R. & Tian, W. 2022. SIRPalpha-Fc fusion protein IMM01 exhibits dual anti-tumor activities by targeting CD47/SIRPalpha signal pathway via blocking the "don't eat me" signal and activating the "eat me" signal. *J Hematol Oncol*, 15, 167.
- Yu, J., Song, Y. & Tian, W. 2020. How to select IgG subclasses in developing antitumor therapeutic antibodies. *J Hematol Oncol.* 13, 45.
- Yu, W. B., Ye, Z. H., Chen, X., Shi, J. J. & Lu, J. J. 2021. The development of small-molecule inhibitors targeting CD47. *Drug Discov Today*, 26, 561-568.
- Zeller, T., Lutz, S., Munnich, I. A., Windisch, R., Hilger, P., Herold, T., Tahiri, N., Banck, J. C., Weigert, O., Moosmann, A., von Bergwelt-Baildon, M., Flamann, C., Bruns, H., Wichmann, C., Baumann, N., Valerius, T., Schewe, D. M., Peipp, M., Rosner, T., Humpe, A. & Kellner, C. 2022. Dual checkpoint blockade of CD47 and LILRB1 enhances CD20 antibody-dependent phagocytosis of lymphoma cells by macrophages. *Front Immunol*, 13, 929339.
- Zeller, T., Munnich, I. A., Hilger, P., Pauls, I., Windisch, R., Kreissig, S., Wichmann, C., Peipp, M., Humpe, A., Schewe, D. M. & Kellner, C. 2023a. Co-Blockade of CD47 and LILRB1 Enhances Daratumumab-Mediated Phagocytosis of T Lineage Acute Lymphoblastic Leukemia Cells by Macrophages. *Ann Hematol*, 102 (Supplement 1), S61-S62.
- Zeller, T., Munnich, I. A., Hilger, P., Pauls, I., Windisch, R., Kreissig, S., Zimmermann, P., Kiepe, N., Wichmann, C., Moosmann, A., Humpe, A., Schewe, D. M., Peipp, M. & Kellner, C. 2024. Combining Daratumumab with Dual Immune Checkpoint

- Blockade of CD47 and LILRB1 Enhances Phagocytosis of T-ALL Cells by Macrophages. *Oncol Res Treat,* 47 (Supplement 2), 318.
- Zeller, T., Munnich, I. A., Windisch, R., Hilger, P., Schewe, D. M., Humpe, A. & Kellner, C. 2023b. Perspectives of targeting LILRB1 in innate and adaptive immune checkpoint therapy of cancer. *Front Immunol*, 14, 1240275.
- Zhang, Y., Lu, N., Xue, Y., Zhang, M., Li, Y., Si, Y., Bian, X., Jia, Y. & Wang, Y. 2012. Expression of immunoglobulin-like transcript (ILT)2 and ILT3 in human gastric cancer and its clinical significance. *Mol Med Rep*, 5, 910-6.
- Zhang, Y., Wang, H., Xu, X., Liu, H., Hao, T., Yin, S., Zhang, C. & He, Y. 2021. Poor Prognosis and Therapeutic Responses in LILRB1-Expressing M2 Macrophages-Enriched Gastric Cancer Patients. *Front Oncol*, 11, 668707.
- Zheng, J., Umikawa, M., Cui, C., Li, J., Chen, X., Zhang, C., Huynh, H., Kang, X., Silvany, R., Wan, X., Ye, J., Canto, A. P., Chen, S. H., Wang, H. Y., Ward, E. S. & Zhang, C. C. 2012. Inhibitory receptors bind ANGPTLs and support blood stem cells and leukaemia development. *Nature*, 485, 656-60.
- Zou, R., Zhong, X., Liang, K., Zhi, C., Chen, D., Xu, Z., Zhang, J., Liao, D., Lai, M., Weng, Y., Peng, H., Pang, X., Ji, Y., Ke, Y., Zhang, H., Wang, Z. & Wang, Y. 2023. Elevated LILRB1 expression predicts poor prognosis and is associated with tumor immune infiltration in patients with glioma. *BMC Cancer*, 23, 403.
- Zuck, M., Dinh, H., Wall, V., Lam, S., Chandrasekaran, R., Zapata, F., Loh, T., Loh, L., Bouchlaka, M., Graddis, T., Zuck, M., Kamal, P. & Probst, P. 2021. Discovery and preclinical characterization of anti-LILRB2 antibodies that rescue T cells from macrophage-mediated immune suppression. *J Immunother Cancer*, 9 (Supplement 2), A299.

## 6. Acknowledgements

An dieser Stelle möchte ich meinen aufrichtigen Dank an all diejenigen aussprechen, die mich während der Promotion fachlich und persönlich unterstützt haben.

Zunächst gilt mein Dank Herrn Prof. Dr. Andreas Humpe für die Möglichkeit der Durchführung dieses Forschungsprojekts in der Abteilung für Transfusionsmedizin, Zelltherapeutika und Hämostaseologie am LMU Klinikum.

In besonderer Weise möchte ich mich bei meinem Doktorvater Prof. Dr. Christian Kellner bedanken, für die Überlassung des spannenden Themas, für die hervorragende Betreuung, für sein unermüdliches Engagement und für die inspirierenden Diskussionen, die mir stets neue Perspektiven eröffnet und Begeisterung an wissenschaftlichem Arbeiten geweckt haben.

Ebenso gilt mein Dank den weiteren Mitgliedern der Betreuungskommission PD Dr. Christian Wichmann und PD Dr. Andreas Moosmann für ihre Unterstützung in wissenschaftlichen Fragen, ihr konstruktives Feedback, sowie die Unterstützung mit Reagenzien.

Außerdem möchte mich herzlich bei allen ehemaligen und aktuellen Mitgliedern der Forschungsgruppen am Max-Lebsche-Platz bedanken: Dr. Sebastian Lutz, Sophie Schabernack, Ira Münnich, Lena Halang, Fiona Rosmus, Lukas Bürtsch, Sophie Kreissig, Dr. Roland Windisch, Stefani Xhaxho, Patricia Hilger, Dr. Linping Chen-Wichmann und Dr. Irene Pauls. Vielen Dank für die immer freundliche Atmosphäre, die Geduld und Mithilfe beim Mikroskopieren der über 40.000 Makrophagen und die fachlichen, sowie auch die dringend nötigen nicht-wissenschaftlichen Gespräche.

Ebenso bedanken möchte ich mich beim Team der Thrombozytenspende für die Versorgung mit LRS-Kegeln, sowie beim Team der Medizinischen Klinik und Poliklinik III des LMU Klinikums, insbesondere bei Dr. Jan Banck, Natyra Tahiri, sowie bei Prof. Dr. Tobias Herold für die Unterstützung bei der Sammlung von Blutproben von Patientinnen und Patienten. Herrn Prof. Dr. Oliver Weigert danke ich für die Bereitstellung der Mantelzell-Lymphom-Proben.

Ebenso gilt mein Dank den Spenderinnen und Spendern von Thrombozyten, sowie den Patientinnen und Patienten, die der Nutzung Ihrer Proben im Rahmen dieses Forschungsprojekts zugestimmt haben.

Nicht zuletzt gilt mein Dank meiner Familie, insbesondere meinen Eltern Wolfgang und Martina, meinen Freunden, sowie meiner Freundin Antonia. Euer Verständnis, eure Geduld und eure Unterstützung haben dieses Studium und diese Promotion erst ermöglich. Ihr habt mich stets daran erinnert, warum ich diesen Weg eingeschlagen habe, und dafür bin ich euch unendlich dankbar.

### 7. Affidavit



LUDWIG-MAXIMILIANS-UNIVERSITÄT MÜNCHEN

Dekanat Medizinische Fakultät Promotionsbüro



### **Eidesstattliche Versicherung**

Zeller, Tobias Sebastian			
Name, Vorname			_

Ich erkläre hiermit an Eides statt, dass ich die vorliegende Dissertation mit dem Titel

## Enhancement of Antibody-Dependent Cellular Phagocytosis of Lymphoma Cells by the Blockade of HLA Class I Receptors

selbständig verfasst, mich außer der angegebenen keiner weiteren Hilfsmittel bedient und alle Erkenntnisse, die aus dem Schrifttum ganz oder annähernd übernommen sind, als solche kenntlich gemacht und nach ihrer Herkunft unter Bezeichnung der Fundstelle einzeln nachgewiesen habe.

Ich erkläre des Weiteren, dass die hier vorgelegte Dissertation nicht in gleicher oder in ähnlicher Form bei einer anderen Stelle zur Erlangung eines akademischen Grades eingereicht wurde.

Augsburg, den 16.10.2025	Tobias Sebastian Zeller		
Ort, Datum	Unterschrift Tobias Sebastian Zeller		

Eidesstattliche Versicherung Stand: 07.01.2025

### Übereinstimmungserklärung 8.





Dekanat Medizinische Fakultät Promotionsbüro



# Erklärung zur Übereinstimmung der gebundenen Ausgabe der Dissertation

mit der elektronischen Fassung				
rsion der eingereichten Dissertation mit dem Titel:				
ellular Phagocytosis of Lymphoma Cells by the Blockade LA Class I Receptors				
n und gebundenen Exemplaren übereinstimmt.				
Tobias Sebastian Zeller				
Unterschrift Tobias Sebastian Zeller				

Übereinstimmung abgegebener Exemplare

Stand: 07.01.2025

### 9. List of Publications

### Original research articles

Schewe, D. M., Vogiatzi, F., Munnich, I. A., **Zeller, T.**, Windisch, R., Wichmann, C., Muller, K., Bhat, H., Felix, E., Mougiakakos, D., Bruns, H., Lenk, L., Valerius, T., Humpe, A., Peipp, M. & Kellner, C. 2024. Enhanced potency of immunotherapy against B-cell precursor acute lymphoblastic leukemia by combination of an Fc-engineered CD19 antibody and CD47 blockade. *Hemasphere*, 8, e48.

Zeller, T., Lutz, S., Munnich, I. A., Windisch, R., Hilger, P., Herold, T., Tahiri, N., Banck, J. C., Weigert, O., Moosmann, A., von Bergwelt-Baildon, M., Flamann, C., Bruns, H., Wichmann, C., Baumann, N., Valerius, T., Schewe, D. M., Peipp, M., Rosner, T., Humpe, A. & Kellner, C. 2022. Dual checkpoint blockade of CD47 and LILRB1 enhances CD20 antibody-dependent phagocytosis of lymphoma cells by macrophages. *Front Immunol*, 13, 929339.

### **Review articles**

**Zeller, T.**, Munnich, I. A., Windisch, R., Hilger, P., Schewe, D. M., Humpe, A. & Kellner, C. 2023. Perspectives of targeting LILRB1 in innate and adaptive immune checkpoint therapy of cancer. *Front Immunol*, 14, 1240275.

Peipp, M., Klausz, K., Boje, A. S., <u>Zeller, T.</u>, Zielonka, S. & Kellner C. 2022. Immunotherapeutic targeting of activating natural killer cell receptors and their ligands in cancer. *Clin Exp Immunol*, 209, 22-32.

#### **Abstracts**

Kiepe, N., Zimmermann, P., Pauls, I., <u>Zeller, T.</u>, Kreissig, S., Wichmann, C., Peipp, M., Humpe, A., Lenk, L. & Kellner, C. 2025. Targeting FMS-Like Tyrosine Kinase 3 (FLT3) in B-Cell Acute Lymphoblastic Leukemia with an Fc-Engineered Antibody. *Ann Hematol, accepted for publication* <u>Zeller, T.</u>, Munnich, I. A., Hilger P., Pauls, I., Windisch R., Kreissig, S., Zimmermann, P., Kiepe, N., Wichmann, C., Moosmann A., Humpe, A., Schewe, D. M., Peipp, M. & Kellner, C. 2024. Die Kombination von Daratumumab mit dualer Immun-Checkpoint-Blockade von CD47 und LILRB1 steigert die Phagozytose von T-ALL-Zellen durch Makrophagen. *Oncol Res Treat*, 47 (Supplement 2), 318.

Zeller, T., Munnich, I. A., Hilger, P., Pauls, I., Windisch, R., Kreissig, S., Wichmann, C., Peipp, M., Humpe, A., Schewe, D. M. & Kellner, C. 2023. Co-Blockade of CD47 and LILRB1 Enhances Daratumumab-Mediated Phagocytosis of T Lineage Acute Lymphoblastic Leukemia Cells by Macrophages. *Ann Hematol*, 102 (Supplement 1), 14.

Zeller, T., Lutz, S., Munnich, I. A., Windisch, R., Hilger, P., Herold, T., Tahiri, N., Banck, J. C., Weigert, O., Moosmann, A., von Bergwelt-Baildon, M., Flamann, C., Bruns, H., Wichmann, C., Baumann, N., Valerius, T., Schewe, D. M., Peipp, M., Rosner, T., Humpe, A. & Kellner, C. 2022. Immun-Checkpoint Co-Blockade von CD47 und HLA-Klasse I-Rezeptoren zur Steigerung der CD20-Antikörper-vermittelten Phagozytose von Lymphomzellen. *Oncol Res Treat*, 45 (Supplement 2), 162.

Hilger, P., **Zeller, T.**, Vogiatzi, F., Muller, K., Munnich, I. A., Windisch, R., Wichmann, C., Nimmerjahn, F., Valerius, T., Peipp, M., Humpe, A., Schewe, D. M. & Kellner, C. 2022. Steigerung der CD38 Antikörper-vermittelten Phagozytose von T-ALL Zellen durch Fc Engineering und CD47 Blockade. *Oncol Res Treat*, 45 (Supplement 2), 92.

Zeller, T., Lutz, S., Munnich, I. A., Windisch, R., Hilger, P., Herold, T., Tahiri, N., Banck, J. C., Weigert, O., Moosmann, A., von Bergwelt-Baildon, M., Flamann, C., Bruns, H., Wichmann, C., Baumann, N., Valerius, T., Schewe, D. M., Peipp, M., Rosner, T., Humpe, A. & Kellner, C. 2022. Dual immune checkpoint blockade of LILRB1 and CD47 enhances antibody-dependent cellular phagocytosis of lymphoma cells by CD20 antibodies. *Eur J Immunol*, 52 (Supplement 1), 136.